Numerical Simulation of a Mesoscale Convective System over the east coast of South Africa

By Ross Blamey

Supervisor:
Prof. Chris Reason

Department of Oceanography
University of Cape Town

A dissertation submitted to the Faculty of Science in fulfilment of the requirements for the Degree in
Master of Science

February 2007

UNIVERSITY OF CAPE TOWN

Abstract

Weather stations across the northern KwaZulu-Natal coastline recorded over 100 mm of rainfall over the 11/12 February 2005, with Cape St. Lucia and Richards Bay measuring 111 mm and 96.8 mm, respectively. This heavy rainfall was associated with a mesoscale convective system (MCS) that initiated through small convective storms beginning early in the afternoon on 11 February 2005 and eventually decayed in the early morning hours on the 12th. The high-lying topography of the eastern escarpment and high diurnal surface heating possibly provided the trigger for the event. It was also identified that a combination of synoptic features in and around South Africa contributed to the evolution of the system.

This particular MCS is investigated with a non-hydrostatic numerical model (MM5) to help determine which processes were important in its initiation and development, as well as what factors contributed to the associated heavy rainfall. The model is also used to conduct sensitivity tests to determine the role that local features, such as the regional topography and sea surface temperature, played in the evolution of the system. Through the various MM5 simulations, it was evident that the eastern escarpment played a key role in triggering the convective event, while it also had an influence on the low level winds that advected moisture into the region. A sea surface temperature sensitivity simulation highlighted the important role that the Agulhas Current plays in supplying moisture to fuel extreme precipitation events in South Africa. The significance of resolving large-scale features in the mid-latitudes in numerical simulations of weather events in South Africa was identified when

excluding these features from the simulation. Through these simulations it was identified that the development of the MCS and the heavy nocturnal precipitation was due to a combination of the continuous moisture supply into the region, a conditionally unstable atmosphere, and uplift due to low level convergence and the local topography.

Acknowledgments

I would like to thank my parents, for the love and support that they have given throughout my life. I am also grateful for all the motivation and support given to me by my family, friends and members of the Oceanography Department.

Sincere thanks go to Kabumbwe Hansingo and Jeremy Main for all their time and patience in assisting with the modelling and other computer related issues. Thanks also to the South African Weather Service, in particular to Lee-Ann Clark, Pieter Visser and Karel de Waal, for providing some of the data and images used in this thesis.

The Meteosat satellite data were provided by EUMETSAT (www.eumetsat.int), with some assistance from Jochen Kerkmann. The NAVOCEANO SST data were obtained through the online PO:DAAC Ocean ESIP Tool (POET) at the Physical Oceanography Distributed Active Archive Center (PO:DAAC), NASA Jet Propulsion Laboratory, Pasadena, CA (http://podaac.jpl.nasa.gov/poet). The NCEP data is provided by the NOAA/Earth Systems Research Laboratory Physical Sciences Division (ESRL:PSD), Boulder Colorado, from their website http://www.cdc.noaa.gov/.

Finally, I would like to thank my supervisor, Prof. Chris Reason, for his interest, valuable input and guidance through this thesis.

Contents

List of Figures and Tables

.....

Chapter 1

Introduction

Severe weather phenomena, such as flooding, lightning, tornadoes, hail, strong winds, not only often result in the loss of life, but also typically lead to damage to infrastructure and to crops resulting in detrimental impacts on the economy. That, combined with the fact that large portions of the South African population live in the rural areas (with limited access to medical services) or below the poverty line, results in them being more vulnerable to such severe weather phenomena than in many other parts of the world. Although there has been fair amount of research on forecasting flash floods and the associated flood producing systems over the last few decades (e.g. Maddox et al. 1979; Doswell et al. 1996; Smith et al. 2001), most of this research has been conducted on weather systems outside of Africa. Therefore, it is essential that continued global research is performed on the types of systems that may have a large negative impact on society.

Another perspective is that these severe weather producing systems often provide much of the all important rainfall to a semi-arid country, such as South Africa. Thus, a greater understanding of these weather producing systems would be beneficial to all parties involved. Some of the standard requirements to observe these systems include a radar network with a large spatial coverage, regular radiosonde data, satellite imagery as well as a weather station network with a large spatial coverage. These instruments are also required to provide the observational data that can be used to validate numerical model output. However, this is one area were South Africa, along with most other African countries, lags behind. Despite the limited data available, more knowledge about severe weather producing systems is needed in order to provide a more reasonable forecast, which would benefit all sections of the population. The types of severe weather producing systems that occur in South Africa include cut-off lows (e.g. Singleton and Reason, 2006; 2007), a variety of thunderstorms, ranging from single cells storms through to the larger mesoscale convective systems (Laing and Fritsch, 1993b; Garstang and Tyson, 2000, Tyson and Preston-Whyte, 2000), and occasionally tropical cyclones in the northeastern and

eastern parts, such as Dominia and Eline in 1984 and 2000, respectively (Dyson and van Heerden, 2001; Reason and Keibel, 2004).

In this thesis, focus is placed on the large, organized, convective storm known as a mesoscale convective system (MCS). A case study of a mesoscale convective event that took place over northern KwaZulu-Natal in February 2005 is presented and analysed. Mesoscale convective systems occur in different regions of the world, including South Africa, and are known to produce a host of severe weather phenomena. Currently, most of the previous research has been conducted on MCSs that have been located outside of the Southern African region. Thus, an important aspect of the ongoing research is to examine MCSs over South Africa and how they may impact on society. Some insight may be provided by comparing the results of the literature on overseas events to South African case studies. A greater understanding of such systems is needed so that more accurate forecasts may be developed in future, as well as mitigating the disaster they potentially may cause. A better understanding of the processes that govern the development and life cycle of these systems is also vital. More details on these particular convective systems are provided in the following chapter.

The objectives of this thesis are twofold, with the first relating to the development of the MCS and the associated heavy precipitation and the second being to obtain a better understanding of how some of the local features may have helped in the development of the system. The main section of this thesis involves the use of a numerical mesoscale model to simulate the particular MCS case study. This simulation will hopefully aid in determining which processes played a key role during the development and life cycle of the event as well as identifying the processes responsible for the heavy precipitation along the north coast. The selected model is the non-hydrostatic fifth generation mesoscale model (MM5; Dudhia, 1993) from the Pennsylvania State University – National Center for Atmospheric Research (PSU/NCAR). This mesoscale model has been applied to MCS cases in other regions of the world with some success (e.g. Tucker and Crook, 1999; Chen et al., 2000; Romero et al., 2000; Xu et al., 2001; and many others). This type of research may provide some insight on how well equipped the MM5 model is at handling a mesoscale convective event over Southern Africa, particularly in the eastern region,

where the local topography may play a key role in the formation and life cycle of these events. Sensitivity tests using the MM5 model are also performed to see how topography and sea surface temperatures within and surrounding the province of KwaZulu-Natal (KZN) may have influenced the development of the system and its associated heavy rainfall. A further sensitivity test is also performed in order to identify the role in which synoptic features in the mid-latitudes may have influenced the evolution of the system.

KZN is situated on the east coast of South Africa, which is located on the southern tip of the African continent. South Africa is bounded on the west by the cold Benguela Current, which is a region of strong ocean upwelling, while the east coast on the other hand is bounded by the warm Agulhas Current. The influence this warm current has on the surrounding coastal regions is a well researched topic, where evidence has been presented that it has an influence on the summer rainfall and severe weather events in the region (e.g. Jury et al. 1993; Crimp and Mason, 1999; Rouault et al. 2002) as well as regional circulation patterns (Reason, 2001). The South African coastal regions are separated from the elevated plateau (approximately 1-2 km above sea level) by a well-defined escarpment that extends above 3km in certain places within the Drakensberg mountain range in KZN and the Lesotho Maluti Mountains. It is this escarpment that limits the low level moisture penetration to the interior of the country from the Southwest Indian Ocean. In addition to strong SST and orographic gradients, Southern Africa is also unique in terms of other influential gradients (Reason, 2006), such as the spatial distributions of soil moisture and vegetation type and cover, with the west coast very much drier than the east coast.

Coastal South Africa could possibly be divided into three rainfall regions: the east coast, which is found to be predominantly a summer rainfall region, the west coast, a winter rainfall region and the south coast which may receive significant rainfall throughout the year. Most of the rainfall over the east coast and also the interior of the country is of convective origin (Tyson and Preston-Whyte, 2000). These authors suggest that the degree of convectivity over South Africa is determined not only by the diurnal heating cycle of the near surface air, but also by the prevailing dynamics of particular synoptic conditions and by mesoscale and local effects. They also noted that the severe storms in the region are often the result of different forcing

mechanisms ranging from the synoptic scale down to the local scale. For the 1965-85 period, Preston-Whyte et al. (1991) found that 4 synoptic types, namely the Tropical-Temperate Trough, Westerly Wave, Ridging High and East Coast Low, accounted for 81 percent of the rainfall over KwaZulu-Natal. A common synoptic situation promoting storm formation is a trough in the tropical easterlies, while frontal passages to the south are also known to frequently trigger storms (Tyson and Preston-Whyte, 2000). Garstang et al. (1987) found that the generation of convective storms over the escarpment of the northeast South African region was associated with westerly waves propagating across the southern tip of Africa, which then interact with the topography of the escarpment. Another interesting observation from the research done by Preston-Whyte (1970) revealed that 64% of mean hourly rainfall in Durban occurred between 19:00 and 06:00 (LST), with a maximum occurring at 21:00. It was thought that local offshore mountain plain winds from the Drakensberg produced this late-evening rainfall peak. It appears that it is usually a case that synoptic and mesoscale forcing as well as the local heating cycle combine to produce severe weather in South Africa.

This thesis is divided into the following chapters: Chapter 2 discusses MCSs and the environment they develop in, as well as what makes these systems unique. The data, methodology and numerical model setup that is used in this thesis is presented in chapter 3, while the case study is presented in chapter 4. This is followed by the presentation of results from the numerical simulation in chapter 5. The results of the sensitivity tests are presented and analyzed in chapter 6. The discussion of the results is found in chapter 7 and conclusions are presented in chapter 8.

Chapter 2

Introduction to Mesoscale Convective Systems

2.1. Definition

The term *mesoscale convective system* (MCS) is used to describe an ensemble of convective storms that satisfy certain spatial and temporal criteria. These particular systems are the largest of the convective storms, where *mesoscale* refers to the size of the weather system, *convective* refers to the type of storm, and *system* means simply that they are organized into one big system. Due to atmospheric dynamics varying greatly in space and time scales, Orlanski (1975) proposed a new way of dividing the three major scales (microscale, mesoscale and macroscale) more precisely temporally and spatially into three scales, respectfully denoted α, β, γ. Mesoscale convective systems are generally divided into two scales:

1. Meso-α scale – length scales of 250-2500 km and duration of $\geq$ 6 hrs
2. Meso-β scale – length scales of 25-250 km and duration of less than 6hrs

However, within a given meso-α scale system, there may be meso-β scale convective components (e.g. McAnelly and Cotton, 1986). MCSs are primarily a product of the amalgamation of smaller convective storms and are organized into a single cloud system.

The term "mesoscale convective system" may lead to some confusion when classifying systems, due to the numerous types and criterion associated with the term. In general, these systems may be divided into two categories, which are linear systems and quasi-circular systems (see figure 2.1). The method of identifying the type of system is predominately done by satellite and radar images. Earlier definitions of MCSs usually categorized them as having a length exceeding 250km and persisting at least 3 hours (e.g. Bartels et al. 1984). However, due to the variety of MCSs, a very broad definition could be accepted that they are a long-lived ($\geq$3 hours) cumulonimbus cloud system that contains a nearby precipitation area of roughly 100 km or more in at least one direction (Parker and Johnson 2000; Houze 2004).

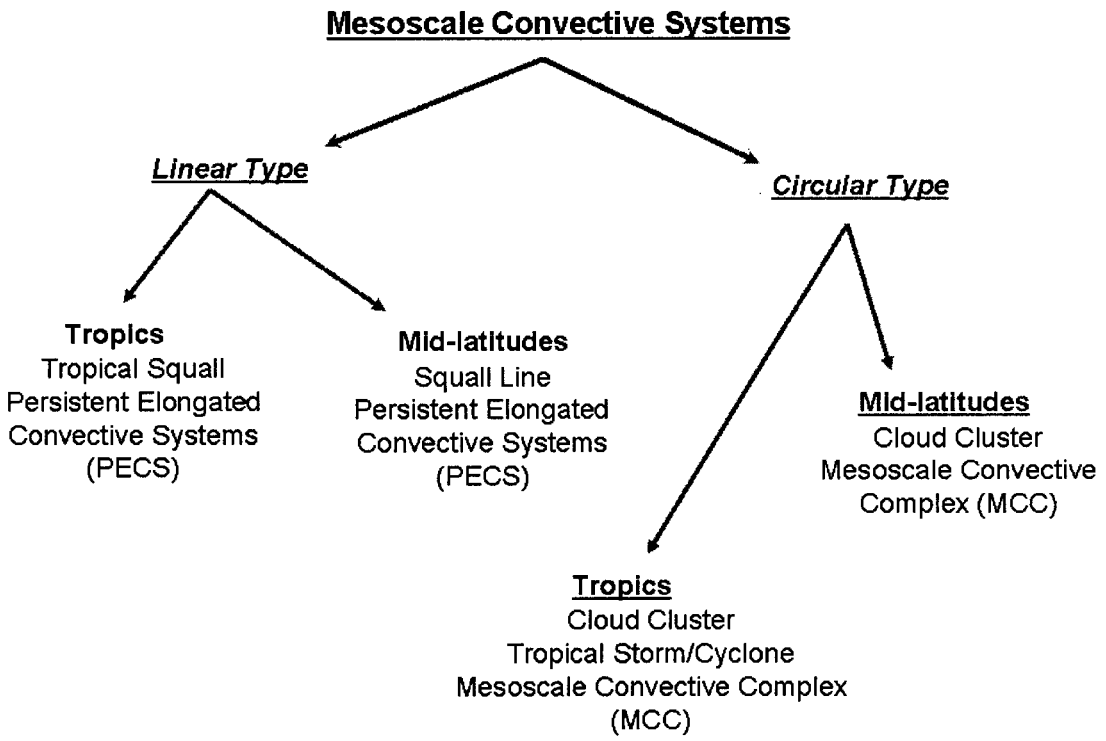

Figure 2.1: Diagram of the different types of MCS found in the tropics and mid-latitudes (adapted from Maddox, 1980)

Probably the most common of the MCSs is the *squall line*, which is found in both the tropics and mid-latitudes. The term "squall line" used to be applied to the cold front and associated with gust winds (Federal Meteorological Handbook, 2005 - hereafter referred to as *FMH, 2005*). Nowadays, the term is commonly applied to any linear convective storm system or any thunderstorm line. Some authors, such as Parker and Johnson (2004a, b, c) have even suggest that linear squall lines could be considered as a phase in the development of many MCSs. These linear systems are usually dominated by a line of convective cells in the front, followed by stratiform rainfall. Prefrontal squall lines are the largest and most violent squall lines that are found in the mid-latitudes (Cotton, 2000). The largest of the MCSs is the *mesoscale convective complex* (MCC), defined by Maddox (1980), and falls under the meso-α scale as a quasi-circular system. To put it into perspective, these systems can develop a cloud shield extent of up to 400 000km^2 (Laing and Fritsch, 1997). The definition of a MCC is based on cloud top temperature, size, duration and eccentricity/shape (table 2.1; Maddox, 1980). It is the eccentricity criterion that usually separates this specific system from other MCSs. Some systems obtained the size and duration of MCCs, but

failed to show a quasi-circular appearance. Hence, another definition was required for these large more linear type systems, which were then given the name of *persistent elongated convective systems* (PECS; Anderson and Arritt, 1998). Another form of MCS is that of *cloud clusters*, which are systems containing convection that is organised in a rather random configuration (Cotton, 2000).

	MCC	**PECS**
Size*	A - $\geq$ 100 000 km^2 B - $\geq$ 50 000 km^2	Same as MCC
Cloud shield Temperature*	A - $\leq$ 32° C B - $\leq$ 52° C	Same as MCC
Shape/Eccentricity	$\geq$ 0.7 at max. extent (i.e. round or oval)	0.7 $\leq$ eccentricity $\geq$ 0.2 (i.e. does not have to be round, but must not be linear)
Duration	Size definition must be meet for a period $\geq$ 6 hours	Same as MCC
Terminate	Size definitions A and B are no longer satisfied	

Table 2.1: Definitions of an MCC and PECS, based on the research by Maddox (1980) and Anderson and Arritt (1998).

* There are two size categories (A and B) for the MCC, which refer to the two cloud shield temperatures (A and B). So in order to satisfy the definition it must have an outer cloud shield temperature of below -32°C and a size greater than 100 000km^2, and an inner cloud shield of greater than 50 000km^2 and colder than -52°C.

2.2. Global Distribution

MCSs are distributed throughout the tropics and mid-latitudes, over both land and ocean. A summary of the distribution of these systems can be found in the review by Houze (2004). This author discusses how the use of different satellite images enables researchers to see the global distribution of these systems through features such as lightning distribution, ice in clouds and regions of convective versus stratiform precipitation. Certain types of MCSs, such as MCCs, require additional features to satisfy the conditions favourable for formation. In a study of South American MCCs, Velasco and Fritsch (1987) found that areas which exhibit frequent and widespread

deep convection (such as the Amazon River Basin) did not necessarily result in the formation of MCCs. This indicates that there are other factors which result in the convection being organized into a MCC. Through a global study of MCCs, Laing and Fritsch (1997) noted that these have a strong tendency to occur in certain regions of the world, which include (see figure 2.2):

- The gradient zones between outgoing long-wave radiation maxima and minima (especially along the periphery of significant OLR minima).
- The lee (relative to prevailing mid-level flow) of elevated terrain

MCSs have been documented in many regions of the world, including parts of North and South America, Europe, Asia, Australia and Africa (Maddox, 1980; Velasco and Fritsch, 1987; Miller and Fritsch, 1991; Laing and Fritsch, 1993a, 1993b, 1997, 2000; Anderson and Arritt, 2001; García-Herrera et al. 2005 and others). However, most of this research on these weather systems has been conducted outside of Africa. The little research that has been done on African systems has mainly focused on systems in the Sahel Region (e.g. Laurent et al. 1998; Laing et al. 1999; Mathon et al. 2002).

There has not been much research conducted on MCS in South Africa, but the little that has been done has found that the systems appear to follow the global trend (Laing and Fritsch 1993b, 1997). The systems over South Africa are predominately an austral summer (November-March) phenomenon and are perceived to be an important feature of the South African climate due to the substantial contribution they make to total annual rainfall (Garstang and Tyson, 2000). These authors suggest that the occurrence of MCSs over South Africa is a product of many interacting process, which operate on scales ranging from the synoptic scale to local conditions. The possible primary controls of cumulus convective development appear to be the atmospheric stability and availability of moisture in the lower levels and the divergence field (Tyson and Preston-Whyte, 2000; Garstang and Tyson, 2000). A common feature over subtropical Southern Africa is a large semi-permanent anticyclone, which is responsible for the temperature inversions and stable layers often found in the region (Cosijn and Tyson, 1996). This stability will inhibit convective cloud growth and therefore reduce the amount of rainfall in the region. Therefore, conditions for deep cumulus convection are required to penetrate the stable layers.

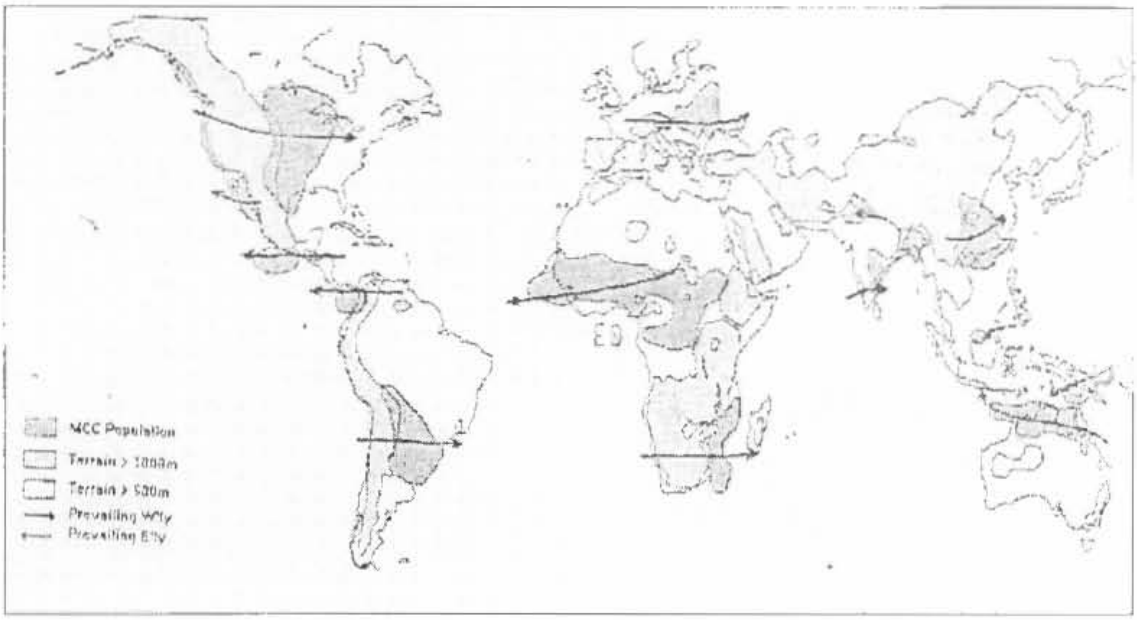

Figure 2.2: The distribution of MCC populations, elevated terrain and the prevailing mid-level flow (from Laing and Fritch, 1997).

2.3. Life Cycle

Mesoscale convective systems, particularly MCCs, display a clear life cycle pattern. The stages within the life cycle are identified by changes in the shape and size of the system, as well as the changing atmospheric conditions (Maddox, 1980). The four main stages are *First storms*, *Initiation*, *Maximum extent* and *Termination* (e.g. Laing and Fritsch 1997; Jirak et al. 2003). The *First storm* stage is the appearance of the initial thunderstorms, *initiation* is the time when the size definition is first met, *maximum extent* is the time when the cold cloud shield reaches a maximum size, and *termination* occurs when the system no longer satisfies its size definition.

The systems also appear to have a similar onset times for the different life cycle stages as seen below (e.g. Maddox, 1980; Velasco and Fritsch, 1987; Millar and Fritsch, 1991; Laing and Fritsch 1993a, b; Laing and Fritsch 1997; Anderson and Arritt, 1998):

1. First thunderstorms develop in the mid-to-late afternoon
2. By sunset, their individual cold-cloud shields have amalgamated into a mesoscale structure

3. In the early night time hours, the system obtains MCS size criteria
4. Reaches maximum size after midnight
5. Dissipates a few hours after sunrise

The onset of certain stages within the life cycle occurs at different times in some parts of the world. Laing and Fritsch (1993b) found that the first thunderstorms developed in mid-afternoon (approximately 12h00 UTC) in Africa. The season in which the systems are studied could also have an impact on the different onset times of the stages, an example of this is shown by Anderson and Arritt (1998) who found that a large percentage of MCCs in the U.S. during 1992 and 1993 initiated at different times during the summer and spring months.

In terms of the duration of these convective systems, it has been found that there is a nearly linear relationship between the average convective system radius and its life cycle (Machado et al. 1998). This supports the findings of Laing and Fritsch (1997) who noted that MCCs with large cold cloud shields usually last longer than those with small shields. The general definition of MCS require them to have a duration longer that 3 hours, but the larger MCCs usually last around 10–13 hours from storm initiation to the time they shrink to below the minimum MCC size criteria (McAnelly and Cotton, 1989; Millar and Fritsch, 1991; Laing and Fritsch 1997; Jirak et al. 2003, Ashley et al. 2003).

The characteristic of these systems to occur predominately during the night time is believed to be related to processes of radiation and latent heating (see Cotton, 2000). This author suggests that the radiation that is absorbed or emitted at the base or top of the cloud cover plays a role in this night time characteristic (figure 2.3). During the night, radiation emitted by the earth is absorbed at the base of the stratiform cloud cover, where a fraction of it is re-emitted towards the earth and another fraction is emitted upwards (this continues at each layer). Due to clouds being relatively good absorbers of infrared radiation, this process results in less of the re-emitted radiation reaching the inner clouds. At the top of the cloud cover there is a net loss of radiation due to the air above it not being able to absorb a lot of the emitted radiation and hence none is re-emitted downwards to the top of the cloud. The end result is that there is a net warming at the base of the cloud and cooling at the top, which results in the cloud

layer being unstable, resulting in convective overturning. Obviously this pattern will differ in the day time hours, since shortwave radiation from the sun is absorbed in the cloud tops. Another feature resulting in an unstable cloud layer is latent heating (Cotton, 2000). Latent heating, which results from condensation on cloud droplets, freezing and vapour deposition growth of ice crystals, causes a warming of the mid-levels and hence a rising motion. Below the mid-levels, there is a cooling due to melting precipitation particles. This cooling will ultimately have an affect on the mesoscale circulation within and around the system, which is discussed in the next section of this chapter.

2.4. MCS development and the Environment:

2.4.1 Initiation and development

In a summary of the synoptic conditions that favour the development of mid-latitude MCCs, Maddox et al. (1986) found that these systems often occur in a region favouring upward vertical motion ahead of a middle-level shortwave trough, in an environment that is conditionally unstable. These authors also note that other features during the development of such systems includes low level warm advection, low levels winds that increase in speed and veer during the night, as well as the atmosphere becoming more moist with time. It could be argued that synoptic-scale processes are required to provide the right conditions for convection to take place, while mesoscale features/processes are required to focus these conditions into a specific region or to initiate convection (Doswell, 1987). Romero et al. (2000) suggest that synoptic and mesoscale conditions must remain favourable for the development of an MCS over a specific region and last for several hours. This situation is needed so that convection can be continuously generated in the specific region, which then allows the system to become long-lived and quasi-stationary. This claim is supported by Cotton (2000) who suggests that the genesis of MCSs usually requires sustained forcing from the large-scale environment in order to trigger formation. However, in the absence of strongly forced environments, mesoscale features become important for the development and evolution of the convective event (Stensrud and Fritsch, 1993, 1994). Synoptic-scale conditions that may encourage the development of convection include upward vertical motion, water vapour flux convergence at low

levels, high water vapour content and potential instability in the atmosphere (Maddox et al. 1979). A common forcing is low-level convergence of moist air, which could be a result of numerous mechanisms such as mountain slope circulations, convergence along large-scale frontal boundaries or convergence along the Intertropical Convergence Zone (Cotton, 2000). Common initiation mechanisms for the more linear MCSs are a synoptic or mesoscale boundary, such as a dryline, trough or front (FMH, 2005).

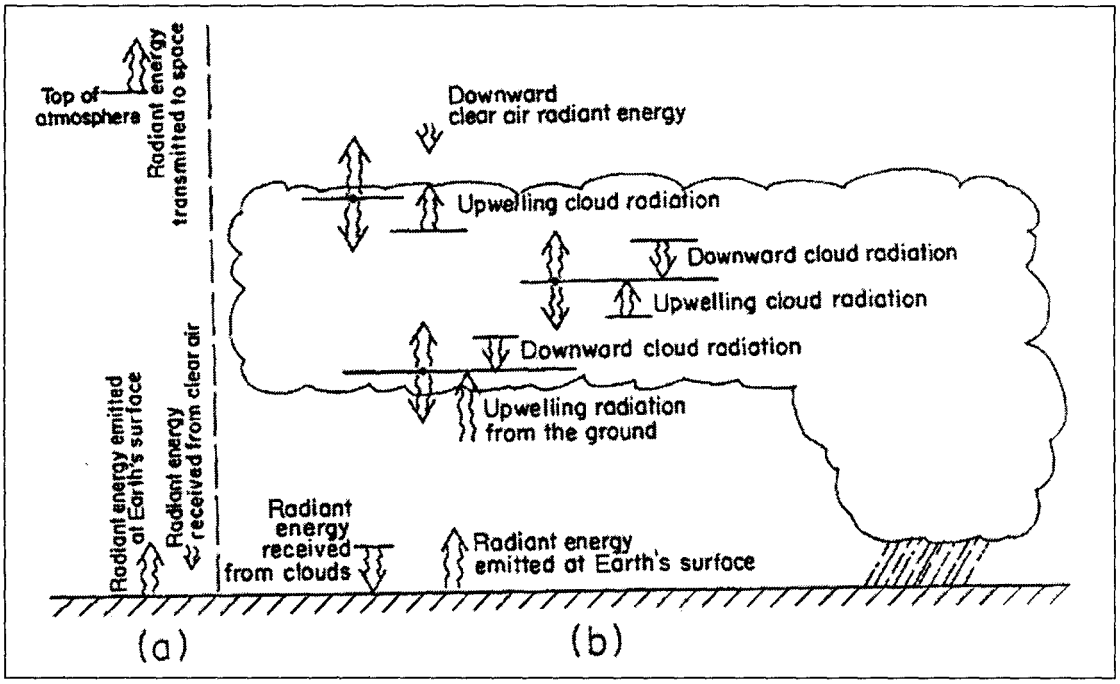

Figure 2.3: Illustration of infrared radiant energy absorbed and received at different levels in the atmosphere (From Cotton, 2000). Left panel illustrates a cloud-free atmosphere, while the right panel illustrates a stratiform-anvil cloud layer. Length of arrows is proportional to the amount of radiant energy per unit area.

Once the initiation of convection has taken place, there appear to be two processes in the life cycle that are vital for this initial convective event to be formed into a MCS, as described by Cotton (2000). The first of these is the merger of anvil clouds of neighbouring storms, which results in a cold pool of air forming near the surface. This pool of air is known as the "cold pool" and forms due to cooling of the air by evaporation and melting of precipitation (Houze et al. 1989, Weisman 1993; Cotton 2000). Weisman (1992) suggests that the generation of a deep cold pool is significant in sustaining a MCS. It is believed that both CAPE and the relative humidity of the low to mid-levels are significant in determining cold pool strength and depth

(Rotunno et al. 1988). These authors also suggest that the low equivalent potential temperature (low-θ_e) air from the mid-levels also plays a role by enhancing evaporational cooling, which then strengthens the downdrafts as well as the cold pool. The downdraft and the cold pool then interact to form the mesohigh at the surface and to drive surface outflow, resulting in low-level convergence and the initiation of a gust front (Houze et al. 1989; Weisman, 1992). Weisman (1993) suggests that if the cold pool spreads in a windless environment it is likely to produce convergence and lifting along its leading edge which can then trigger new cells.

2.4.2 General air flow

The merger of the anvils is also seen as important due to the heating effects in the middle and upper atmosphere as a result of latent heating. This results in the formation of a tropospheric low pressure region which may then drive a mesoscale circulation (e.g. Houze et al. 1989; Cotton 2000). At the interface of the cold pool and the inflow of warm, moist air, a horizontal pressure gradient develops, which is directed outward from the meso-high. This results in low-level moist air being lifted into the system. The lifting of this low level air is also aided by the meso-low aloft (Houze et al. 1989; Cotton 2000).

There appear to be two general conceptual models that are accepted for the more quasi-linear systems, with the one referring to the more symmetric MCS and the other an asymmetric MCS (Houze et al. 1989; Houze et al. 1990). The symmetry of these systems, in terms of the shape of the cloud and precipitation distribution, is related to the cyclonic and anticyclonic vortices forming on the northern and southern ends (in the northern hemisphere), respectively. This is discussed in more detail in the next section of this chapter. The most recognized model of a mature linear MCS appears to be the one produced by Houze et al. (1989), which reveals the general overview of air flows, circulations, and features found in a mature linear MCS (figure 2.4). In this model, there are two major airflows, with the one being high equivalent potential temperature (high-θ_e) front-to-rear flow that is initiated at the gust front and enters the convective updraft while accelerating upwards and then rearwards. This flow is believed to result in the formation of the stratiform precipitation that forms behind the convective line (Houze et al. 1989). The second major flow is that of the downward-

sloping rear-to-front flow, which is also commonly referred to as the rear-inflow jet (RIJ). Unlike the front-to-rear flow, this flow contains low-θ_e air and enters the rear of the storm in the midlevels below the trailing anvil cloud in the stratiform region and advances towards the convective line. This flow then descends as it reaches the convective line and combines with precipitation downdrafts. The descending flow is due to evaporative cooling of raindrops, melting of precipitation and the downward directed pressure gradient force in the stratiform region (Cotton, 2000; Houze 2004). The rear inflow does not develop until the system becomes tilted upshear and it appears to be related to vertical wind shear and magnitude of CAPE (Weisman, 1992).

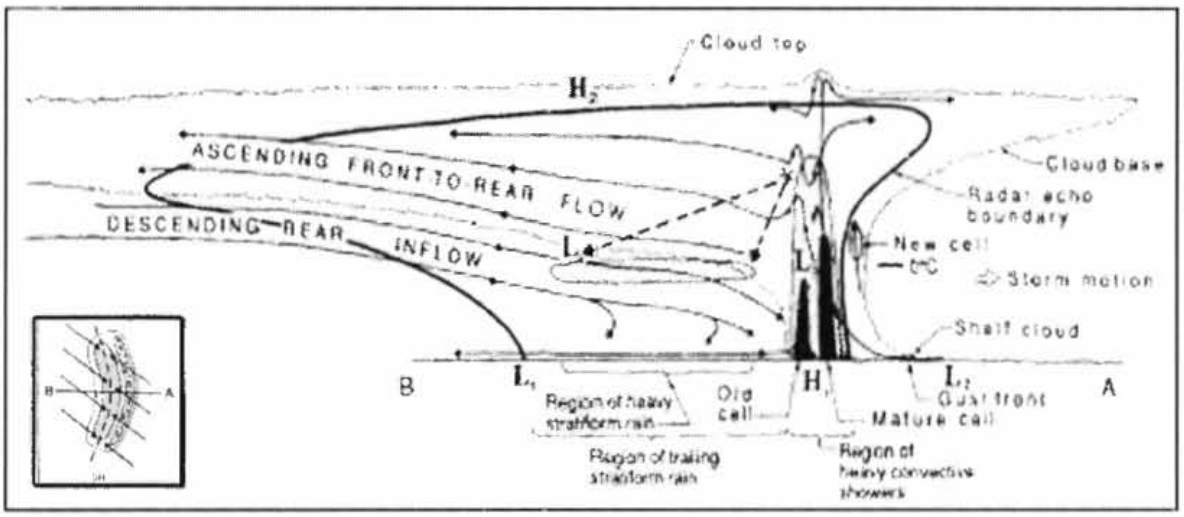

Figure 2.4: Houze et al's (1989) conceptual model of a squall line with a trailing stratiform area viewed in a vertical cross-section, which is viewed parallel to its motion (see, insert).

Initially it was thought that this inflow was driven by thermodynamic processes only (e.g. Smull and Houze, 1987; Lafore and Moncrieff, 1989), but more research has shown that the cause for this air flow may be as a result of dynamic processes. The strength of this flow appears to be linked to the thermodynamic instability of the environment (Weisman, 1992). Research by Schmidt and Cotton (1990) revealed that gravity waves resulting from heating in the convective line could possibly produce the rear inflow. Houze (2004) suggests that the rear inflow is mainly produced by the gravity wave theory, while the role of thermodynamic processes more that likely aids

in producing descent in the inflow. This rear inflow is also mainly found in leading-line/trailing stratiform type MCSs, but research has found that non-squall type MCS still have a mid-level inflow, which was usually determined by the flow in the large-scale environment (e.g. Kingsmill and Houze, 1999).

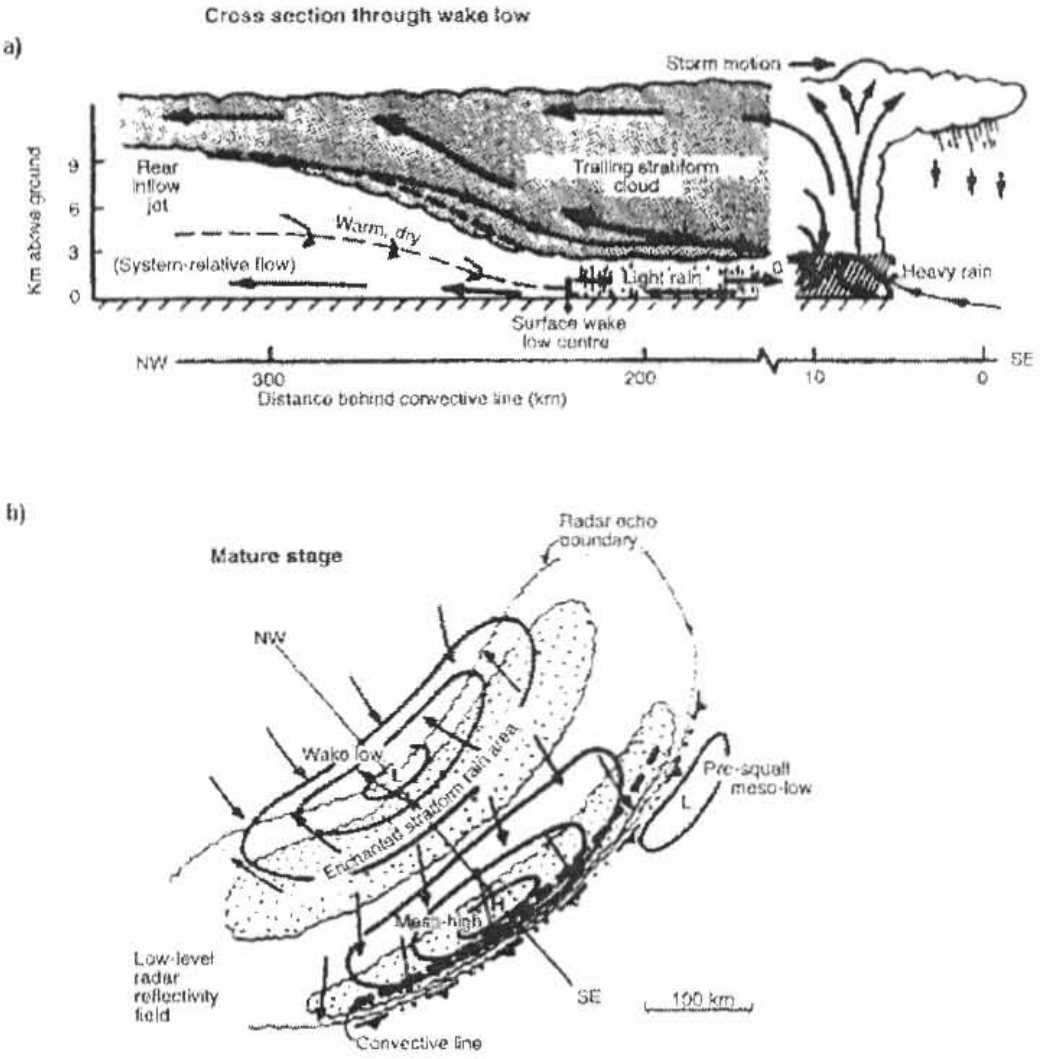

Figure 2.5: Schematic cross-section through the wake low (a) and surface pressure and wind fields and precipitation distribution during the mature stage of a squall line (b). Arrows indicate stream lines, not trajectories (from Johnson and Hamilton, 1988).

Cotton (2000) also suggests that stretching of the air column in the stratiform region (particularly during the night time hours), due to rising air in the mid-levels and sinking air below it, may also result in air flow from the rear of the system. This author also suggests that the convective region also plays a role in the rear-to-front flow by a similar stretching of the air column. The stretching is a result of buoyant air

rising in the updraft region, while strong downdrafts (form due to water loading, melting and evaporation of precipitation) occur just behind it. This stretching results in a low pressure region known as the wake low (between 2-4 km above ground level), which draws air in from the rear. The descending rear-to-front flow is also believed to play a role in the formation of a low pressure region at the surface due to adiabatic warming of the sinking air (Johnson and Hamilton, 1988). Other surface pressure patterns associated within the quasi-linear system include a low pressure immediately ahead of the line (pre-squall mesolow), while a high pressure region (mesohigh), caused by evaporation and melting of convective precipitation, forms just behind the convective line. Johnson and Hamilton (1988) summed up these pressure patterns in a schematic, which is found in figure 2.5. These pressure patterns are known to shift polewards, along with the stratiform precipitation region, in the Northern Hemisphere asymmetric systems (Loehrer and Johnson, 1995).

2.4.3 Rotation, Rossby radius and longevity

Something that makes MCSs unique is their ability to survive in a region where conditions are not always favourable. Due to their size and duration, as well as the area they draw air from, the Coriolis force is important (Cotton, 2000). As the system begins to get larger, low level air is drawn from further afield, which eventually will become large enough for the airstream being drawn in to respond to the Earth's rotation. At the same time, air being drawn into the mid-levels also begins to respond to the Earth's rotation. At this stage, the system now contains a slow cyclonic rotation as more air is drawn into the system. This cyclonic circulation is sometimes evident in the mid-level clouds after the main convection and stratiform rainfall has dissipated, and will be discussed later in this chapter, in the section titled "MCSs and MCVs". At the top of the system, the rising air reaches the stable tropopause and results in the air spreading outward horizontally. This part of the system receives little heating, which results in a meso-high forming at the top. The horizontally spreading air eventually spreads far enough for the rotation of the Earth to come into play, resulting in an anti-cyclonic rotation. Due to the variation of the Coriolis force with latitude, systems in the higher latitudes do not have to be as large as those in the tropics to experience the same rotation.

Cotton et al. (1989) pointed out from observations and modelling studies that deep convection becomes less intense as the system reaches maturity and the flow becomes increasingly geostrophically balanced and non-divergent. In general, large quasi-circular mesoscale convective systems develop an organized region of high or low pressure, which is sustained for many hours, and hence the wind field adjusts to this pressure field and becomes influenced by the Earth's rotation so that the flow then approaches geostrophic balance. However, another apparent force has to be taken into consideration when flow occurs around curved isobars. This force is known as the centrifugal force and either acts in the same direction as Coriolis or the opposite direction along a curved plane (depends on the central pressure). When Coriolis, the pressure gradient force and the centrifugal force are in balance then the system is referred to being gradient balance. Cotton (2000) suggested that although the systems hardly ever reach true balance, it is the adjustment toward a balanced state, which separates MCSs from ordinary convective storms. This adjustment ultimately plays a role in the systems survival as it enters a zone where conditions are unfavourable to sustain it.

As rotation of the system develops, it also develops inertial stability. This means that if the system moves into a region of increased static stability (i.e. more stable environment) it can continue to survive as an organized system, whereas a non-rotating system will rapidly decay (Cotton, 2000). The scale at which a MCS develops enough rotation to be dominated by inertial stability is known as the "Rossby radius of deformation, (λ_R)". In other words, the Rossby radius of deformation could be described as the length scale at which the rotational effects become as important as buoyancy effects in the development of the flow about the MCS. This value varies with latitude and static stability, being larger at lower latitudes, so that tropical systems will have to be larger than their mid-latitude counterparts in order to be inertially stable. Also, if the MCS is larger than λ_R, it will have an influence on the gravity waves emitted in the convective cells (Cotton, 2000). Convective cells heat the atmosphere during precipitation, resulting in gravity waves that propagate horizontally and vertically out of the system. This propagation results in the heating and kinetic energy that is generated in the cells being distributed away from the system. Thus, if the system is larger than λ_R, it will result in the heating and kinetic

energy being more efficiently converted into a nearly-balanced rotating circulation (Menard and Fritsch, 1989; Cotton et al. 1989; Cotton 2000).

Research by Cotton et al. (1989) led to a more dynamically based definition of an MCC in which they related the horizontal scale of MCCs to the Rossby radius of deformation. They describe a mature MCC as:

"*A mature MCC represents an inertially stable mesoscale convective system which is nearly geostrophically balanced and whose horizontal scale is comparable to or greater than the Rossby radius of deformation*" Cotton et al. (1989: pg 780).

These authors also proposed that this dynamical definition distinguishes the MCC from the shorter lived, smaller mesoscale convective systems in the mid-latitudes and is a basis for comparing tropical mesoscale systems with mid-latitude MCCs.

Laing and Fritsch (1993b) suggested that the close relationship between MCCs, tropical storms, tropical depressions and MCC produced mesoscale vortices support the definition proposed by Cotton et al. (1989); i.e., that a MCC is an attempt by the atmosphere to produce an inertially stable and geostrophically balanced system with a radius larger than the Rossby radius of deformation. Anderson and Arritt (1998) found that the correlation between size and duration of MCC events in their research and other studies, such as Laing and Fritsch (1997), agrees with this dynamical description, because they suggest that the likelihood that the spatial scale of the MCC exceeds the Rossby radius of deformation increases with the size of the MCC (all else being equal).

In a global summary of MCCs, Laing and Fritsch (1997) document that most systems appear to obtain maximum size during the night. Houze (2004) suggests that this timing is probably a result of both dynamic and thermodynamic properties that limit the size of the system. The dynamic factor refers to the already mentioned Rossby radius, while the thermodynamic factor refers to the thermodynamic structure of the boundary layer. One possible factor that helps sustain the boundary layer during the night time hours is that of the low level jet (LLJ). LLJs are responsible for the inflow of high-θ_e air and appear to be prominent features in the MCS environment (e.g.

Maddox and Doswell III, 1982, Maddox, 1983; Miller and Fritsch, 1991; Smull and Augustine, 1993; Chen et al. 1998; Laing and Fritsch, 2000; Vera et al. 2005 and many others). The systems in the U.S. usually thrive on moist air masses brought in by the LLJ, which come from the warm waters of the Gulf of Mexico, while the air mass that feeds the South American systems usually comes from the tropical rainforest regions of the Amazon and Parana River basins (Velasco and Fritsch, 1987; Vera et al. 2005). Miller and Fritsch (1991) noted that most of the MCC population centres in the Western Pacific Region occur downstream of a long fetch of low level flow over very warm water. The upper level jets (ULJ) are also prominent features in the formation of MCSs (e.g. Maddox, 1983; Cotton et al. 1989). The systems often form in certain exit zones of the ULJ or migrate latitudinally as the jet does during the different seasons (e.g. Velasco and Fritsch 1987; Miller and Fritsch 1991).

The termination of the system usually occurs when it moves into an environment that is more stable and convectively less favourable (Maddox et al. 1986). The termination stage is usually identified as to when the system no longer meets the requirements of being classified as a MCS. Maddox (1983) noted that during this stage the LLJ no longer feeds moisture into the system and that cool air advection replaces the warm advection in the lower troposphere. These unfavourable conditions are usually as a result of the changing synoptic patterns.

There are a variety of MCSs that all contain their own unique flow patterns, which cannot all be fully discussed in this study. The discussion presented here highlights the fact that there has been extensive research into these types of systems and for brevity, not all of it can be included. There are also many processes that are not fully understood and this also requires further attention. This section has dealt with some of the major features and characteristics that have been associated with MCS.

2.5. MCSs and MCVs

As mentioned previously, in the Northern Hemisphere the remnants of the cyclonic circulation in the mid-levels (2–6 km above ground level) is sometimes evident in visible satellite imagery after the main cloud system has dissipated. This remaining circulation can often be identified by the presence of spiral bands and is more

commonly known as a Mesoscale Convective Vortex (MCV). Nearly all of the MCVs that have been documented have occurred within the United States (e.g. Menard and Fritsch, 1989; Bartels and Maddox, 1991; Trier et al. 2000a; 2000b; and others).

The diameters of these systems can range from tens to hundreds of kilometres and have temporal scales ranging from hours to days (e.g. Bartels and Maddox, 1991; Bartels et al. 1997; Weisman and Davis 1998). They have been found to generate within the stratiform precipitation region of the mesoscale system, during the mature and later stages of the life cycle (e.g. Leary and Rapport, 1987; Zhang and Fritsch, 1988b; Menard and Fritsch, 1989). Probably the most distinguishing features of MCVs is that of their shape and spiral pattern which, from satellite images, suggests that cyclonic rotation is taking place. Bartels and Maddox (1991) noted that most MCVs in their case study originated from "MCC-like" systems, but only half originated in systems that actually satisfied all the MCC criteria. Another interesting observation made by these authors is that MCVs develop primarily in the same regions as MCCs and even show similar migration patterns as MCCs.

However, MCVs are not only restricted to MCC type systems since research has revealed that vortices may develop at the ends of the quasi-linear systems (Weisman, 1993; Skamarock et al. 1994). These vortices are commonly referred to as "book-end vortices". As mentioned previously, there are two general conceptual 2-D models for the quasi-linear MCS, which are symmetric and asymmetric MCS (figure 2.6; Houze et al. 1989; Houze et al. 1990). Within a symmetric MCS in the Northern Hemisphere, cyclonic and anticyclonic mid-level vortices of equal strength develop on the northern and southern ends of the convective system, respectively. The asymmetric MCS also has these cyclonic and anticyclonic vortices, but the cyclonic vortex in this case is more dominant. This often led to the distortion of the trailing-stratiform precipitation region, where the stratiform region was biased toward the poleward (northern) end of the line in the Northern Hemisphere systems. The strengthening of the cyclonic vortex is usually as a result of Coriolis force (Weisman, 1993; Skamarock et al. 1994; Weisman and Davis, 1998). Davis and Wiseman (1994) suggest that the origin of such vortices could be attributed to the upward tilting of system-generated horizontal vorticity by the leading line convective updrafts. The main source for this horizontal vorticity was found at the cold pool-updraft interface. Houze (2004) suggests that this

pattern of the MCS initially being symmetric in structure and then becoming more asymmetric later in the life cycle is the most common life cycle scenario.

It has also been documented that some MCVs are associated with subsequent convective activity where occasionally this subsequent convective activity is know to produce severe weather (Bartels and Maddox, 1991; Menard and Fritsch, 1989; Trier at al. 2000a). This subsequent convective activity is known to take place on the periphery of the MCV circulation, where it is short-lived, or closer to the MCV centre, where it is longer-lived (Trier et al. 2000a; 2000b). MCVs may also enhance the rear-inflow jets, which then may aid in strengthening the surface winds and result in more damage (Weisman and Davis, 1998).

On the synoptic scale, Trier et al. (2000a) identified three basic types of surface environments associated with MCV cases. These included MCVs occurring along or to the north of an east-west orientated quasi-stationary front, in advance of slowly moving cold fronts and those that were not associated with any synoptic thermal boundaries. Just over half of their MCV cases were associated with the first type of surface pattern. In terms of features in the mid-troposphere, Bartels and Maddox (1991) noted that MCVs appear to be associated with a long-wave ridge. This ridging pattern in the large-scale environment has also been documented in other case studies (e.g. Bartels et al. 1997; Trier et al. 2000a).

Bartels and Maddox (1991) suggest that key factors controlling whether an MCV is generated or not may be due to both the scale and duration of latent heating, and the character of the background synoptic or mesoscale settings, such as shear, vorticity and divergence, in which the convective system develops. These authors found that the MCVs in MCSs were favoured by weak flow, weak vertical shear, weak background relative vorticity, and strong gradients of humidity. Through the use of model simulations, Weisman and Davis (1998) were able to show that in the quasi-linear systems, mesoscale vortices are produced for an entire range of shears.

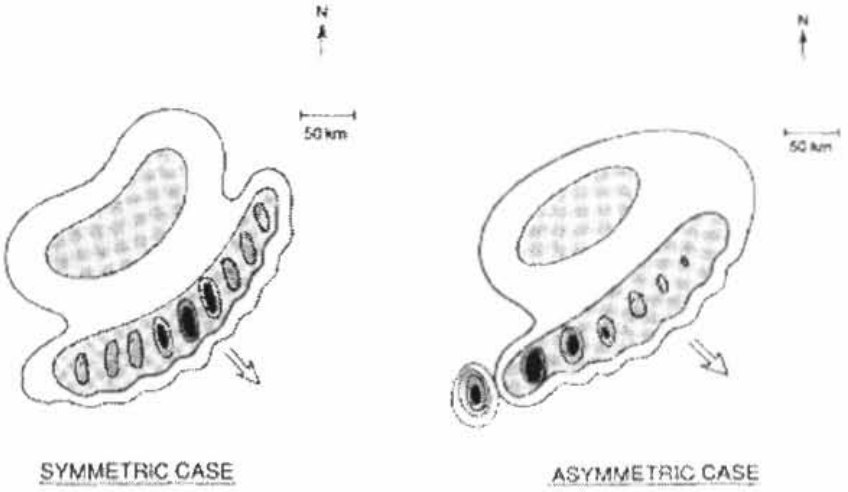

Figure 2.6: Schematic produced by Houze et al. (1990) which depicts the symmetric (left) and asymmetric (right) leading-line/trailing stratiform type MCS. Where, levels of shading imply increasing radar reflectivity.

There is still a lack of knowledge regarding these systems and as more research is placed on MCVs, hopefully a greater understanding of how, where and when these systems develop will be achieved. It appears that quite a few of these systems are spawned from "MCC-like" systems, which suggests that it is only the larger or longer lived MCS that may produce MCVs. However, often research has shown that these vortices also occur in the quasi-linear systems and influence the symmetry of the system. Although, the initial research from Bartels and Maddox (1991), suggested that only a few of these systems developed a year, some small or short-lived systems may go undetected. More recently, it has become evident that new technology is allowing for more of these systems to be detected and researched (e.g. Trier et al. 2000a). To the author's knowledge there does not appear to have been any of these systems documented within the Southern Hemisphere.

2.6. MCS Propagation

Most methods of determining MCS tracks involve studying their cold cloud shields using satellite imagery. In the U.S., MCCs are found to move with the mean flow in the 700-500 mb layer, which is eastward (Maddox, 1980). The strength of the midtropospheric flow could possibly have an affect on the significance and location of

flooding, because it is likely to determine the speed at which the MCC passes through an area (Trier and Parsons, 1993). During the mid-summer, many of the systems in the U.S. curve equatorward in the late stages of their life cycle (Velasco and Fritsch, 1987). Systems in mid-latitude South America are found to track west to east in late spring, but show a more equatorward track during mid-summer (Velasco and Fritsch, 1987). Looking at the large systems over southeastern Africa, Laing and Fritsch (1993b) found that the systems forming near the eastern escarpment tend to move east or northeastward towards the high equivalent potential temperature (high-θ_e) associated with warm waters (Agulhas Current) along the southeastern African coast (figure 2.7). Similar findings were found in the Western Pacific Region (WPR), where the systems tended to depart from the prevailing mid-level flow, which appeared to be towards the low-level high-θ_e air (Miller and Fritsch, 1991). Research by Parker and Johnson (2000) found that most of the systems they researched in the central United States were fed from the front. Systems tend to propagate to the right (left) of the prevailing mid-level flow in the Northern Hemisphere (Southern Hemisphere), which could be due to the low-level high-θ_e air which is always to the right (left) of these systems (Miller and Fritsch, 1991). However, it must be noted that some authors (e.g. Parker and Johnson, 2000; Pettit and Johnson, 2003) have found that some systems may be fed by an inflow of high-θ_e air from behind the system.

The above mentioned large scale flow may be useful in helping determine the movement of the system, but a greater understanding of the factors aiding in its propagation is required. In a summary of the literature on MCSs by Houze (2004), this author attributes the propagation of the systems to a range of modes. The first mode being the role in which "cold pool dynamics" has on the propagation of the system. As mentioned previously, the cold pool is the area beneath the system and is formed due to cooling of the air by evaporation and melting of precipitation. Simply put, the cold pool then pushes outwards as a gravity current and results in lifting the conditionally unstable air at its border, generating new convection at its leading edge. However, Houze (2004) does not regard this process as being able to explain all the aspects of propagation. This could be demonstrated by convective cells sometimes forming way in front of the gust front. This formation, known as *discrete propagation*, is believed to be determined by the sum of two components of the flow. Corfidi et al. (1996) attempted to predict the movement of MCC, by looking at the

movement of the mesobeta-scale (Orlanski, 1975) convective elements (MBEs). They constructed a very simple conceptual model, which shows the MBE movement as the vector sum of the mean flow in the cloud layer and the propagation component. The authors found that this technique seemed to provide a good estimate of the rate of movement and also revealed that there is an overwhelming tendency for MBEs to propagate towards or "into" the low level jet (LLJ). Although Corfidi (2003) noted that the LLJ appears to play a role in the vector motion of MCS, other features appear to have a bigger influence in the motion. Houze (2004) suggests that the mean large-scale environmental wind velocity may possibly be used as a proxy for the cold pool propagation of an individual cumulonimbus, while the LLJ may possibly be used as a proxy for the discrete jumping.

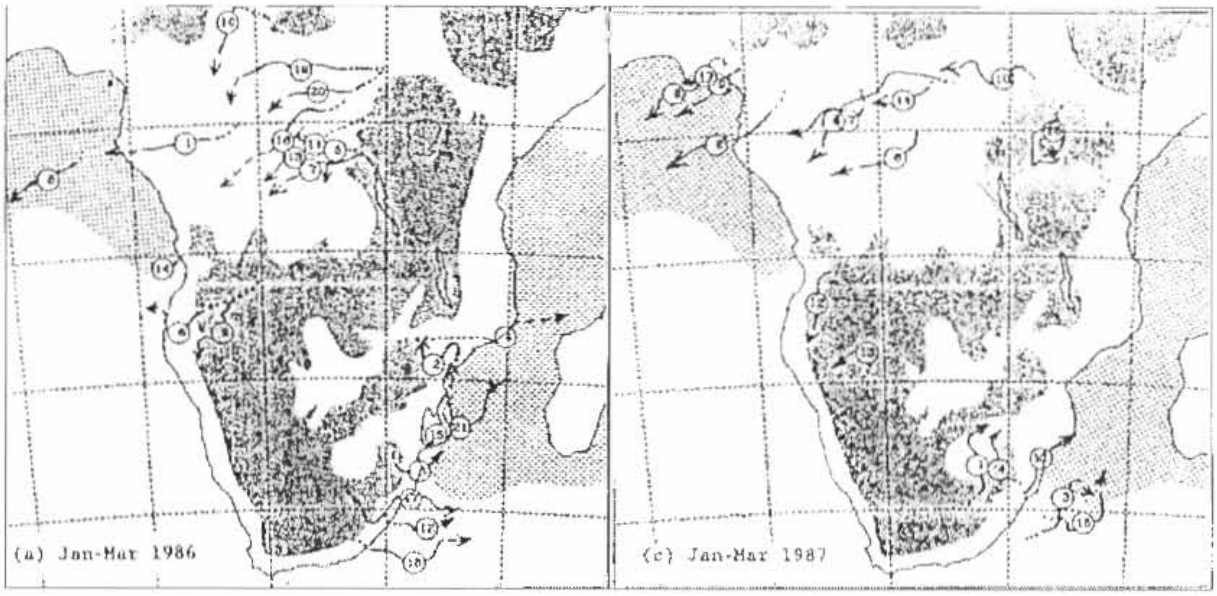

Figure 2.7: Tracks of MCCs during January-March 1986 (left) and January-March 1987 (right) over Africa (from Laing and Fritsch, 1993b).

Other possible modes of propagation include waves generated by the MCS itself, such as waves generated within the convection region as discussed previously. These waves then propagate out of the system and may initiate new convective cells (e.g. Schmidt and Cotton, 1990; Mapes, 1993). Also, waves generated outside of the system may also contribute to the propagation of the system, such as Kelvin waves interacting with convection in the Intertropical Convergence Zone (ITCZ) over West Africa (e.g. Mounier et al. 2005) or gravity waves driven by diurnal heating in the Andes, South America (Mapes et al. 2003).

2.7. MCS and Precipitation

In convective storms, precipitation is usually classified into two types, stratiform or convective. The type of precipitation is mainly controlled by vertical air motions, static stability, horizontal kinematics and shear of the horizontal winds in the vertical (FMH, 2005). At any given time, the type of precipitation is usually determined by the dominant mechanism which is causing the vertical motion. Most MCSs contain both stratiform and convective precipitation, but one of them usually dominates at a given stage of the life cycle. Cotton (2000) suggests that within MCSs, 60% of the precipitation is from the convective region, while the other 40% occurs in the stratiform region. These systems also appear to have a distinct precipitation pattern, where the heaviest precipitation occurs within the first half of the storm's life cycle (Kane et al. 1987; Jirak et al. 2003). McAnelly and Cotton (1986) found that the maximum hourly rain rate occurs early in the intense growth rate, followed by a steady decrease, while the resultant rain volume reaches a maximum 1-2 hours prior to the maximum infrared area. The system is then transformed into a larger precipitating system of increasingly lighter and more stratiform anvil rainfall, which gradually decreases in size as it decays.

Regions of convective cells are usually distributed in two ways, which mainly depend on the type of MCS. They are either embedded within a large area of developing stratiform (e.g. cloud clusters or MCC) or they could be restricted along the system's leading edge (e.g. squall line). These cells are related to the low level cold pool, convergence, both low level and deep layer wind flow and shear, and the underlying topography (FMH, 2005). To distinguish between areas of convective and stratiform precipitation, radar reflectivities less than 40 dBZ are classified as stratiform precipitation, while greater than 40 dBZ are regarded as convective precipitation areas (e.g. Geerts, 1998; Parker and Johnson, 2000; Jarik et al. 2003). The convective regions are made up of intense vertical cores of updrafts and downdrafts coinciding with heavy precipitation, whereas the stratiform region, which is larger, contains the lighter precipitation. The stratiform region is believed to be a product of the dissipation of older convective cells and partly by broader-sloping mesoscale ascent (Houze et al. 1990; Houze, 1997; Parker and Johnson, 2000). Large local precipitation

totals often occur when deep convective cells are organized in such a way that they move repeatedly over a given area (Doswell et al. 1996).

The organizational modes of MCS are generally based upon this distribution of stratiform precipitation in relation to the convection region (Parker and Johnson, 2000). Using satellite imagery and radar data, these authors classify the linear modes of MCS into three categories: trailing stratiform, leading stratiform and parallel stratiform MCSs. The organization of the MCS is believed to play a role in flash flooding, especially in cases where a trailing stratiform precipitation region occurs (Doswell et al. 1996). Looking at the structure of extreme rain producing MCSs, Schumacher and Johnson (2005) found that there was great variability in the radar-indicated structures of these systems. Factors that appear to have an influence on the distribution of precipitation and determining stratiform region shapes include the flow during the formation of the system as well as the storm relative winds (Cotton, 2000; Parker and Johnson, 2000). Thus in terms of forecasting such events, the speed and direction of the environmental mid- and upper-level winds relative to the storm's motion need to be taken into consideration. The use of radar has allowed researches to investigate the internal structure of MCSs, in order to identify the distribution of convective cells with the stratiform precipitation (e.g. Bluestein and Jain, 1985; McAnelly and Cotton, 1989; Houze et al. 1990; Parker and Johnson 2000).

It has also been suggested that in some regions, such as the United States, MCSs play an important role in the warm season precipitation (Fritsch et al. 1986; Kane et al. 1987; Ashley et al. 2003). There has been fair amount of research placed on these systems with most of it focused on the forecasting of such phenomenon due to the potential damage they may cause through extreme weather phenomena, such as flash floods, hail, lightning and even tornadoes. Most flash-flooding events in the U.S. appear to be associated with MCSs (Doswell et al. 1996). This finding is supported by more recent research by Schumacher and Johnson (2005) who found that out of 116 extreme rainfall events in the US, 65% were linked to MCSs. These systems are even more of a threat when a group or series of them develop. A group of Mesoscale Convective Weather Systems (MCWSs) is only defined as a "series" if the respective precipitation patterns of two or more MCWS coincide by more than 20% and if each subsequent event begins 12h or less following dissipation of the previous event

(Fritsch et al. 1986). These authors claim that a series MCWSs are very likely to be the most prolific precipitation produces in the U.S., rivalling or even sometimes exceeding that of a hurricane.

2.8. Research Questions and Motivation

This chapter has made an attempt to identify some of the key features associated with MCSs and the environment in which they develop. It is apparent that there has not been much research based on the systems found in Southern Africa. The gap in the literature on MCSs in this region needs to be addressed and even the little work that has been done needs updating. The vast majority of the literature also appears to be based on systems found in the Northern Hemisphere.

There still remains a lot of uncertainty in selecting the best methods for monitoring and forecasting MCSs. It is due to the size of these systems and the influence they have on the surrounding environment that a weather network with a large spatial coverage is required to monitor such events. The development of satellite technology since the late 1970's has played an influential role in identify and monitoring these events. In terms of forecasting MCSs, most of the modern methods involve the use of numerical models, which still have their shortcomings. Some of the well known problems associated with numerical modelling will be discussed in more detail in chapter seven. This highlights the fact that more research using these types of models is required.

For this thesis, a single case study of a mesoscale convective system that took place over the northern parts of KZN is presented and analyzed. The main aim of this thesis is to provide a better understanding of the evolution of the system as well as the associated severe precipitation. Through the use of a numerical mesoscale model, sensitivity tests are also conducted in order to identify the role local features played in the development and evolution of the system.

Possible questions that this thesis aims to address include:

- How well does the current South African weather network detect the MCS?

- What factors resulted in the development of the system and the associated heavy precipitation?
- What role did local features, such as topography and SSTs, play in the evolution of the system and the heavy precipitation production?
- What is the sensitivity of the model to initial and boundary conditions?
- What are the implications for forecasting such events in South Africa?

It must be stressed that this thesis is not aimed at identifying and researching the entire South African MCS population, but investigates a single event. The end goal is to produce a better understanding of the evolution of this particular event and the associated heavy rainfall by using a numerical mesoscale model. This may provide some idea as to how successful the MM5 model may be in simulating and potentially forecasting such events in the near future, which will have an impact on mitigating the damage that these storms create.

Chapter 3

Data and Methodology

3.1. Introduction

This thesis may be broken into two sections, with the first covering the types of data used to provide the observations for this particular event and the second being the use of models to help in identifying processes important in the formation and development of the convective event. This chapter provides an introduction to the data that was used, as well as why and how it was applied to this research. An introduction of the models that are utilized is also provided, as well as the setup.

3.2 Station Data

This research incorporates station data obtained from the South African Weather Service (SAWS; www.weathersa.co.za). The stations where the data are taken from are located throughout the KwaZulu-Natal province, as well as two of the surrounding provinces (Free State and Mpumalanga). The type of data that is utilised for this research includes rainfall, wind speed and direction, temperature, pressure, relative humidity and radiosonde data. Most of this data is available at hourly intervals, but this is restricted to certain stations located through out the province. Upper air soundings for Durban were also obtained from the University of Wyoming (http://weather.uwyo.edu/) sounding archive.

This station data are then used in two ways, with the first being able to provide a better understanding of the environment in which the MCS developed and secondly to validate the model output. Due to station data not being obtainable from Mozambique, global daily merged precipitation data, supplied by the Global Precipitation Climatology Project (GPCP; Huffman et al. 2001), are used to see the full extent of the precipitation. This daily one degree precipitation data are created by the Laboratory for Atmospheres at the NASA Goddard Space Flight Center.

3.3 Radar and Satellite

3.3.1 Radar

Two main instruments have been used to study MCS, the first being satellites and the second being radar. Nowadays, these instruments are used simultaneously in order to gain a better understanding of the different weather systems. The original identification and definition of MCSs was (and still is) based on IR satellite images, such as the MCCs by Maddox (1980). Each method has there own benefits (see table 3.1), which is why some studies have incorporated both satellite and radar (e.g. Bluestein and Jain, 1985; McAnelly and Cotton, 1986; Leary and Rapport, 1987; Jirak et al. 2003 and many others).

Satellite	**Radar**
Cloud-top temperatures	Type of precipitation (e.g. stratiform, convective, etc)
Size	Meso-β-scale convective features
Shape (eccentricity)	Interaction of convective clusters
Duration	Arrangement of convective cells
Movement	Movement

Table 3.1: A summary of what the satellite and radar instruments can be used for.

Jirak et al. 2003, suggest that satellites are good identifying the different MCSs, but they do not provide much information on the underlying convection and internal precipitation, which is why radar should also be used for a more detailed study. Considering that it is possibly due to the meso-β-scale convective features which determine some of the characteristics of the MCS systems (size, duration, precipitation; McAnelly and Cotton, 1986; Houze, 2004), it can be understood why the knowledge of the internal structure of an MCS is important, and hence the use of radar is needed.

Radar can also be used to help determine the two different precipitation types during the life cycle of the MCS, as well as the location of the convective cells in relation to the stratiform precipitation. As discussed in the previous chapter, it is this distribution of convective and stratiform precipitation that has also been used to classify the

different linear types of MCSs (e.g. Parker and Johnson, 2000). Through the use of both satellite images and radar, Leary and Rapport (1987) showed that the locations of intense cells corresponded to the highest (coldest) cloud tops in the satellite imagery.

The radar images used in this research, which are produced using TITAN, are supplied by the SAWS. The Thunderstorm Identification, Tracking, Analysis and Nowcasting (TITAN) project, which began in 1982, was initially used to objectively identify and analyze thunderstorms with the focus being on evaluating cloud-seeding activities aimed at rain enhancement in South Africa (Dixon, 2005). This program has expanded over the years and now supports a range of activities and no longer just the storm-specific applications. For information regarding the TITAN project the reader is directed towards the TITAN website (www.titan.com).

3.3.2 Satellite

For this case study, images supplied from EUMETSAT (www.eumetsat.int) are used to study this event. Meteosat Second Generation (MSG) is the new generation of European geostationary meteorological satellites, which provides continuous observation of the earth's full disk. It is equipped with the Spinning Enhanced Visible and Infrared Imager (SEVIRI) imaging radiometer (see Schmetz et al. 2002). This instrument is a 12-channel imager used for observing the earth–atmosphere system. Eleven of the channels observe the earth's full disk and the other channel, the high resolution visible (HRV) channel, only covers half of the full disk in the east–west direction and a full disk in the north–south direction. These 12 channels cover a large spectral range, from visible to infrared, and are known as either 'warm' or 'solar' channels (VIS0.6, VIS0.8, NIR1.6, HRV) or 'cold' channels (IR3.9, IR6.2, IR7.3, IR8.7, IR9.7, IR10.8, IR12.0, IR13.4). Eleven of the channels have a sampling distance of three kilometres at nadir and are able to scan the full disk of the earth (3,712 x 3,712 pixels), while the HRV channel produces images with one kilometre sampling at nadir. Due to the satellite being geostationary it can perform frequent imaging over the same area, which will allow detection of changes in the atmosphere. The imaging-repeating cycle of MSG is 15 minutes and the images contain 10 bits per pixel.

The raw data which is produced by the SEVIRI instrument is then pre-processed at EUMETSAT headquarters in Darmstadt (Germany), where it is then transformed into image data which is ready to be used, with calibration and geo-location information appended. Some other meteorological data, such as wind, cloud analysis, atmospheric humidity and atmospheric instability, is also computed at EUMETSAT and is then made available to users within 15 minutes after image reception. Level 1.5 image data is the result of the processing of the satellite raw data (Level 1.0 data) and is probably one of the main products of the MSG system. The name 'Level 1.5' refers to image data that has been corrected for all unwanted radiometric and geometric effects, has been geolocated using a standardised projection, and has been calibrated and radiance linearised (Fowler, 2006). This data is then placed into an appropriate computer program/s to extract or compute the required images.

For a more detailed description of how MSG works and what other data products available it is suggested that the reader visits the EUMETSAT website (www.eumetsat.int), as well as an article by Schmetz et al. (2002) and documentation by Fowler, 2006.

3.4 Re-analysis and Analysis Data

Atmospheric circulation patterns during the event are examined using two different datasets. Both these datasets have been used before to analyze atmospheric circulation patterns during heavy rainfall events over Southern Africa (e.g. Rouault et al. 2002; Singleton and Reason, 2006, 2007).

3.4.1. NCEP re-analysis data

The first is the NCEP-NCAR re-analysis data (Kalnay et al. 1996), which are available at a 2.5° horizontal resolution. This global data, which contains a temporal resolution of six hours is available at all standard pressure levels from 1000 to 10 hPa. It should be noted that there has been concern for possible errors found in the NCEP data in the Southern Hemisphere prior to 1979, which could be due to the lack of observations to validate the data (Kalnay et al. 1996; Tennant, 2004). The Southern Hemisphere is dominated by oceans, which makes validating the reanalysis data

difficult. However, the introduction of satellites in the late 1970's resulted in another source of data that could be utilized in the data assimilation and provide a more accurate representation of the atmosphere conditions.

3.4.2. The MRF Model

The second dataset utilized is that of the National Center for Environmental Prediction (NCEP) Medium Range Forecast (MRF) model, which has a horizontal resolution of 1° (Kanamitsu 1989; Kalnay et al. 1990; Kanamitsu et al. 1991). To initialise this global forecast model, data from the global observation network is used. The MRF model also has a temporal resolution of six hours and the data are available at all standard pressure levels through the atmosphere. This model was also used to provide data for the initial conditions for the mesoscale model. This is because of the higher spatial resolution of the data compared to the NCEP data.

3.5. The MM5 Model and Simulation setup

3.5.1. Model Configuration

The model used in this thesis is version 3 of the nonhydrostatic fifth generation mesoscale model (MM5; Dudhia 1993; Grell et al. 1994) from the Pennsylvania State University – National Center for Atmospheric Research (PSU/NCAR). This model has been used to research MCS in nearly all parts of the world, ranging from the U.S., Africa, Europe to parts of Asia (e.g. Tucker and Crook, 1999; Chen et al. 2000; Romero et al. 2000; Xu et al. 2001; and many others). However, this particular model has not extensively been applied to extreme weather events in the Southern Hemisphere.

The MM5 model employs a terrain following σ-coordinate system (i.e. lower levels follow the terrain, while the upper surface is flat), where σ_p is defined by:

$$\sigma_p = (p_0(Z) - p_t) / (p_0(Z_s) - p_t)$$

Where P_0 is a reference pressure that depends only on the height above sea level, P_t is the pressure at the top of the model and Z_s is the height of the earth's surface. In this

case a total of 23 σ-levels are utilized, starting from the surface up to 100 hPa. Most model setups usually have the vertical grid spacing stretched so that there is a finer resolution within the PBL. The lowest level in the model is represented with a value of $\sigma = 1$, while the top of the model is defined as $\sigma = 0$. Pielke (2002) suggests that the idea of defining a coordinate surface coincident with the bottom topography allows for a more efficient use in computer resources, as well as simplifying the application of lower boundary conditions.

3.5.2. Initial and Boundary Conditions

When modelling these systems, it must be kept in mind that there may be more than one convective forcing mechanism, which all operate on different spatial scales, such as a front compared to variations in local topography. Therefore the resolution in the model must be able to capture the large scale features, the smaller scale forcing mechanisms as well as the processes within the convective event. This is why nesting is so valuable in modelling because one can use the coarse grid to capture the synoptic scale features, such as fronts and troughs, while nesting allows for the explicit representation of the convective processes. For this particular simulation (hereafter referred to as the control simulation) two domains were incorporated with two way nesting. The nesting ratio utilized is the standard 3:1 for two-way interaction in the MM5 model. The coarse domain, with a 18km resolution, contains 271 x 370 grid points centred at 20°S, 30°E (figure 3.1). The fine domain, with a horizontal resolution of 6km, consists of 112 x 148 grid points. The input used for the nest comes via its boundaries with coarse domain, while input from the nest to the coarse mesh comes from the nest interior.

Topography was taken from the U.S. geological Survey (USGS) 5-minute resolution dataset for the coarse domain (figure 3.2), while the fine domain used the 2-minute resolution USGS data. These data are available to download along with the rest of the MM5 programs. To highlight the differences between the topography between the two domains used in the control simulation, an east-west vertical cross-section along 29°S is produced. It can be seen in figure 3.3 that there are slight differences in the representation of the topography between the two domains, most noticeably at the highest points. The graphs appear to be similar, but it should be noted the number of

horizontal grid points along the x-axis used to create each graph, whereby the domain two graph uses about three times as many grid points compared to the domain one.

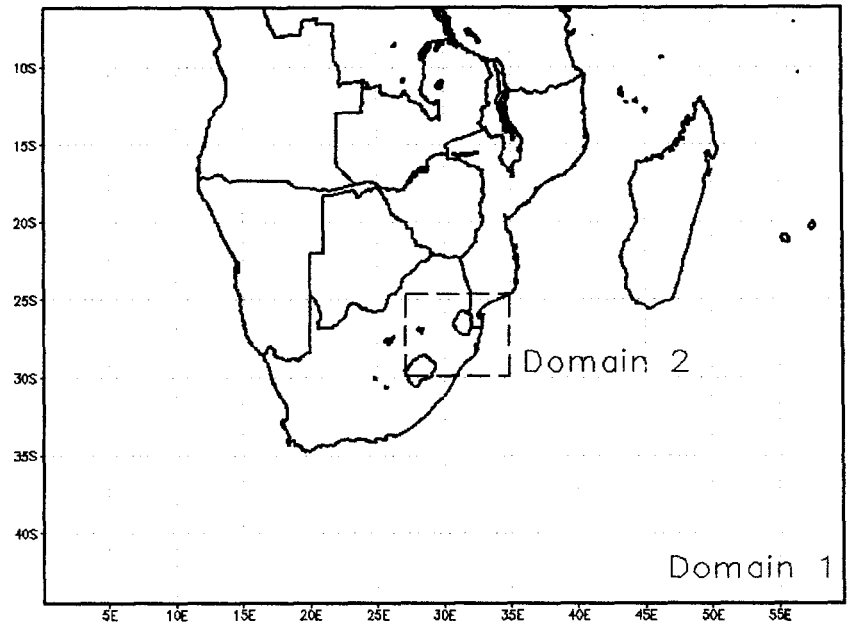

Figure 3.1: The two domains used for model simulations of the event.

The model has the option of three sets of source land-use/vegetation categorizations, where each grid cell of the model is assigned the chosen category, and this then determines surface properties such as albedo, roughness length, longwave emissivity, heat capacity and moisture availability. For the control simulation the 10 min (~19km) resolution global vegetation dataset is used.

To construct the initial and boundary conditions for the model, 1°x 1° resolution data from the MRF model was horizontally interpolated onto the MM5 grid and then vertically integrated to the model σ-levels. The sea surface temperature (SST) used is taken from the weekly average version 2 of the NOAA Optimum Interpolation SST (OISST; Reynolds et al. 2002), which has a resolution of 1°x 1° and is made available from the Climate Diagnostic Center (CDC). These boundary conditions from the MRF model were imposed every six hours for the outer grid, while for the nested grid, boundary conditions were applied from the mother grid at each time step with two-way nesting applied to ensure that output from the higher resolution grids are fed back into the mother grid. The forecast length of the model is 4320 minutes (72 hours)

beginning on the 10 February 2005, while the model produced output every 60 minutes.

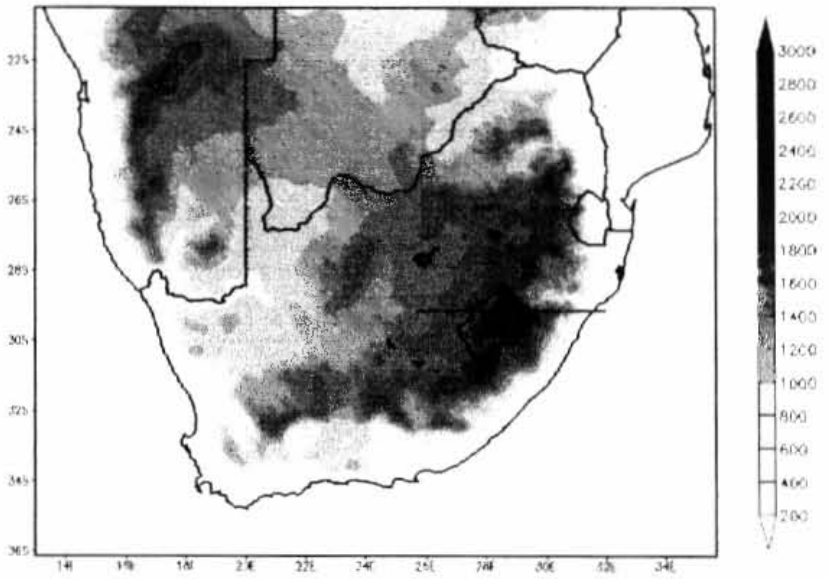

Figure 3.2: The topographic setting (starting at 1000m at an interval of 200m) of Southern Africa. Image created using the U.S. geological Survey (USGS) 5-minute resolution dataset.

3.5.3. The physics options

As previously discussed, there has been so much attention given to the different parameterizations of sub-gridscale processes that are incorporated within the model simulations and forecasts. Presently, there is still a fair amount of debate and uncertainty surrounding it, where the main focus is based on which parameterization works better than others. However, saying this, it does appear that some parameterization options do produce superior results when compared to the others, but selecting the best is very subjective. Ultimately, it should just be taken into consideration that the parameterizations used will not be able to represent all the complex atmospheric processes, of which some of the laws governing these processes are still not fully understood. Thus, results may differ slightly when using the different physics options and the process of trial and error is probably the best way to obtain the best results.

There are many options available in MM5 for the physical parameterizations. For this particular study, the planetary boundary layer physics were parameterized using the

MRF scheme (Hong and pan, 1996). The surface temperature and moisture over land were calculated using the five-layer soil model (Dudhia, 1996). Cloud cover is taken into account when calculating surface fluxes, as well as atmospheric temperature tendencies caused by longwave and shortwave radiation components.

MM5, like most models, uses a hybrid precipitation approach, whereby it uses both an explicit moisture scheme and a cumulus parameterization scheme. The explicit scheme is used to simulate resolved-scale precipitation, while the cumulus parameterization is used for the sub-grid precipitation. For this thesis, an explicit precipitation scheme is used on the 6 km grid, while the Grell cumulus scheme (Grell et al. 1994) is used on the coarse domain for the control run. This was done to prevent conflict between explicitly resolved convection and the parameterisation scheme in the nested domain. The Resiner explicit microphysics parameterization (Reisner et al. 1998) is used to represent the resolvable-scale cloud and precipitation processes. In this scheme, five prognostic equations are used for water vapor, cloud water, rainwater, cloud ice, and snow for the resolvable-scale motion. It includes the effects of evaporation, condensation, hydrostatic water loading, melting, freezing, deposition, sublimation and supercooled liquid water.

3.5.4. Backward Trajectories

In order to obtain a better idea of the moisture transport into the region during the storm initiation and life cycle, backward trajectories are computed. These trajectories were calculated by using the Hybrid Single Particle Lagrangian Integrated Trajectory model (HYSPLIT4), which was developed by the Atmosphere Resources Laboratory (ARL) at NOAA (Draxler and Taylor, 1982). To compute the trajectories, gridded fields of meteorological variables are required at regular temporal intervals, and in this case the model uses the MM5 simulated meteorological fields as input. For a complete description of all the equations and model calculation methods for trajectories and air concentrations, the reader is directed to the article by Draxler and Hess (1997).

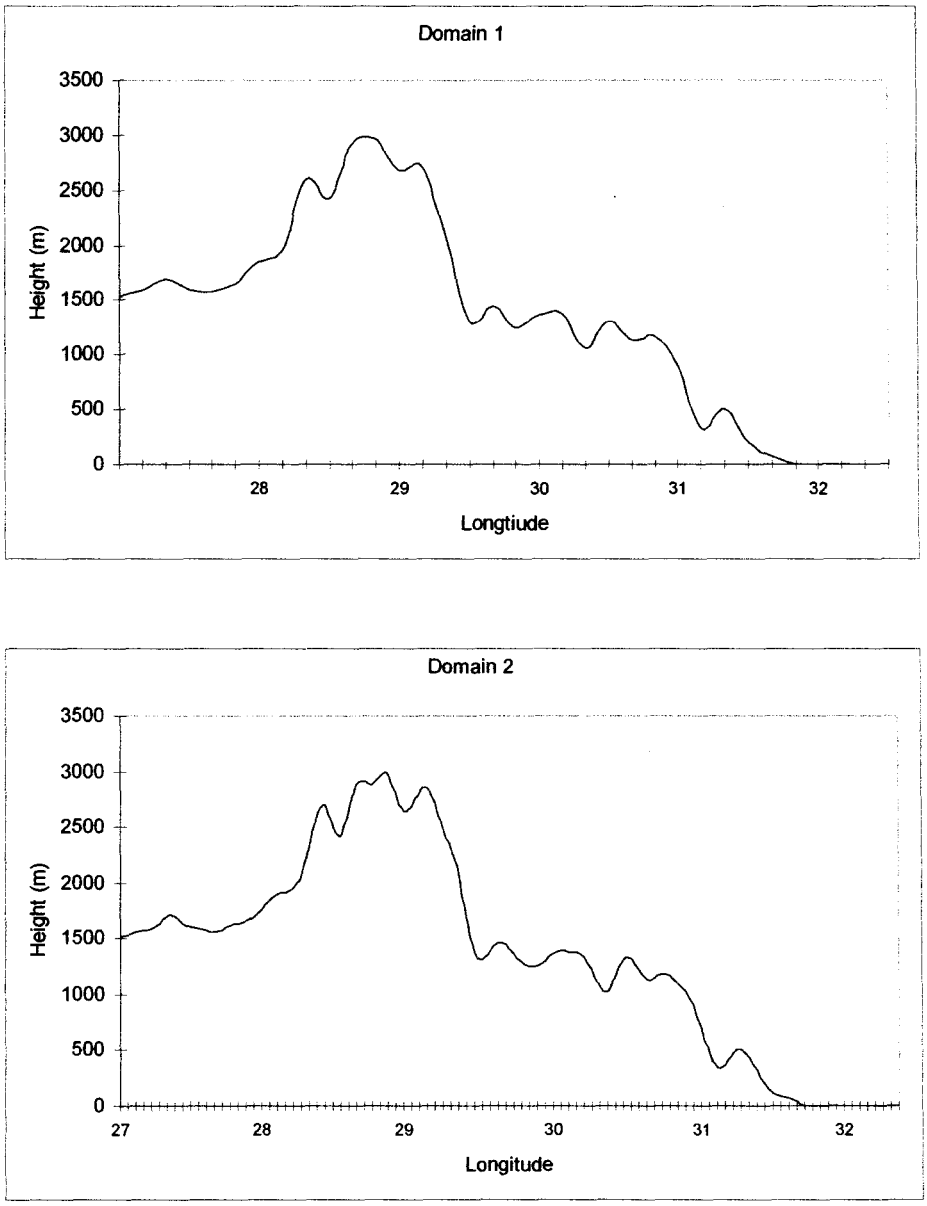

Figure 3.3: Vertical cross-sections (from line in figure 3.2) showing the differences in terrain between the two domains, with the top being domain one and the bottom being domain two.

3.5.5. MM5 Sensitivity Tests

In order to determine the role in which certain features, such as topography or SST, played in the development and life cycle had of the event, a sensitivity study is preformed. The setup of each experimental run was exactly the same as discussed above, but certain changes were made to each individual run. For this thesis it appears certain features, namely the SST of the surrounding ocean, the topography of the

escarpment and synoptic features in the mid-latitudes, played a role in the evolution of the system.

3.5.5.1. Sea Surface Temperatures

Previous research has shown that surface fluxes of sensible and latent heat from the Agulhas Current may play a crucial role in the development of heavy rainfall systems in South Africa (e.g. Rouault et al. 2002; Singleton and Reason 2006, 2007). It has been shown that these surface fluxes appear to be underestimated in certain reanalysis datasets (Rouault et al. 2003). Rouault et al. (2000) noted that the core of the Agulhas Current was likely to transfer 5 times as much water vapour to the atmosphere as the surrounding water. This suggests that the initial conditions placed in a mesoscale model need to resolve the core of the Agulhas Current and the strong SST gradients in order to provide a more realistic representation of the surface fluxes.

The SST data used in the control run contained a horizontal resolution of 1°, which may be too low to resolve the core of the Agulhas Current as well as the steep SST gradients. Thus, higher resolution SST data are required so that these key features may be resolved. In this case, the higher resolution 18 km weekly interpolated multi-channel SST (MCSST) dataset, which is produced by the National Oceanography Office (NAVOCEANO; http://poet.jpl.nasa.gov/), was used. Due to its weekly temporal resolution, the data was kept constant throughout the simulation. This data is taken from the Advanced Very High Resolution Radiometer (AVHRR) sensor aboard the NOAA-14 and NOAA-16 polar orbiting satellites (Stowe et al. 1991). The AVHRR sensor has five channels that operate in the visible to thermal infrared portion of the spectrum, whereby two of the channels collects visible wavelength data and the other three gather information in the infrared wavelengths. It has been in operation since 1981, but for the MCSST data it is only available from 2001 till present. SST anomalies are also created using this data by comparing it to the Reynolds optimally interpolated SST climatology data (Reynolds and Smith, 1994; Reynolds et al. 2002).

3.5.5.2. Topography

To highlight the role of topography in the initiation and life cycle of the event, a run is performed whereby the topography is reduced by 75%. As shown in figure 3.2, the eastern parts of South Africa contain regions of high topography, where it extends up to 3000m in certain places. Mountains may aid in producing heavy rainfall through orographic uplift of potentially unstable air or they may assist in developing long-lived, stationary low-level convergence zones that provide a source for new convection to develop (Spencer and Stensrud, 1998). Therefore, topography may have a large influence on the simulation of a mesoscale convective event.

Katzfey (1995) used a hydrostatic mesoscale model to simulate three extreme precipitation events that occurred over the South Island of New Zealand and found that orography had a strong influence on the amount of precipitation. This author found that the simulated precipitation was improved when the orography was more realistic and the horizontal resolution increased. Tucker and Crook (1999) used the MM5 numerical model to examine a MCS, with the main focus being that of the initiation process and associated influences as well as the dependence on model resolution. Two different model runs were compared, one at 3 km resolution and the other at 6.67 km resolution. The biggest difference between the two runs was that the higher resolution topography had higher surface elevations. Although the lower resolution model was able to simulate the initiation of the MCS because it was able to produce the mountain convection from which it evolved, it had difficulty simulating the eastward propagation of the convective line. However, other areas of mountain convection were not well represented by the lower resolution model, indicating that a higher resolution model was needed to represent all the mountain convective activity.

The western Mediterranean is another region where numerical simulations have been used to identify the influence of topography on flash floods events attributed to MCSs (Romero et al. 1998 and Romero et al. 2000). The role of topography has also been identified as playing an important role in extreme precipitation events in other parts of the world (e.g. Buzzi and Foschini, 2000; Chen et al. 2005). Topography is also known to have an influence on features associated with MCSs, such as the LLJ (e.g. Pan et al. 2004). Bernardet et al. (2000) suggest that the sensitivity of the convective

systems to the topography is directly associated with the thermal and wind distribution caused by the topography.

The role that topography plays in extreme precipitating events in South Africa has been identified in numerous studies. Laing and Fritsch, (1993b) found that the eastern escarpment plays an important role in the development of MCCs in the region, which is common initiating mechanism for these types of systems around the world (Laing and Fritsch, 1997). The local coastal topography is also known to play a major role in promoting the ascent of moist air as well as blocking the propagation of systems, such as cut-off lows (e.g. Singleton and Reason, 2007). Thus, a sensitivity test is performed to identify the role the eastern escarpment played in this particular convective event as well as how the coastal topography may have influenced the development of heavy precipitation.

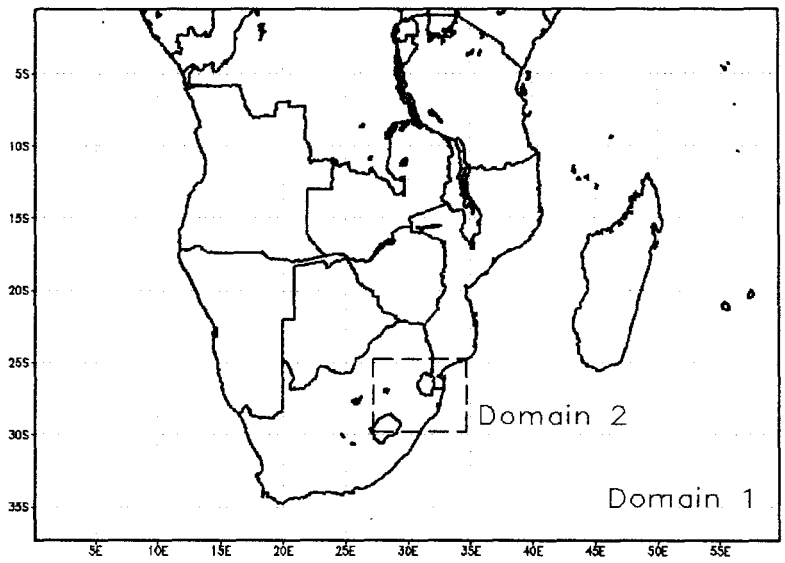

Figure 3.4: The position of the two domains used in the mid-latitude sensitivity test.

3.5.5.3. Mid-latitudes

Large-scale mid-latitude weather systems, such as extratropical cyclones and associated fronts, anticyclones and waves, found propagating eastwards south of South Africa are known to have an influence on weather patterns within the country (Tyson and Preston-Whyte, 2000). Other westerly disturbances, such as cut-off lows may also influence weather events over South Africa (Singleton and Reason, 2006,

2007). Thus, a further simulation was conducted whereby the 18 km domain was positioned further equatorward compared to that of the control simulation, such that the southern location of the domain was situated at 37°S (see figure 3.4), with all else being equal. This was done to highlight the importance of these synoptic features found in the mid-latitudes and also to possibly identify what influence they may have had in this particular case study.

Chapter 4

The Case Study

4.1. The Event

The selected case study for this research involves a mid-latitude mesoscale convective system that initiated over the high topography of the Drakensberg Mountain range along the eastern escarpment in the early afternoon on the 11 February 2005. This particular system is of interest due to the large amounts of rainfall it produced, particularly along the north coast of KwaZulu-Natal (KZN; figure 4.1). Some rain gauges along the northern coastline recorded over 100mm during the night/morning of the 11/12th, with the maximum being 119mm recorded at Uloa Agricultural Office. Swaziland, bordering the South African provinces of KZN and Mpumalanga, also received heavy rainfall during the event, since a few stations recorded over 50mm, with the maximum being 101mm at Mananga station.

Most of the rainfall that fell along the northern coast occurred during the night time hours, which is illustrated by figure 4.2. It must be taken into consideration that rainfall data was not obtained for Mozambique, which may have resulted in a different rainfall distribution had this data been available. Rainfall images, supplied by GPCP, show the full areal extent of the precipitation produced by the system (figure 4.3). However, this rainfall dataset is provided at a 1° horizontal resolution, which may result in the full intensity of the precipitation not being captured at a particular location.

It is apparent that this single event had a large influence on the February rainfall for the region, leading to some regions having above average rainfall for the month (figure 4.4). Using monthly rainfall data over the last 25 years, one calculates that average February rainfall at Cape St Lucia and Richards Bay is 156.9 and 157.7 mm, respectively (figure 4.5a). During the event (11/12th February 2005), these two stations recorded 111.0 and 99.6 mm, respectively. This data shows the impact that this single event had in accounting for about two thirds of the average February

rainfall at both stations. Not only did this event have an impact on the February rainfall, but also on that for the core summer rainy season (December-February; figure 4.5b). Research in an Australian case has shown that if a region experiences anomalously wet conditions during a season, then the resulting excess moisture may aid in the development of a MCS (e.g. Perrin and Reason, 2000). However, for the current case it appears that the northern parts of KZN experienced below average rainfall for January, the month before the event (figure 4.3), which further shows the impact this event had on the DJF rainfall period.

4.2. The Synoptic and Local Settings

4.2.1. Synoptic Settings

The synoptic charts (figure A4.1 in appendix) and MRF model output (figures 4.6, 4.7 and 4.8) reveal that during the event, a ridge of high pressure south of the country, a frontal system south-east of the country and a surface trough over the interior of the country were prominent synoptic features. At the 500 hPa level, a weak westerly wave passed over the southern parts of the country during 11 February (figure 4.7). These synoptic conditions are likely to have interacted to provide favourable conditions for the development of convective precipitating systems along the east coast.

On 10 February, a weak cold front system was located to the south of the country, with an anticyclone approaching from the west, and a trough was present over interior South Africa (figure A4.1a). Another anticyclone system was situated in the Southwest Indian Ocean, with another low pressure sitting between the country and this anticyclone. These synoptic conditions resulted in easterly and northeasterly winds at the surface along the KZN coastline. At the mid-levels, a weak westerly wave was situated to the southwest of the country.

By the 11th, the anticyclonic system from the South Atlantic began to ridge south of the country, while the weak cold front had propagated towards the east (figure A4.1b). A ridging anticyclone, which is a common occurrence during the summer rainfall season and has a peak in frequency during the months of October and February, is

known to produce widespread rainfall over the eastern parts of Southern Africa (Tyson and Preston-Whyte, 2000). These authors suggest that the widespread rainfall is usually as a result of a combination of events, such as weakening inland pressure gradients, the changing curvature of the flow, mesoscale orographic forcing and upper level divergence in the westerly wave.

This ridging high pressure south of the country was also associated with moderate onshore winds from the southwest Indian Ocean onto the east coast (figure 4.9). The Southwest Indian Ocean has also been known to fuel heavy rainfall events along the Eastern Cape (Crimp and Masson, 1999; Rouault et al. 2002). These low level winds supply moisture into the region due to them moving across the warm SST of the Agulhas Current (figure 4.10). Moisture flux images reveal that a large quantity of moisture was advected into the storm region at the 1000hPa level during the event (figure 4.11). These NCEP moisture flux values, which are calculated from specific humidity and wind data, indicate that the largest amount of moisture was advected into the region during the night of 11/12 February (between 140 and 180 g kg^{-1} ms^{-1} between 18h00 and 00h00 UTC 11 February; figure 4.11) and this may have resulted in the increase of rainfall at this time.

Moisture convergence at the lower levels was also a persistent feature during the life cycle of the event. It should be noted that for the purpose of this thesis, areas containing convergence are represented with positive values in the horizontal plots, while areas of divergence are represented with negative values, unless stated otherwise. The moisture convergence figures (figure 4.12) indicate that at 12h00 UTC February 11, there was considerable moisture convergence along the eastern escarpment, which then spread westwards and northwards during the afternoon. By 00h00 UTC, the most intense moisture convergence was located along the northern parts of KZN as well as the interior. The maximum values along the northern KZN region are consistent with an increase of rainfall in this region. During the late morning of the 12th, moisture divergence was then prominent over southern KZN.

A surface interior trough, in the easterly flow over inland South Africa, is also a favourable mechanism for the development of convective rainfall. This semi-stationary heat low is often associated with low-level convergence and upper level

divergence to the east of the surface trough, leading to rainfall over eastern South Africa (Tyson and Preston-Whyte, 2000). Plots of upper level divergence (figure 4.13) reveal that large sections of northern KZN and northeastern South Africa were dominated by divergence during the 11th and morning of the 12th. At 12h00 UTC on the 11th (not shown), there did not appear to be any strong divergence in the region where the storm initiated and by 18h00 UTC a large portion of KZN was dominated by convergence, which is during the development of the convective event. During the period when most rainfall occurred, upper level divergence was dominant.

Previous research has suggested that frontal systems to the south east of the country may also influence the development of this type of convective system. For example, Garstang et al. (1987) found that the generation of convective storms over the escarpment of the northeast South African region are associated with westerly waves propagating across the southern tip of Africa, which then interact with the topography of the escarpment. However, in this case, the front was rather weak and did not extend too far inland.

Southwesterly winds at mid-levels (500 hPa), associated with the westerly wave passing over the southern part of the country, only reached the KZN province early in the afternoon on February 11th (figure 4.7). These winds then weakened as the wave propagated out towards the Indian Ocean during the early morning hours on the 12th. Divergence in the mid-levels showed slightly different results to the pattern found in the upper levels. Over KZN, it was apparent that the mid-levels were dominated with convergence during the time the storm initiated (not shown). Mid-level convergence was also present along the north coast during the night, while by the morning of the 12th mid-level divergence dominated.

At upper levels (200 hPa), winds speeds greater than 10 m.s^{-1} were experienced over parts of KZN and offshore to the southeast and the east of the coast (figure 4.8). During the day, these winds fluctuated back and forth from westerly and southwesterly directions, but for a brief period during the night the winds then veered to become northwesterlies before returning to westerlies. In the MCS formation environment, upper level jets (ULJ) are also prominent features, with the systems usually developing near the right exit zones (in the Northern Hemisphere) of the ULJ

(e.g. Maddox, 1983; Cotton et al. 1989). This situation results from the regions of upper air divergence and convergence developing due to the effects of both curvature of the streamlines and confluence and diffluence within the jet stream (Tyson and Preston-Whyte, 2000). These authors note that over South Africa, the right front exit side (poleward side) of the jet is associated with divergence, while the left front side (equatorward side) is associated with convergence. This pattern of upper air convergence and divergence may provide enhanced conditions of convection on the poleward side of the jet and unfavourable conditions on the equatorward side. As shown in figure 4.13, there was upper level divergence over the northern parts of KZN during the later stages of the convective event, during the period of most rainfall. However, the early stages of the event were not dominated by divergence and by 18h00 UTC on February 11, most parts of KZN contained upper level convergence.

The MCS began to decay during the morning of 12 February, when the synoptic conditions no longer provided suitable conditions to sustain convection. The ridging high pressure system shifted further eastwards, resulting in the wind patterns changing. As a result, there was also less fuel for the system, which was evident by the decrease in the amount of moisture feeding the system (figure 4.11). By mid-afternoon on the 12th, the strong upper level winds were situated to the north of KZN and to the interior and were south-westerly in direction. The changes in the wind field at lower levels also resulted in moisture convergence in the region being replaced by moisture divergence (figure 4.12). The interior trough had also weakened, which is evident by the pressure increasing from 1004 hPa to 1008 hPa. By this time, the weak westerly wave in the mid-levels had also propagated eastwards towards the Indian Ocean. As a result, unfavourable conditions for convection now exited leading to the decay of the system.

4.2.2. Radiosonde Data

Radiosonde data are not actively collected in many parts of Southern Africa and are only routinely available for some South African stations. The closest radiosonde station to this event is Durban, approximately 300 km to the east of where the storm initiated and about 250 km south of Richards Bay. From this data, we can then

determine some of the basic severe weather parameters used to evaluate the stability of the atmosphere (see appendix B). These parameters are then compared with the categories defined by NOAA's National Weather Service (hereafter referred to as NWS; www.crh.noaa.gov/).

The 09h00 UTC 11 February Durban sounding (figure 4.14a) indicates that the atmosphere at the time was conducive to the development of convective systems. This was evident by the conditionally unstable atmosphere that contained large amounts of convective available potential energy (CAPE) with a value of 2896J/Kg and a very high precipitable water (PW) content of approximately 48 mm. The lifted index (LI), which is generally used as a stability measure, contained a value of -6.55°C and illustrates the favourable conditions for storm development. A LI value less than -6°C is usually accepted as being a very unstable environment (NWS). Another method used to evaluate the threat of severe weather is that of the severe weather threat index or SWEAT. An atmosphere with a SWEAT value of over 300 is usually identified as having the potential to produce severe thunderstorms (NWS). On the 11th, the Durban sounding only contained a SWEAT value of 234, which suggests that the potential of severe thunderstorms was not too high. The total totals index (TT), which accounts for both the static stability and 850mb moisture, contained a value of approximately 49 °C. This value is slightly less than the value the NWS use, which ranges from 50-55°C, in order to determine the possible development of severe thunderstorms. However, these categories have been developed for the U.S. and may not be appropriate for the generally more stable South African atmosphere.

The sounding also revealed that near-surface conditions were hot and humid, while above this layer, the atmosphere was cooler and close to saturation between the 950 and the 800 hPa levels. Another feature was the presence of a low level inversion (approximately at the 750 hPa level). This pattern of warm, moist air overlain by cool, drier air is conducive to the development of convective events. In terms of wind patterns, the sounding indicated that the winds veered with height, surface winds were southeasterly, and southwesterly/westerly at mid-levels due to the ridging anticyclone and mid-level westerly wave to the south. No evidence of a LLJ existed however.

The 00h00 UTC 12 February Durban sounding (figure 4.14b) had different results to the 09h00 UTC sounding, but still showed that the atmosphere was conducive to the development of convection. Noticeable changes in this sounding from the previous one include the large drop in CAPE (82 J/kg), a decrease in the TT (45°C) and a decrease in the LI (-1.34°C) whereas there were increases in the SWEAT index (364) and an increase in the precipitable water content (51.29 mm). A very weak nocturnal inversion existed, while the atmosphere between the 850-500 hPa layer was nearly saturated. This sounding also reveals the difference in wind conditions throughout the atmosphere. Winds were now south-southeasterlies at the lower levels (southwesterly at lowest level), but stronger westerlies at mid-levels and still veering with height. There also appears to be some evidence of a LLJ present, which may be identified by the wind speeds greater than 25 knots at the 800-900 hPa level.

The type of convective storm (i.e. single cell, multicell or supercell) that develops is strongly dependent on the vertical wind shear in the storm's environment (Wiseman and Klemp, 1982, 1986). Wiseman and Klemp (1982) found that different shear strengths in the lowest 6km of the atmosphere produced different storms types. In a numerical study, they found that the weak shear environments appeared to produce weaker short-lived single cell storms, low to moderate shear produces secondary development similar to observed multicells, while strong shear produce split storms which are similar to observed supercells. These authors also noted that the buoyancy in the region also plays an important role in the development of the type of storm. This relationship between the buoyancy and wind shear in the lowest 6km is represented in the form of the bulk Richardson number (BRN; see appendix B).

From the 09h00 UTC sounding, the bulk Richardson number (BRCH on the sounding) had a value of 301.5, which indicates the possibility that unsteady, multicellular growth may occur (Weisman and Klemp, 1982, 1986). By the 00h00 UTC sounding, this value had dropped to 35.15, which is still greater than the minimum value (30) required for multicelluar storm development (Weisman and Klemp, 1982). However, Weisman and Klemp (1986) suggest that it should be taken into consideration that the magnitude of BRN indicates what type of convection may occur in a given environment, but it does not necessarily indicate the severity of the convective system.

The use of severe weather parameters suggests that during the day of the 11 February 2005, the atmosphere was conducive to the development of thunderstorms. Some of these parameters even suggested that the development of severe thunderstorms was likely. However, it must be kept in mind that the Durban data was a few hundred kilometres from where the event initiated and reached the maximum extent, so caution must be taken when interpreting this radiosonde data.

4.2.3. Station Data

It is evident from the mesoscale surface charts (appendix figure A4.2) that SAWS stations spread across KZN recorded relatively high surface temperatures (28-32°C) and dew point temperatures (15-24 °C) during the afternoon of the 11 February 2005. As a result, strong diurnal surface heating as well as the topography may have provided a trigger for the event. The SAWS stations also recorded high humidities, particularly along the north coast (mid to high 90%'s) during the afternoon of event.

These mesoscale charts also indicate that surface convergence took place inland during the afternoon on the 11th, which is inferred by the opposing surface winds. The onshore winds along the east coast are also obvious. From the SAWS weather station data, is was evident that the winds at Durban started off as northeasterlies during the morning of the 11 February before veering and becoming southeasterlies to southerlies for most of the afternoon and night. The winds at Richards Bay had a very similar pattern, starting off as northeasterlies during the morning of the 11th, but slowly started veering to southeasterlies during the night and then backed to northeasterlies early on the 12th. This wind pattern suggests that moisture from the surrounding ocean may have been transported into the region. During the afternoon of 11 February, the winds at Durban steadily increased from 2-3 m.s^{-1} to a maximum of around 9 m.s^{-1} in the evening, while at Richards Bay Airport the winds fluctuated between 2 and 4 m.s^{-1} and sharply increased to reach a maximum of approximately 8 m.s^{-1} around midnight. This station data is consistent with the MRF model output (figure 4.6) that showed there were no winds stronger than 10m.s^{-1} at the surface during the event. At both these stations, the wind then weakened during the morning on 12 February.

4.2.4. Topography, SSTs and LLJ

From the global research that has been conducted on these systems, it appears that topography plays a role in the formation of MCS, particularly MCCs, with the majority of the forming downwind of elevated terrain (figure 2.2; Laing and Fritsch, 1997). Formation of convective systems along mountains ranges are also known as "*orogenic*" systems. In South Africa, it is the Drakensberg Mountain range that plays a role in the initiation of these systems. Laing and Fritsch (1993b) found that most African systems developed downstream (relative to the midtropospheric flow) of mountain ranges. MCS (particularly MCC) genesis in southeastern Africa is found to take place east of the South African escarpment, which is downstream relative to the midtropospheric westerly flow (figure 2.7). This situation is partially similar to the one found in the subtropical/mid-latitude South American MCCs, where Velasco and Fritsch (1987) found that systems tended to be concentrated immediately downwind of the major mountain range (Andes) and embedded within the latitudinal belts of maximum mid-level westerlies. Past research has revealed that the South African escarpment serves as the initiating point for convection that propagates to the east and also occasionally produces severe local storms (e.g. Garstang et al. 1987). Not only does the topography contribute to the initiation of storms and increased precipitation, but it also alters other significant features associated with MCSs, such as the low level jet (e.g. Pan et al. 2004).

An interesting feature apparently missing for the KZN event considered here is that of a prominent low level jet (LLJ). figure 4.6 indicates that only small areas along the east coast contained low level wind speeds greater than $10 m.s^{-1}$. Even at the 850 hPa level (not shown), where friction is less, there does not appear to be any LLJ. The station and radiosonde data also showed that wind speeds in the region never exceeded 10 $m.s^{-1}$ in the lower levels. However, scatterometer surface winds derived from measurements from the QuikSCAT satellite winds (figure 4.15) suggest that during the event, winds impacting on the east coast did reach speeds greater than 10 $m.s^{-1}$. This difference in wind speeds found in the MRF model and that of QuikSCAT could possibly be due to the difference in the resolution of data and methods of obtaining the wind data.

As discussed in chapter two, LLJ are responsible for the inflow of high-θ_e air and have been found to be prominent features in the MCS environment. It was mentioned that systems that have been documented from around the world all appear to be associated with a LLJ and a nearby moisture source, such as a warm ocean. In South Africa, strong precipitation events have been associated with a LLJ bringing moisture from the Agulhas Current region (Rouault et al. 2002; Singleton and Reason, 2006 2007). However, the heavy precipitation events researched by these authors were different systems (cut-off lows) to that of an MCS and therefore can not be directly compared to this case study. It may also be that the 1° resolution of the MRF data that does not enable LLJ identification, although it was clearly present in the cut-off low cases at this resolution.

The LLJ is also believed to play an important role in determining the movement of the systems, but it was also previously discussed that there are many other factors that may play a role in their propagation. Research by Corfidi et al. (1996) suggests that the movement of these systems is generally a result of the mid-level flow as well as the low level jet. As shown in figure 2.7, most systems over southeastern Africa were found to move east or northeastwards towards the high equivalent potential temperature (high-θ_e) associated with warm waters along the southeastern African coastline (Laing and Fritsch, 1993b). Similar findings to that of Laing and Fritsch (1993b) appear to occur in this case study, where the system initially propagated in the direction of the mid-level flow, which was dominated by south-westerly winds (figure 4.7). At the same time, low-level winds originated from the east and later from the northeast, which is consistent with the propagation of the MCS. An interaction at these levels may explain the propagation of the system.

Sea surface temperatures (SST) along the east coast during the event were warmer than usual (figure 4.10). The winds over the ocean region continued to supply moisture into the system during the night time hours (figure 4.11), which may have resulted in the system strengthening and the long life cycle. During the late morning of the 12th, the winds weakened and moved further offshore. It is usually the case that when the LLJ weakens or no longer feeds the system that the convective system begins to decay (Maddox, 1983), as indeed occurred here.

4.3. Satellite Imagery

4.3.1. Development and Shape

In terms of MCS life cycles, the system studied here appeared to follow the global trend, as well as the pattern identified for Southern African systems by Laing and Fritsch (1993b). Initially, it developed as a few single cell storms along the Drakensberg Mountain range, which then merged and developed as a single cloud system (figures 4.16). The merging or interaction of individual storms into one big system is a common feature found in the development of these systems (Maddox et al. 1986). As the system grew in strength it propagated eastwards and then towards the northeast. From the satellite images, it appears that the system only obtained MCS status around 16h00-17h00 UTC on February 11 and lasted approximately ten hours, until it started to decay just before 03h00 UTC the next morning. The system appeared to reach maximum extent between 22h00-00h00 UTC on February 11. The long life cycle of this MCS may have been due to it being in close proximity to its moisture source.

Cloud top temperature data (figure A4.3) indicates that the system was dominated by convective elements (i.e. very cold cloud top temperatures) initially, while the latter stages of the life cycle more likely contained stratiform precipitation. As discussed in chapter two, this precipitation pattern is common in MCSs. The cloud top temperature contours used in figure A4.3 were selected due to them being used to identify certain types of MCS, such as the MCC (Maddox, 1980). This author classified an MCS as an MCC if it fulfilled certain criteria (see table 2.1), with one of these criteria being the size of the cold cloud shield. Two cold cloud shields were defined in the original definition, with the larger one being the -32°C shield and the smaller being the -52°C. The -72°C contour range was used to show areas of strong convection.

The visible channels and the IR channels show a clear initiation of the system beginning around 13h00 UTC on February 11 (not shown). High resolution visible images (HRV) may also be utilized during the day time and they provide a higher resolution picture of the event. From the HRV images it appears that the initiation was likely due to orographic effects, figure 4.17 indicates that the storm formation was near the Drakensberg Mountains. These HRV images also clearly show the individual

storms merging as time passes. It must be noted that due to errors in the satellite computer program, the continental and political boundaries in the image have shifted westward, therefore caution must be taken when analysing the image. Unfortunately, HRV images require sunlight in order to be of any use; therefore these images can not be used during the night time hours when the MCS developed into a mature system.

Another interesting observation for the event is the evolution of the shape of the system, which initially started out as a linear system, but later in the life cycle became more circular in appearance. As mentioned previously, the shape of the system is usually one of the methods applied to help determine the type of MCS. The linear systems are more commonly referred to as squall lines, while the quasi-circular systems are usually referred to as being MCCs. Some authors (e.g. Parker and Johnson, 2004a, b, c) have suggested that the squall line could possibly be described as a phase in the development of many MCS, which may possibly be the case here.

This shape could be characteristic of the quasi-linear MCSs symmetry structure during the life cycle. It was discussed in chapter two that the symmetry of quasi-linear systems may change during the latter stages of the life cycle. Thus, during the early stages in the life cycle the systems usually show a symmetric appearance, whereas in the later stages, are more asymmetric. This change results from vortices generated by upward tilting of the system-generated horizontal vorticity by the leading line convective updrafts and then later on, the Coriolis force. Most research on this characteristic has been documented for Northern Hemisphere systems, and it is usually the northern end (poleward end) that experiences the extra cloud mass and precipitation structure. This result suggests that, in the Southern Hemisphere, the bias would be towards the southern end. Currently, there appears to be no research done on the symmetry of systems found in the Southern Hemisphere. In the IR satellite images for this case study, it is evident that in the later stages of the life cycle, extra development took place on the southern end of the system during the night (see figure 4.16 f-i).

The system began to decay in the morning of February 12, since the synoptic conditions were no longer favourable for convection. Once the system began to dissipate, some form of anticyclonic circulation (from animations of the images)

became apparent in the remaining clouds (see figure 4.16 k-l). This rotation could refer to the mesoscale convective vortex (MCV; as discussed in chapter two) that is found in the decaying parts of an MCS. However, there does not appear to be any distinct circulation pattern in the NCEP reanalysis data and MRF model output, but these relatively lower resolution datasets may prevent finding this mesoscale feature.

4.4. Radar - Internal Structure

Research has shown that even though MCSs have a characteristic cloud shield, there is a complex case to case variability in its radar substructure (e.g. Leary and Rapport, 1987; McAnelly and Cotton 1986; Hilgendorf and Johnson, 1998; Jirak et al. 2003). As discussed in chapter two, the underlying precipitation structure is one method of determining the type of MCS. From the radar images produced by SAWS, it is evident that the system developed over the high topography along the eastern escarpment (figure 4.18). As the system developed, cells begun to merge and the system began to propagate to the east/northeast. These images show how the early stages of the life cycle were dominated by a few convective cells, while later in the life cycle, stratiform precipitation appeared to be more dominant. These radar images can be compared with the cloud top temperature images to show that the cold temperatures in the cloud are consistent with convective elements of the storm.

It must be noted that the Bloemfontein radar station was not in operation during the period, hence some of the initial development of the storm was not captured. Unfortunately, the SAWS radar network does not cover the north coast region of KZN, which is why there appears to be no radar reflectivity in the region during the event. Thus, for this particular case it appears that the radar system was only useful in capturing parts of the initiating phase as well as some of the early propagation and does not really assist in determining the internal structure of the system during the mature phase.

4.5. Summary

On the 11 February 2005, a mesoscale convective system developed along the east coast of South Africa. This particular system resulted in a large amount of

precipitation along the north coast of KZN, with most of this heavy precipitation occurring at night. Satellite and radar images were used to identify the location of the event as well as the different life cycle stages, starting with the initiation stage through to the dissipation stage. It appeared that the storm initiated as single cell storms over the high-lying topography of the eastern escarpment. These single cells then merged and strengthened during the night. As the system strengthened, it began to propagate in an easterly direction, towards the northern Agulhas Current region. The system decayed during the early morning hours of the 12 February and by midday there was little evidence in the cloud patterns that this event took place.

The data suggests that a ridging anticyclone, an interior trough and a westerly wave in the mid-levels, played a key role in the evolution of the convective system. It is also apparent that mesoscale features also had an influence on the development and life cycle of the system. Doswell et al. (1996) suggest that in order for deep convection to be produced, three criteria must be satisfied. These three criteria refer to the existence of low-level moisture, upward motion and a conditionally unstable environment. For this particular case study it has been shown that moisture influx and convergence occurred at low levels within parts of KZN. The soundings for Durban revealed that the atmosphere at the time was conditionally unstable and near saturated in the lower levels. This sounding suggests that that the possibility of deep convection was likely to occur. Strong diurnal surface heating as well as the high topography along the eastern escarpment may have provided a trigger for the event. Moderate onshore winds blowing over the warm Agulhas Current appeared to supply moisture into the region, which sustained the system through the night. Convergence in the lower levels and upper level divergence also resulted in favourable conditions for storm formation.

Changes in the synoptic pattern led to the decay of the system. These unfavourable conditions included the eastward propagation of the anticyclone, weakening of the interior trough as well as changes in the resulting winds. As a result, the inflow of low level moisture weakened and the patterns of convergence and divergence became unfavourable for convection. Changes at the mid-levels included the westerly wave propagating out into the Indian Ocean, which influenced the wind pattern and the convergence/ divergence pattern.

This chapter focused on some of the instruments and datasets required to provide the observations for an MCS that developed over the eastern parts of South Africa. From this, some of the favourable conditions that were required to initiate and develop this have been established. As suggested by Romero et al. (2000), in order for a MCS develop, the synoptic and mesoscale conditions must remain favourable for the development of such a system over a specific region and last for several hours, which appears to be the case here. However, in order to study this further, a numerical mesoscale model is used in the following chapters to provide a more thorough investigation of the event at a higher temporal and spatial resolution.

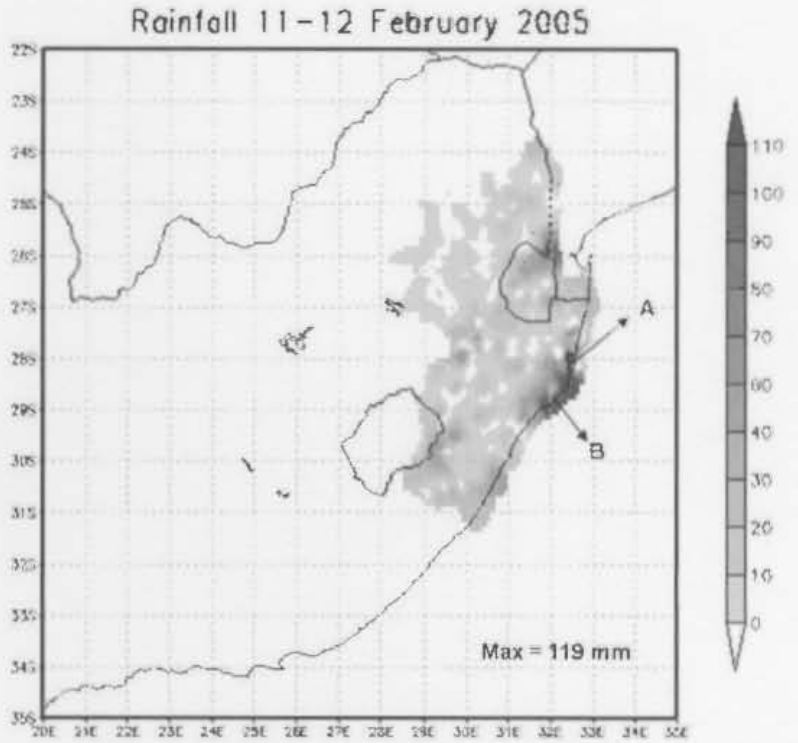

Figure 4.1: Accumulated precipitation (10 mm interval) from 334 stations across the eastern region of Southern Africa for the 11 - 12 February 2005.

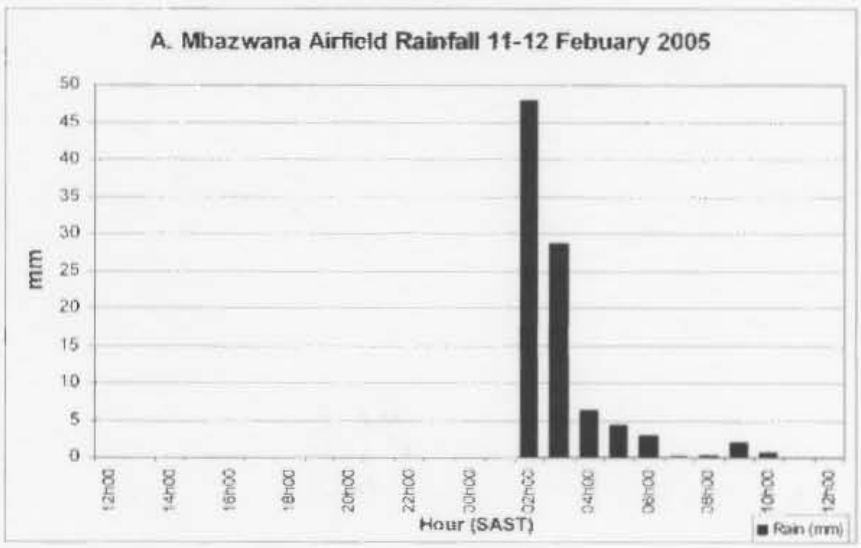

Figure 4.2: Graphs of hourly precipitation for stations at Mbazwana Airfield (top) and Richards Bay (next page). The location of these two stations is marked A and B on figure 4.1, respectively.

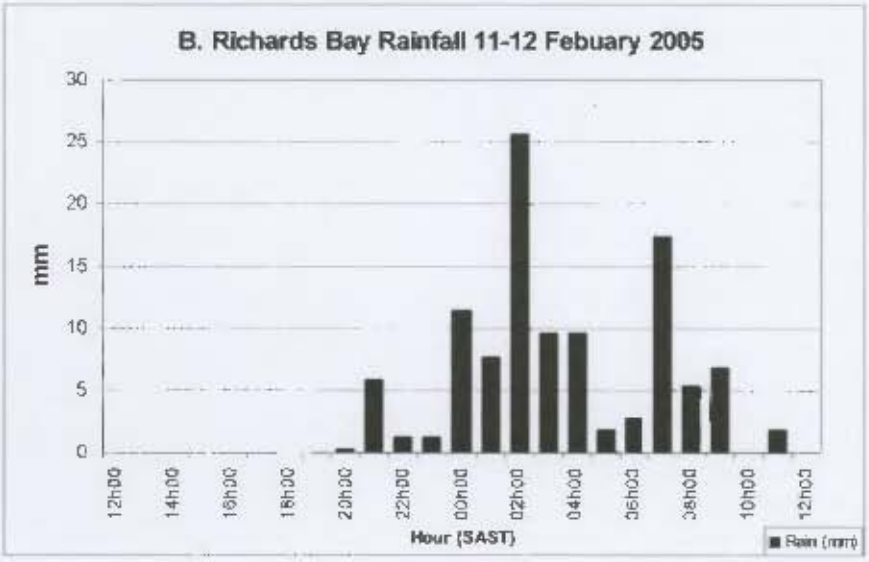

Figure 4.2 cont: Graph of hourly precipitation for the station at Richards Bay. The location of these two stations is marked B on figure 4.1.

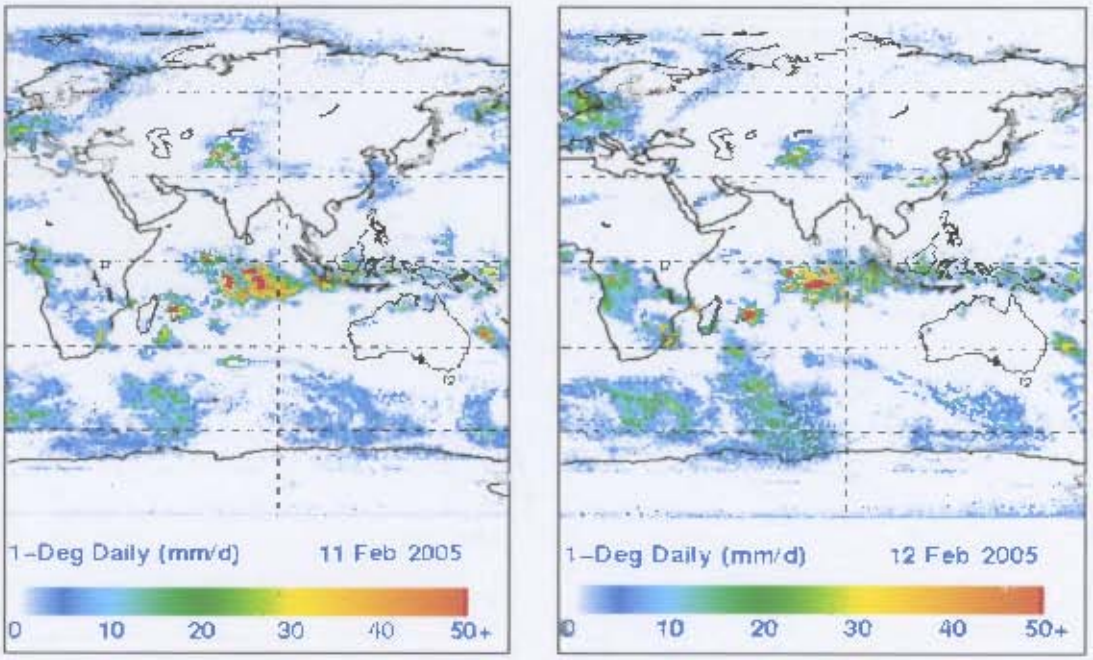

Figure 4.3: GPCP images showing the daily precipitation for parts of the globe (1 degree spatial resolution) on the 11th (left) and 12th (right).

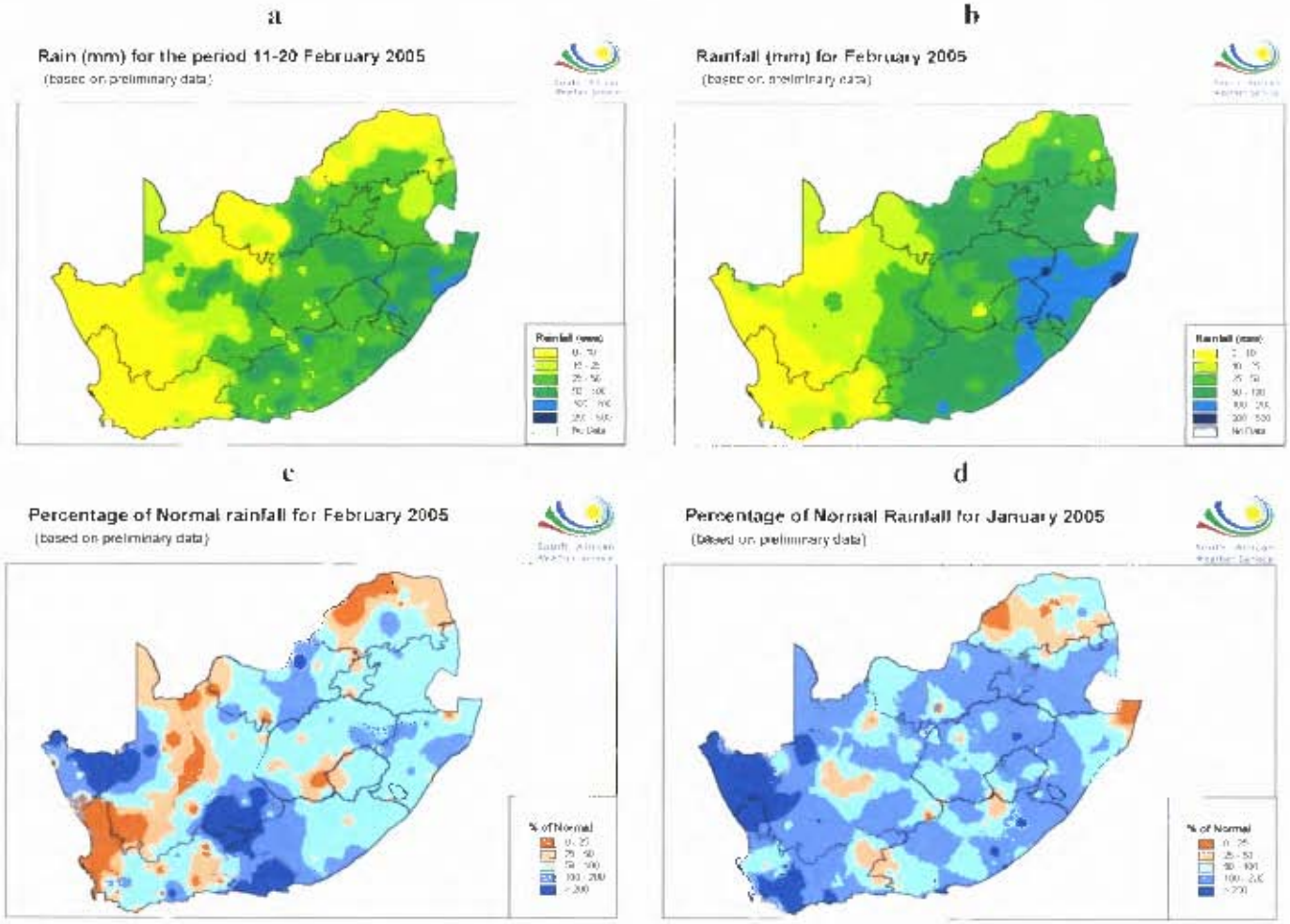

Figure 4.4: SAWS rainfall maps showing a) Recorded rainfall for the 11-20 February 2005. b) Rainfall for the month of February, c) percentage above normal rainfall for the month of February 2005 and d) percentage above normal rainfall for the month of January 2005 over South Africa.

a)

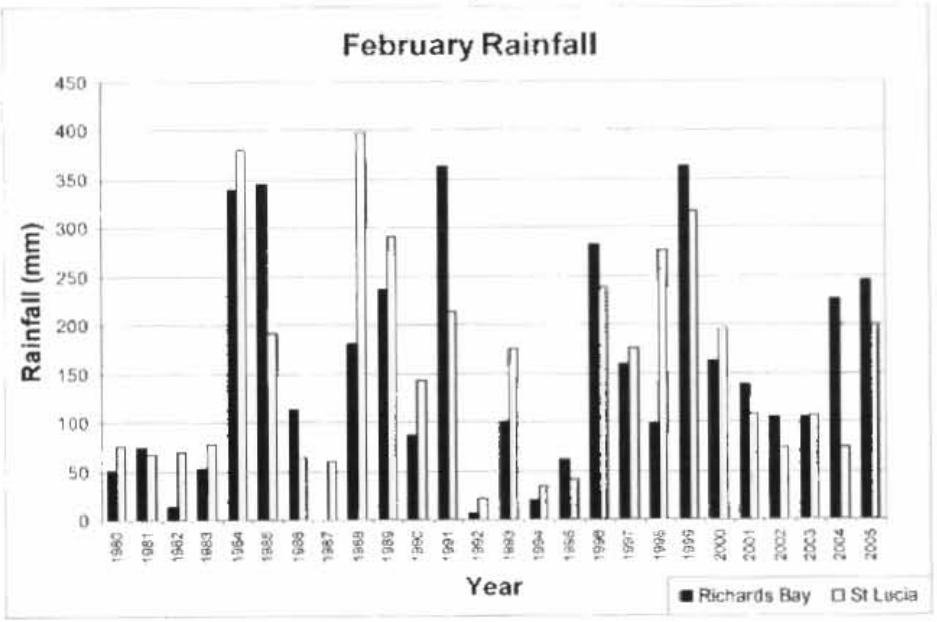

b)

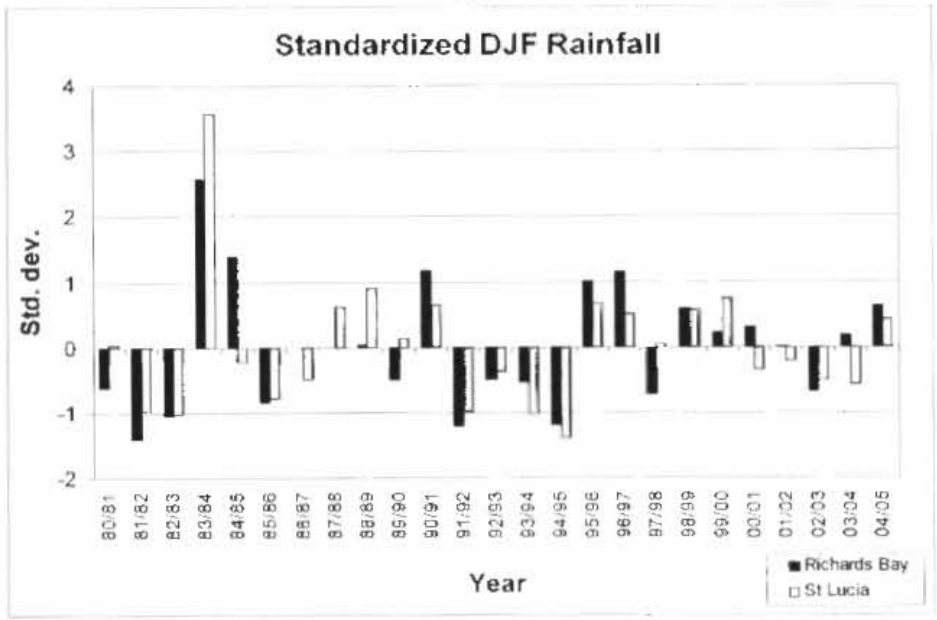

Figure 4.5: Graphs showing a) February rainfall and b) standardized December-February rainfall for Richards Bay and Cape St Lucia stations for the period 1980-2005.

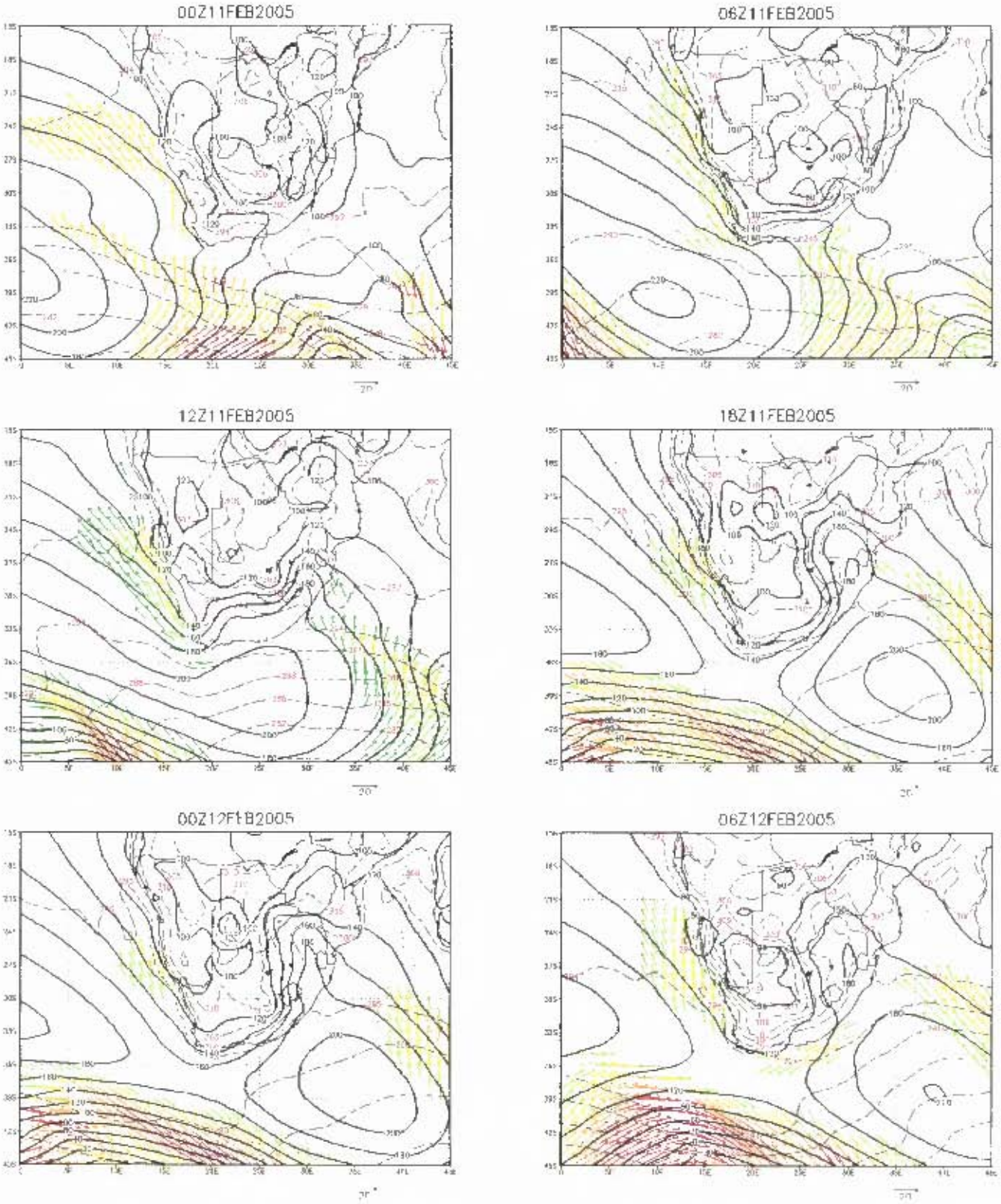

Figure 4.6: Temperature (dashed contours; interval 2 degrees k), geopotential height (think contours; interval 20m) and winds with speeds greater than 10 $m.s^{-1}$ (36 km/h) at the 1000 hPa level, derived from the MRF model. Starting at 00h00 UTC on the 11^{th} and ending at 06h00 UTC on the 12 February, at 6-hourly intervals.

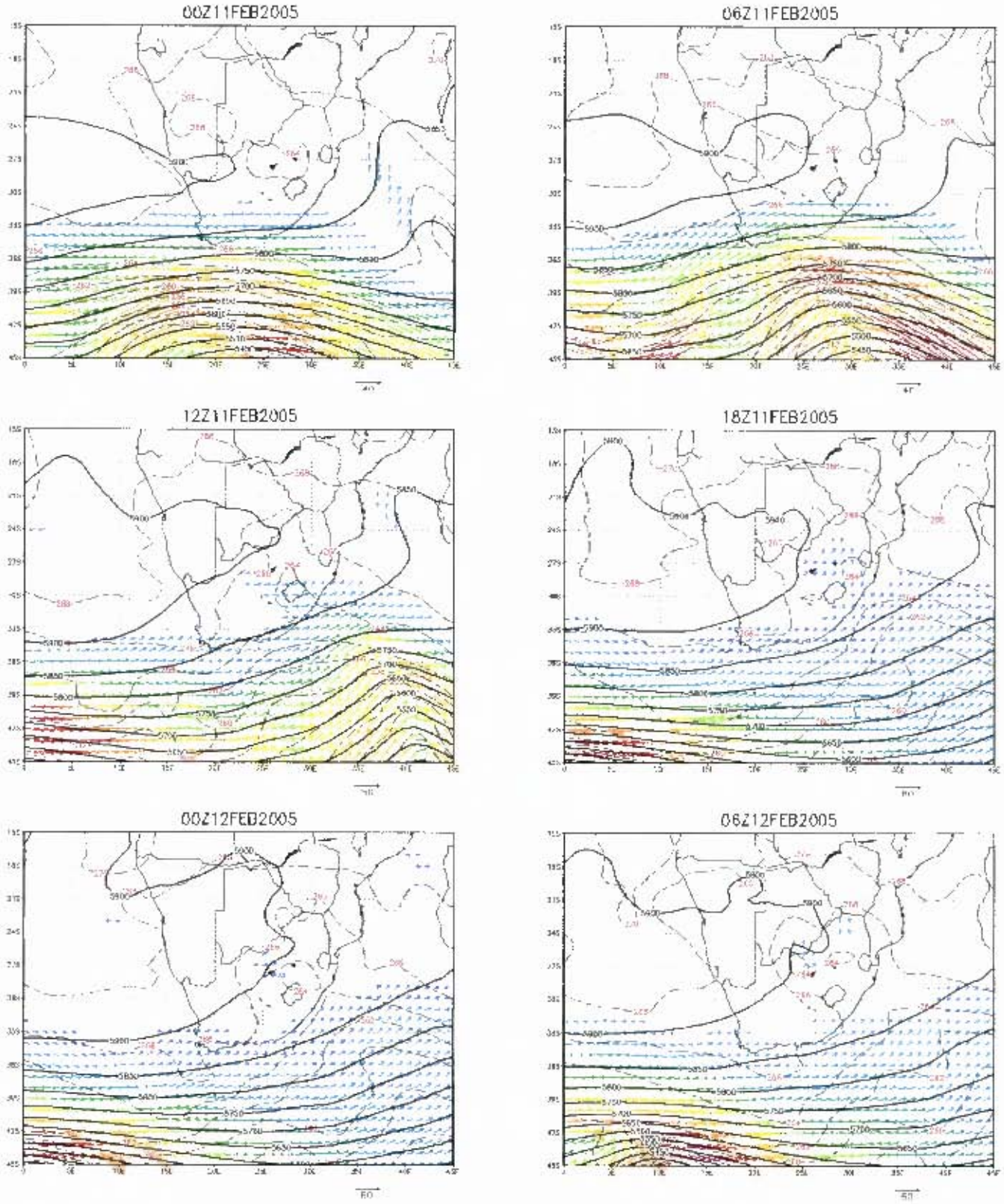

Figure 4.7: Same as figure 4.6, except at the 500 hPa level and that the contour interval for geopotential height is 50m.

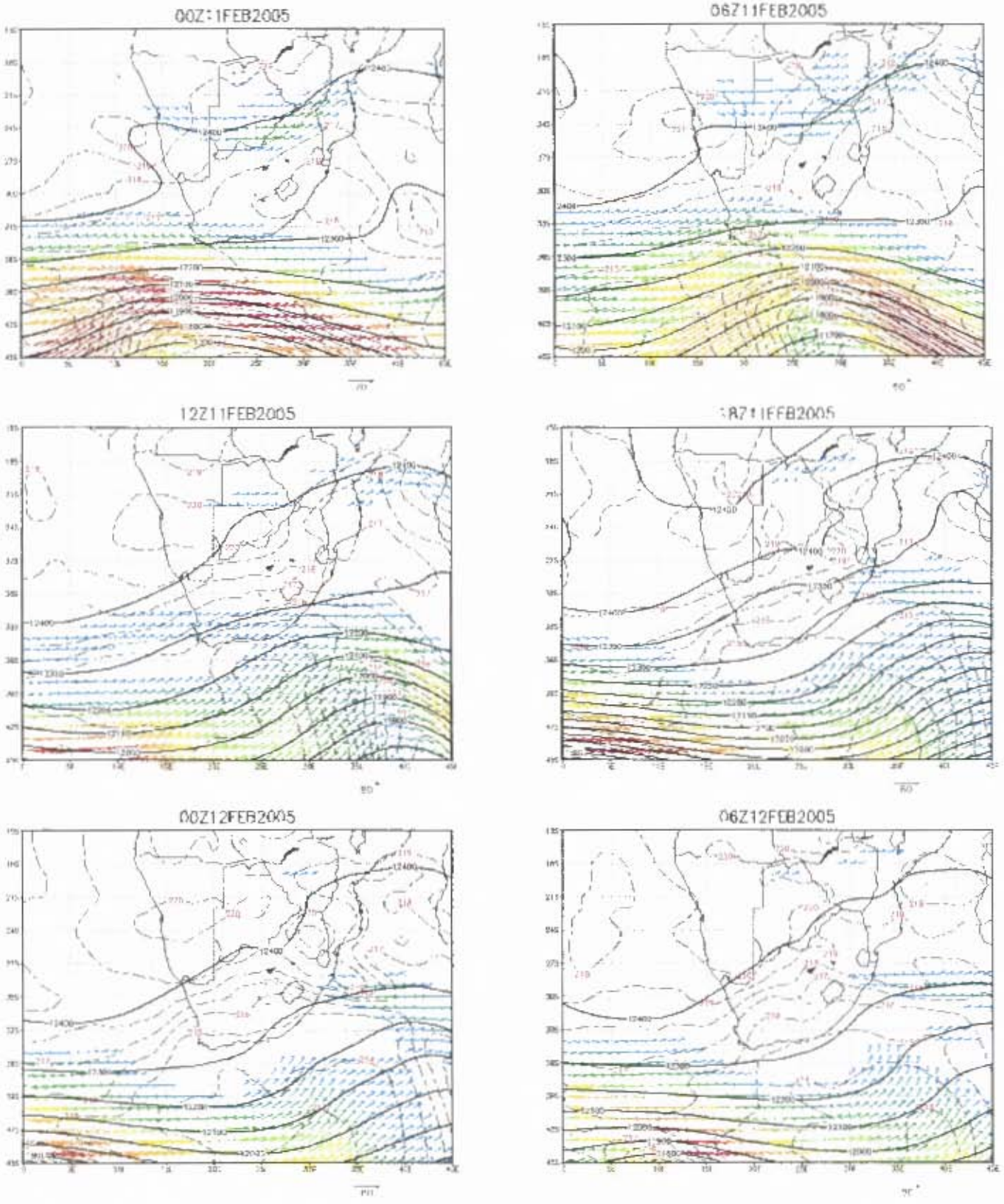

Figure 4.8: Same as figure 4.6, except at the 200 hPa level. Only wind speeds greater than 20 $m.s^{-1}$ are shown and that the contour interval for geopotential height is 100m.

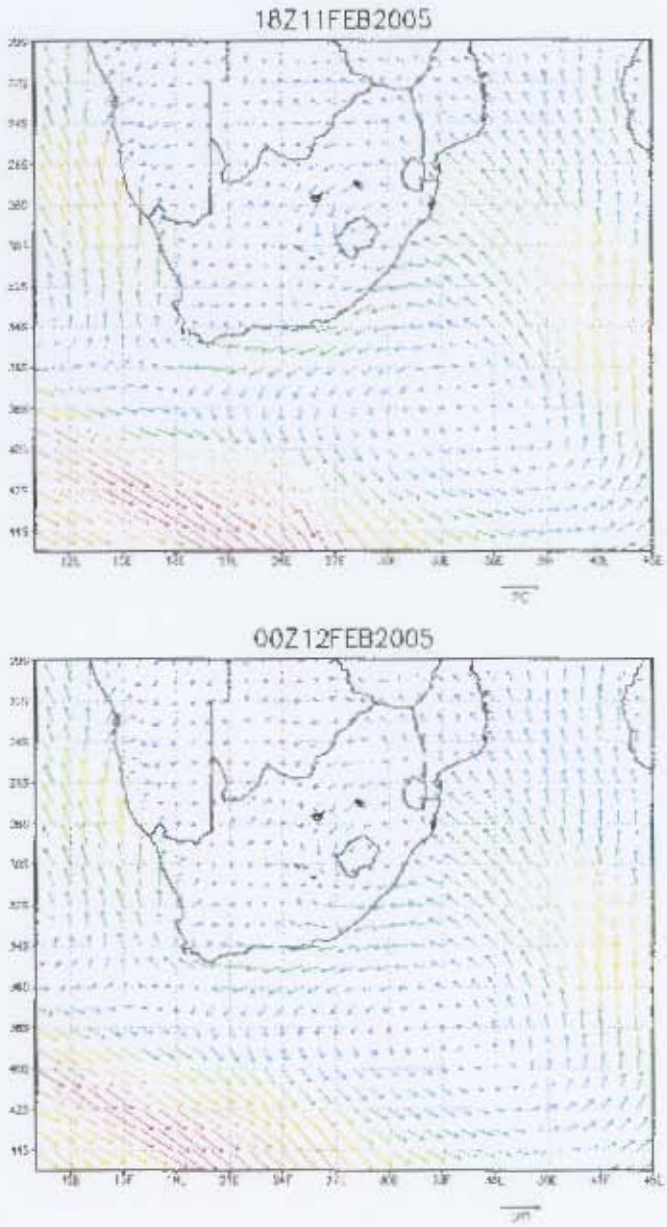

Figure 4.9: MRF winds at the 1000 hPa level, illustrating the moderate onshore winds at 18h00 UTC (top) and 00h00 UTC (bottom) along the east coast of South Africa as a result of the ridging high pressure system.

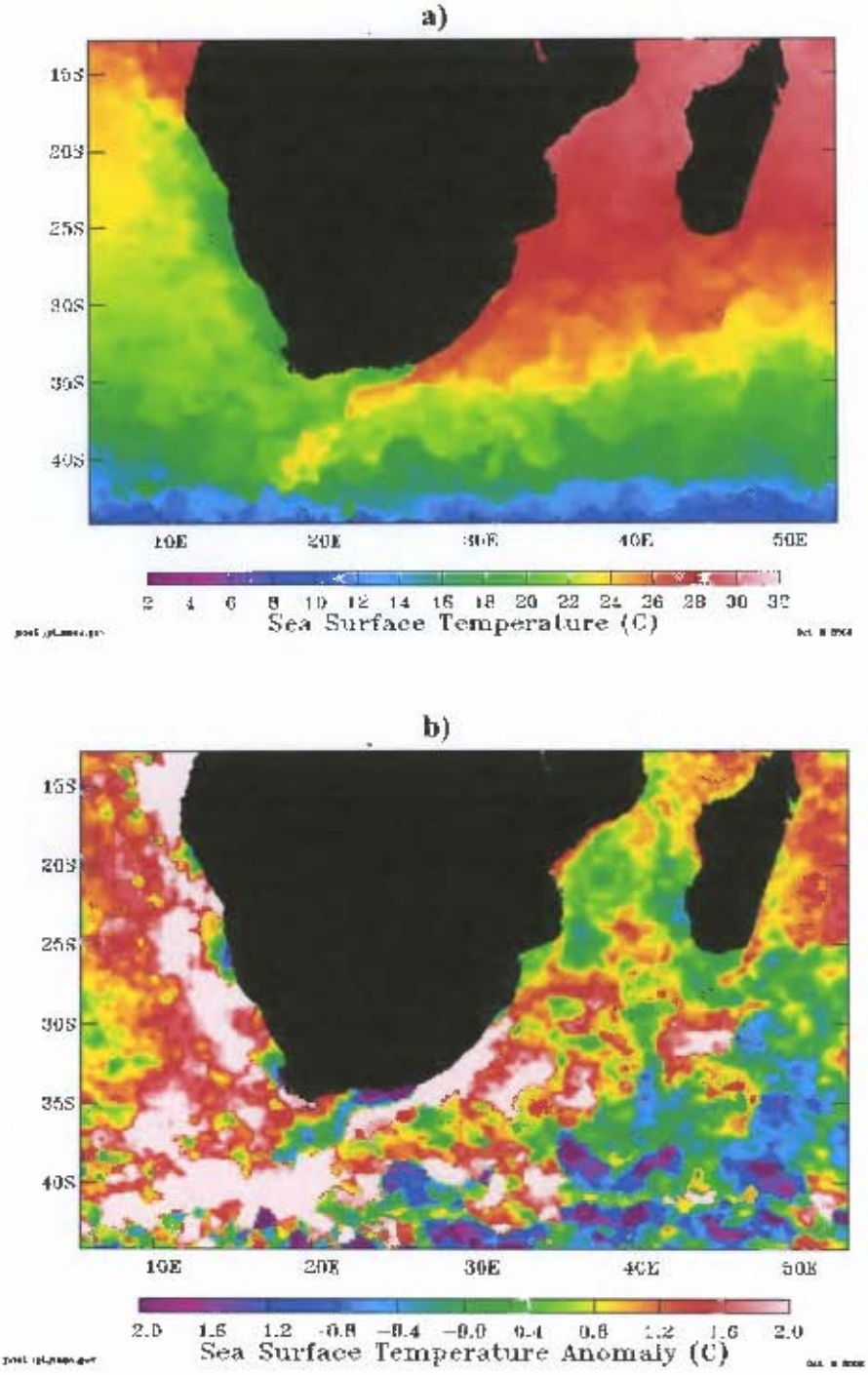

Figure 4.10: Sea surface temperatures during the week of the event (a), and SST anomalies of that week (b). These SSTs are derived from the NOAA (National Oceanic and Atmospheric Administration) Polar Orbiting Advanced Very High Resolution Radiometer (AVHRR).

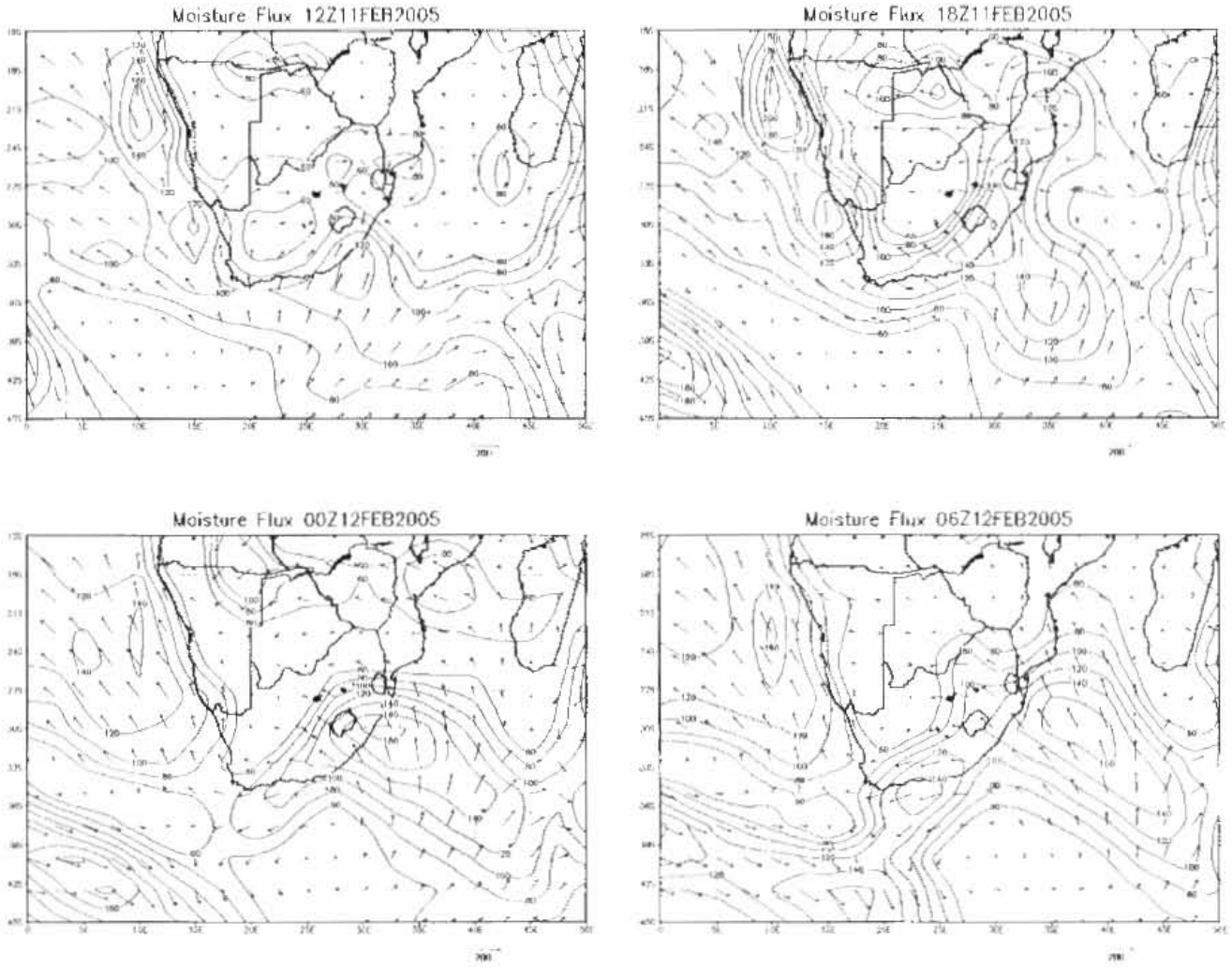

Figure 4.11: NCEP 6-hourly moisture flux values (interval 20 g. kg^{-1} $m.s^{-1}$) at the 1000 hPa level.

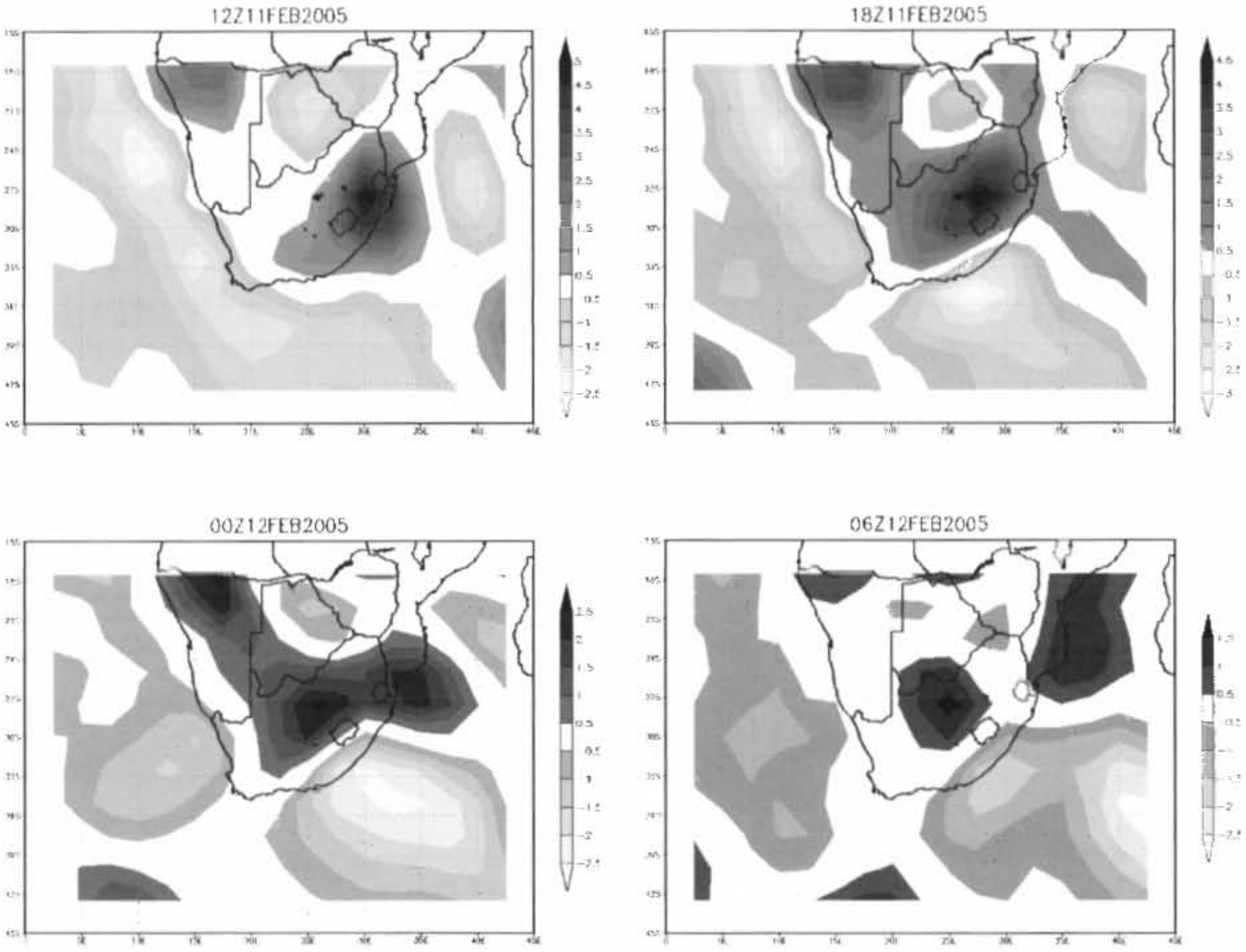

Figure 4.12: Moisture flux convergence (positive values) at the 1000 hPa level (interval 0.5 $g.kg^{-1}.s^{-1}$). Derived from NCEP reanalysis data and shown at 6 hour intervals starting at 12h00 UTC and ending at 06h00 UTC. Positive values indicate convergence.

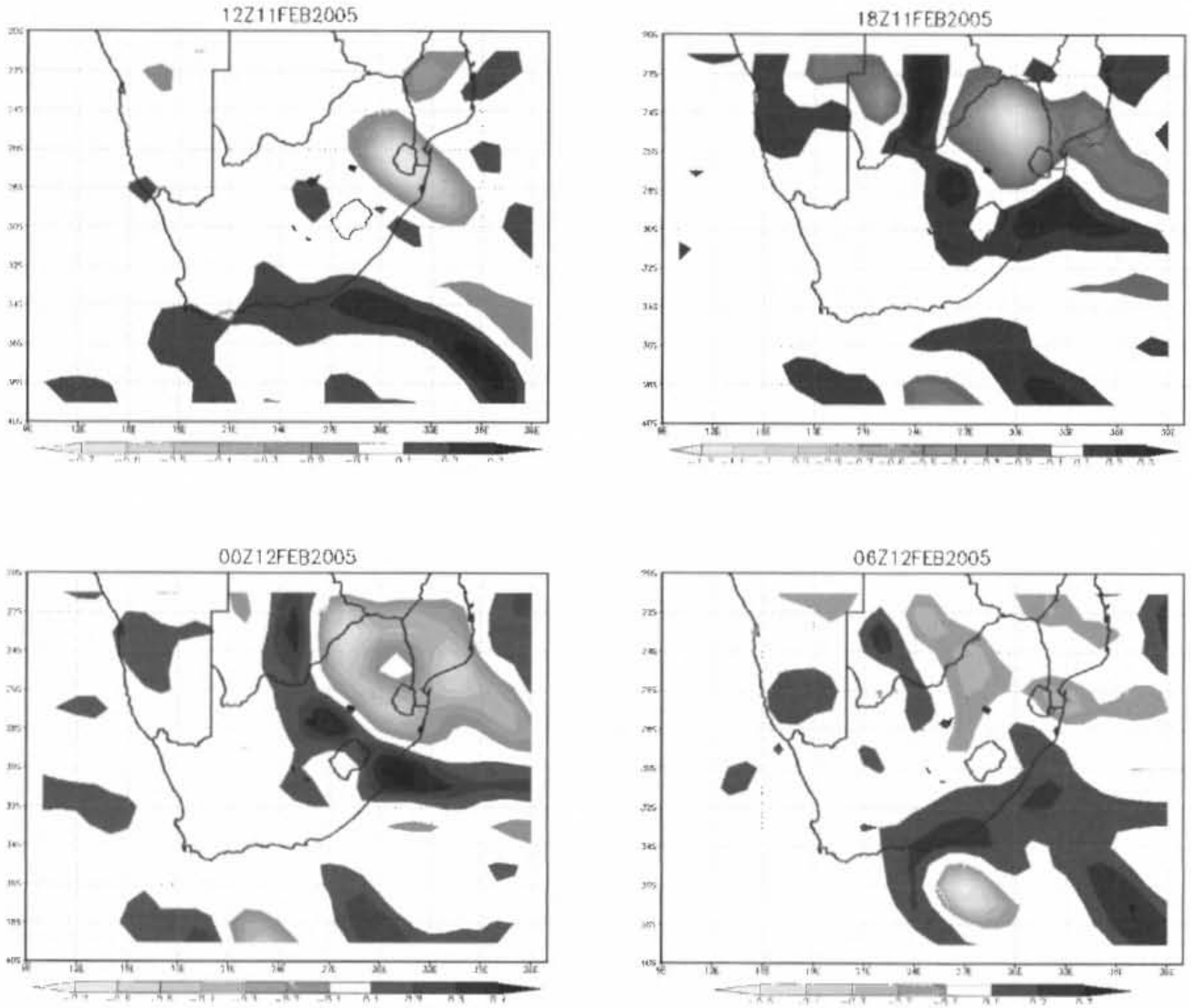

Figure 4.13: Divergence (negative values) at the 200 hPa level (interval, 0.1 x 10^{-3} s^{-1}), calculated from the MRF model output. Starting at 12h00 UTC on the 11 February, with a 6 hour interval and ending at 06h00 UTC on the 12th.

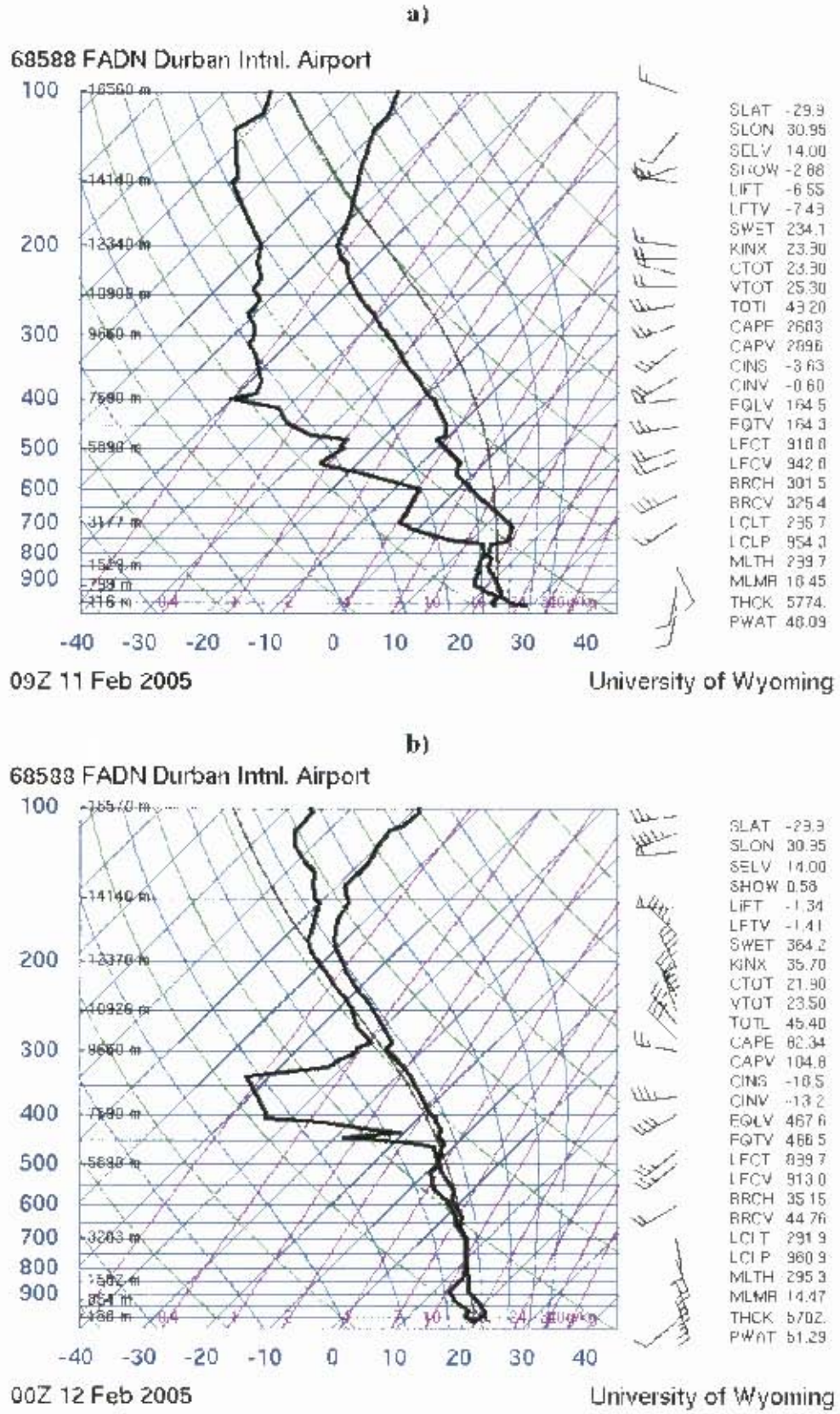

Figure 4.14: Plot of the Radiosonde data collected from the Durban station at a) 09h00 UTC 11 February 2005 and b) 00h00 UTC on the 12th. Left solid line = dewpoint temperature (°C), right solid line = temperature (°C)

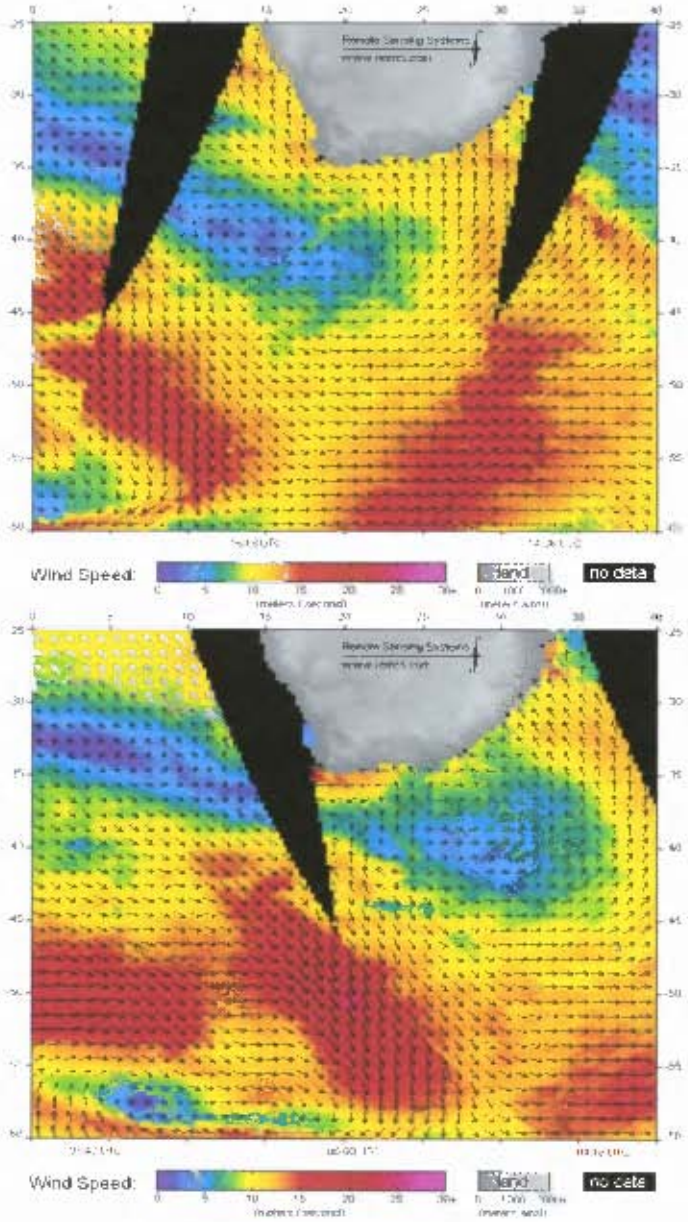

Figure 4.15: Winds derived from microwave scatterometer SeaWinds (more commonly known as QuikSCAT; www.remss.com) at a 0.25° resolution for the evening of the 11th (top) and the morning of the 12th February 2005 (bottom).

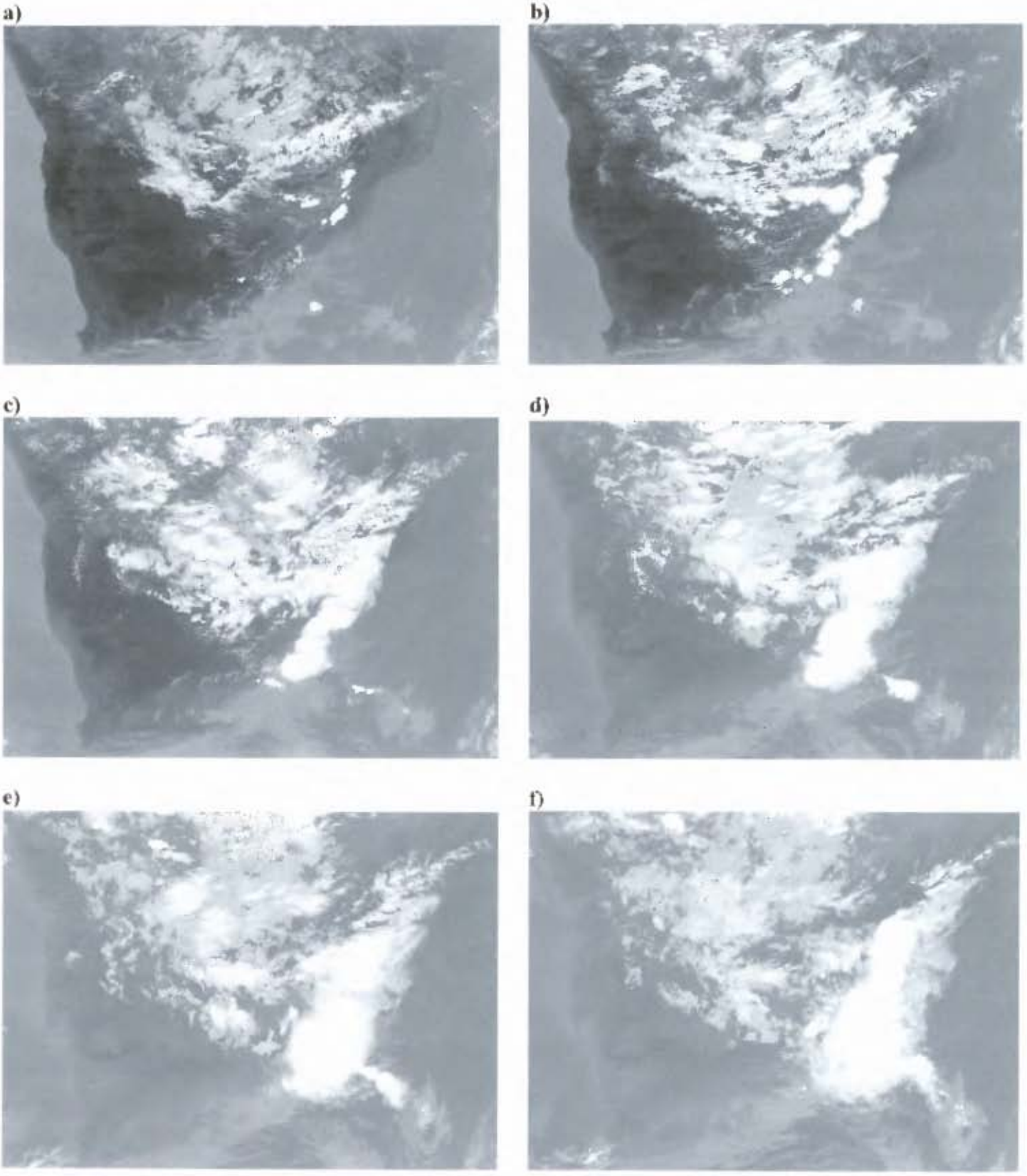

Figure 4.16: Meteosat infrared satellite images at two hour intervals (from left to right) starting at a) 11h42 UTC (top left) through to f) 21h42 UTC (bottom right)

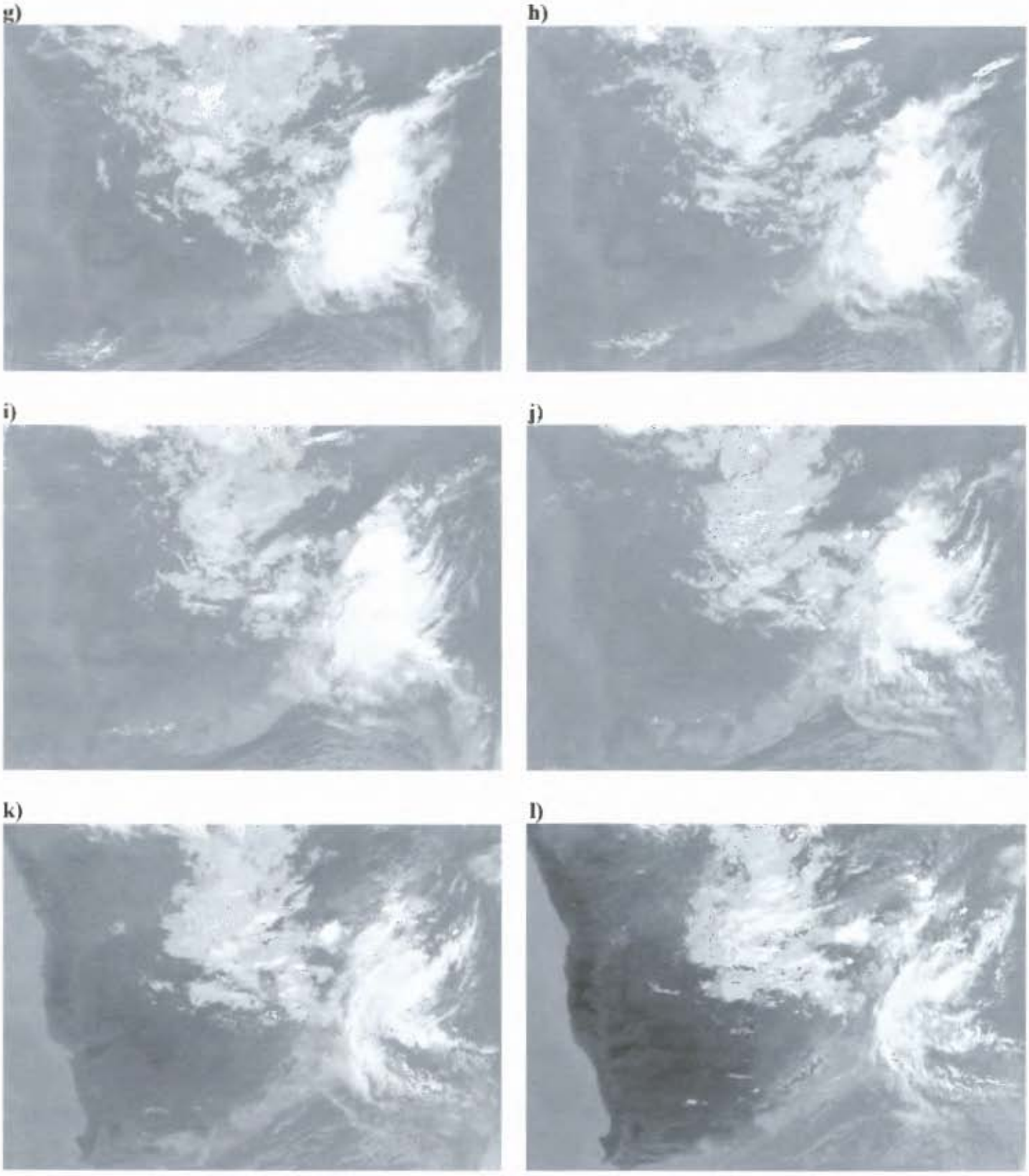

Figure 4.16 cont: From left to right Starting at g) 23h42 UTC through to l) 09h42 UTC.

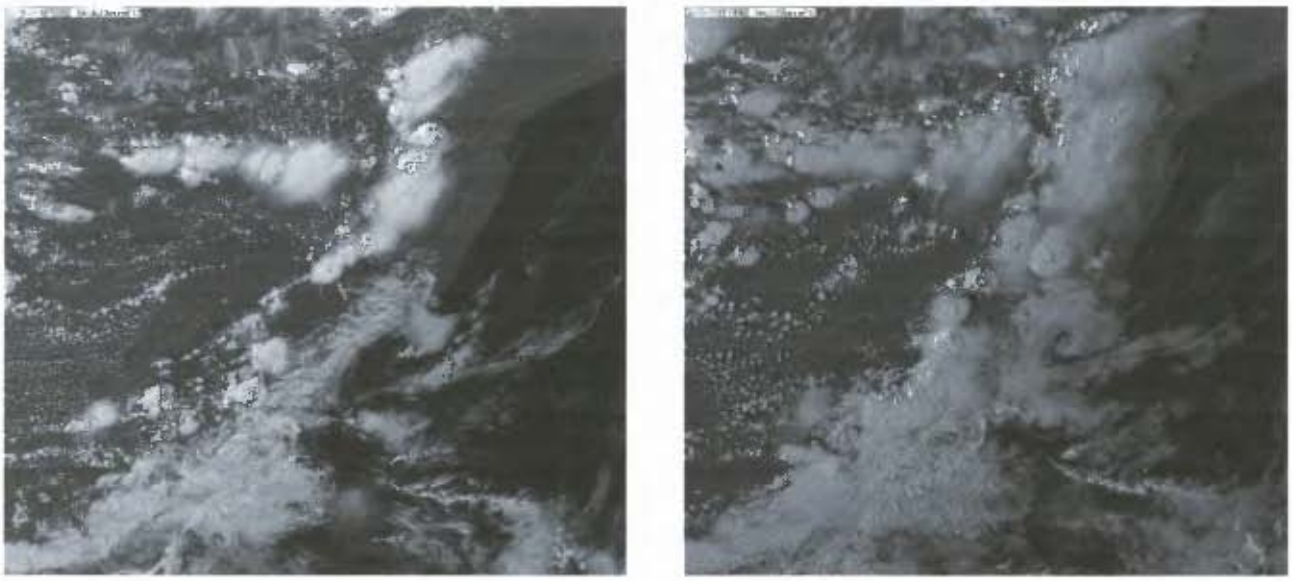

Figure 4.17: HRV images showing the development and merging of the individual storms at 13h12 UTC (left) and 14h42 UTC (right).

a) 12h00 **b) 14h00**

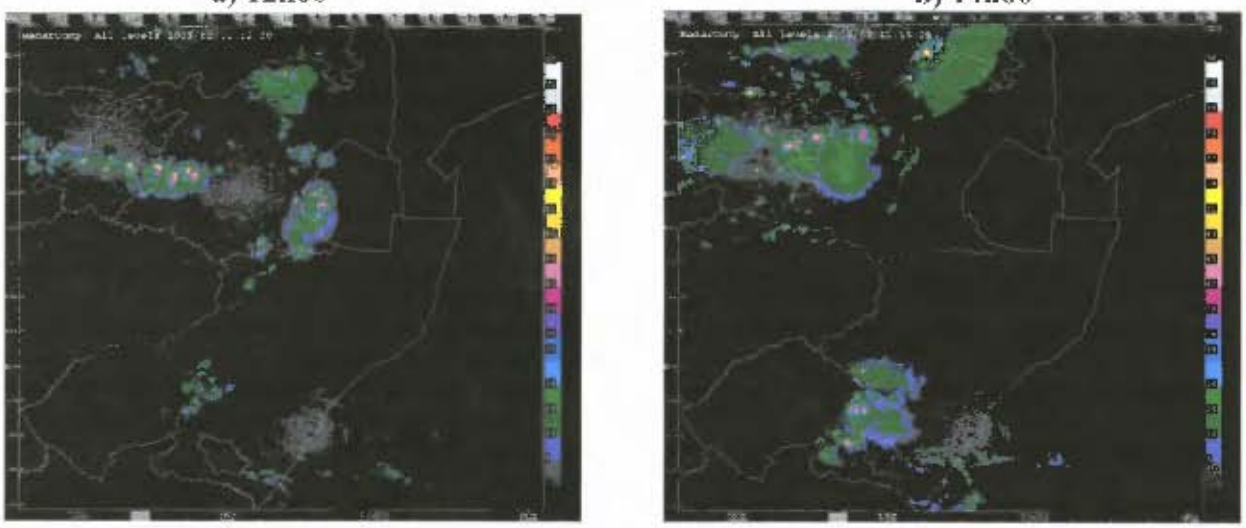

Figure 4.18: TITAN radar reflectivities at 2 hour intervals going from left to right starting at a) 12h00 UTC through to b) 02h00 UTC.

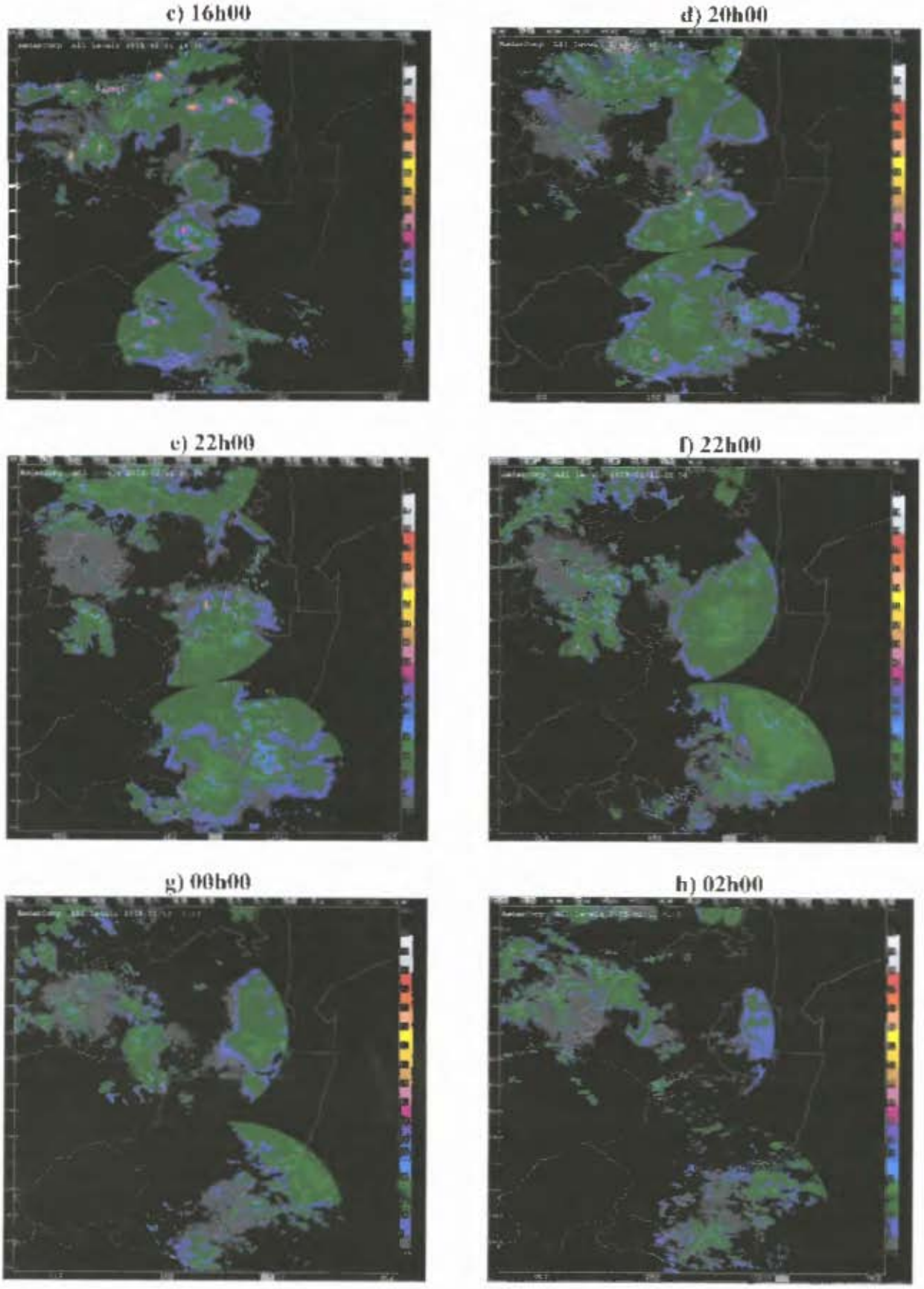

Figure 4.18 cont: Radar reflectivities at 2 hour intervals going from left to right starting at c) 16h00 UTC through to h) 02h00 UTC.

Chapter 5

Numerical Model Analysis

5.1. Introduction

The first objective of this chapter is to assess the ability of the MM5 mesoscale numerical model to simulate the mesoscale convective event presented in chapter four. Validating the numerical model simulation is done by two methods, with the first being the comparison of the simulated synoptic and local conditions with that of the observed conditions obtained from the MRF model output and SAWS weather station data. The second involves comparing key features of the convective event, such as its simulated development and associated precipitation, with that of the observations provided by satellite imagery and SAWS station data. This analysis was performed to determine whether the simulation produced the most important features of the event, as presented in the previous chapter.

The second objective of this chapter is to then identify the mechanisms that may have contributed to the heavy precipitation along the coastal regions of KZN. This is done by looking at key features on the horizontal and vertical scale in the simulation that may have aided in the production of this heavy precipitation.

It was identified through trial and error that initialising the model at 00h00 UTC 10 February 2005 produced the best results in terms of storm development, life cycle and location. The initial and boundary conditions, which are taken from the MRF model, are imposed at this time and every six hours throughout the simulation. Further details about the model setup and the parameterisations that represent the sub-grid scale processes are described in Chapter three.

5.2. Validation of MM5 Model Simulation

5.2.1. Synoptic and Mesoscale Conditions

Figure 5.1 shows mean sea level pressure and areas of strong wind (> 10 $m.s^{-1}$) at the lowest level from the MM5 model simulation. As found in the MRF analysis (see figure 4.6) and the SAWS synoptic charts (see figure A4.1), the propagation of the ridging high pressure system to the south of the country in the control simulation appears to be an influential feature during the event (figure 5.1). This synoptic feature was located to the southwest of the country during the early morning hours of 11 February 2005 and then propagated to the south of South Africa by midday. By the early morning on the 12 February, this feature had then propagated out into the Southwest Indian Ocean. The simulated ridging anticyclone played an important role in supplying the onshore winds into the east coast, which is discussed in more detail later in this chapter. Figure 5.1 also reveals the presence of an interior trough simulated during the time of the event. This simulated trough appears weaker (1010 hPa) compared to that found in the SAWS synoptic charts (1004 hPa) at the same time. However, later that afternoon the trough did strengthen slightly with the central pressure decreasing to 1008 hPa.

At the 500 hPa level, the MM5 simulated synoptic pattern also appears to be consistent with that of the MRF analysis (figure 5.2). The eastward propagation of a westerly wave at this level was found in the MRF analysis data (see figure 4.7) and it also appears in this MM5 simulation. The simulation seems to get the timing of this westerly wave correct, since the wave approaches South Africa in the early morning of 11 February and by the afternoon is situated to the southeast of the country. The control model simulation also compares favourably with the synoptic pattern at the 200 hPa level found in the MRF analysis (figure 5.3) in terms of the geopotential height patterns and the location and strength of the upper level jet.

The low level simulated circulation also compare favourably as those found in the MRF model analysis. Figure 5.4 shows the circulation pattern (wind stream and speed) at the 0.995 sigma level, which is the lowest level in the model. As illustrated in the previous chapter, possibly the most important circulation at this level was the

onshore flow into the east coast (see figure 4.9) and this does appear to be simulated in the control model run. In the simulation it is evident that during the early morning on the 11 February, northeasterlies dominated the lower levels along the east coast of South Africa, which then veered as the day progressed, becoming southeasterlies by the early afternoon. As the ridging anti-cyclone propagated out into the Southwest Indian Ocean, the wind pattern shifted and returned to northeasterlies by the early morning on the 12th. However, there are also differences between the simulated winds (figure 5.4) and that of the observations (not shown), with the most obvious being the strength of the wind off the east coast of South Africa. When compared to the MRF model output, it appears the control model simulation captures the wind direction correctly, but slightly underestimates the strength of it. It also appears to underestimate the wind strength when compared to surface winds derived from measurements from QuikSCAT (see figure 4.15). These weaker winds found in the model simulation could be as a result of the slightly weaker pressure gradient situated to the southeast of the country.

The circulation pattern in the MM5 simulation at the 0.525 sigma level (figure 5.5) also appears to compare favourably with the MRF model output (not shown). The propagation of a westerly wave past the south of the country during the morning of 11 February can be identified in the wind circulation pattern. This particular synoptic feature at this level was evident in the MRF analysis. Westsouthwesterly winds were dominant during the initiation of the system, while southwesterlies dominated as the westerly wave propagated further eastwards. The maximum model wind speeds found in this simulation at this level also compare favourably with the MRF model output (not shown).

Comparison of the low level model winds with that of the SAWS station data for Durban and Richards Bay shows that the model winds are slightly stronger than those observed during the morning and early afternoon of 11 February (figure 5.6). However, these values do fluctuate after this and at times the simulated winds are weaker, (e. g. Durban after 18h00 UTC). It must be kept into consideration that the model simulation does depend heavily on the initial and boundary conditions, which is supplied by the coarser resolution MRF model. It could be due to this low resolution input data that results in the different winds being experienced. Other

features, such as local topography, could also lead to differences between the simulated and observed values. It should also be noted that the grid (resolution) of the model has to be taken into consideration, since a station represented in this model run will represent data found in an 18 km grid.

Figure 5.6 also shows a comparison between the humidity found in the model compared to that of three SAWS weather stations (see figure 5.7 for station location). It reveals that the model underestimates the relative humidity along the coast, particularly during the early morning on the 12 February. However, it should be noted that model does seem to capture the pattern of increasing humidity along the coastal region during the afternoon on the 11 February as well as the humidity pattern found in Bloemfontein. This apparent agreement may help with the precipitation pattern, and influence the location and distribution of heavy precipitation. These differences in the humidity between the model and SAWS stations could also be due to factors mentioned above. It was found in chapter four that high surface diurnal heating possibly played a role in triggering the event. The model appears to portray the temperature pattern found at all the three stations, but appears to underestimate the temperature at the Bloemfontein location during the afternoon of the 11^{th} (figure 5.6).

Overall, simulation of the synoptic features compares favourably to those observed in the MRF model analysis, QuikSCAT winds, and SAWS station data. There are some subtle discrepancies found in the simulation which possibly have resulted due to the low resolution input data. Despite these differences, the model appears to perform sufficiently well to enable it to be used to better analyse the evolution of the event.

5.2.2. MCS and Precipitation Simulation

There have been numerous variables that have been used as a proxy for MCS and the associated convection. Examples of this include Bernardet et al. (2000) who used values of vertical velocity as a proxy for convection, while Chen et al. (2000) use rain water values to identify the MCS in the model. Outgoing longwave radiation (OLR) is another common method used as a proxy for precipitation or at least cloud cover. Xu et al. (2001) used sea level pressure (SLP) fields as a proxy to identify and determine the location of the MCSs in their study. As illustrated in chapter two, distinctive

pressure regions can be located with and around MCSs, which is why SLP could be used as a proxy for these systems.

Using OLR from the control simulation as a proxy for the system, figure 5.8 reveals that the simulated system initiated along the high topography of the eastern escarpment (see figure 5.7) in the early afternoon on 11 February 2005, which agrees with the satellite observations (see figure 4.16). It appears that at first a few single cell systems developed which then merged into a single system during the afternoon and early evening. The system gained its maximum size during the night at approximately 23h00 UTC and then began to decay in the early morning hours of the 12th. This life cycle pattern depicted in the OLR appears to follow that found in the satellite imagery found in chapter four. However, a few noticeable differences between the OLR figures and the observations are apparent. The shape of the system differs slightly from that of the observations, since the system was observed to retain a more linear shape for a longer period than found in the simulation (figure 5.8). The timing of the system was also slightly off, since it initiated slightly later than observed in the satellite images and also appeared to last longer as well. However, the duration of the simulated system appears to be similar to that found in the observations.

Appendix figure A5.1 shows the OLR and precipitable water found in the nested domain of the control simulation. It is also evident that areas of low OLR values (i.e. substantial convective cloud cover) coincide with high values of precipitable water (> 4.5 cm). This suggests that these two variables could be used to monitor the location and propagation of the MCS. It also highlights the linear nature of the precipitable water distribution and its links with topography (see figure 5.7).

For the purpose of this thesis, the simulation is evaluated in terms of both the development of the storm (e.g. timing and spatial distribution), as well as elements of precipitation, such as location and areal extent. Figure 5.9 indicates that the model precipitation pattern has a similar spatial distribution to the observed precipitation (figure 4.1). However, the model appears to over-estimate the precipitation amount along the north coast. For example, simulated precipitation at Richards Bay (see figure 5.7 for location) was over 140mm, compared to the 99 mm observed from the SAWS weather station. It is also apparent that there is excess precipitation simulated

in the high-lying topography regions of the northeast escarpment. It should be noted that the simulation of accumulated precipitation in the nested domain (figure 5.9b) is also over-estimated in the same regions. However, there are also regions where the model significantly under-estimated the precipitation, such as Cape St Lucia region (see figure 5.7 for location). Cape St Lucia station was observed to have received approximately 110 mm during the event, but in the simulation it received less than 10 mm. Over- or under-estimating precipitation appears to be a common problem in mesoscale modelling, which is discussed in chapter seven, and is possibly related to the parameterization of convection and cloud microphysics.

SAWS weather station data indicates that majority of the intense precipitation took place along the north coast of KZN during the late night time hours and early morning hours (i.e. between 22h00-02h00 UTC) 11/12 February. The model simulation appeared to follow a similar pattern (figure 5.10). These figures show the early precipitation pattern along the eastern escarpment as the system developed, which then spreads eastwards as the system propagated to the east. The heaviest precipitation along the north coast then took place during the night time hours, which is similar to that found from the SAWS weather stations. Figure 5.11 shows that this heavy precipitation during the night was associated with strong upward vertical velocities as well as high values of rain water mixing ratio. The characteristics of this convective system are further examined at the time of the heaviest precipitation in order to identify features that may have influenced this precipitation pattern.

5.3. Winds, Convergence and Instability

In order to understand the factors involved in the development of the heavy precipitation along the coastal region, one needs to consider the role of certain processes important for convective development. Doswell et al. (1996) suggest that in order for deep convection to be produced, three criteria must be satisfied. These three criteria refer to the existence of low-level moisture, upward motion and a conditionally unstable environment in the region.

Figure 5.12 indicates that low level moisture convergence was found over large sections of KZN during the convective event. Low level moisture convergence was

initially found only along the escarpment and parts of the KZN coastline during the early afternoon on the 11th, but during the late afternoon and evening, this feature was found along the entire coastline as well as over most parts of northern KZN. During the night, low level moisture convergence was still found over the northern parts of KZN, but was mainly restricted to the coastal region. During the night and early morning hours of 12 February, low level moisture convergence also occurred along the Mozambique coastline and in parts of Swaziland. By late morning on the 12 February, areas of low level convergence in KZN became smaller and widespread (not shown), while some were replaced by low level divergence. This moisture convergence pattern was also found slightly higher up in the atmosphere at the 0.870 sigma level (not shown), since low level convergence was initially located along the escarpment, but by late afternoon and during the night, moisture convergence was present along the northern parts of KZN and Swaziland. It is interesting to note that convergence at this level persisted throughout the night and early morning hours over the northern coastline near 29°S.

A common feature in the development of MCSs that appears to be absent in the simulation of this event is that of a LLJ (figure 5.12). This feature was also not evident in the MRF analysis, but this could be due to its coarser resolution. By 12h00 UTC 11 February there was a moderate southeasterly wind impacting on the coast (see figure 5.4), which may have be responsible for supplying moisture into the region. This feature was prominent even during night time hours and was also evident in the surface wind pattern derived by QuikSCAT (see figure 4.15). These moderate winds then began to weaken during the night and shift further offshore (as the anticyclone propagated eastwards), and hence reducing the amount of moisture into the region. A similar wind pattern is found in the 0.870 sigma level (not shown) indicating that the strong onshore advection of moisture occurred in the lower 1500m of the atmosphere. The wind pattern at the 0.870 sigma level illustrates the persistent onshore winds into the northern coastline. The timing of the heavy precipitation along the north coast appears to be similar to that of the onset of these winds into the region.

Figure 5.11 indicated that moisture advection also took place at the 750 hPa level into the region of heavy precipitation during the night. This advection was due to the anti-cyclonic circulation pattern found at this level along the east coast. This circulation

pattern was also evident at the 800 and 700hPa levels (both not shown), but was not so clear at the levels above this. This anticyclonic feature, which propagated from the southwest (along the Eastern Cape coast), appears to have originated from a mesoscale high pressure system that had developed behind the cold front. The frontal system had passed along the southern parts of the country during the 10/11 February 2005 (see figure a4.1). Holland and Leslie (1986) describe this coastal ridging phenomenon as a ducted ridging event. These authors presented a numerical simulation of such an event that took place over southeast Australia. In there case study, they noted that the initiating mechanism is either a front impinging on the divide (Australia Mountain Range), or a rapid intensification or eastward movement of an anticyclone. As noted by these authors, this phenomenon is found in Australia, South America and South Africa. By the late morning hours this feature in the case study had propagated further off the east coast and had weakened, which possibly resulted in reducing the amount of moisture advected into the region. This dissipation pattern is similar to that described by Holland and Leslie (1986), since the ridging event weakens as it propagates up along the coast. It should be noted that this feature cannot be confirmed in the observations due to the lack of observation data and poor resolution of the data available.

These findings in the simulated wind strength and circulation patterns is supported by figure 5.13, which depicts wind speed and zonal wind speeds, which is used to highlight the dominant direction, found in the control simulation along cross-section B-B' (see figure 5.9). From these cross-sections it is evident that during the event, winds with an easterly component were found in the lower levels in the simulation, which extended up into the mid-levels in certain regions. At the same time, the mid-to upper level winds were predominantly from a westerly direction. In similar cross-section, using meridional wind speeds (not shown) instead of zonal wind, it is evident that the early afternoon winds in the lower levels contained a more southerly component than easterly. These cross-sections support the findings in figures 5.4 and 5.12, which indicate that onshore winds were impinging the KZN coastline in the lower levels during the event. The ducted coastal ridge is also evident in the vertical cross-sections. However, a slight difference is that the vertical cross-sections suggest that this phenomenon possibly extended up to the 500 hPa level, which was not so apparent in the horizontal figures (not shown).

In order to get a better understanding of the conditions through the troposphere during the heavy precipitation event, east-west vertical cross-sections are produced. These cross-sections are taken along transect A-A' in figure 5.9, which is through one of the regions that received heavy precipitation during the event. A vertical cross-section illustrating vertical velocity, wind vectors and relative humidity through the region that received a copious amount of precipitation is shown in figure 5.14. This figure shows that during the times of maximum hourly precipitation, the region experienced onshore winds and strong vertical uplift. This strong vertical uplift extends from the lower levels up to the mid-levels (even to the upper levels at times) while high relative humidities were present in the lower atmosphere. The vertical uplift was a prominent feature during the late afternoon and night, where it first featured further inland around 15h00 UTC on February 11, and then was no longer present along the coastal region after about 03h00 UTC the next morning. The regions of strong vertical extent always occurred near the coastal region, which could be due to the inflow of low level moisture and the coastal topography forcing this moist air to rise.

Figure 5.15 reveals the divergence/convergence pattern through the atmosphere during the times in which the region which received heavy precipitation. It can be seen that low level convergence and mid-level divergence was prominent over the coastal region during the periods of heavy precipitation. From figures 5.14 and 5.15, it is evident that the upward motion was associated with the strong vertical coupling between low level convergence and mid-level divergence. The low level convergence appeared to fluctuate in strength during the night, weakening at times before strengthening again. This coupled convergence/divergence pattern may result in the intensification of the convective system due to air being forced to rise due to the low level convergence and then spreading outwards in the mid-levels due to the divergence, allowing more air to rise.

The location of the low level convergence also coincided with regions containing a mixing ratio greater than 0.4 $g.kg^{-1}$ (figure 5.16). These columns of mixing ratio greater than 0.4 $g.kg^{-1}$ at times extended well into the mid-levels during the periods of strong uplift, showing that the moist air originating from the ocean extended well above the boundary layer. During the morning hours (approximately after 03h00

UTC), the coupled divergence/convergence pattern weakened (not shown), while the amount of moisture in the atmosphere also decreased.

Figure 5.16 also plots the equivalent potential temperature (θ_e) and reveals the presence of a thermal ridge located in the region of maximum rain water mixing ratio. This thermal ridge does not appear to extend much into the middle troposhere and is only evident during the evening and night time hours. When the cross-section was extended further eastwards (not shown), a steep vertical gradient in the equivalent potential temperature (θ_e) was also present during the heavy precipitation periods during 11 and 12 February 2005. These steep vertical gradients of equivalent potential temperature suggest that moisture was transported into the region from the surrounding ocean (Juneng et al. 2006).

Convective instability was calculated by obtaining the difference in equivalent potential temperature between the 0.995 and the 0.525 sigma levels (interval °C; figure 5.17). A convectively unstable environment usually contains dry mid-levels with near saturated conditions in the lower levels. These figures suggest that during the event the atmosphere was convectively unstable, particularly along the northern regions of KZN in the afternoon and evening. In the early night time hours, this convectively unstable air over northern KZN seemed to have dissipated becoming more stable, but in the early morning hours of 12 February 2005, the stability of the atmosphere in the region began to weaken and favour convective development again. The topography along the coastal regions is not as significant as that found inland, which suggests that the unstable atmosphere found during the event may have played a key role in the development of convection.

Precipitable water is also plotted on figure 5.17 and it can be seen that values exceeding 50 mm were located in parts of KZN during the late afternoon and evening hours. During most of the night and following morning, northern KZN experienced values of precipitable water exceeding 40 mm. It should be noted that further inland, in the region where the system initiated, the precipitable water values never exceeded 30 mm. Certain parts of Swaziland also received heavy precipitation and it can be seen that this region also contained high values of precipitable water during 11 and 12 February. At the same time, this region also contained a convectively unstable

atmosphere and hence favourable conditions for convective development. It is also apparent that the linear nature of the precipitable water distribution and its links with topography are more evident in figure 5.17 than found in figure A5.1.

The convective instability figures are supported by the soundings produced using the MM5 simulation output for the Richards Bay and Durban region (figure 5.18). The soundings from the simulation for Durban reveal that a near saturated condition at low levels was overlain by a drier atmosphere in the mid-levels. The soundings for Richards Bay did not appear to have the same moisture pattern, since the atmosphere in the mid-levels at this location were a lot closer to saturation compared to the Durban soundings. All the soundings, except the 00h00 UTC Richards Bay sounding, show the presence of a strong southeasterly wind in the lower levels, particularly for Durban station soundings. Soundings at both stations indicated that the winds were veering with height in the simulation, which is evident by surface winds were southeasterly, while at the mid-levels there were strong southwesterly/westeries.

Severe weather parameters for the Durban 09h00 UTC 11 February (not shown) sounding taken from the simulation reveal that the atmosphere was not as conducive to severe storm development as determined from the observed at the same time (see figure 4.14). The simulated atmosphere contained less CAPE (741 J/kg) and SWEAT (218) than observed, as well as a lower precipitable water content (44.3 mm). The model sounding also had a lower totals total index (46°C) and lifted index (-1.5 °C) compared to the observed sounding, while it also indicated that the model atmosphere was slightly further away from saturation than observed. As the simulation progressed, the atmosphere became more conducive to the development of convection in the Durban region. The 12h00 UTC 11 February Durban sounding from the simulation had an increase in nearly all severe weather parameters that have been used, when compared to the 09h00 UCT sounding. The simulated atmosphere had a CAPE value of 719, a SWEAT value of 375, a TT value of 48 °C, a lifted index value of -2.5 °C and a precipitable water vale of 46.6 mm. However, these severe weather parameter values were still weaker than those observed.

The 12h00 UTC (not shown) and 18h00 UTC 11 February Richards Bay soundings from the simulation were the most conducive to the development of convection. The

only noticeable difference between the two was that the 18h00 UCT had a higher precipitable water content and was closer to saturation throughout the profile compared to the 12h00 UTC. Apart from those differences, both these soundings had similar severe weather parameter values, which both showed the atmosphere was favourable for the development of convective systems. The 12h00 UTC (18h00 UTC) sounding from the simulated had a CAPE of 1541 (1425) J/kg, SWEAT value of 221 (228), a TT value of 48 (47) °C, a PW value of 49.8 (58.4) mm and a lifted index of -3.6 (-3.5) °C. However, no radiosonde data is collected in the Richards Bay region, thus no comparisons can be made between the soundings from the simulation with the observed state of the atmosphere.

The Bulk Richardson's number (BRN), which is usually and indicator of convective storm type and is calculated from values of CAPE and vertical wind shear in the lower 6 km of the atmosphere (Wiseman and Klemp, 1982, 1986), indicated that in the simulation the Richards Bay region was more conducive to the development of multicellular convective systems, when compared to the Durban region. This is evident by the higher values of BRN found in the Richards Bay region. For example the Richards Bay 18h00 UTC sounding contained a BRN of 44.53, while the Durban sounding had a value of 24.08 at the same time. The highest BRN value obtained from both stations in the simulation was 487.5 at the 00h00 UTC Richards Bay sounding and the lowest being 11.88 at the 12h00 UTC Durban sounding. It should be noted that the BRN values found for the simulated Durban soundings were less that the observed in figure 4.14. This could possibly be due to the lower CAPE values found in the simulation.

5.4. Backward Trajectories

In order to obtain a better idea of the moisture transport into the region of the storm initiation and life cycle, backward trajectories was computed. The trajectories were calculated using the Hybrid Single Particle Lagrangian Integrated Trajectory model (HYSPLIT4). This model was developed by the Atmosphere Resources Laboratory (ARL) at NOAA (Draxler and Taylor, 1982). To compute the trajectories, gridded fields of meteorological variables are required at regular temporal intervals in this case, the trajectory model uses the MM5 simulated meteorological fields as input.

Backward trajectories were computed for regions near storm initiation and along the coastal regions where maximum precipitation occurred. This method also allows one to see where air parcels from different pressure levels originated from. A total of four parcels were released backwards, with all of them starting from different levels, which corresponding to the lower, mid and upper levels of the atmosphere.

Previous research has shown that moisture sources for the South African summer precipitation region include the neighbouring tropical oceans (D'Abreton and Lindesay, 1995; Cook et al. 2004), tropical Africa (D'Abreton and Lindesay, 1993; Cook et al. 2004) and the Agulhas Current region off the South coast (Jury et al. 1993; Rouault et al. 2002; Singleton and Reason, 2006, 2007). During the height of summer when convective activity is typically greatest (January), kinematic trajectory modelling has revealed that moisture transport into the summer precipitation region of South Africa is mainly from the northeast with a maximum at around 850-700 hPa (D'Abreton and Tyson, 1996). Cook et al. 2004 found that most wet spells in the summer South African precipitation region coincide with increased influx of moisture from the Southwest Indian Ocean and convergence over the precipitation region.

Figure 5.19a reveals that the low level air parcels involved in the initiation of the storm, originated from the northeast of South Africa 36 hours prior to the storm. These air parcels travelled in a southwestward direction along the northern Agulhas Current before heading inland towards the escarpment. SST images (figure 4.10) in chapter four indicated that anomalously warm waters were experienced off the east coast during the event, which possibly resulted in more moisture being evaporated. The air parcels in the lower levels then ascended as they approached the region of storm initiation. Air parcels from the mid- and upper levels both appeared to have originated to the west of South Africa. These air parcels then transported cool, drier air into the region at mid-levels contributing to convective instability over KZN when this air overlaid the warm, moist unstable marine air.

Backward trajectories from Richards Bay and Uloa Agricultural College (figures 5.19b and c, respectively), which are two of the stations that received significant precipitation, reveal similar patterns of air flow as discussed above. In both cases, the air parcels in the lower atmosphere originated from the northeast and then travelled

across the warm Agulhas Current waters along the east coast. This trajectory path possibly led to an enhancement of the precipitation in the region due to the air parcels travelling across a relatively very warm ocean. Note that weather stations along the northern coastline of KZN had recorded very high humidities during the event (see chapter four for details). There is also evidence that air parcels in the mid-levels above Richards Bay originated at the lower levels over the ocean before rising into the mid-levels, while those at the same level above Uloa Agricultural College originated from the drier South African interior mid-levels.

It should also be noted that these backward trajectories are consistent with the wind patterns at the different levels prior to and during the event. From the station data and MRF model output, it was evident that the winds on the 10 February 2005 were dominated along the east coast by northeasterlies, which continued through till the morning hours of the 11th. By the afternoon on the 11th, these winds had veered to southeasterlies, which continued throughout the day and into the night, before backing to northeasterlies the following morning.

Air parcels ending up over Swaziland (figure 5.19d), originated from the warm ocean off the Mozambique and South African coastline. Mananga station (see figure 5.7), which is the location of the end point in backward trajectory in figure 5.19d, received over 100mm of precipitation during the event. The low level trajectories reflect the strong easterly winds apparent in this region (see figure 5.12). In this case, the origin of the upper level air parcels appear to have originated at the lower levels over the warm ocean then the air parcels were forced to rise due to the local topography or low level convergence (e.g. figure 5.12).

5.5. Summary

This chapter has focussed on the numerical simulation of the mesoscale convective event that was analysed in the previous chapter. The setup of the control simulation was based on the findings of chapter four, as well as a trial and error process that was used to identify the best simulation of the event. When comparing the MM5 control simulation to the SAWS station data and MRF model output, it was found that the simulation did have some success in replicating the main features of the event. The

model was able to simulate the salient features of the event, but it had difficulty in simulating the precise location and intensity of the heavy precipitation. However, there were subtle discrepancies in the synoptic and mesoscale conditions in the simulation, which may have had an influence on the precipitation over-estimation along the coastal region. However, it is more likely that the precipitation over-estimation is related to the parameterization of convection and cloud microphysics in the model. These discrepancies found in the model may have been due to the initial and boundary conditions used to simulate this event or the parameterizations selected.

The simulations indicated that the topography along the eastern escarpment played a role in the initiation of the system. From OLR images, it was evident that after initiating along the escarpment, the system propagated towards the east/northeast in the direction of the northern Agulhas Current region. This track suggests that the building of the system took place at the flanks most exposed to the inflow of low level air. This low level air was rich in moisture due to it travelling across the warm northern Agulhas Current. Through backwards trajectories, it was identified that in the region of heaviest precipitation, lower level air parcels originated out over the warm waters of the southwestern Indian Ocean 36 hours prior to the event. These air parcels then travelled above Agulhas Current, which is rich in moisture, before arriving along the northern coastline of KZN. The wind pattern for the 11 and 12 February 2005 suggests that the moisture was brought in from the southeast, but it should be noted that northeasterly winds were present on the 10th and early morning of 11 February 2005. These northeasterly winds were likely to have supplied some of the moisture for the early phases for the convective event.

Once the model simulation was validated with the precipitation, station data, MRF model analyses and satellite observations, an investigation to the mechanisms resulting in the heavy precipitation was conducted. The simulated over-estimation of the heavy precipitation along the north coast may also have been a result of the persistent low level convergence and inflow of moist air into the region throughout the night and early morning hours. It was found that all three criteria required for the development of deep convection, as described by Doswell et al. (1996), were satisfied along the northern coastline of KZN. It was shown that the region contained a consistent southeasterly/easterly wind, which led to the transport of moisture rich air

into the region. This transport is evident from the region containing a precipitable water content greater than 40 mm throughout the late afternoon and night and a mixing ratio greater than 0.4 $g.kg^{-1}$ extending from the surface up to the mid-levels. This region also contained a conditionally unstable atmosphere, which was illustrated through figures containing the difference in equivalent potential temperature between two layers, as well as the soundings. Through vertical cross-sections taken through one of the heavy precipitation regions, it was identified that persistent patterns of coupled low level convergence and mid-level divergence were present. It was also evident that strong upward motion was associated with this strong vertical coupling between low level convergence and mid-level divergence, which likely aided in the production of the heavy precipitation. Thus, there was a large quantity of moisture available along the northern KZN coastline, a conditionally unstable atmosphere and strong uplift for a prolonged period during the night. These conditions provided a very favourable environment for the copious amount of precipitation experienced in the region. Although, these synoptic and mesoscale features found in this model simulation appear similar to those described by Maddox et al. (1986) that are found in the development of MCCs, this particular system was not quite large enough or of long enough duration to be classified as a MCC.

It was also identified in the simulation that a mesoscale anticyclonic feature over the east coast may have also resulted in the advection of moisture into the region during the night and early morning hours. This feature was most prominent at the 800,750 and 700 hPa levels and possibly originated either from the frontal system impinging on the coastal topography or the eastward propagation of the anticyclone, as found in southeast Australia (Holland and Leslie, 1986). This feature should not be mistaken for a mesoscale convective vortex (MCV), which have been noted to develop in the dissipation stages of MCSs (refer to chapter two). The presence of an MCV was not evident in the observations and it also did not appear to be evident in the simulation. This could be due to various reasons for this particular case study, such as the system possibly did not have a long enough duration for the winds to be influenced by Coriolis. It should also be noted that MCVs attend to feature more in the dissipating stages of MCCs than the other types of MCSs (e.g. Bartels and Maddox, 1991). It could also possibly be due to the local topography that inhibits the development of such a feature over the east coast. However, more case studies are required in order to

identify if and when the development of such a mesoscale feature takes place in South Africa.

It appears that changes in the synoptic features had an influence of the dissipation of the mesoscale convective system. The ridging anticyclone propagated further eastwards resulting in the core of strong winds weakening and moving further offshore. This may have resulted in a weakening of the moisture advection into the system, which was evident from the decreasing precipitable moisture values and the mixing ratio in the region. The mesoscale anticyclone feature found in between the lower and mid-levels also weakened at this stage and possibly also resulted in less moisture being transported into the east coast. The forcing of the convective system also appeared to fade away in the morning of 12 February since there no longer any low level convergence and upper level divergence after that time. The atmosphere also became more stable and less favourable for the development of convection. Once these factors weakened during the morning of 12 February 2005, the production of the heavy precipitation came to an end and the mesoscale system began to dissipate.

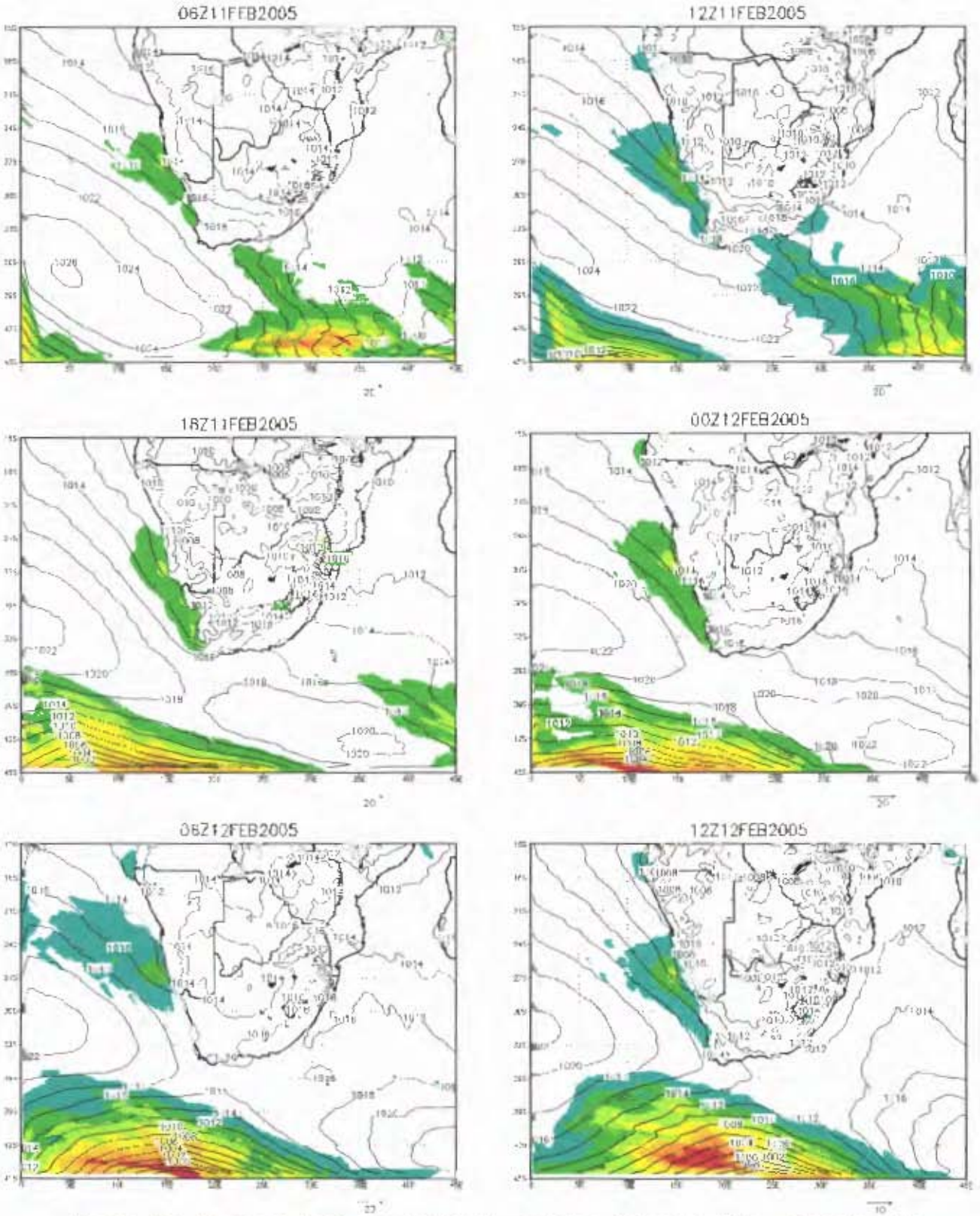

Figure 5.1: Mean sea level pressure (black contours; interval 4 mb) and winds with speeds greater than 10m.s^{-1} at the 0.995 sigma level, derived from the control simulation. At 6-hourly intervals, starting at 06h00 UTC on the 11th and ending at 12h00 UTC 12 February.

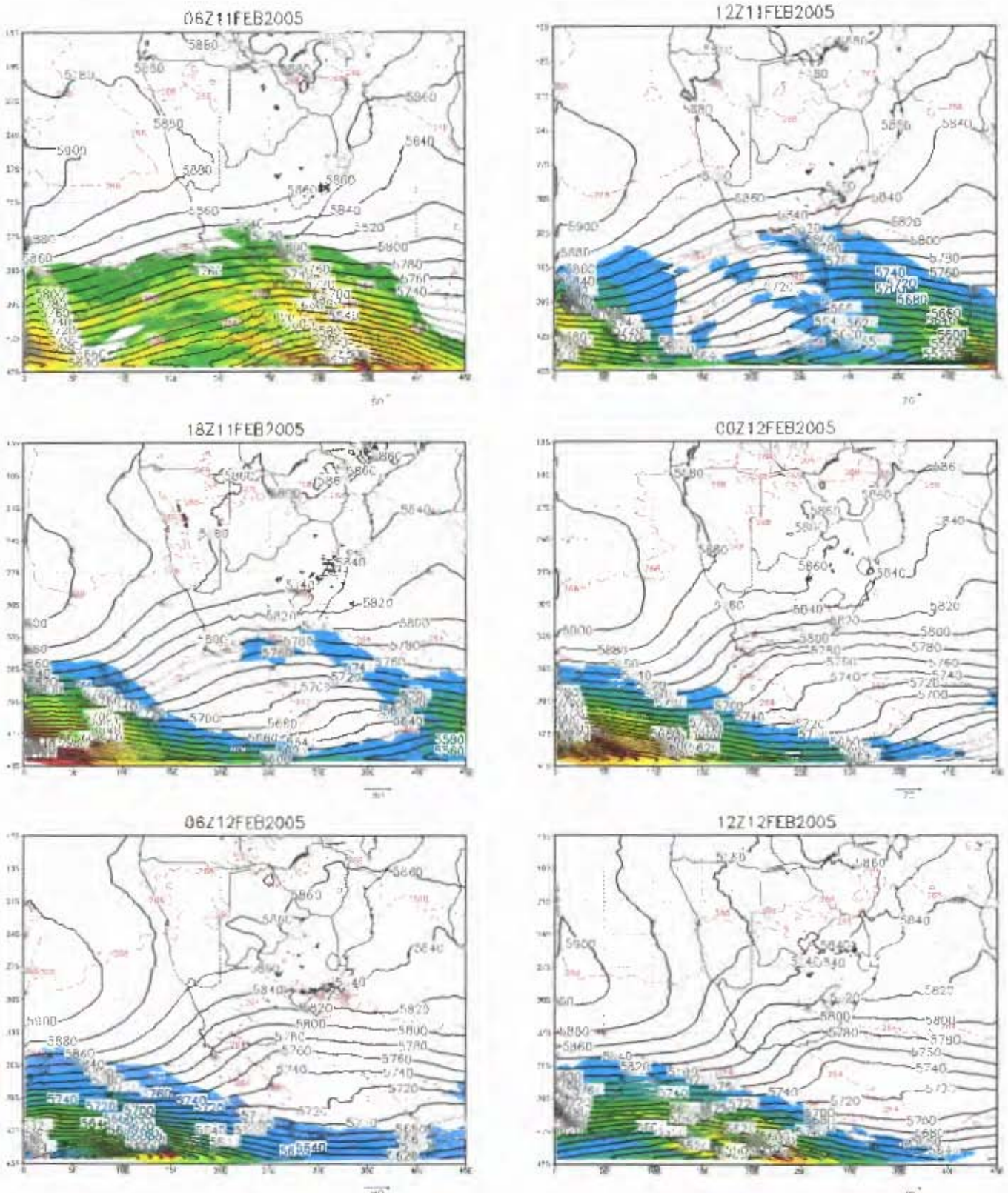

Figure 5.2: Temperature (dashed contours; interval 4 degrees k), geopotential height (solid contours; interval 20m) and winds with speeds greater than 20 $m.s^{-1}$ at the 500 hPa level, derived from the control simulation. At 6-hourly intervals, starting at 06h00 UTC on the 11th and ending at 12h00 UTC 12 February.

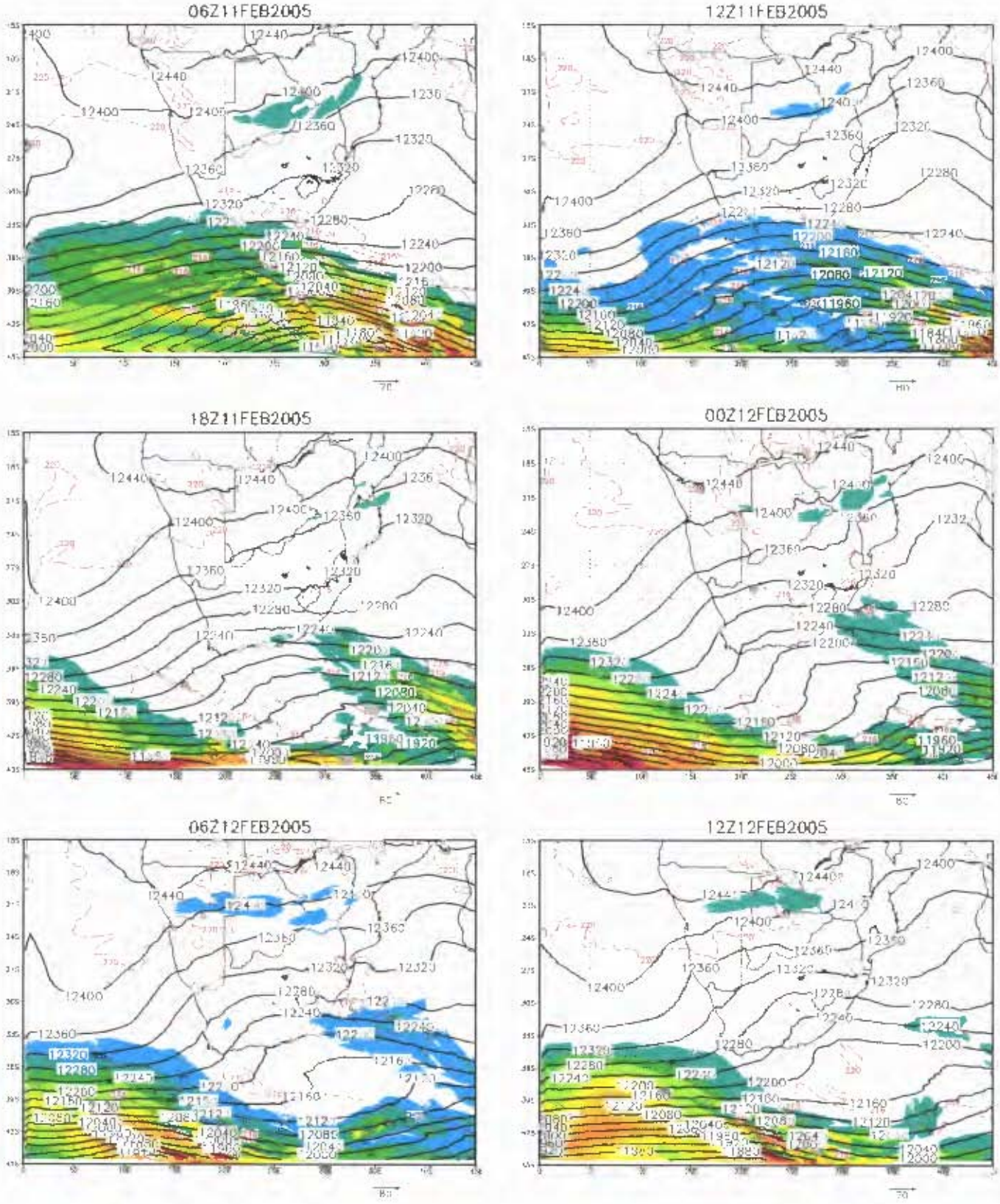

Figure 5.3: Same as figure 5.2, except at the 200 hPa level, geopotential height has an interval of 40m and winds with speeds greater than 25 $m.s^{-1}$ are shown.

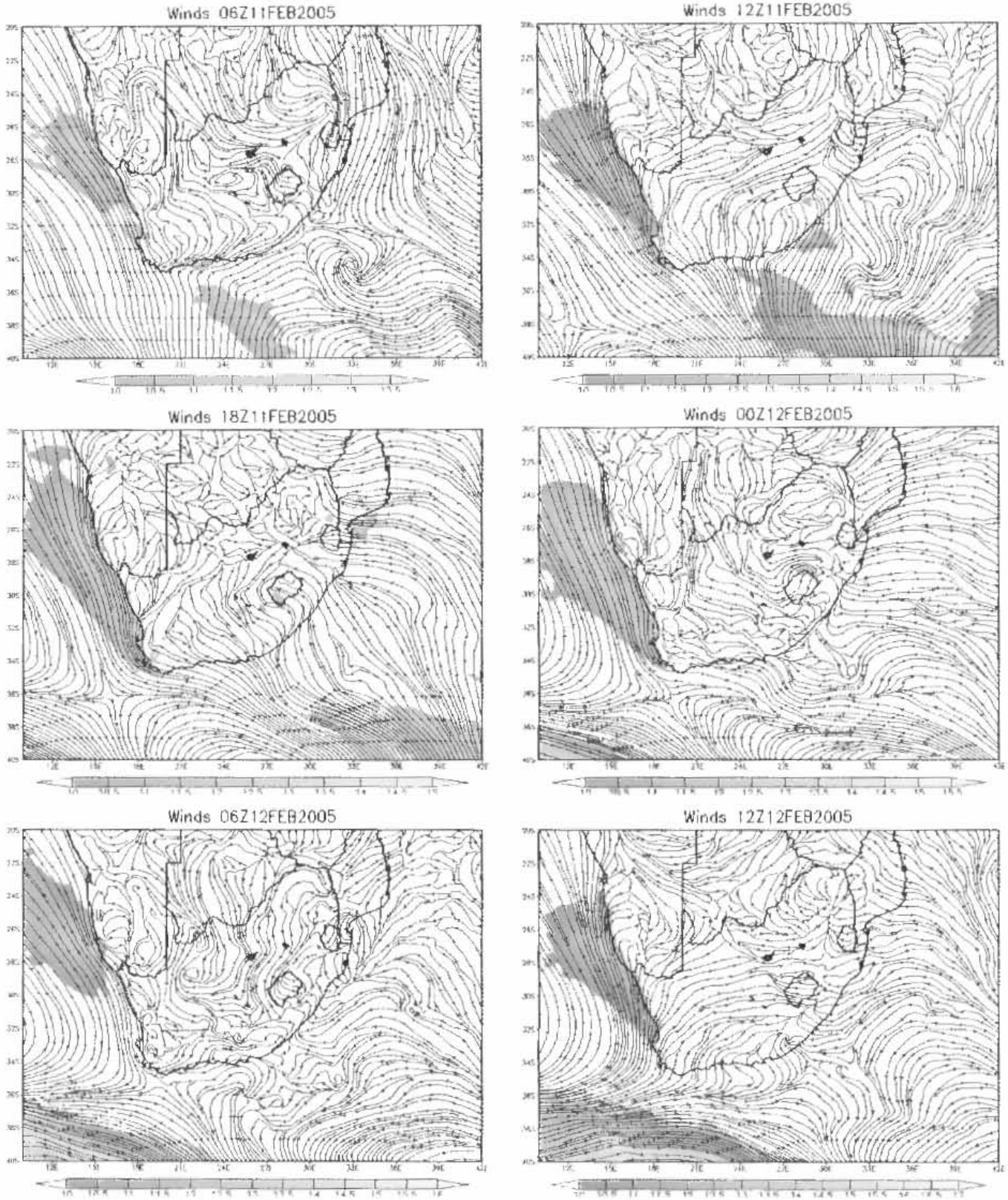

Figure 5.4: Circulation pattern in the control simulation at the 0.995 sigma level and regions where wind speeds greater than 10m.s^{-1} are shaded (interval; 0.5 m.s^{-1}).

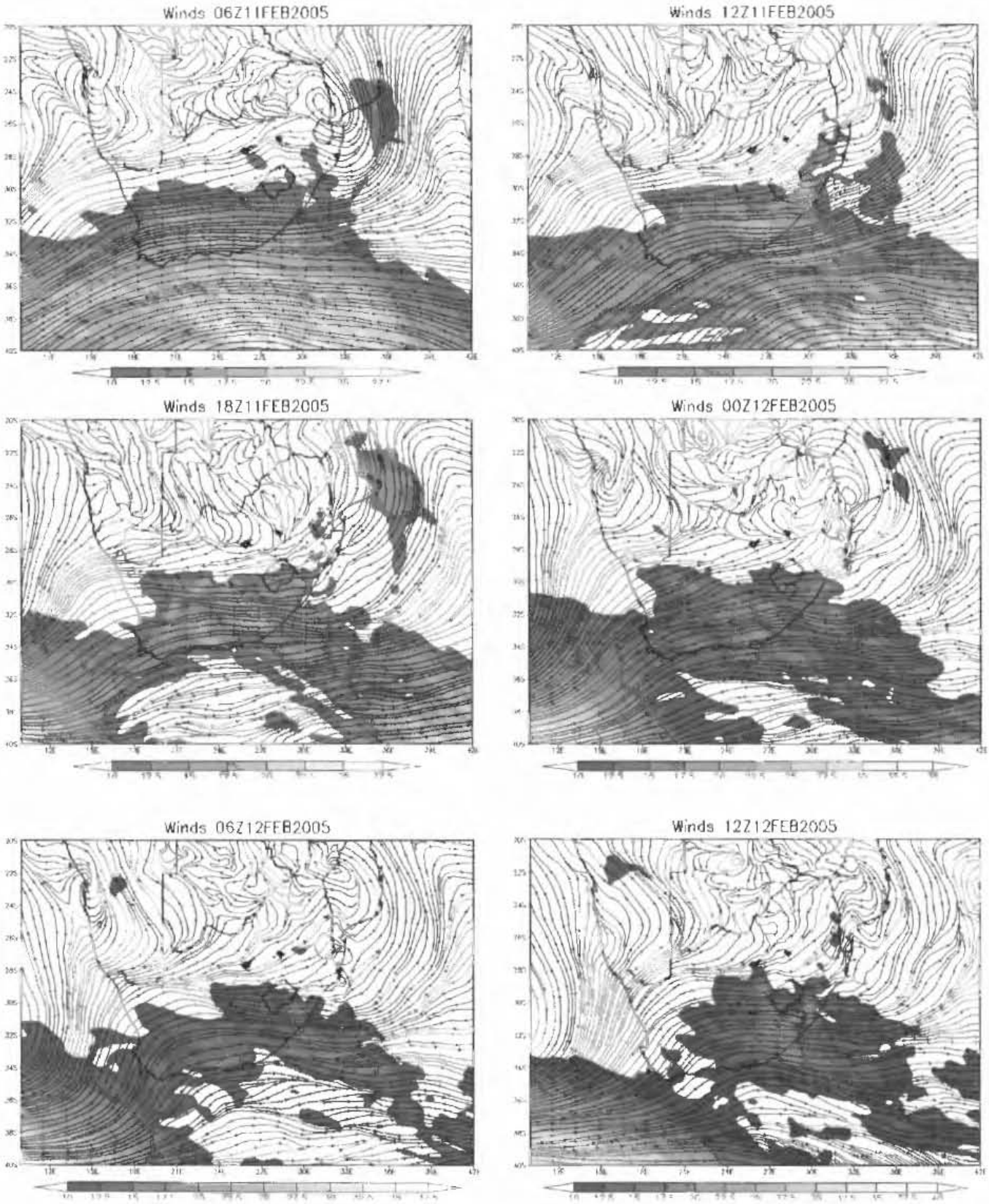

Figure 5.5: Same as figure 5.4, except at the 0.525 sigma level and that the shaded interval is at 2.5 $m.s^{-1}$.

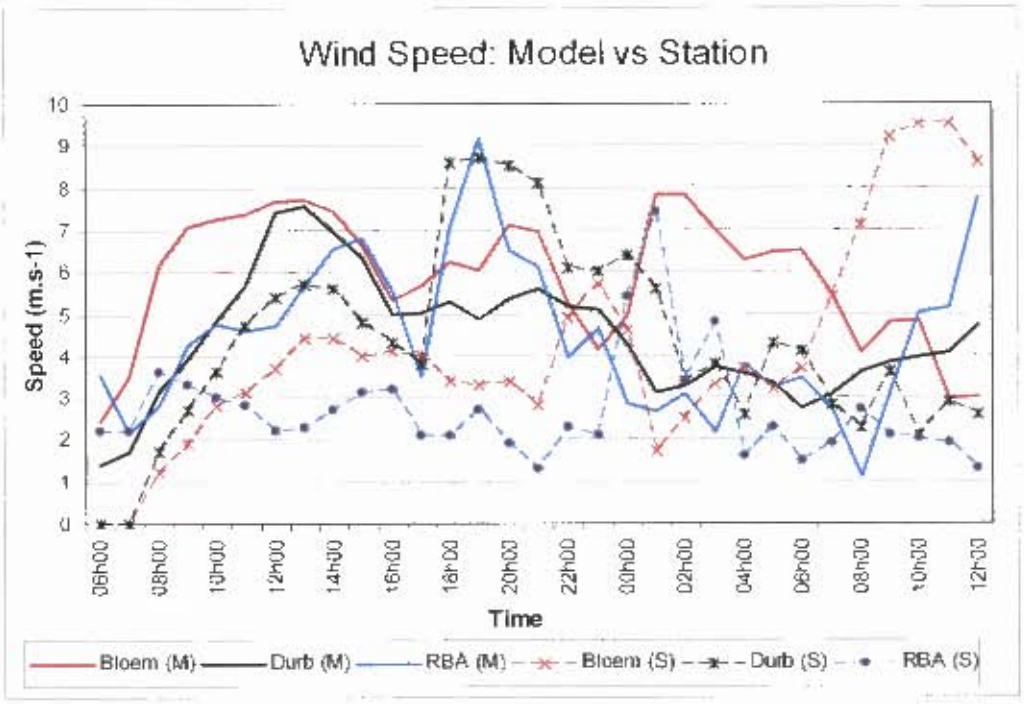

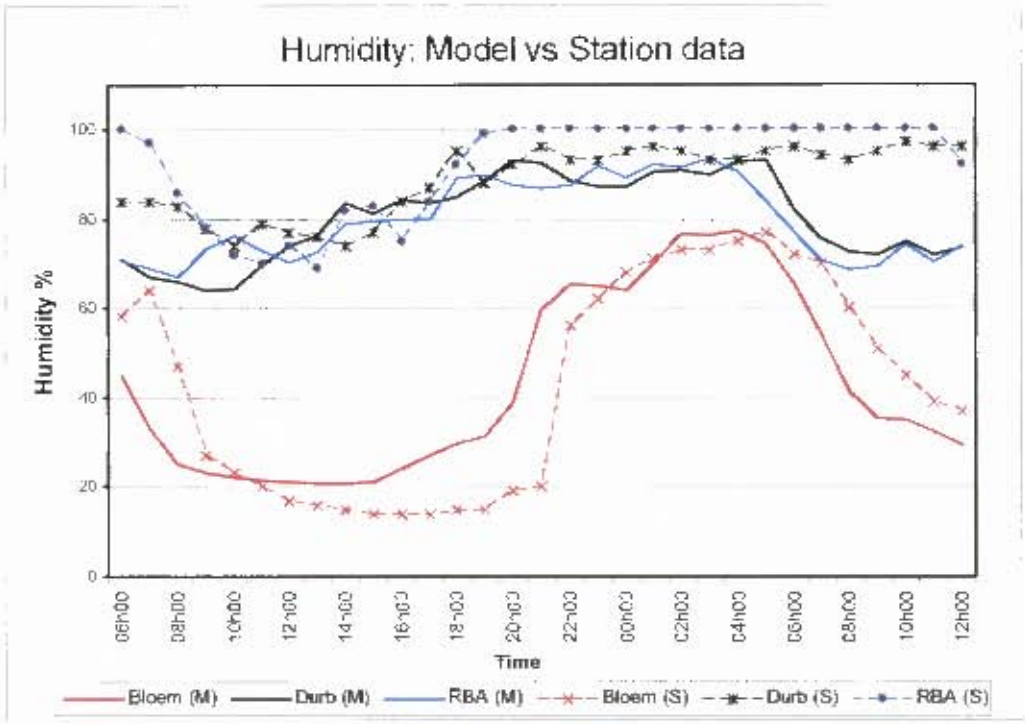

Figure 5.6: Comparisons between model output and SAWS station data for three locations in South Africa. The top graph compares wind speeds, while the bottom graph compares humidity.

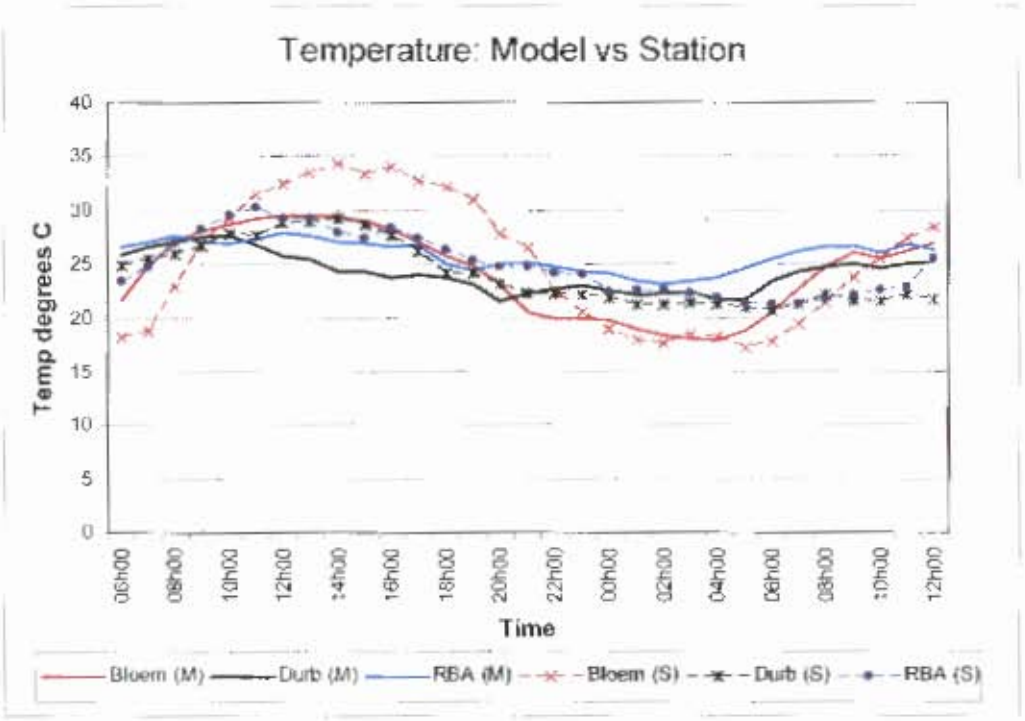

Figure 5.6 cont: Comparisons between temperature from model output and SAWS station data for three locations in South Africa.

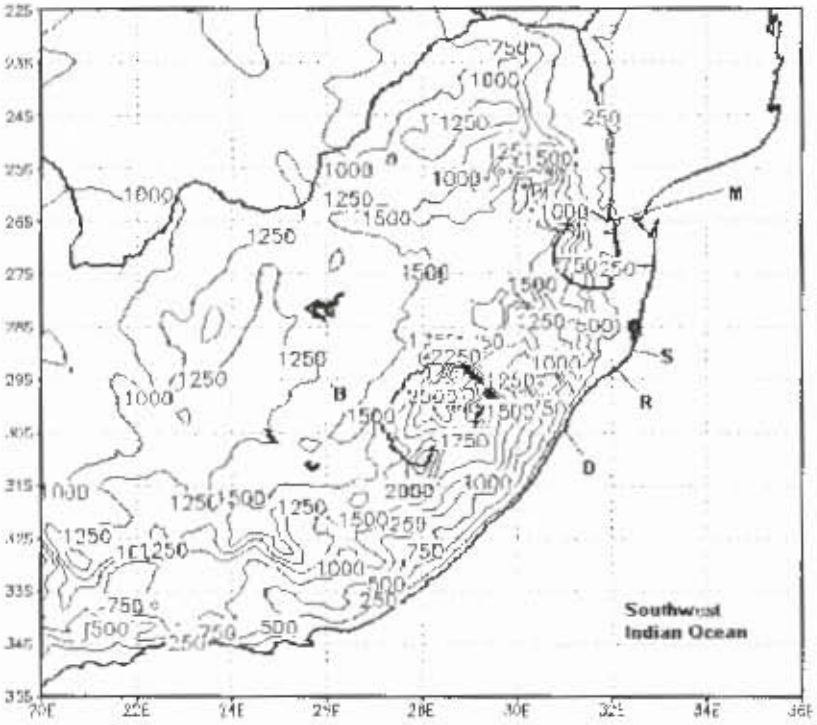

Figure 5.7 : Map showing the topography (250m contour interval) of the eastern half of South Africa, as well as the location of some of the weather stations (D – Durban; R – Richards Bay; S – Cape St Lucia; M – Mananga station and B – Bloemfontein).

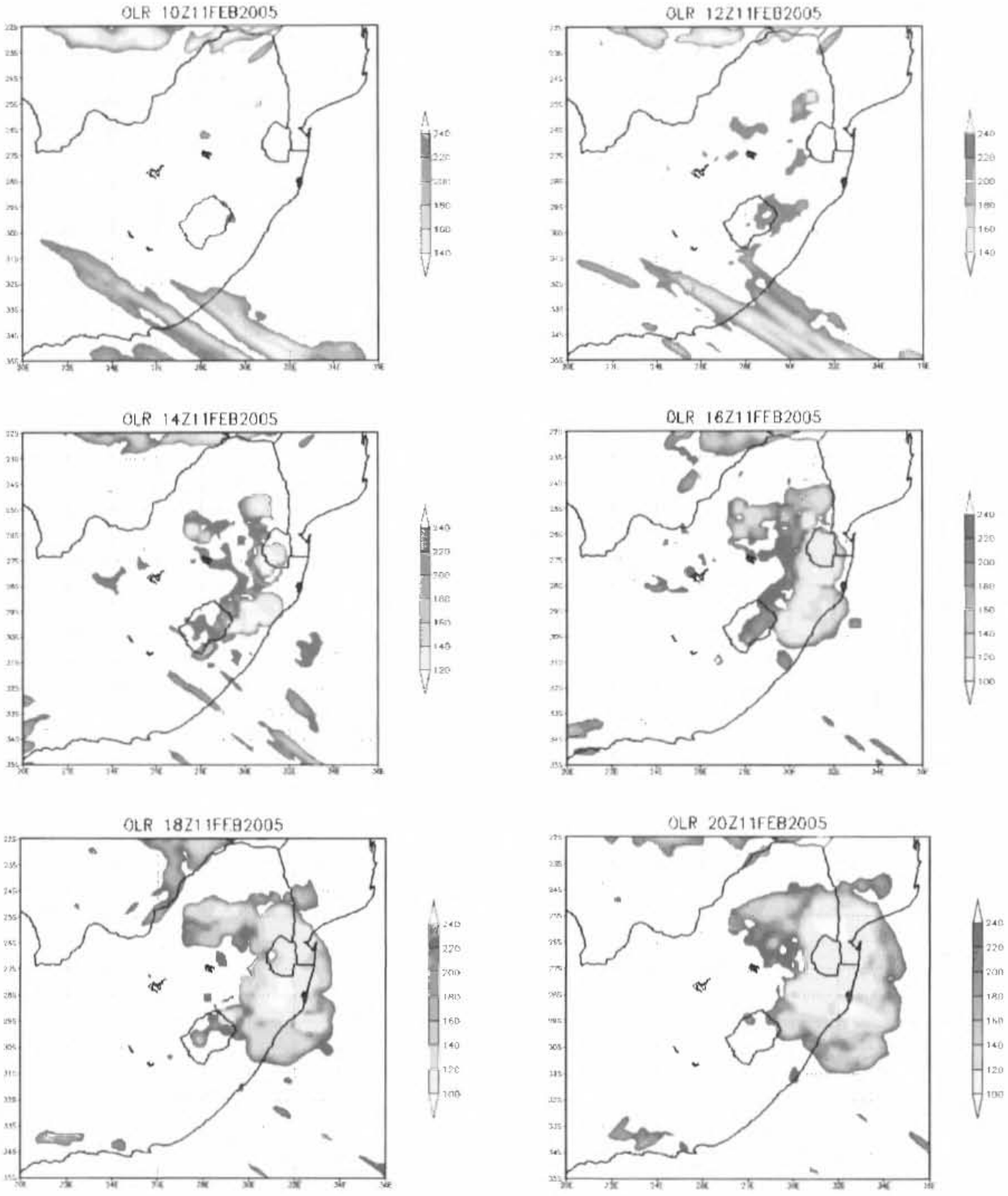

Figure 5.8: Domain one outgoing longwave radiation (interval, 20 w.m^{-2}) derived from the control simulation. Starting at 10h00 UTC on the 11 February and ending at 20h00 UTC (at 2 hour intervals).

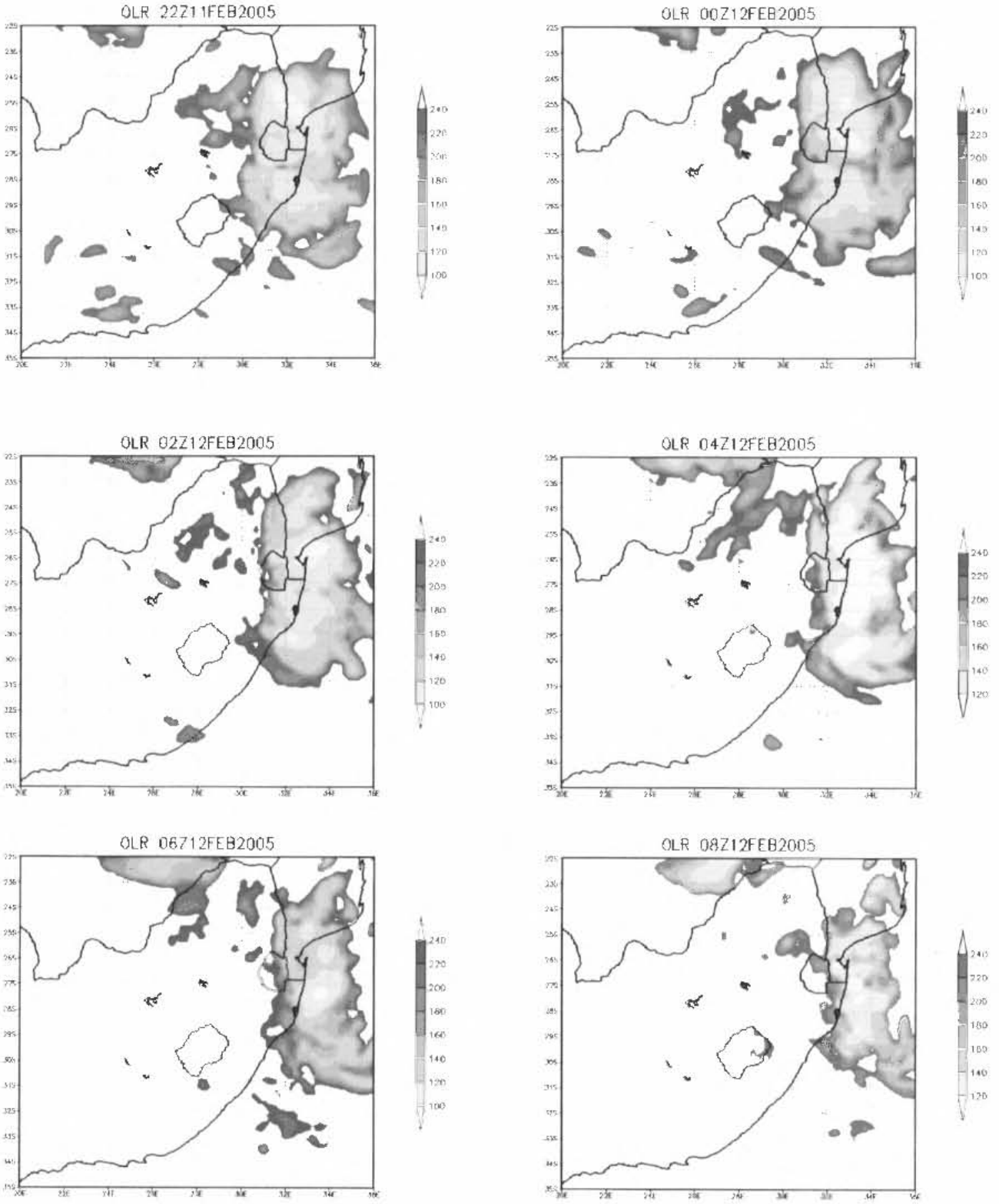

Figure 5.8 cont: From 22h00 UTC 11 February to 08h00 UTC on the 12th.

a)

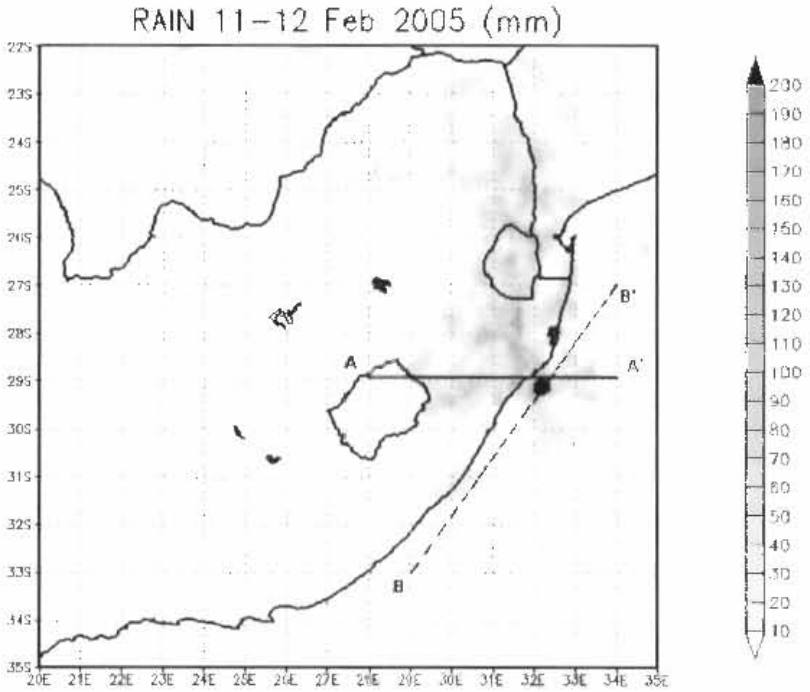

b)

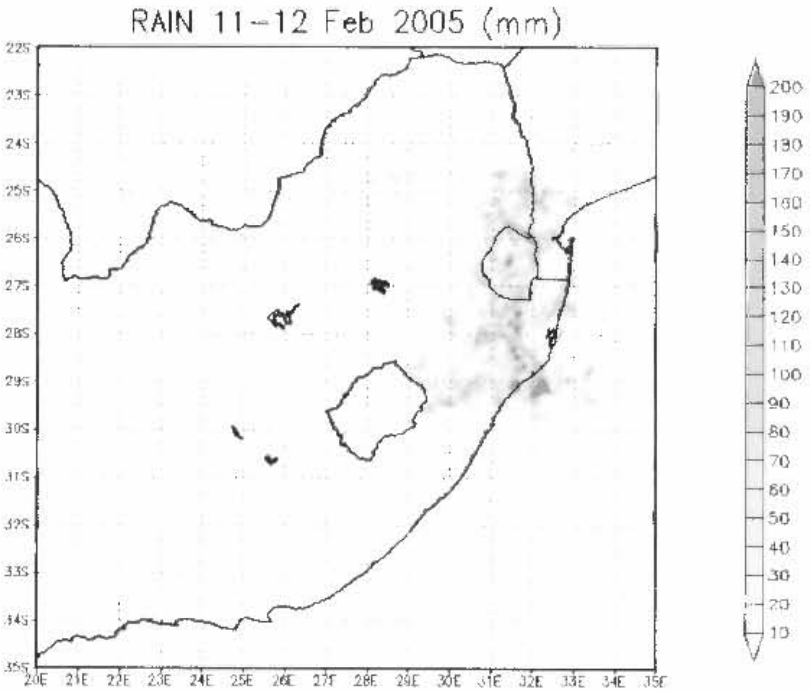

Figure 5.9: MM5 simulated precipitation for the 11 and 12 February 2005 for a) domain one and b) nested domain.

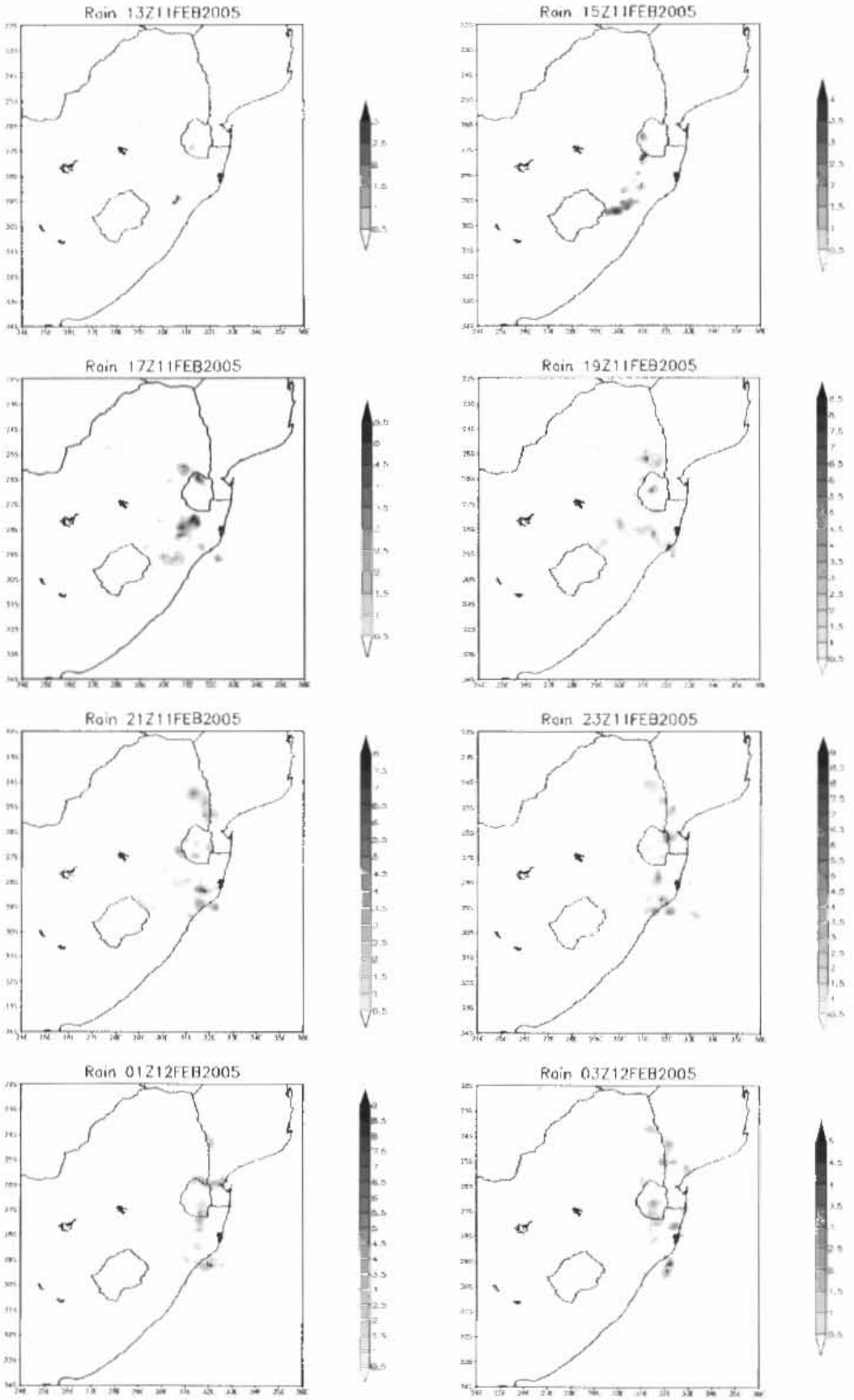

Figure 5.10: Hourly simulated precipitation (interval at 0.5 mm) from the control run. At 2 hour intervals, starting at 13h00 UTC 11 February and ending 03h00 UTC on the 12th.

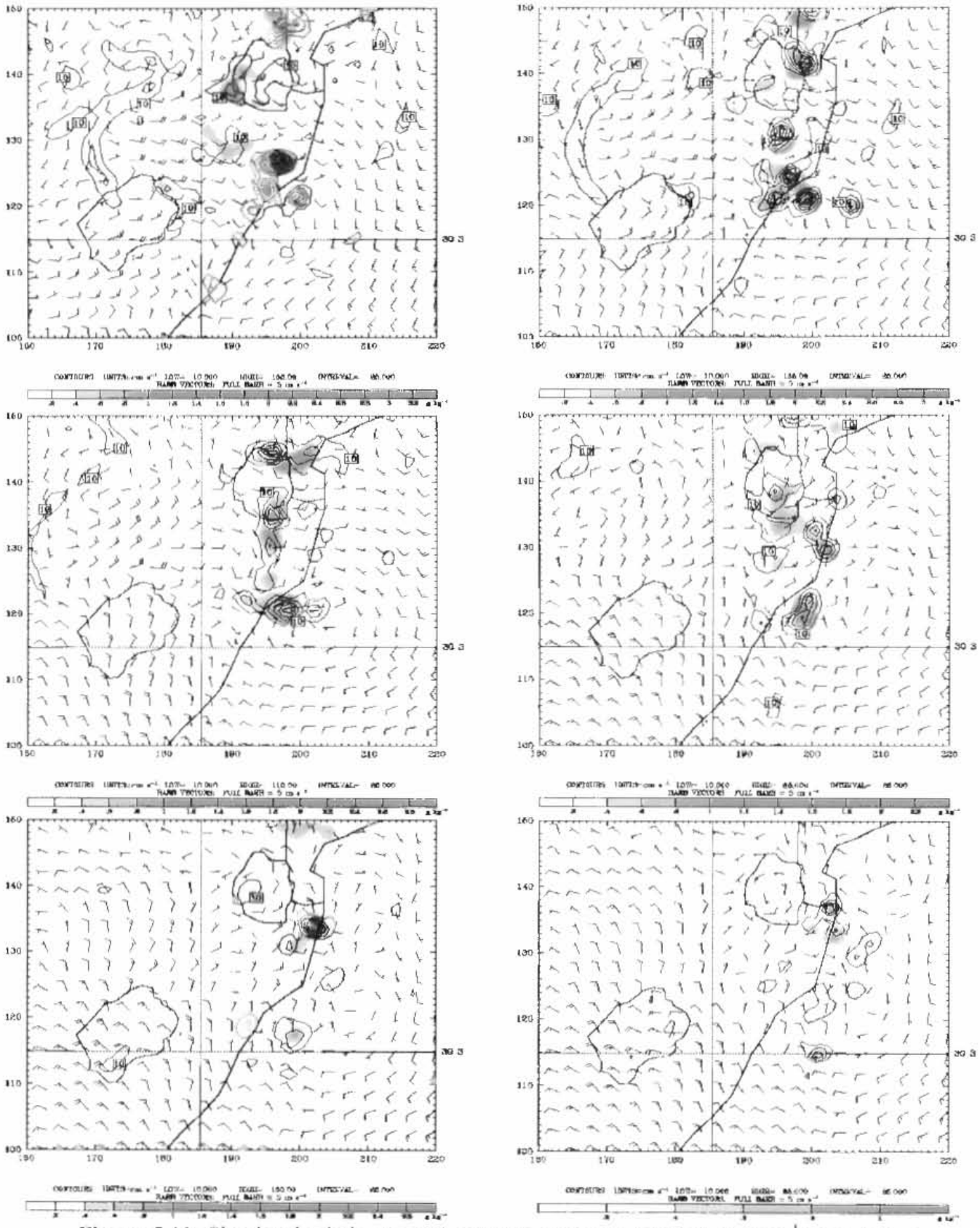

Figure 5.11: Simulated winds, vertical velocity (contour; interval 25 cm.s^{-1}) and rain water mixing ratio (shaded; starting at 0.4 g kg^{-1}) at the 750 hPa level. Starting at 20h00 UTC on the 11th and ending at 06h00 UTC on the 12th, at 2 hour intervals (left to right). Only areas with upward motion (greater than 10 cm s^{-1}) are shown for clarity.

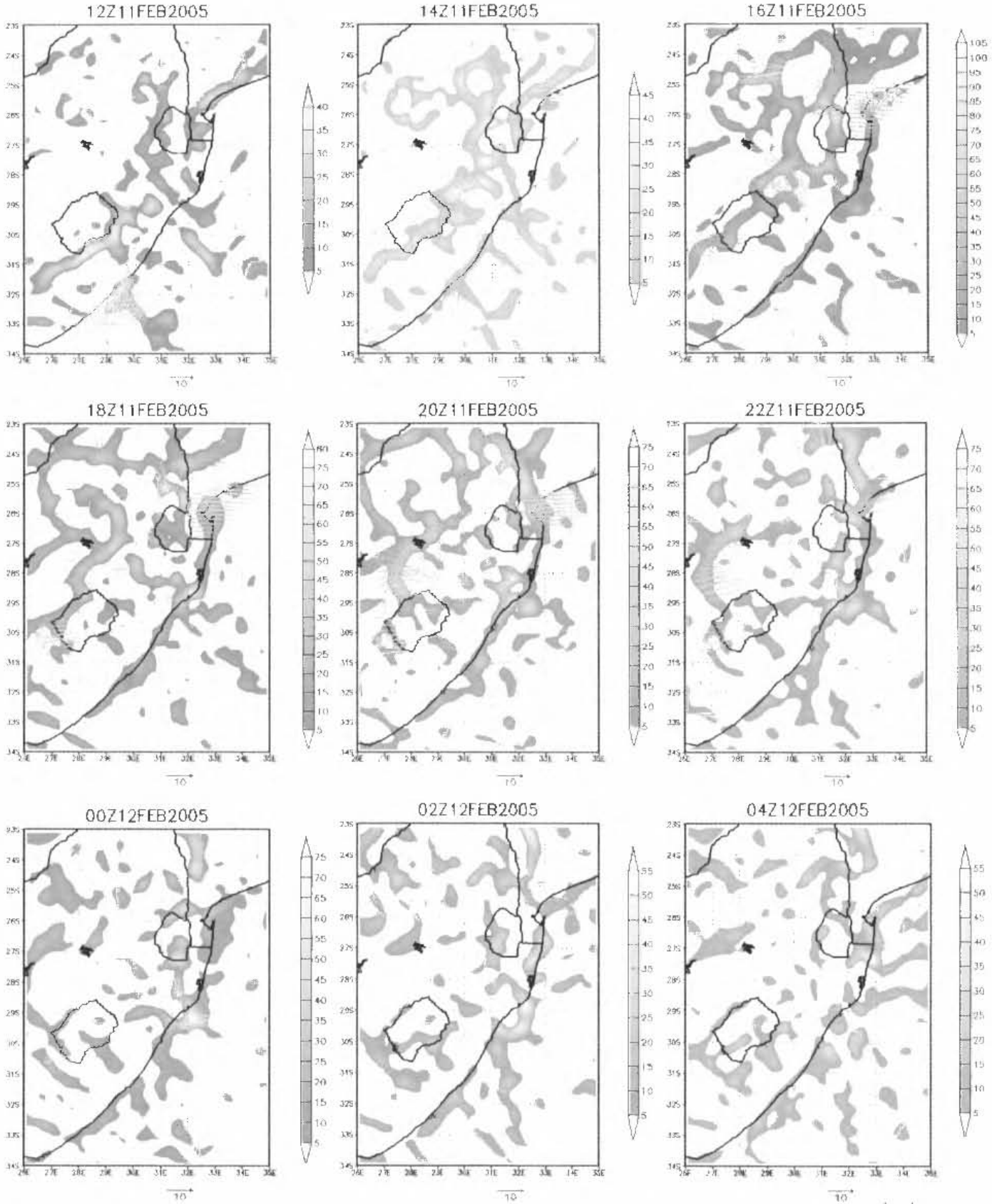

Figure 5.12: Moisture convergence (shaded positive values with interval of 5 $g.kg^{-1}.s^{-1}$) and wind speeds greater than 10 $m.s^{-1}$ at the 0.955 sigma level from the control simulation. Starting at 12h00 UTC 11 February through to 04h00 UTC on the 12th, at 2 hour intervals. Note that divergence has been omitted for clarity.

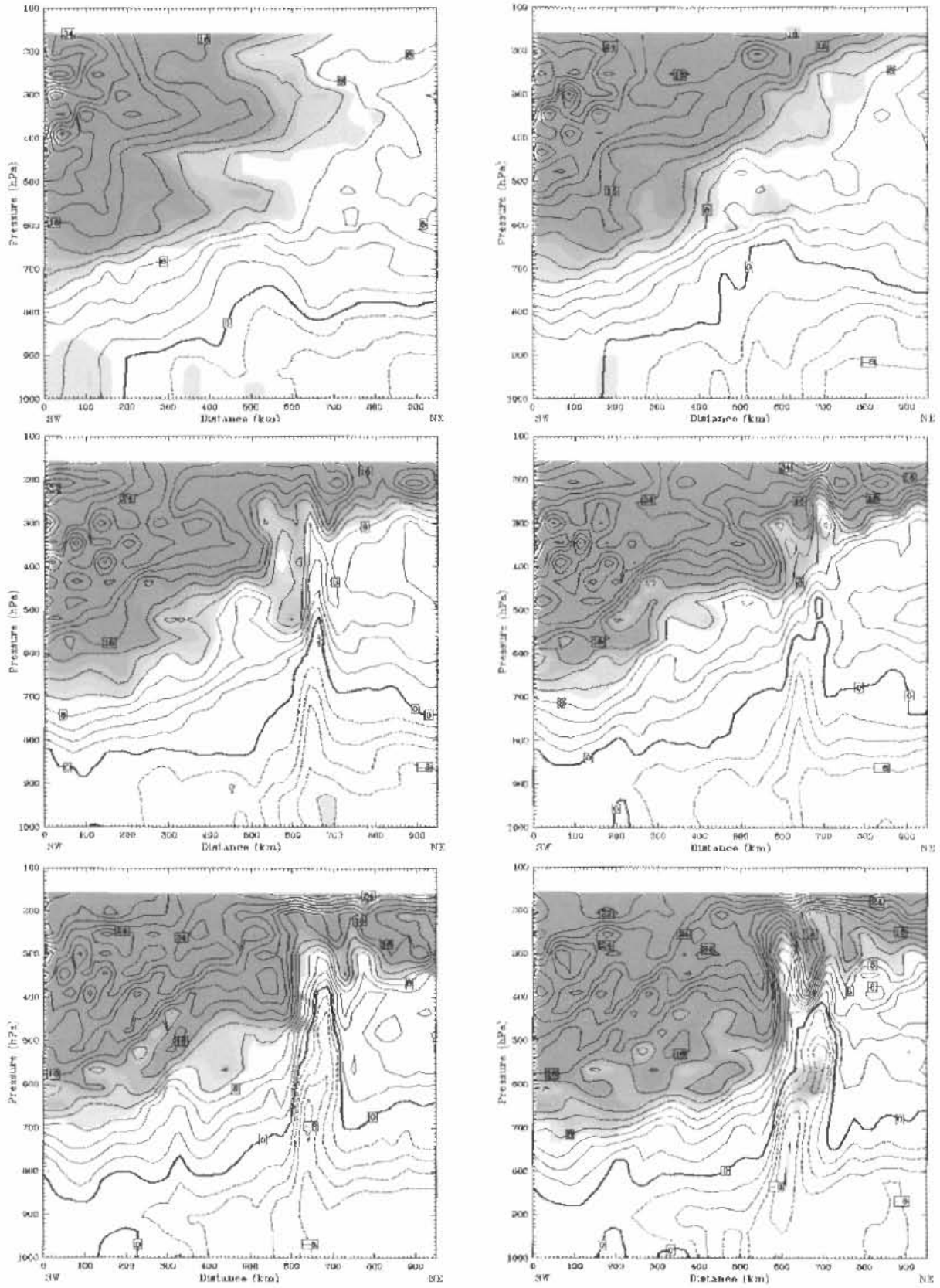

Figure 5.13: Vertical cross-sections of wind speeds starting at 10 $m.s^{-1}$ (shaded; 5 $m.s^{-1}$ interval) and zonal wind speeds (contour; 2 $m.s^{-1}$ interval) from the control simulation along B-B' in figure 5.9. From left to right starting at 14h00 UTC 11 February (top) and ending at 00h00 UTC (bottom).

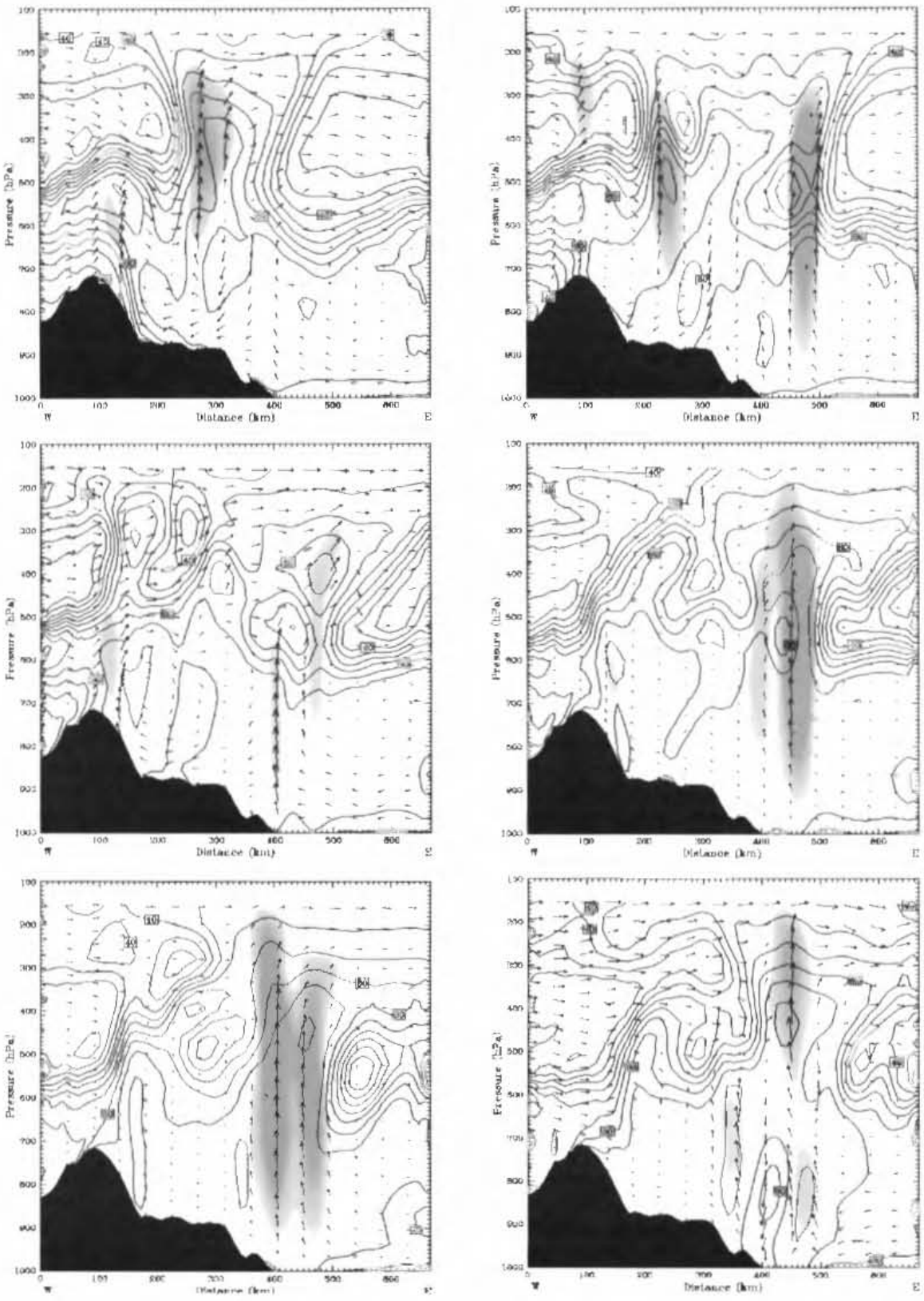

Figure 5.14: Vertical cross-section along A-A' (see figure 5.9) of wind vectors, vertical velocity greater than 40 cm.s^{-1} (shaded) and relative humidity (contours with an interval of 10%) from the control simulation. From left to right, the figures are for 15h00 UTC 11 February (top left) through to 01h00 UTC (bottom right) at a 2 hour interval.

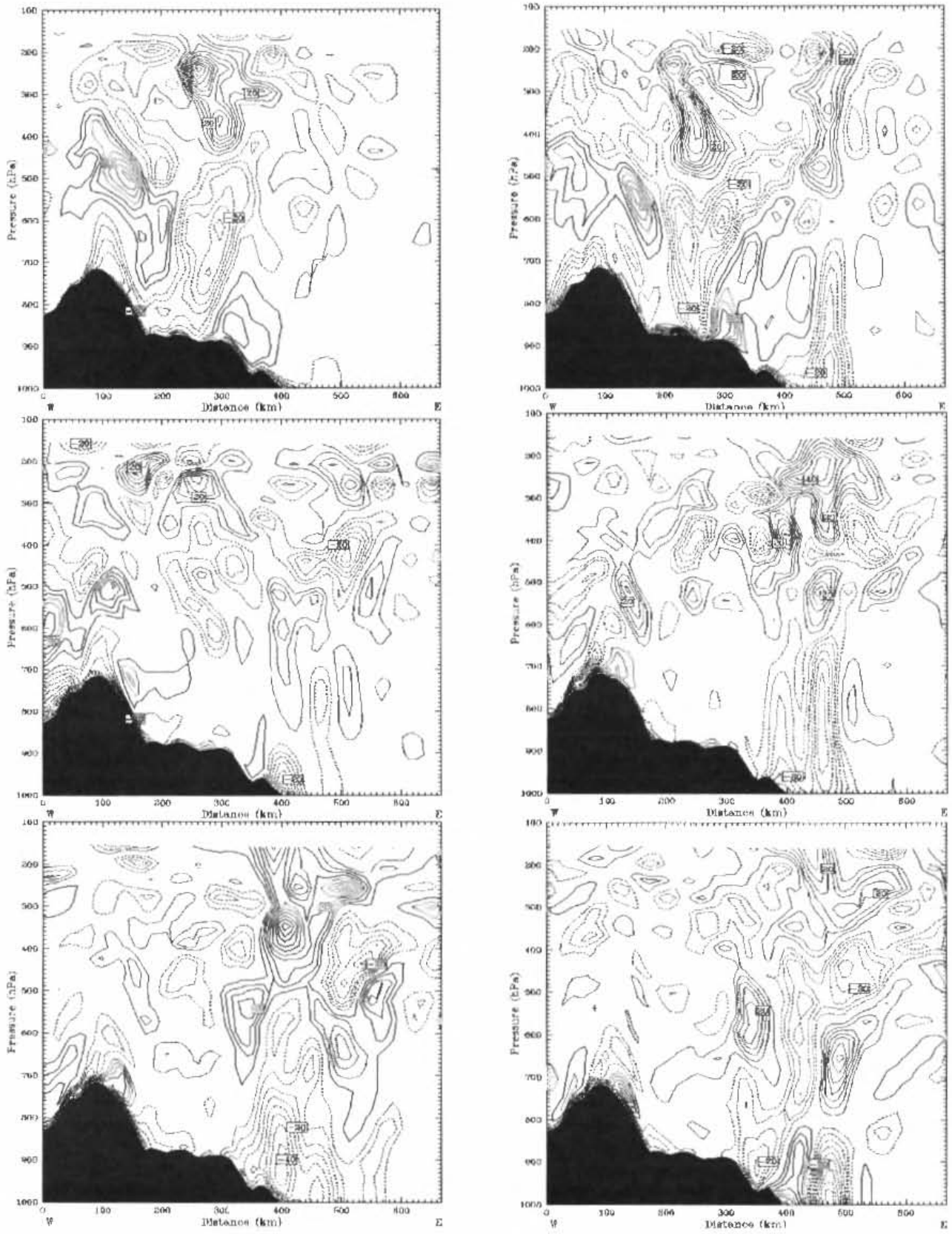

Figure 5.15: Vertical cross-section of divergence (interval 5 s^{-1}) along line A-A' found in figure 5.9. Starting at 15h00 UTC 11 February (2 hour intervals) and ending at 01h00 UTC. Note that in these figures divergence is positive (solid contours) and convergence is negative and dashed.

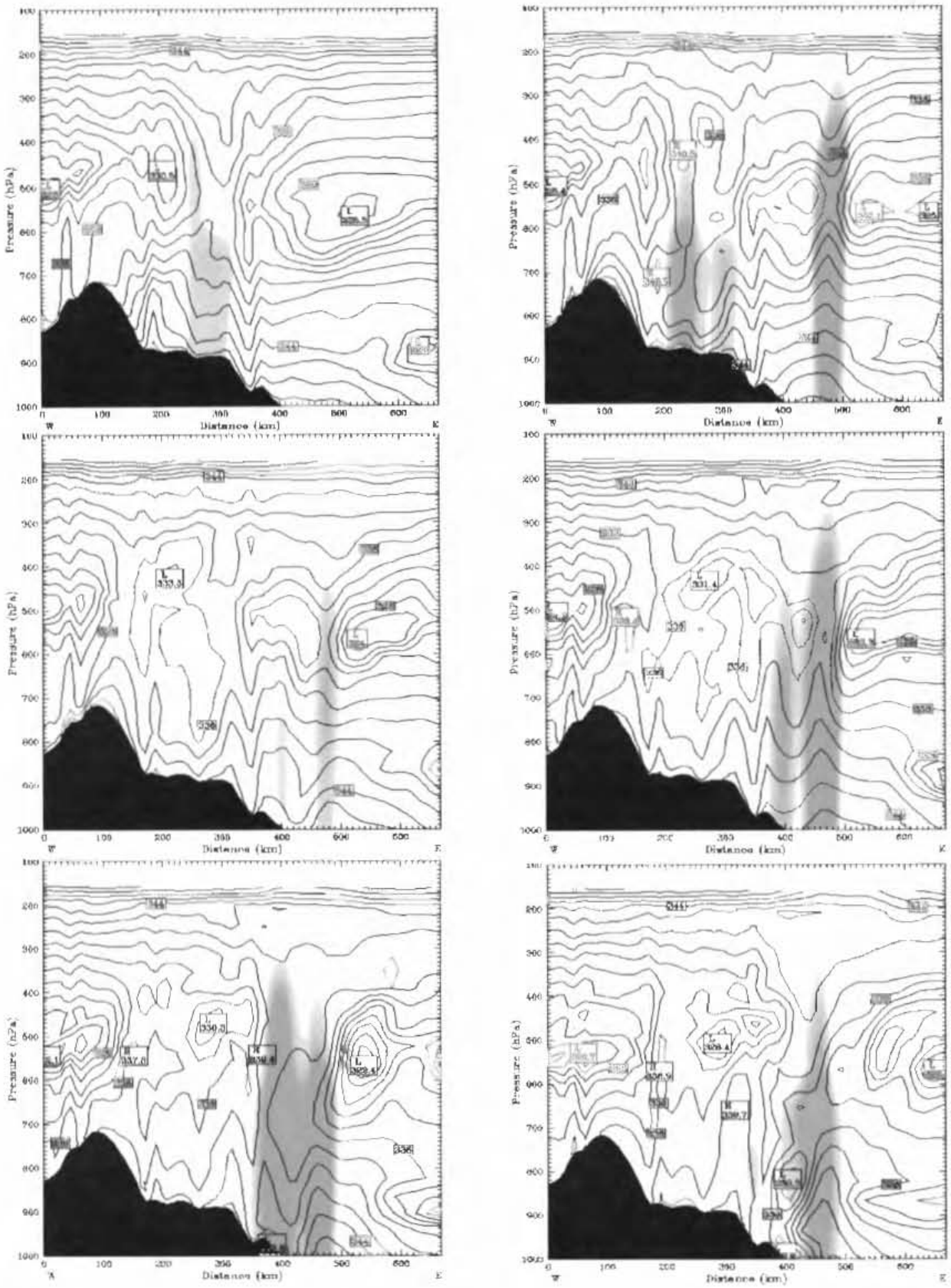

Figure 5.16: Vertical cross-section of equivalent potential temperature (interval 2°K) along line A-A' found in figure 5.9. The gray shaded region indicates areas with a rain water mixing ration greater than 0.4 g.kg^{-1}. Starting at 15h00 UTC 11 February (2 hour intervals) and ending at 01h00 UTC.

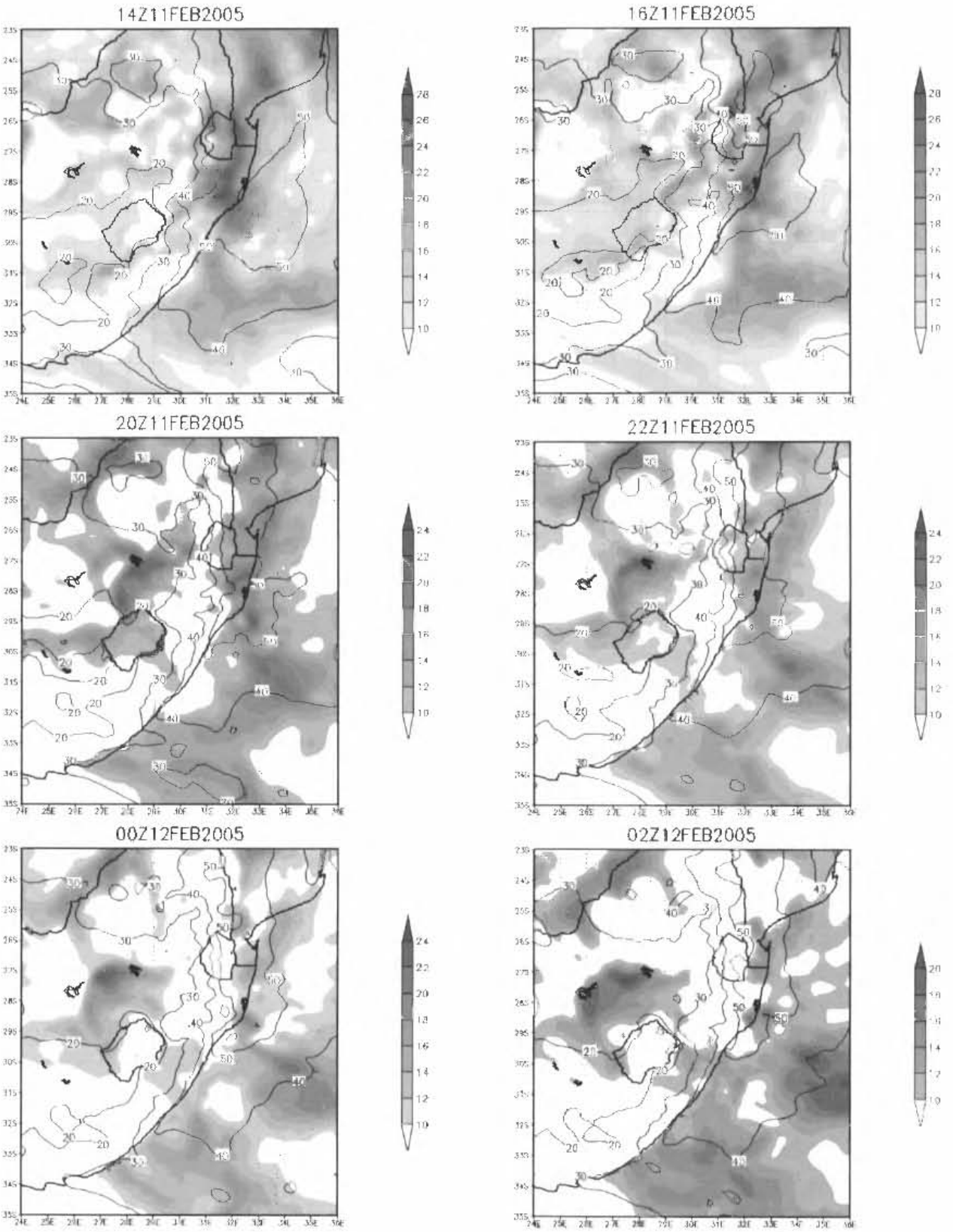

Figure 5.17: Convective instability (shaded; 2°C interval starting at 10°C) and precipitable water (contour, 10 mm interval) over the eastern parts of South Africa. Starting at 14h00 UTC 11 February and ending at 02h00 UTC, at 2 hour intervals.

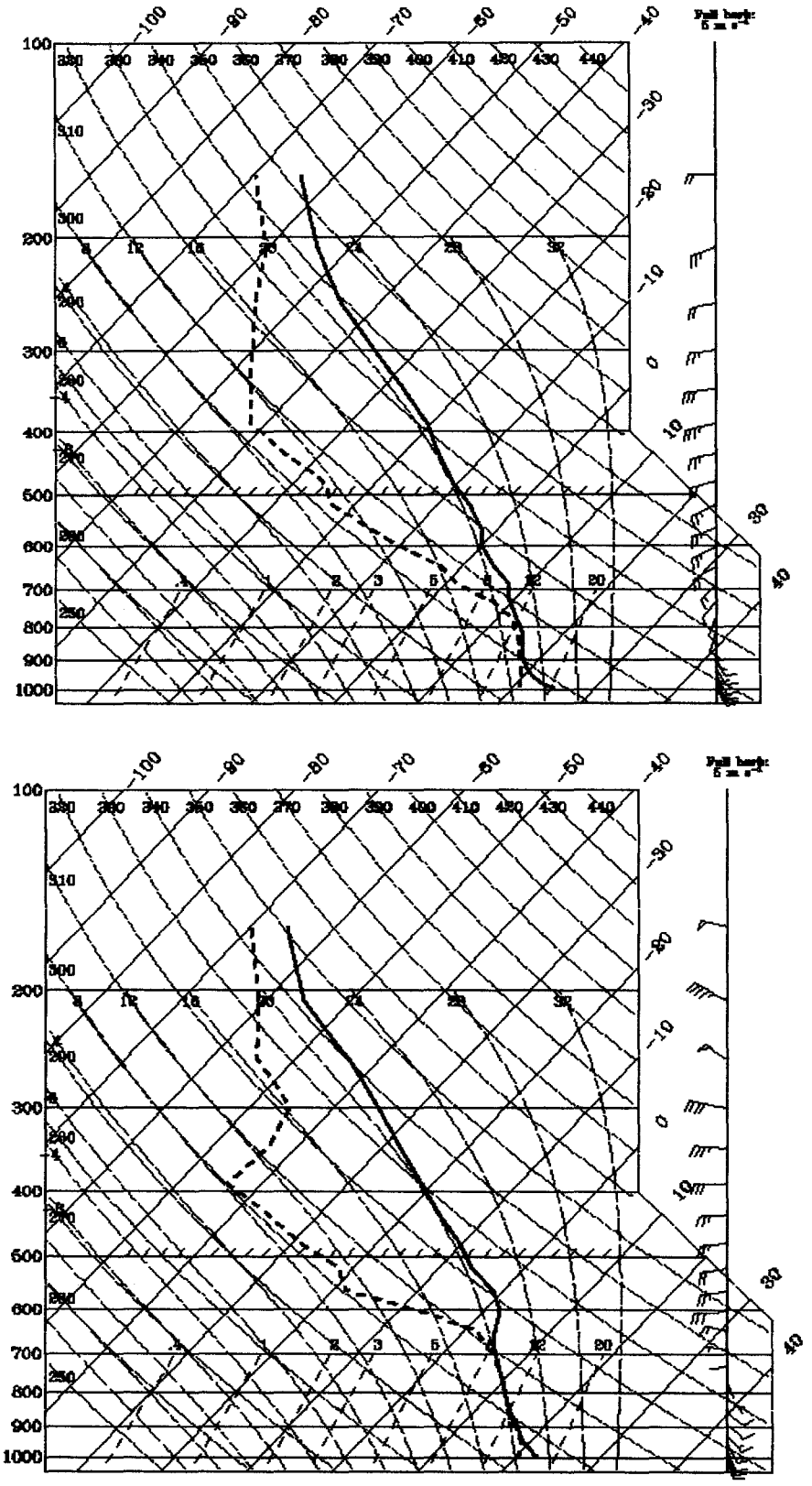

Figure 5.18: Soundings from the control simulation located at 29.97°S; 30.95°E (Location of Durban station) at 12h00 UTC 11 February 2005 (top) and 00h00 UTC 12 February 2005 (bottom).

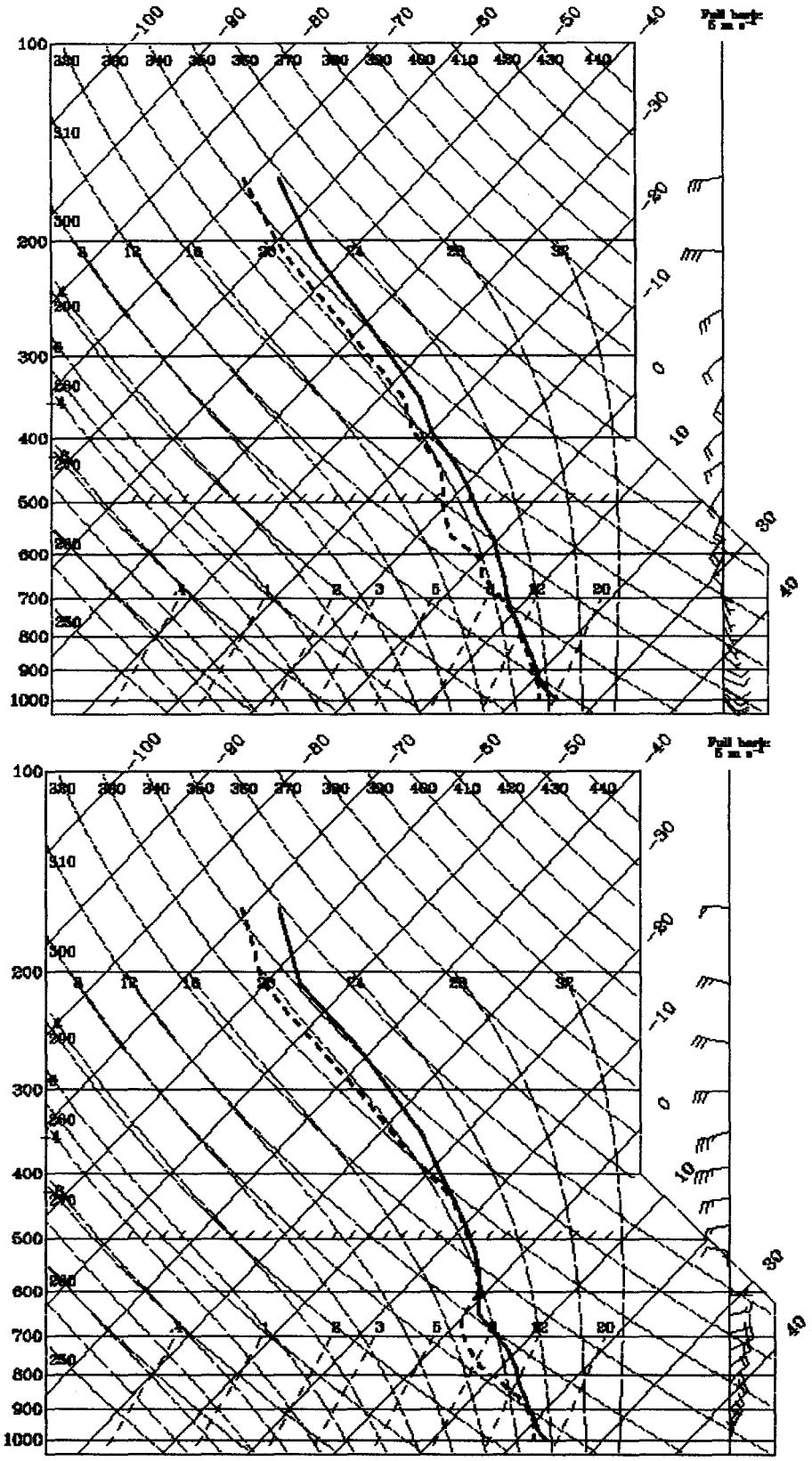

Figure 5.18 cont: Soundings from the control simulation located at 28.73°S; 32.8°E (Location of Richards Bay station) at 18h00 UTC 11 February 2005 (top) and 00h00 UTC 12 February 2005 (bottom).

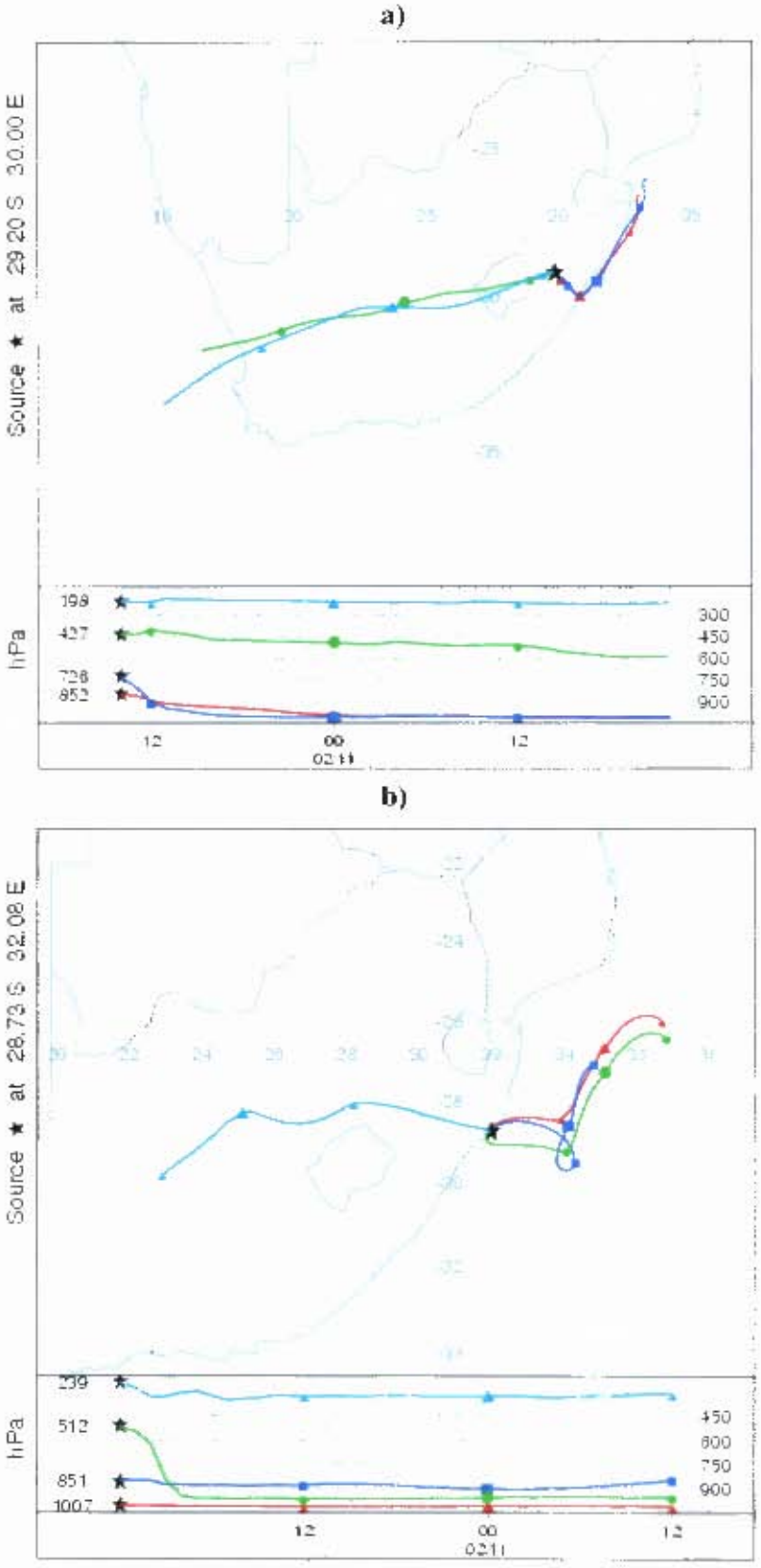

Figure 5.19: 36 hour backward trajectories of air parcels released at a) 14h00 (UTC) 11 February 2005 and at b) Richards Bay station at 00h00 UTC on the 12th. The location coordinates are found on the left hand side of the image, while the altitude of the different air parcels are found in the bottom panel.

c)

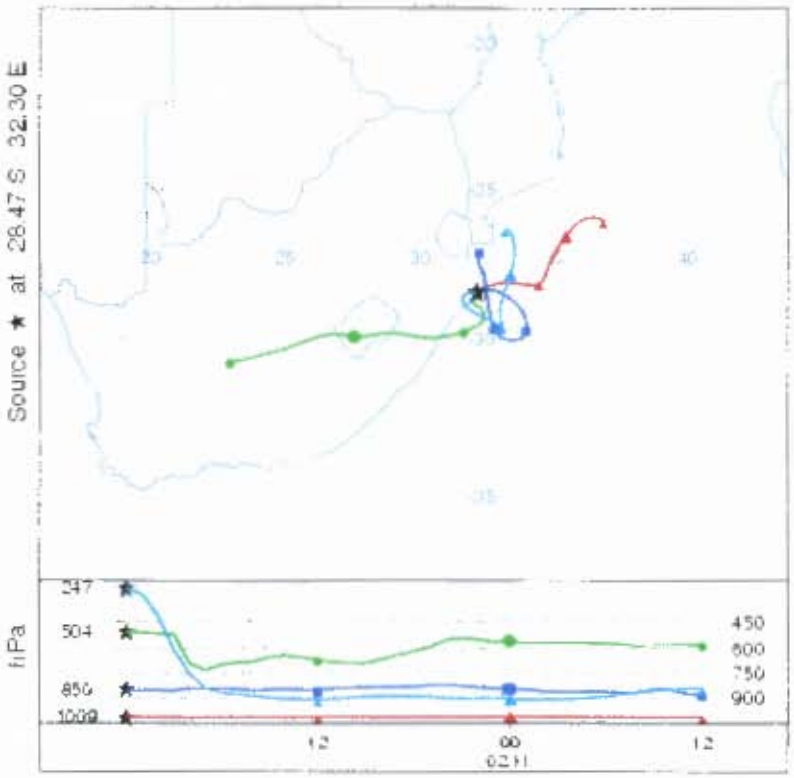

d)

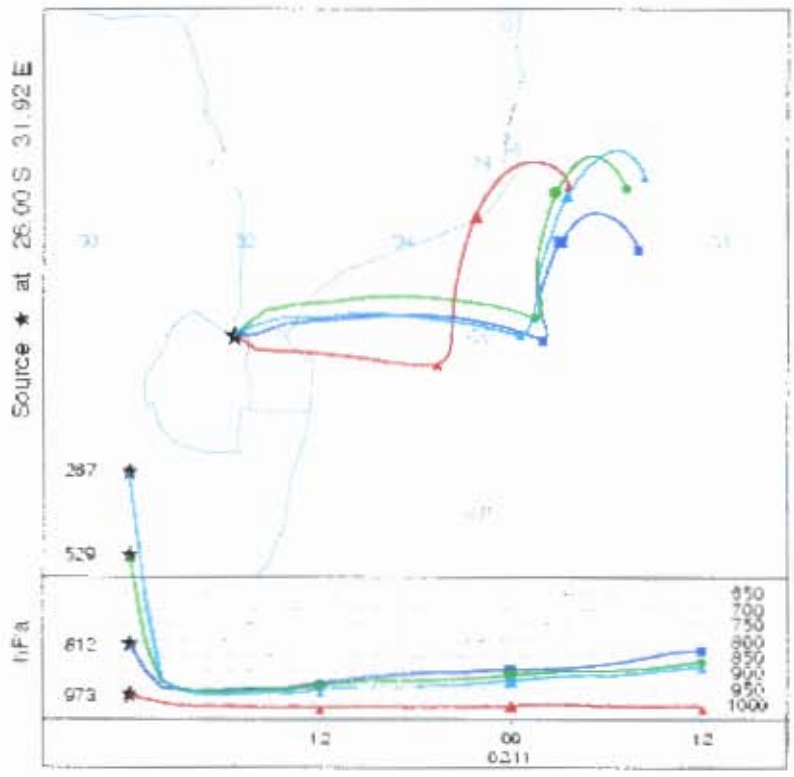

Figure 5.19 cont: 36 hour backward trajectories of air parcels released at c) Ulloa Agricultural College and d) Mananga station at 00h00 UTC 12 February 2005.

Chapter 6

Sensitivity Tests – The Role of SST, Topography and the Mid-latitudes

6.1. Introduction

The importance of the initial and boundary conditions in mesoscale models has become increasingly recognized over the last few decades. From this case study, there are two local features that appeared to have played a significant role in the life cycle of the system, but to what extent remains uncertain. Topography appeared to have had an influence in the initiation of the system, while the Agulhas Current region appeared to play a crucial role in supplying moisture for the system to develop. On the synoptic scale, weather phenomena in the mid-latitudes south of South Africa are also known to influence the weather patterns over the country. In chapter four it was evident that certain synoptic features propagating eastwards along the southern part of South Africa played a role in the evolution of this particular convective event.

This chapter provides the results from three other simulations, which are used to identify the role of the above mentioned features found within and around South Africa. In the process, it will also highlight the sensitivity of the simulation when a certain aspect is changed, namely the representation of the topography, SSTs and mid-latitudes. Each simulation is presented separately, with a brief introduction on the feature that is being changed is given, which is then followed by the results and discussion. Further details about the general model setup for the simulations can be found in chapter three. As mentioned in the previous chapter, the success of numerical simulations of mesoscale convective systems is usually determined by the simulated precipitation distribution and intensity as well as features of the systems development, such as the initiation or propagation. Thus, for this section the results of the precipitation and OLR from the simulation are compared with the observed conditions and the results from the control simulation. This is then followed with a brief discussion of what may have influenced the

results found in the simulations, more specifically what features or factors on the synoptic scale and local scale may have influenced any differences.

6.2. SST Sensitivity Test

6.2.1. Introduction

The Agulhas Current is an influential feature found along sections of the South African coastline. As suggested by Rouault et al. (2003), the influence of the Agulhas Current as a moisture source for heavy rainfall events, may be substantially underestimated by certain reanalysis datasets since the narrow core of the current cannot be adequately represented by the operational models. This is possibly due to the underestimation of surface fluxes of sensible and latent heat in the Agulhas region in the NCEP and European Centre for Medium-range Weather Forecasting (ECMWF) reanalysis data (Rouault et al. 2003). To asses the potential contribution of a better resolved Agulhas Current in the storm evolution, a higher resolution SST dataset was used in another model simulation. The higher resolution data used is that of the AVHRR SST data, which was discussed in more detail in chapter three. Figure 6.1 shows a comparison between the two datasets that are used in the different model simulations. From this figure it can be seen that the lower resolution data still captures the general surface temperature gradients, but the higher resolution SST data better represents the finer scale features, such as the core of the Agulhas Current and the steep SST gradients. In the AVHRR SST data, there is no data over land, which may have some impact on the model simulation, thus the OISST data is superimposed over this region.

6.2.2. Convective System and Precipitation

The intensity of the precipitation appears to be greater in the SST sensitivity simulation (figure 6.2) when compared to that found in the control case (see figure 5.9). This is shown by the increase in the simulated precipitation over most parts of KZN. However, it is apparent that the precipitation distribution in KZN is similar to the observed (see figure 4.1), since most of the heavy precipitation occurred along the north coast, particularly

around the Richards Bay region. It is also evident that the SST sensitivity simulation achieved a better result in simulating the precipitation that occurred over the KZN interior and the small amounts found along the southern parts of the KZN coastline. The precipitation distribution also indicates that a large quantity fell over the ocean just off the east coast, but this cannot be validated due to the lack of observations from this region. It should also be noted that an under-estimation in precipitation occurred along the northern parts of Swaziland, particularly in the Mananga station region, which received in excess of a 100 mm during the event.

In terms of storm development, it is evident from the OLR images (figure 6.3) that the system in SST sensitivity simulation developed along the eastern escarpment during the afternoon of 11 February 2005. The evolution pattern appears very similar to that found into the control simulation (see figure 5.8), since after initiating, the single storm cells merged and evolved into a large mesoscale system. Comparisons between the OLR figures in the control simulation and the SST sensitivity simulation reveal that the system obtained a similar size in both simulations, as well as obtaining the maximum size around the same period (between 22h00-00h00 UTC). There is evidence that the simulated system in the SST sensitivity simulation appeared to decay at a slower rate in the early morning hours of the 12th, when it was located over the Agulhas Current region. Figure A6.1, showing hourly precipitation, support the OLR results, since most of the heavy precipitation along the northern coastal region took place during the evening and night on the 11 February in the SST sensitivity simulation, which is similar to that found in the control run. It is also apparent that the heavy precipitation off the east coast continued to take place in the early morning hours of the 12th, which supports the suggestion that the system took slightly longer to dissipate, as found in the OLR images.

From the precipitation and the OLR results, it is evident that the higher resolution SST, with all else being equal, leads to an excess of precipitation simulated over the coastal regions as well as over the Agulhas Current region. It was obvious that very similar features of the simulated MCS, such as size and evolution, occurred in the SST sensitivity simulation when compared with the control run. However, a noticeable difference was

the size of the system in the latter stages of the SST sensitivity simulation, since it was still well developed along the poleward section during the morning hours of 12 February. It should be remembered that in the satellite imagery (in chapter four) there also appeared to be a bias towards the development of the poleward side of the system, since it was found to be larger and more developed. This could explain the excessive precipitation found off the east coast in the SST sensitivity simulation. It is possible that the higher resolution SST data may have influenced the evolution of the system over the coastal regions and neighbouring Agulhas Current.

6.2.3. Synoptic and local conditions

The low level synoptic conditions (figure 6.4) in the SST sensitivity simulation are very similar to that found in the control run. During the morning of 11 February, a frontal system passed to the south of the country. This feature is still visible during the early afternoon in the OLR images (figure 6.3). The presence of an interior trough is also evident in figure 6.4. However, as identified in the control simulation, this feature appears weaker than that found in the observations, which is shown by the higher values of SLP. As found in the control simulation, the pattern of an anticyclone ridging to the south of the country during the 11-12 February is evident in the SST sensitivity run. The feature was located to the southwest of the country during the morning hours of the 11th and by the late afternoon it had propagated further eastwards to the south of the country. As will be discussed later in this section, this single feature played a key role in the lower level circulation patterns over the KZN region during the event.

Figure A6.2 shows temperature, geopotential height and areas of strong wind at the 500 hPa sigma level found in the SST sensitivity simulation. The propagation of a westerly wave from the west during the early morning hours of 11 February is apparent. By midday it was located over the southern parts of the country, before propagating out into the Southwest Indian Ocean during the late afternoon. It is evident that the synoptic pattern at this level is very similar to that identified in the control run. Results from the

SST sensitivity simulation suggest that at 200 hPa level (not shown), the synoptic conditions were also identical to those found in the control simulation.

At the 0.525 sigma level, the direction and magnitude of the winds in the SST sensitivity simulation (not shown) are also similar to that found in the control run. With westsouthwesterly winds dominating at this level over the eastern region of South Africa on 11 February, which are then replaced with westerly winds during the morning of the 12^{th}.

Circulation patterns at the lowest level in the SST sensitivity simulation showed that continuous onshore flow along the east coast took place during the event (figure 6.5). The direction and magnitude of the winds at this level in the SST sensitivity simulation are similar to the corresponding winds in the control simulation. As identified in the control simulation, the anticyclone ridging to the south of the South Africa played an important role in the development of these onshore winds. It is likely that in the SST sensitivity simulation, these onshore winds advected more moisture into the region due to the higher resolution SST data used in the initial conditions. It is also expected that the development of the ducted ridge, which occurred at the lower to mid-levels (figure A6.3), would have aided in the onshore moisture advection. It is evident that the onshore flow component of the ridge coincided with regions that contained strong upward motion and a high precipitable water content.

Vertical cross-sections of wind speed and zonal wind (figure 6.6) off the east coast suggest that the onshore winds in the lower levels were a dominant feature through much of the event in the SST sensitivity simulation. Vertical cross-sections of meridional wind (not shown) along the same transect indicate that the early afternoon flow contained more of a southerly component compared to the late afternoon and night flow. There is also evidence of a weak easterly LLJ developing during the night, which was not identified in the control run. In this case, this feature is arbitrarily defined as a narrow low-level region of winds exceeding speeds of $10 m.s^{-1}$ in the lower levels, which was likely to have advected more moisture into coastal KZN and hence, resulted in more precipitation.

Figure 6.7, the 1000hPa moisture flux values from the SST sensitivity simulation, indicates that large quantities of moisture were advected into the region during the event. During the afternoon, most of the moisture used to fuel the system originated from the southeast of KZN. This southeasterly advection pattern continued until the evening, after which it was then replaced by easterly advection. This moisture advection pattern is consistent with the circulation in the lower levels of the atmosphere, as identified in figures 6.5 and 6.6.

Figure 6.8 shows the low level moisture convergence found over the eastern region of South Africa during the event in the SST sensitivity simulation. During the early afternoon the low level moisture convergence was mainly confined to the eastern escarpment, but by mid-afternoon, low level moisture convergence was found all along the coastal region. The low level moisture convergence along the coastal regions was a prominent feature through most of the night and early morning hours. This moisture convergence over the coastal region was also evident in the control run (figure 5.12) and the convergence values between the two simulations are very similar.

The large quantity of moisture advected at the lower levels over the coastal region is reflected in soundings taken from the SST sensitivity simulation. It is apparent that soundings taken over the Durban and Richards Bay region (both not shown) suggest that the lower atmosphere was near saturation during the afternoon and night. The soundings also indicate that the atmosphere was conditionally unstable, which is supported by figure A6.4 and that the region in which the MCS was located contained a high precipitable water content (over 50mm during the night).

Vertical cross-sections along transect C-C' in the SST sensitivity simulation (see figure 6.2) suggest that the nocturnal heavy precipitation was due to a combination of factors that were present for much of the night. These factors included strong low level convergence and mid-level divergence that took place in a region that contained a high moisture content (figure 6.9). Strong upward vertical velocities and persistent onshore

flow in the lower levels over the coastal regions were also identified in the vertical cross-sections (not shown). It was also evident from these cross-sections that the coastal regions of heavy precipitation, contained high relative humidity values (not shown), which were also found in SAWS station data along the northern coast. However, most importantly, these vertical cross-sections indicate the factors favourable for convection were evident through most of the late afternoon, through to the morning hours the following day. This ongoing pattern likely resulted in the heavy precipitation along the north coast of KZN.

6.3.4. Simulation Summary

An analysis of the synoptic conditions found in the SST sensitivity simulation suggests that similar large scale features were present during the evolution of the event, as identified in the control run. These features had an influence on the evolution of the event by influencing the circulation patterns throughout the atmosphere. The results also suggest that that local conditions identified in the SST sensitivity simulation favoured the development of an MCS and the associated heavy precipitation.

It was evident that large quantities of moisture appeared to be advected into the east coast region in the SST sensitivity run, which may explain the increase in precipitation when compared to the control case. Similar favourable conditions for the formation of convection as identified in the control case were found in this simulation, namely the presence of a coupled low level convergence/mid-level divergence pattern, a convectively unstable atmosphere, strong upward vertical velocities and abundant moisture. It is also possible that sustained conditions favouring the development of convection during the late afternoon and night may have resulted in the over-estimation of heavy precipitation in this particular sensitivity simulation.

It is likely that an increase in the SST resolution lead to more moisture being transported into the east coast region, but to what extent this influenced the extreme precipitation pattern is not so obvious. It was also apparent in the SST sensitivity simulation that, when the convective system was positioned over the Agulhas Current region, it took longer to

dissipate. This result suggests that fluxes over this warm current and the close proximity of moisture may have strengthened the system. It should be remembered that the AVHRR data contains a high spatial resolution, but, temporally, it still remains at a weekly a resolution. It is possible that the exclusion of diurnal and sub-weekly SST variability in the run may lead to differences in the simulation.

Ultimately, it has been established that most of the moisture used to fuel the extreme precipitating system originated from the Agulhas Current region. These results reinforce the hypothesis that the Agulhas Current plays a key role in extreme precipitation events found in South Africa, as identified in other research (e.g. Rouault et al. 2002; Singleton and Reason, 2006, 2007). Thus, further research on the influence that this warm current has on MCSs over the east coast and the mechanisms responsible for the advection of moisture in to the region is required.

6.3. Topography Sensitivity Test

6.3.1. Introduction

The eastern escarpment is made up of topography extending up to around 3000m in certain regions and is believed to play a role in triggering mesoscale convective systems in South Africa (Laing and Fritsch, 1993b). It was found in the control simulation that the high-lying topography along the eastern escarpment more than likely had an influence on the initiation of the convective system that took place on the 11-12 February 2005. Thus, most of the focus in this simulation is on the role the eastern escarpment played in the development of this convective system. The coastal topography may have also provided the initial uplift that produced the heavy precipitation along the northern KZN coastline. However, it should be noted that the coastal topography is not as significant in height when compared to the inland topography. Thus, it is likely a combination of factors, including the coastal topography, that result in providing the favourable conditions for heavy precipitation along the coastal region.

Figures 6.10 and 6.11 shows the two topographic settings used in the different model runs, whereby one uses full topography (the control simulation) and the other has the terrain height reduced by 75 % everywhere (the topography sensitivity simulation). It can be seen in these figures that the topography used in the sensitivity test is a lot smoother and contains much weaker gradients. However, it should be noted that it is likely that topographic effects do not entirely disappear when reducing the topography prior to the simulation. As discussed by Romero et al. (2000), the initial fields for the simulation are based on analysis data that will contain orographic effects. In this case, the initial and boundary MRF fields are based on analysis that will have contained some representation of topographic effects, thus the results of such a sensitivity test should be viewed with caution.

6.3.2. Convective System and Precipitation

The precipitation pattern, shown in figure 6.12, appeared to have changed considerably after the terrain was reduced in this particular sensitivity test. It is evident that most of the precipitation is now confined to the extreme northeastern parts of KZN, Mpumalanga, southern Mozambique and parts of Swaziland. In the figure, the colour bar indicating total accumulated precipitation may be misleading, since only one or two small regions received heavy precipitation. When compared with the observed precipitation pattern (figure 4.1) and that of the control simulation (figure 5.9), it is evident that there is clearly much reduced precipitation over the region. Hourly precipitation images (not shown) reveal that most of the precipitation that took place in the extreme northeastern parts of KZN begun in the late afternoon (16h00 UTC), which then extended in a northerly direction and continued until just after 00h00 UTC in Mozambique.

The findings in the precipitation figures are supported by figure A6.5, which shows OLR images depicting the evolution of the convective event. From these OLR images, it is evident that without any significant topography in the simulation, the MCS fails to develop along the eastern escarpment as identified in the satellite imagery. However, another convective system did develop along the northeastern region of KZN in the late

afternoon (around 16h00 UTC), which coincided with the start of the simulated precipitation in that region. This convective system strengthened during the late afternoon and night, slowly propagating northwards into Mozambique. By the early morning hours, it begun to decay at a fairly rapid rate when compared to the MCS found in the control simulation.

The results from this reduced topography simulation suggests the strongly reduced topography may have weakened the associated uplift so that it was insufficient to produce the heavy precipitation in KZN. However, over the extreme northeastern region of KZN, where a convective system developed, it appears that the topographic effects were less important. It is also interesting to note that northern Swaziland (around Mananga station) also received a fair amount of precipitation in this sensitivity simulation, as found in the observations. Hence, the local factors were sufficient to produce the heavy precipitation in the absence of significant topography in this region. In order to identify conditions that favoured the development of the convective system over northern KZN and not elsewhere, an analysis of the synoptic and local conditions is conducted.

6.3.3. Synoptic and local conditions

Figure 6.13 shows sea level pressure and areas with wind speeds greater than $10m.s^{-1}$ at the 0.995 sigma level in the topography sensitivity simulation. Although, the high pressure system ridging to the south of the country is evident, the development of a trough in the interior is not so obvious. The sea level pressure values over the central interior are also higher than those in the control simulation, consistent with the weaker interior trough in the former. Areas of strong wind ($>10m.s^{-1}$) over the west coast and the oceans are similar to those found in the control simulation (see figure 5.1).

At the 500 hPa level, it appears that the synoptic pattern in the topography sensitivity run (figure A6.6) is similar to that of the MRF analysis. The eastward propagation of a westerly wave is evident in both the sensitivity and control simulations at this level. Temperature, geopotential heights and areas of strong wind at the 200 hPa level in this topography sensitivity simulation (not shown) were found to be very similar to the

corresponding control simulation plots (figure 5.3). At 200 hPa, the effects of local topography are relatively weak and the simulation is dominated by the boundary and initial conditions.

Changes in wind circulation and strength are however clearly apparent in the lower level of the topography sensitivity simulation (figure 6.14). Northwesterly and then southwesterly winds dominated over KZN at the 0.995 sigma level in the morning of 11 February. The lack of topography along the eastern escarpment may have resulted in southwesterly winds being present at this level in the late morning and early afternoon hours (see figure 5.4 versus figure 6.14). The winds off the east coast in this simulation only became predominantly onshore during the afternoon and they continued in this direction (southeasterly) until the morning of 12 February 2005. By comparison, the winds at this level in the control simulation became onshore early in the morning of 11 February and likely resulting in more advection of moist marine air at this level and hence, more rainfall. Even though the topography is smoothed and results in less surface friction, there were no significant differences in the wind strength found in the topography sensitivity simulation compared with the control simulation. This result suggests that the effects of topography was more to steer the wind rather than influence its magnitude.

It is evident that the ducted coastal ridge, which was present between the 800-700 hPa levels in the control simulation, failed to developed in this test simulation (not shown) since there was no longer topography to trap the feature (Holland and Leslie, 1986). It was suggested in the control simulation that this feature may have also resulted in onshore moisture advection into the coastal regions of KZN and its absence in this topography sensitivity simulation may help explain the reduced precipitation.

At the 0.525 sigma level (figure 6.15) it can be seen that the topography sensitivity simulation has a similar circulation pattern to the control simulation (see figure 5.5). However, one noticeable difference is that the mid-level winds appear to be more southwesterly compared to the westsouthwesterly winds found in the control simulation.

The winds also appear slightly stronger in the topography sensitivity simulation and, over the northern parts of KZN, they appear to contain a more southerly component during the late afternoon hours on the 11 February. As mentioned previously, it has been documented that the mid-level winds often play a role in the direction in which the MCS propagates. Figure A6.5 indicates that the MCS propagated in a northerly direction. Thus, it appears that the mid-level winds played a key role in driving the system in this direction.

Plots of vertical cross-sections of wind speed and zonal and meridional wind speed (figure A.6.7 and not shown, respectively), indicate that, stronger winds with a southerly/westerly component were found lower down in the atmosphere in the topography sensitivity simulation compared to that in the control case. Hence, topography appeared to have blocked these southwesterly winds in the control simulation. The strong onshore winds in the topography sensitivity simulation appeared to be confined to the northern parts of the KZN coastline and they also only become clearly defined later in the afternoon. This pattern highlights the fact that less moisture was likely to have been transported into the coastal region of KZN, due to the weaker onshore winds along the entire coastline and that they did not extend as far up into the atmosphere as in the control run.

Figure 6.16 suggests that the near surface winds played a key role in developing areas of low level moisture convergence. Regions of low level moisture convergence propagate inland along with moderately strong winds (figure 6.16) during the afternoon on the 11 February. The convergence zones are situated over the KZN interior in the early afternoon, and then propagate northwestwards into the Free State region by the evening. However, there is no persistent low level moisture convergence zone located over the eastern escarpment during the afternoon in figure 6.16, unlike that found in the control case (see figure 5.12).

Consistent with figure A6.5, a region of low level moisture convergence existed over northern KZN throughout most of the afternoon and evening. It is also apparent that the

storm development coincided with strong northeasterlies, which helped to fuel the system. Figure A6.8, the convective instability calculated from the difference between equivalent potential temperature at the 0.955 – 0.525 sigma levels, indicates that the convective system developed in an atmosphere that was favourable for the large-scale convection.

In the control simulation, it was noted that high precipitable water values coincided with the location of the convective event (determined from OLR values). Figure A6.8 shows a similar pattern in topography sensitivity simulation, since areas with a precipitable water content greater than 50 mm roughly coincide with the convective system location and propagation. It is also interesting to note that the precipitable water values in figure A6.8 do not contain the same linear distribution as in the control case (see figure 5.9) consistent with the much weaker topography in the sensitivity case.

Vertical cross-sections through northeastern KZN (see figure 6.12 for locations) indicate that, at the time of storm development, a pattern of coupled low level convergence and upper level divergence was evident along the coast (figure 6.17). However, this feature was not present for long, since a few hours after initiating there was no noticeable low level convergence (figure 6.16). During the brief period, when low level convergence and upper level divergence occurred strong upward vertical velocities (figure 6.17) as well as a high rain water mixing ratio (not shown) were also present well into the mid-levels. However, these features, which are favourable for convection, only lasted until early evening.

Vertical cross-sections for the region that contained heavy precipitation in the control simulation (see figure 5.9 for location), show that no periods of sustained convection took place in the topography sensitivity simulation. The reduced topography run shows conditions that do not favour convection and no obvious trigger for convection. During the night, no sustained low level convergence took place (figure 6.18), nor were there any regions of strong vertical velocities. In addition, it is clear the westerly mid-level winds,

which are relatively dry and stable, appear stronger in the topography sensitivity simulation than the control case.

Figure 6.19 indicates that the lower levels are less saturated in this sensitivity case than in the control run. Severe weather parameters from the 12h00 UTC 11 February Durban sounding in the sensitivity simulation (not shown) suggested that the atmosphere had a high CAPE (1641 J/kg), SWEAT (348), PW (48.6 mm), TT (50 °C) and LI (4.6°C) values, which are higher than the values found in the control simulation at the same time. The 00h00 UTC sounding (not shown) taken over the same region indicates that all the severe weather parameters had weakened considerably. However, the 00h00 UTC sounding from Richards Bay region (figure 6.19) revealed a similar pattern to that found at the 12h00 UTC Durban sounding. Severe weather parameters obtained from this Richards Bay sounding indicated the atmosphere was conducive to the development of convection in the region, since these parameters contained very similar values to those found in the 12h00 UTC Durban sounding. These soundings suggest that conditions were favourable for the development of convection over the region in the topography sensitivity simulation but the much reduced topography provided too weak a trigger to initiate the convection.

6.3.4. Simulation Summary

The results of this sensitivity simulation suggest that the eastern escarpment played a key role in the development of the MCS, since the observed convective system failed to develop over the eastern escarpment in this run. Also, the considerable under-estimation of precipitation suggests that the synoptic forcing alone was not capable of producing significant precipitation for this particular event. However, it was apparent that regions over northeastern KZN were still favourable for the development of convection, and a convective system developed there in this reduced topography simulation. The results suggest that, in cases where dynamical factors are not strong enough for the development of upward motion, local topography can play a key role in providing uplift, which may trigger such convective systems.

Differences in wind circulation were evident, with the onshore winds impinging on the KZN coastline weaker than in the control run. These winds also did not extend as far up into the atmosphere and were mainly confined to the extreme northern parts of the KZN coastline when compared to the control simulation. This result suggests that less moisture was likely to have been transported into KZN resulting in less favourable conditions for heavy precipitation development. Therefore, the eastern escarpment may have blocked the southwesterly/westerly winds at the lower levels in the control simulation, resulting in the easterly winds extending further inland and at higher levels in the control simulation, leading to more widespread precipitation.

Another key difference between this topography sensitivity simulation and the control simulation was that no sustained periods favourable for convection occurred over the coastal region. In the control simulation, coupled low level convergence and upper level divergence, strong upward vertical velocities and abundant moisture were present for much of the night, whereas in the topography sensitivity simulation this pattern was only evident for a few hours. In the latter, it was found that the atmosphere over the coastal regions was conducive to the development of convection, since the sounding data contained severe weather parameters which contained higher values than that found in the control case. However there was less moisture in the lower levels of the atmosphere during the 11 February 2005 supporting the previously discussed idea that weaker, more northward displaced, onshore winds advected less moisture into the region in topography sensitivity simulation.

These findings have demonstrated the important role that the eastern escarpment possibly plays in the development of these large convective systems in Southern Africa, as noted by Laing and Fritsch (1993b). Thus, an accurate representation of the local topography is needed in models to further our understanding of how local topography influence extreme weather systems in the region. The analysis has also helped identify the role the coastal topography played in the development of the heavy precipitation in the region by providing additional forcing of the moist onshore flow, which is likely to have continued

to rise due to the convectively unstable atmosphere found in the control simulation. However, it is recognized that these results are from one case study and hence, further simulations using different events are required in order to identify the role of the topography in the region. Other simulations using varying topography settings should also be tested in order to get a better understanding of the role topography plays. It should also be kept in mind that the some of the differences found in the precipitation distribution in this particular simulation may have also been influenced by the parameterization schemes used, most notably the convective parameterization scheme.

6.4. Mid-latitude Sensitivity Test

6.4.1. Introduction

This mid-latitude sensitivity simulation was performed to investigate the importance of the mid-latitude circulation on the evolution of the convective event. Synoptic features found propagating eastwards south of South Africa are known to have an influence on weather systems located within the country (Tyson and Preston-Whyte, 2000). These authors noted that a common synoptic situation promoting storm formation is a trough in the tropical easterlies, while frontal passages to the south are also known to frequently trigger storms. Preston-Whyte et al. (1991) found that for the 1965-85 period, four synoptic types, namely the Tropical-Temperate Trough, Westerly Wave, Ridging High and East Coast Low, accounted for 81 percent of the rainfall over KwaZulu-Natal. Thus, a further simulation was conducted whereby the 18km domain was positioned more equatorward compared to that of the control simulation, such that the southern location was situated at 37° S, instead of 45°S as in the control run (see figures 3.1 and 3.4). However, it is recognized that a similar problem to the smoothed topography simulation will possibly occur in the mid-latitude sensitivity simulation. Since the initial and boundary conditions for the MRF model will still contain some influence of the mid-latitudes. It is not possible to entirely remove the influence of this feature for the experiment.

6.4.2. Convective System and Precipitation

The simulated precipitation along the northern coastline in the mid-latitude sensitivity run was significantly over-estimated (figure 6.20) when compared to the control run or the observations. In addition, a slightly different accumulated precipitation pattern results for the event, with the most noticeable differences occurring in the KZN interior and along the south coast of KZN. However, it is obvious that most of the heavy precipitation in the mid-latitude sensitivity case occurred along the north coast of KZN, which is similar to the findings in the observations and the control run. It was identified in the observations that majority of the intense precipitation took place along the north coast of KZN late at night (i.e. between 22h00-02h00 UTC 11/12 February). However, in the mid-latitude sensitivity simulation, the heavy precipitation along the north coast started a few hours early (figure A6.9), suggesting that the storm development occurred more rapidly.

Using OLR as a proxy for the system (figure 6.21), it appears that the simulated system in this mid-latitude sensitivity simulation showed a similar life cycle pattern as that identified through the satellite imagery in chapter four. However, a noticeable difference is that of the location of the system, which appear to be displaced further to the north (more equatorward) compared to the observed system. This displacement could possibly explain the increase in precipitation identified in the northeastern region of South Africa in the mid-latitude sensitivity simulation. The shape of the system also differs from that of the observations, since the system was observed to retain a more linear shape for a longer period than found in this model simulation (figure 6.21). The initiation time of the simulated system appeared to be closer to the observed than the control case. However, it appears to now strengthen too quick leading to an earlier onset of the heavy coastal precipitation (figure A6.9).

6.4.3. Synoptic and local conditions

Figure 6.22 shows sea level pressure and areas of low level wind stronger than $10 m.s^{-1}$ in the mid-latitude sensitivity simulation. Due to the smaller domain, the ridging anti-cyclone cannot be clearly identified. As mentioned previously, this particular synoptic

system played an influential role in the onshore winds impinging on the east coast, a point discussed in more detail later in this chapter. Figure 6.22 also reveals the presence of a weak interior trough during the event. This trough was weaker in the mid-latitude sensitivity case than in the control run.

In addition, there is evidence of an eastwards propagating westerly wave at the 500 hPa level (figure A6.10), which was also identified in the MRF analysis data and the control simulation. However, due to the domain choice, this feature cannot easily be verified. The mid-latitude sensitivity simulation seems to get the timing of this possible westerly wave correct, since the wave approaches South Africa early on the 11 February and by the afternoon is situated to the southeast of the country. Also, this simulation compares favourably with both the MRF 200 hPa level results and the control case (not shown).

Figure 6.23 shows the wind stream and speed at the lowest level in the model indicating that the circulation is similar to the control case. As found in the control simulation, the most important circulation at this level was the onshore flow into the east coast. However, it is evident that the magnitude of this onshore flow is over-estimated in the mid-latitude sensitivity run when compared to the control run and the MRF analysis. Figure 6.22 and 6.23 indicate that during the late afternoon in the mid-latitude simulation, there were stronger winds present off the east coast at low levels than that found in the control simulation as well as the MRF model output. However, the magnitude of the low level winds in the mid-latitude sensitivity simulation is similar to those derived from measurements from the QuikSCAT satellite winds (figure 4.15). These stronger winds found in the mid-latitude sensitivity run could be as a result of the slightly stronger pressure gradient to the southeast of the country when compared to the control case.

The circulation pattern found in the mid-latitude sensitivity simulation at the 0.525 sigma level (figure A6.11) also appears to differ slightly with that found in the control simulation. Figure A6.11 shows the propagation of a westerly wave past the south of the country during the morning of 11 February 2005, which was also evident in the control model run, but the wind direction differs. At this level, the winds throughout the event are

predominately southwesterlies and at times contain a more southerly component, compared to the more westsouthwesterlies identified in the control case. This difference in the wind direction could possibly account for the more equatorward displacement of the convective system in the mid-latitude sensitivity simulation, as evident in the OLR figures.

Overall, the synoptic features in the mid-latitude sensitivity simulation compare reasonably well to those observed in the control run as well as the MRF model output. There are some discrepancies found in the mid-latitude sensitivity simulation, likely due to the model boundary not extending far enough to the south to capture the large-scale features. The most noticeable difference found between the mid-latitude sensitivity and the control simulation is that of the low and mid-levels winds. These wind differences may have had an influence on the MCS development and location as well as the intensity and spatial distribution of the associated precipitation.

Figure 6.24 indicates that low level moisture convergence was evident over large sections of KZN during the convective event in the mid-latitude sensitivity simulation. The low level convergence pattern found during the life cycle of the event was similar to that found in the control case, since low level moisture convergence was initially found only along the escarpment and parts of the KZN coastline during the early afternoon on the 11^{th}, but during the late afternoon this feature was found along the entire coastline as well as over most parts of northern KZN. During the night, low level moisture convergence was still found over the northern parts of KZN, but was mainly restricted to the coastal region. At the same time, low level moisture convergence also occurred along the Mozambique coastline and in parts of Swaziland in the mid-latitude sensitivity simulation. By the late morning hours on the 12 February 2005, areas of low level moisture convergence in KZN became smaller and weaker (not shown), while some areas were replaced by low level divergence. This convergence pattern was also evident slightly higher up in the atmosphere at the 0.870 sigma level (figure A6.12), with moisture convergence initially located along the escarpment, but by the late afternoon and night, convergence was present along the northern parts of KZN and Swaziland. It

should be noted that moisture convergence at this level persisted throughout the night and early morning hours along the northern coastline around 28°S in the mid-latitude sensitivity simulation, which is slightly further to the north compared to the results found in the control case.

An interesting feature found in the mid-latitude sensitivity simulation is that there appeared to be an apparent LLJ (figure 6.24) during the event. The LLJ is arbitrarily defined as a channel of winds exceeding speeds of $10m.s^{-1}$ in the lower levels. This feature was not obvious in the MRF analysis, but this could be due to its coarser resolution. These stronger low level winds in the mid-latitude sensitivity simulation may be as a result of the slightly stronger pressure gradient to the southeast of the country when compared to the control case.

In the mid-latitude sensitivity simulation, the southeasterly LLJ, first impinged on the coast on the afternoon of February 11 and was still evident later in the evening, mainly along the northern coastal regions. As evident in the control simulation, the timing of the heavy precipitation along the north coast in the mid-latitude sensitivity simulation appears to coincide with the onset of the strong winds into the region. These onshore winds began to weaken during the night and shift further offshore (as the anticyclone shifted eastwards) and hence reduced the amount of moisture into the region. A similar wind pattern is found in the 0.870 sigma level in the mid-latitude sensitivity simulation (figure A6.12), indicating that the strong onshore advection of moisture occurred throughout the lower 1500m of the atmosphere. This advection pattern was also identified in the control simulation, but is likely to be stronger in the mid-latitude sensitivity run due to the stronger winds. Overall, the wind pattern at the 0.995 to 0.870 sigma level in the mid-latitude sensitivity simulation illustrates the persistent onshore winds impinging the KZN coastline during the event.

This low level jet is more apparent when vertical cross-sections are plotted along the east coast. Figure 6.25 shows wind speed and the zonal wind speed found in the mid-latitude sensitivity simulation along cross-section B-B' in figure 5.9. It is apparent that winds

should be noted that moisture convergence at this level persisted throughout the night and early morning hours along the northern coastline around 28°S in the mid-latitude sensitivity simulation, which is slightly further to the north compared to the results found in the control case.

An interesting feature found in the mid-latitude sensitivity simulation is that there appeared to be an apparent LLJ (figure 6.24) during the event. The LLJ is arbitrarily defined as a channel of winds exceeding speeds of $10m.s^{-1}$ in the lower levels. This feature was not obvious in the MRF analysis, but this could be due to its coarser resolution. These stronger low level winds in the mid-latitude sensitivity simulation may be as a result of the slightly stronger pressure gradient to the southeast of the country when compared to the control case.

In the mid-latitude sensitivity simulation, the southeasterly LLJ, first impinged on the coast on the afternoon of February 11 and was still evident later in the evening, mainly along the northern coastal regions. As evident in the control simulation, the timing of the heavy precipitation along the north coast in the mid-latitude sensitivity simulation appears to coincide with the onset of the strong winds into the region. These onshore winds began to weaken during the night and shift further offshore (as the anticyclone shifted eastwards) and hence reduced the amount of moisture into the region. A similar wind pattern is found in the 0.870 sigma level in the mid-latitude sensitivity simulation (figure A6.12), indicating that the strong onshore advection of moisture occurred throughout the lower 1500m of the atmosphere. This advection pattern was also identified in the control simulation, but is likely to be stronger in the mid-latitude sensitivity run due to the stronger winds. Overall, the wind pattern at the 0.995 to 0.870 sigma level in the mid-latitude sensitivity simulation illustrates the persistent onshore winds impinging the KZN coastline during the event.

This low level jet is more apparent when vertical cross-sections are plotted along the east coast. Figure 6.25 shows wind speed and the zonal wind speed found in the mid-latitude sensitivity simulation along cross-section B-B' in figure 5.9. It is apparent that winds

with an easterly component were confined to the lower levels and at times extending up to the mid-levels, while at the mid- to upper levels, winds with a westerly component were dominant. From the wind speed values, it is evident that a LLJ developed in the mid-latitude sensitivity simulation, since in the lower levels there was a strong confined onshore component. Figure 6.24 indicated that during the afternoon on February 11, southeasterly onshore winds were present along the coastline, which was identified in similar vertical cross-section plots showing meridional wind speeds (not shown) instead of zonal wind speeds.

Vertical cross-sections indicate that very similar mechanisms were responsible for the heavy precipitation production along the north coast in the mid-latitude sensitivity simulation. A noticeable difference is the location of the heavy precipitation, which in the mid-latitude sensitivity simulation is found further equatorward compared to the control case. Figure 6.26, a vertical cross-section depicting vertical velocity, wind vectors and relative humidity, shows that during periods of heavy precipitation the region experienced onshore winds and strong vertical uplift. The vertical uplift was a prominent feature during the late afternoon and night, since it first featured around 16h00 UTC and was no longer present after about 02h00 UTC the next morning. The regions of strong vertical extent always occurred near the coastal region, which may have been due to the continuous inflow of low level moisture and the coastal topography then forcing this moist air to rise.

The presence of a coupled low level convergence/upper level divergence pattern was found in regions of heavy precipitation (figure 6.26). It was also evident that the location of the low level convergence coincided with regions containing a mixing ratio greater than 0.4 $g.kg^{-1}$ (not shown). These vertical cross-section figures identify similar features aiding in the production of precipitation as found in the control case.

As found in the control case, the convective instability existed during the event in the mid-latitude sensitivity simulation was convectively unstable, particularly along the northern regions of KZN during the event (figure A6.13). The lower atmosphere over the

northern coastal regions remained convectively unstable throughout the afternoon and night, before increasing in stability during the morning of 12 February. Precipitable water, also plotted on figure A6.13, indicates that values exceeding 50 mm were located along the northern coastal region of KZN during the late afternoon and evening hours, which was also evident in the control run.

The convective instability figures are supported by the soundings produced from the mid-latitude sensitivity simulation for the Richards Bay and Durban region (both not shown). Most of these soundings reveal that a near saturated condition at low levels was overlain by a drier atmosphere in the mid-levels. The soundings also indicate the presence of a strong southeasterly wind, particularly for the Richards Bay soundings. The Richard Bay soundings indicated that the winds were veering with height, which is evident from the surface winds being southeasterly, while in the mid-levels there were strong southwesterly/westerly winds.

6.4.4. Simulation Summary

The mid-latitude sensitivity simulation has been used to identify the role in which the large scale feature in the mid-latitudes may have played in the evolution of the MCS. This was achieved by shifting the location of the 18km domain northwards so that the southern boundary was 37°S. From the mid-latitude sensitivity simulation, evidence has been presented that suggests that due to the mid-latitudes not being fully represented in the simulation, certain features are possibly not well resolved. The main discrepancy in this sensitivity simulation appears to be with the simulation of the winds at various levels. It was evident that the wind direction in the lower levels was well simulated, but the magnitude was over-estimated compared to observations. However, it was noted that surface winds derived from QuikSCAT illustrated stronger winds than was found in the MRF model analysis.

Another interesting inconsistency produced in the mid-latitude sensitivity simulation was that of the evolution of the convective event and its associated heavy precipitation. It was

found that compared to the satellite imagery, the simulated system appeared to be displaced further to the north. This northward displacement may have occurred due to the more southerly component in the mid-levels winds. It is also likely to have accounted for the increase in precipitation in the northern parts of KZN. This increase in precipitation was likely due to a combination of more moisture being transported into the region by the stronger onshore low level winds and the persistent factors favouring the development of convection. These factors include a coupled low level convergence/mid-level divergence pattern, high content of moisture in the lower atmosphere and a convectively unstable atmosphere. It can be seen that the factors that may have been responsible for the heavy precipitation in the mid-latitude sensitivity simulation were similar to those found in the control case. Thus, the results suggest that convective instability over the coastal regions of KZN were favourable for sustaining the development of a convective system.

It was found that a near-surface ducted coastal ridge was present in the control simulation (see figure 5.11). This phenomenon was also identified in the mid-latitude sensitivity simulation (figure A.6.14). However, it is evident that in the mid-latitude sensitivity run, this mesoscale feature was located further south when compared to the control case and it did not appear to last as long, although it still appeared to have an influence on the wind direction into the heavy precipitation region. As discussed previously, the development of this feature was likely linked to the propagation of a frontal system and a synoptic-scale anticyclone ridging south of the country. These two large-scale features are usually located in the mid-latitudes and the northward shifted domain leads to the ducted ridge not being well resolved. However, it should be noted that there are no observations of the ducted ridge in the case study, so the location and role of such a feature still needs to be established.

These findings suggest that in order to produce a reasonable simulation of an extreme weather event in South Africa, it is likely that an accurate representation of the mid-latitudes is required. Synoptic features in the mid-latitude circulation have an influence on mesoscale features in and around South Africa. Thus, the model domain needs to include the mid-latitudes when forecasting or simulating weather phenomenon over

South Africa. These results also emphasize the necessity for obtaining accurate observations of the atmosphere in the mid-latitudes in order to provide reliable initial and boundary conditions for numerical model simulations.

6.5. Summary

This chapter has focused on isolating the influences of certain features found within and around South Africa. Through these simulations, the importance of SSTs, local topography and the mid-latitude circulation on the evolution of the convective system has been examined. The analysis has also highlighted the inconsistencies produced by a numerical model when a single variable is altered in the model forcing. However, these results should be regarded as preliminary since these sensitivity simulations have only been applied to one case study and therefore should not be generalised. In order to get a better understanding of the role each feature plays, simulations such as these must be applied to a range of extreme precipitating systems developing in different environments. It is also recognized that alternative methods of determining the effects of the topography, SSTs and mid-latitudes in such cases can be used, such as the factor separation technique described by Stein and Alpert (1993). This particular factor separation technique may help in fully quantifying the effects these three factors may have had on the evolution of the convective system. Ultimately, it should be recognized that identifying the individual role of each feature in such events may be difficult due to the complex interactions with one another. For example, Garstang et al. (1987) found that the generation of convective storms over the escarpment of the northeast South African region was associated with westerly waves propagating across the southern tip of Africa, which then interact with the topography of the escarpment. Thus, it is likely that a combination of these factors will interact to develop heavy precipitating convective storms in the eastern region of South Africa.

Cook (2000) separated the vertical integrated moisture convergence into four terms: convergence, advection, orographic and transients and then identified the influence that these terms individually had on the development of the South Indian Convergence Zone

(SICZ) and its links to rainfall variability over Southern Africa. A similar type of approach could perhaps be used to identify which features were important for the development of the vertical integrated moisture convergence in this case study and hence give insight to the rainfall processes.

Most of the vertical and horizontal transects performed in this chapter have been repeated in each simulation so that consistency is kept in identifying the factors that favoured or hindered the development of the system and the associated precipitation. All the results presented in this chapter have been derived from the 18 km domain of each simulation since the results of the nested domain (6 km resolution) were very similar. For example, as found in the control case, precipitation for all the sensitivity simulations appeared to have been intensified in the nested domain of the simulation, but the spatial distribution remained fairly similar to that found in the 18 km domain. It should also be remembered that the effects of the parameterizations used in the numerical model cannot be excluded in these simulations. Thus, some of the precipitation irregularities found within each simulation could be due to deficiencies in the parameterization of convection and cloud microphysics. This is discussed in more detail in the chapter that follows.

From the initial results of these sensitivity simulations, it seems that the topography along the eastern escarpment played an important role in triggering the convective event. For example, the system failed to develop along the eastern escarpment during the afternoon of the 11 February 2005 in the topography sensitivity simulation. It was evident that the atmosphere over the coastal region was favourable for the development of convection, but this failed to transpire due to there being insufficient forcing and less moisture in the lower levels. The results also suggest that the local topography steered the low levels winds in the control run and hence, had an influence on the onshore, moisture advecting winds found in the topography sensitivity simulation, since less moisture was found in the lower levels in this run. Thus, it is suggested that it is important for the local topography to be well resolved in numerical model simulations of events taking place of eastern South Africa.

As discussed by Rouault et al. (2003), the role of the Agulhas Current as a moisture source for heavy precipitation events in Southern Africa appears to be misrepresented in operational models (ECMWF, NCEP) due to the underestimation of fluxes from this warm current. It was found in the SST sensitivity simulation that by having an increased SST resolution an increase in the amount of accumulated precipitation occurred over the east coast during the event. Furthermore, it seems that the SST sensitivity test did produce a marginally better precipitation spatial distribution compared to the control case.

It was also obvious that the simulated system in the SST sensitivity test had a bias towards poleward development in the latter stages of its evolution, since it was well developed in this region and took longer to dissipate while positioned over the Agulhas Current. This bias in the development of the poleward section was also identified in the satellite imagery. This suggests that the surface fluxes and close proximity of moisture over the higher resolution SST may have resulted in stronger storm, which is consistent with an increase in precipitation. This reinforces the idea of using high resolution SST data to represent the core of the Agulhas Current and the strong SST gradients in numerical simulation of extreme precipitating events over South Africa.

The role the mid-latitude circulation played in the evolution of the event became evident when the 18km domain of the mid-latitude sensitivity simulation excluded this factor by being bounded at 37°S. It was noted that when this aspect was excluded in the model simulation, slightly different results were identified with the most obvious involving the wind patterns in the low and mid-levels. These changes in the wind patterns appeared to have resulted from the representation of large-scale features in the mid-latitudes and hence, had a large impact on certain features of the convective storm, such as its location and spatial distribution of the associated precipitation. This result suggests that in order to get a more accurate representation of a convective event over the east coast of South Africa, the poleward boundary of the domain should be extended well into the mid-latitudes. It also highlights the importance of resolving the large-scale features located in

the mid-latitudes in the initial and boundary conditions, which may be rather problematic due to the lack of observations in this part of the Southern Hemisphere.

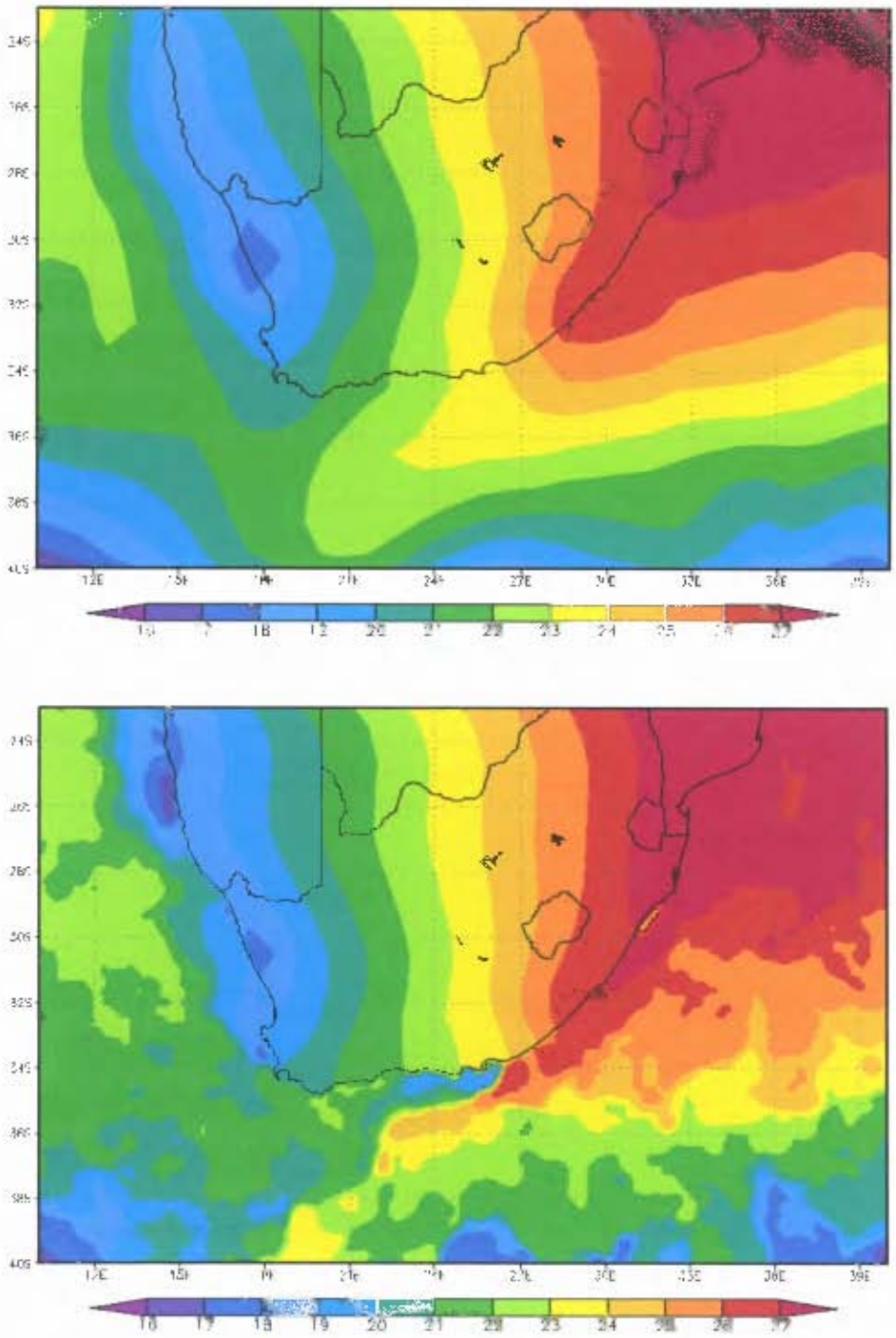

Figure 6.1: The two SST datasets that were used for the models initial and boundary conditions, which are the OISST SST (top) weekly data that includes the 11 February 2005 and the AVHRR SST (bottom) for the same period. (Note that over the land in the AVHRR image the OISST SST data had been superimposed).

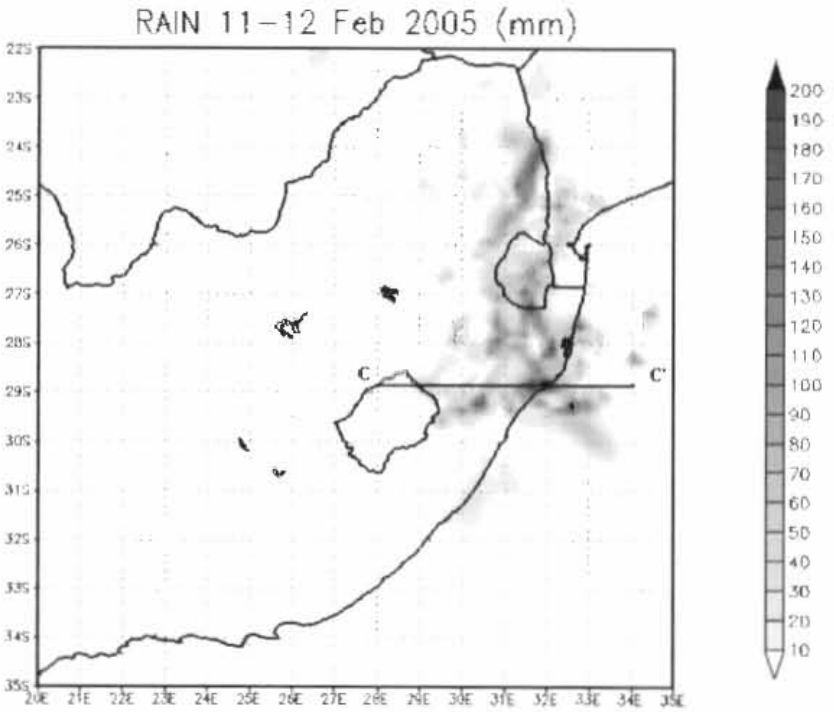

Figure 6.2: Simulated precipitation for the 11 and 12 February 2005 for domain one from the SST sensitivity simulation.

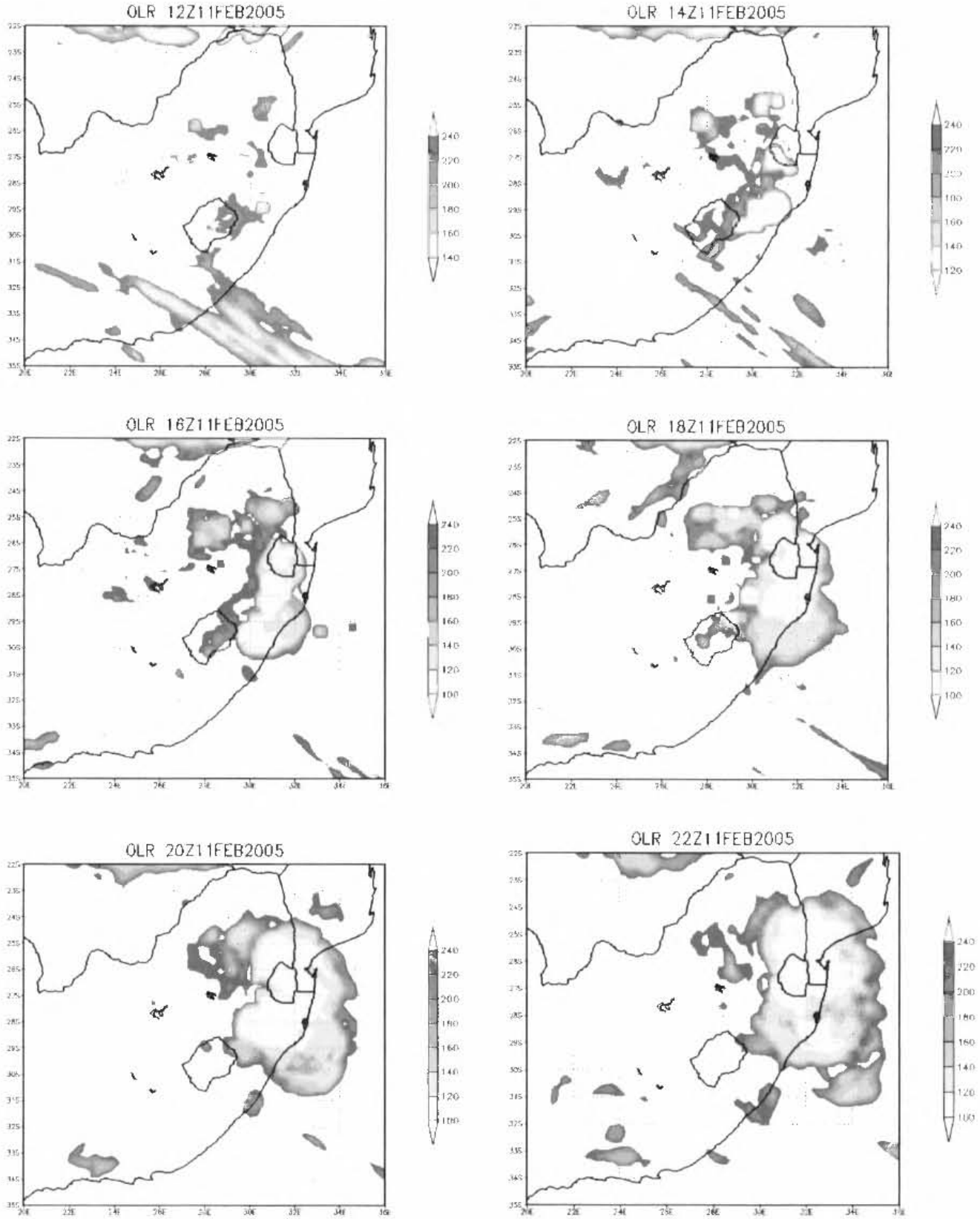

Figure 6.3: Outgoing longwave radiation (interval, 20 w.m^{-2}) derived from the SST sensitivity test. Starting at 12h00 UTC 11 February at 2 hour intervals and ending at 22h00 UTC.

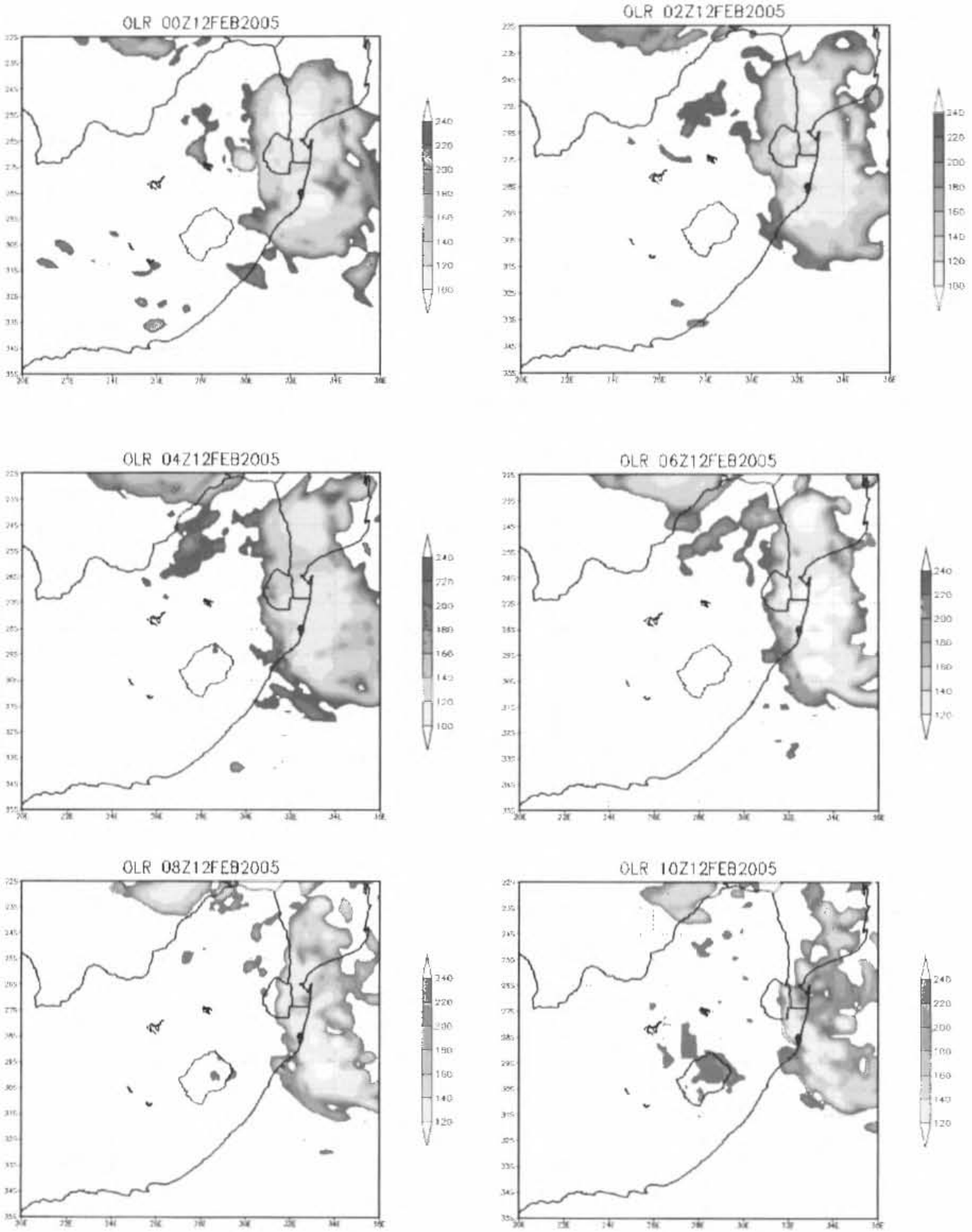

Figure 6.3cont: From 00h00 UTC 11 February (at 2 hour intervals) and ending at 10h00 UTC.

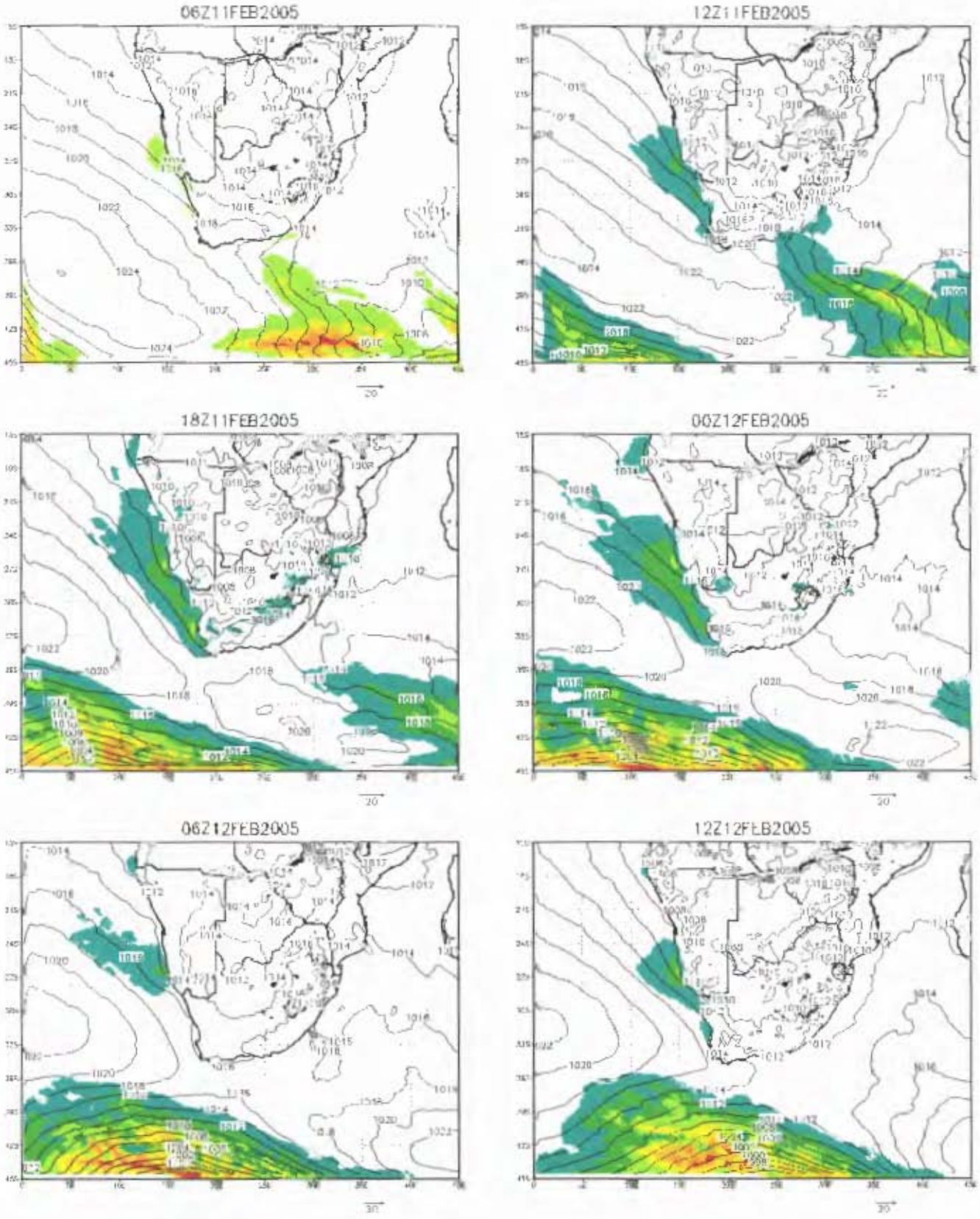

Figure 6.4: Mean sea level pressure (black contours; interval 4 mb) and winds with speeds greater than 10m.s^{-1} at the 0.995 sigma level, derived from the SST sensitivity simulation. Starting at 06h00 UTC on the 11th and ending at 12h00 UTC on the 12 February, at 6-hourly intervals.

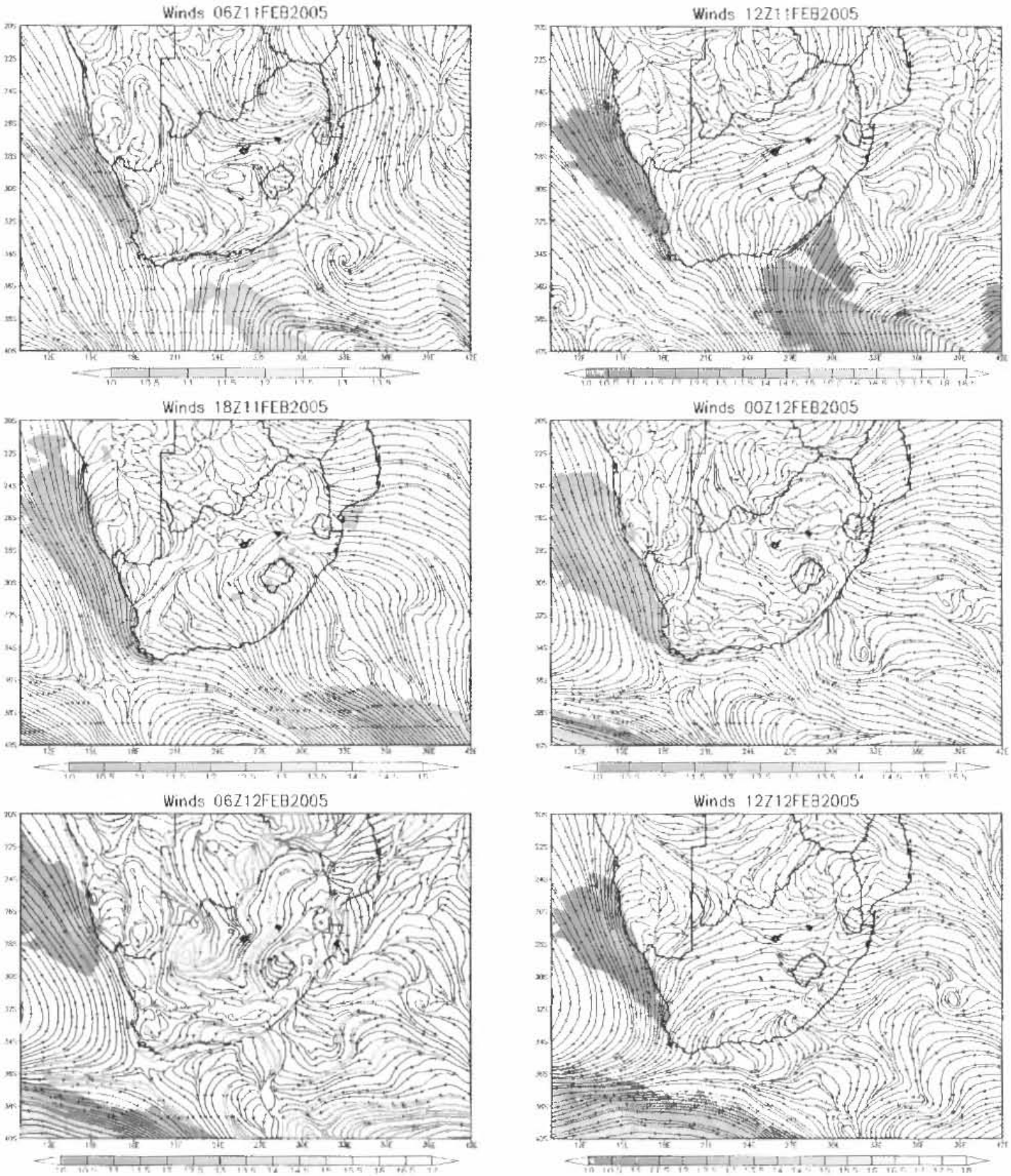

Figure 6.5: Circulation pattern in the SST sensitivity simulation at the 0.995 sigma level and regions where wind speeds greater than 10**m**.s^{-1} are shaded (interval; 0.5 m.s^{-1}).

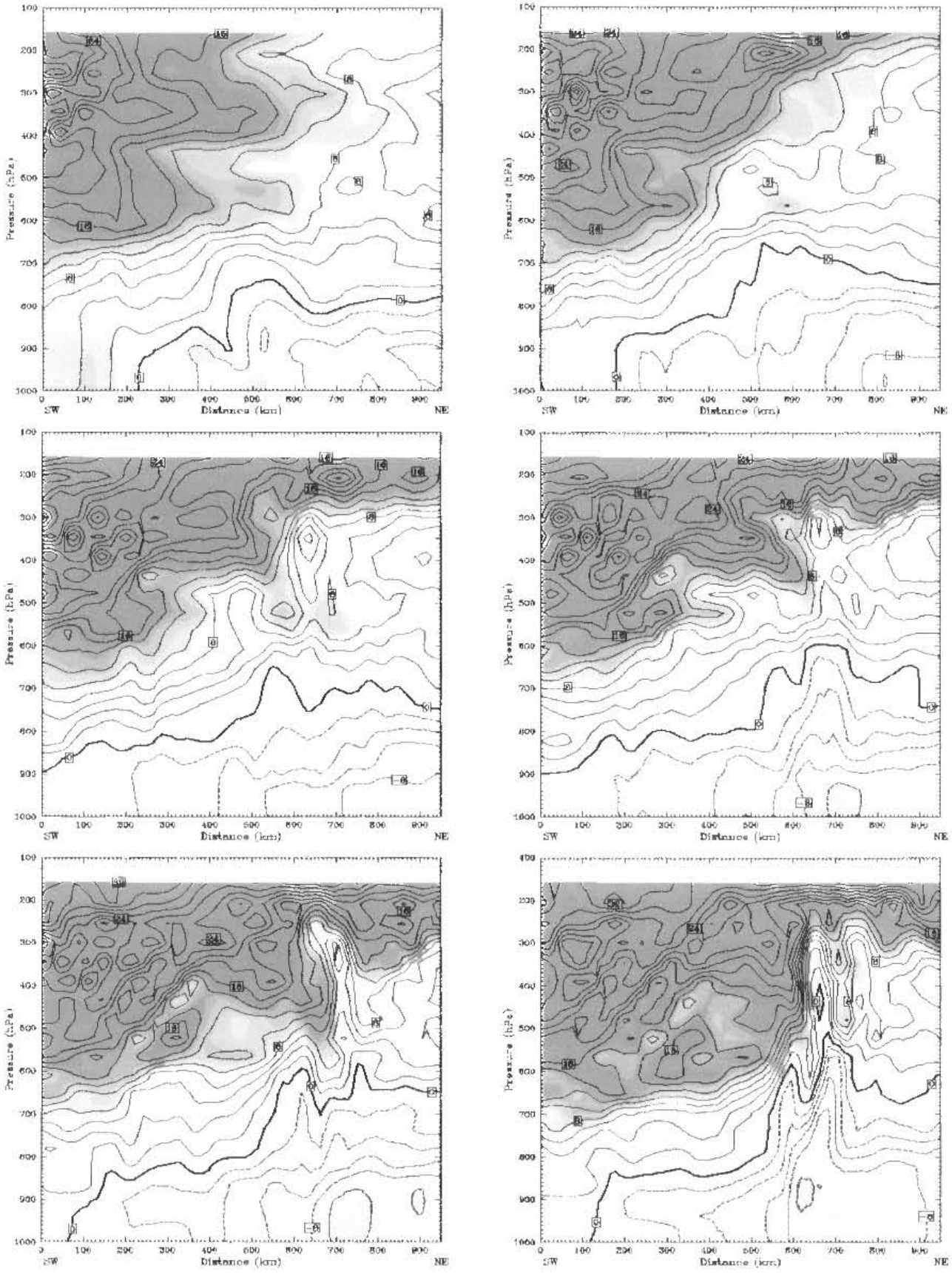

Figure 6.6: Vertical cross-sections of wind speeds starting at 10 $m.s^{-1}$ (shaded; 5 $m.s^{-1}$ interval) and zonal wind speeds (contour; 2 $m.s^{-1}$ interval) along B-B' (see figure 5.9). From left to right starting at 14h00 UTC (top left) and ending at 00h00 UTC (bottom right).

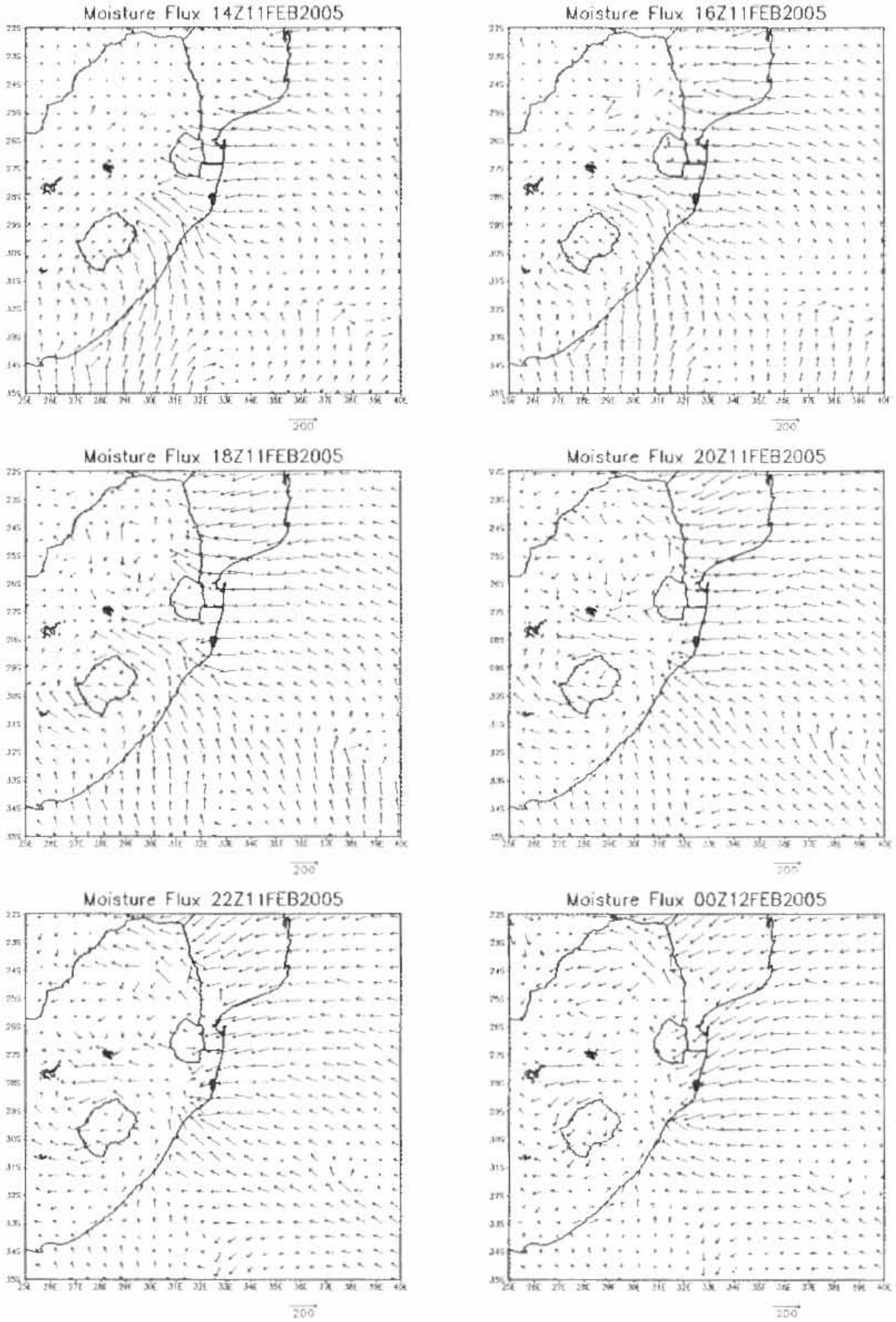

Figure 6.7: 2-hourly moisture flux values (g. kg^{-1} $m.s^{-1}$) at the 1000 hPa level in the SST sensitivity simulation (magnitude of vector arrow denoted in bottom right).

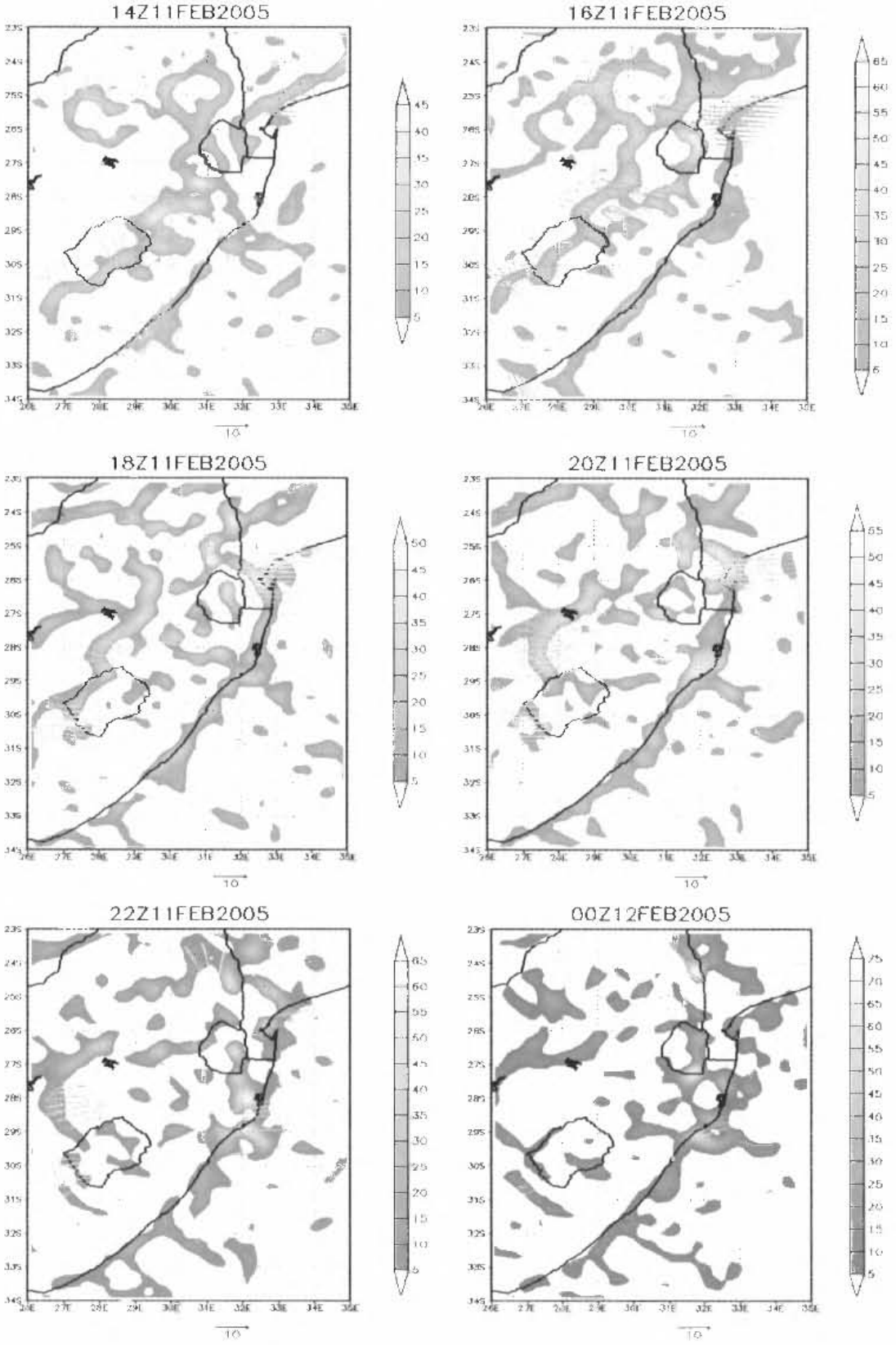

Figure 6.8: Moisture convergence (shaded positive values with interval of 5 $g.kg^{-1}.s^{-1}$) and wind speeds greater than 10 $m.s^{-1}$ at the 0.955 sigma level from the SST sensitivity simulation. Starting at 14h00 UTC on the 11th through to 00h00 UTC on the 12th, at 2 hour intervals. Note that divergence has been omitted for clarity.

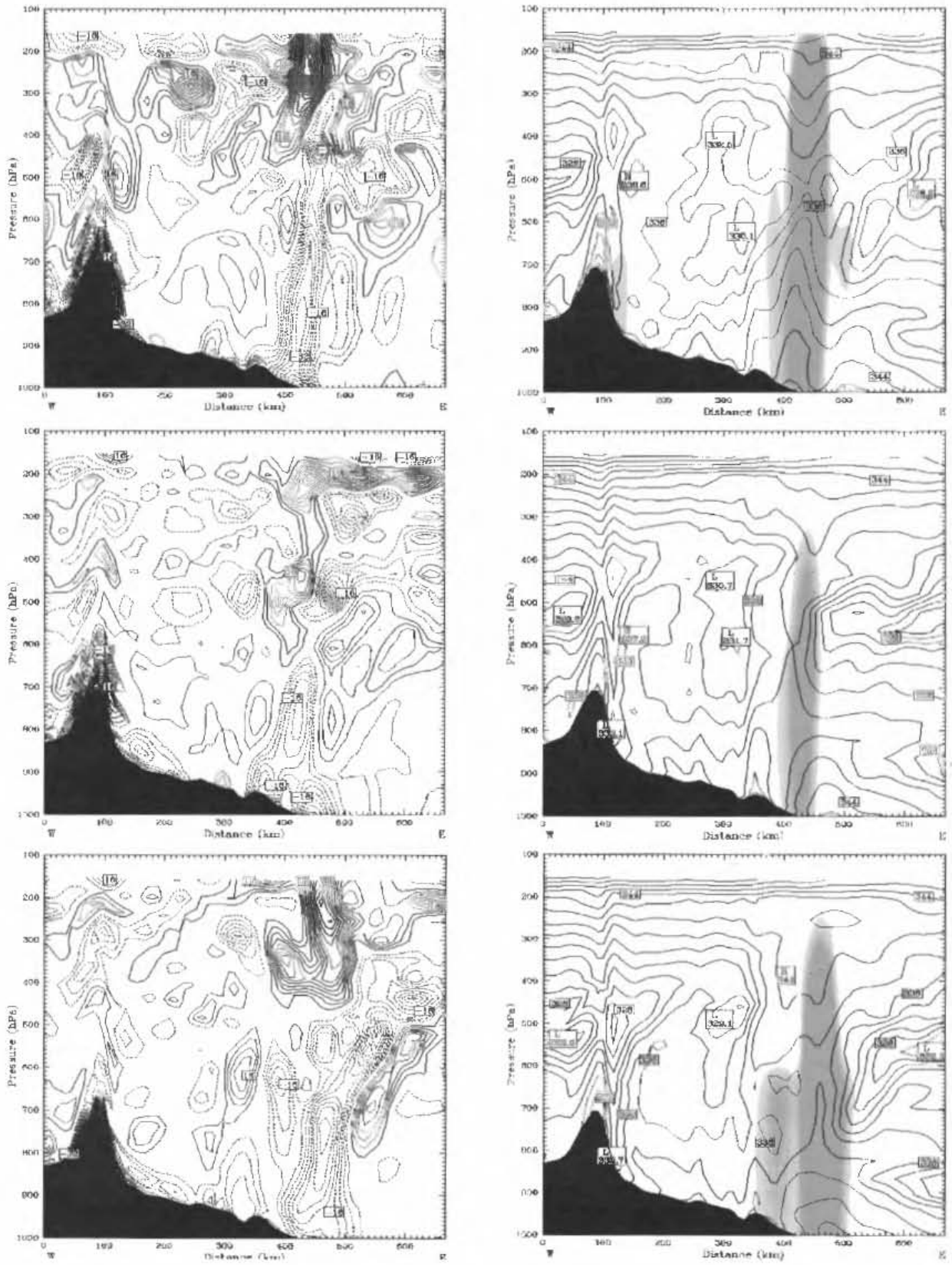

Figure 6.9: Vertical cross-section of divergence (left; interval 4 s^{-1}) and the right figures showing equivalent potential temperature (contour; interval 2°K) and, rain water mixing ration greater than 0.4 $g.kg^{-1}$ (shaded) along line C-C' (figure 6.2). Starting at 20h00 UTC on the 11 February (2 hour intervals) and ending at 00h00 UTC. Note that divergence is positive and convergence is negative and dashed.

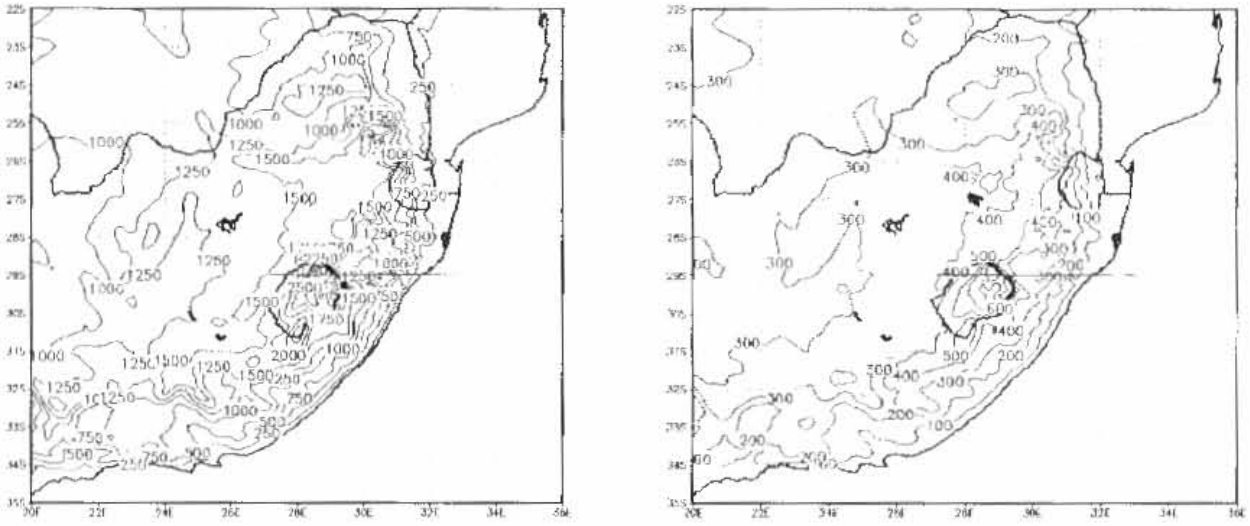

Figure 6.10: The topography of the control simulation on the left (contour interval 250m) and of the sensitivity test on the right (contour interval 100m).

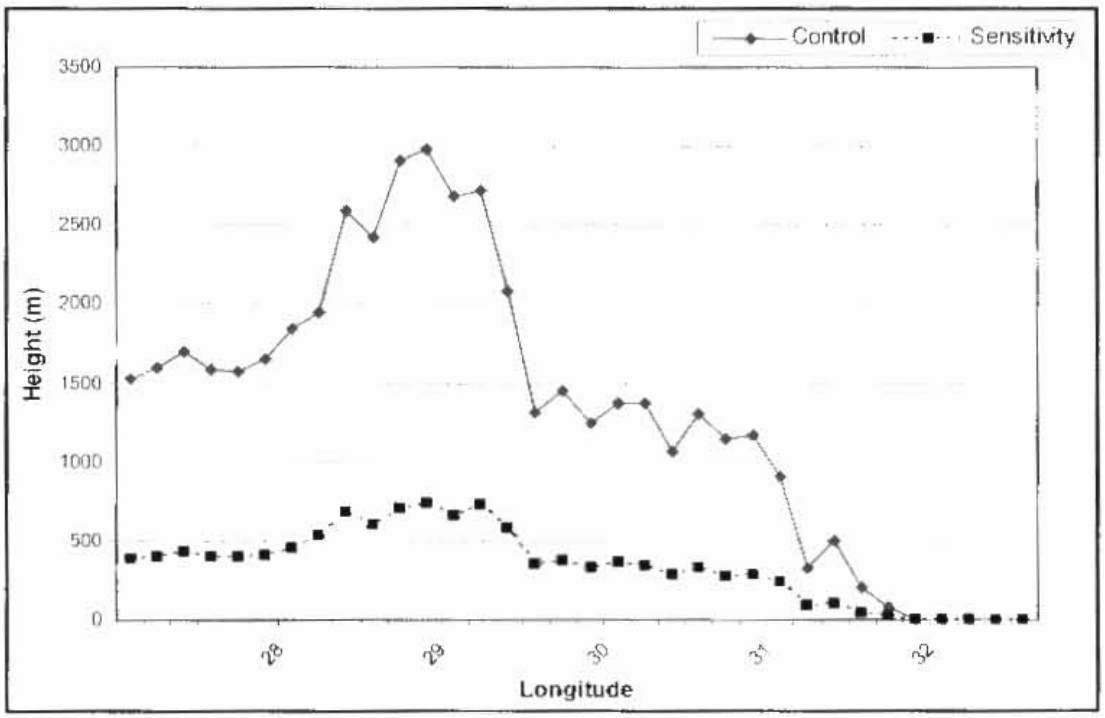

Figure 6.11: Vertical cross-section along 29°S (see figure 6.10) which illustrates the topography difference between the control simulation and that of the topography sensitivity test.

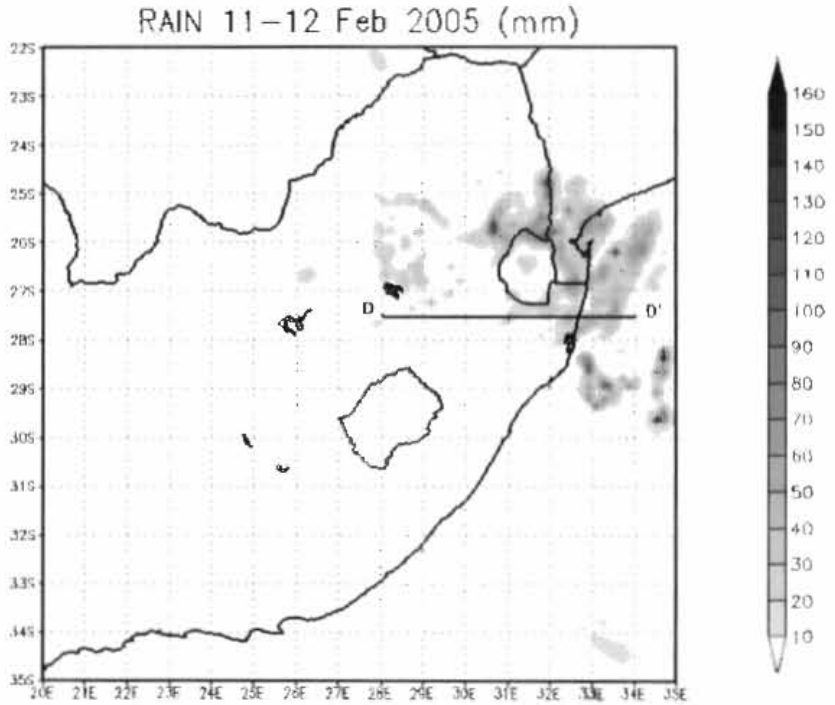

Figure 6.12: Accumulated precipitation for 11 and 12 February 2005 for domain one in the topography sensitivity simulation.

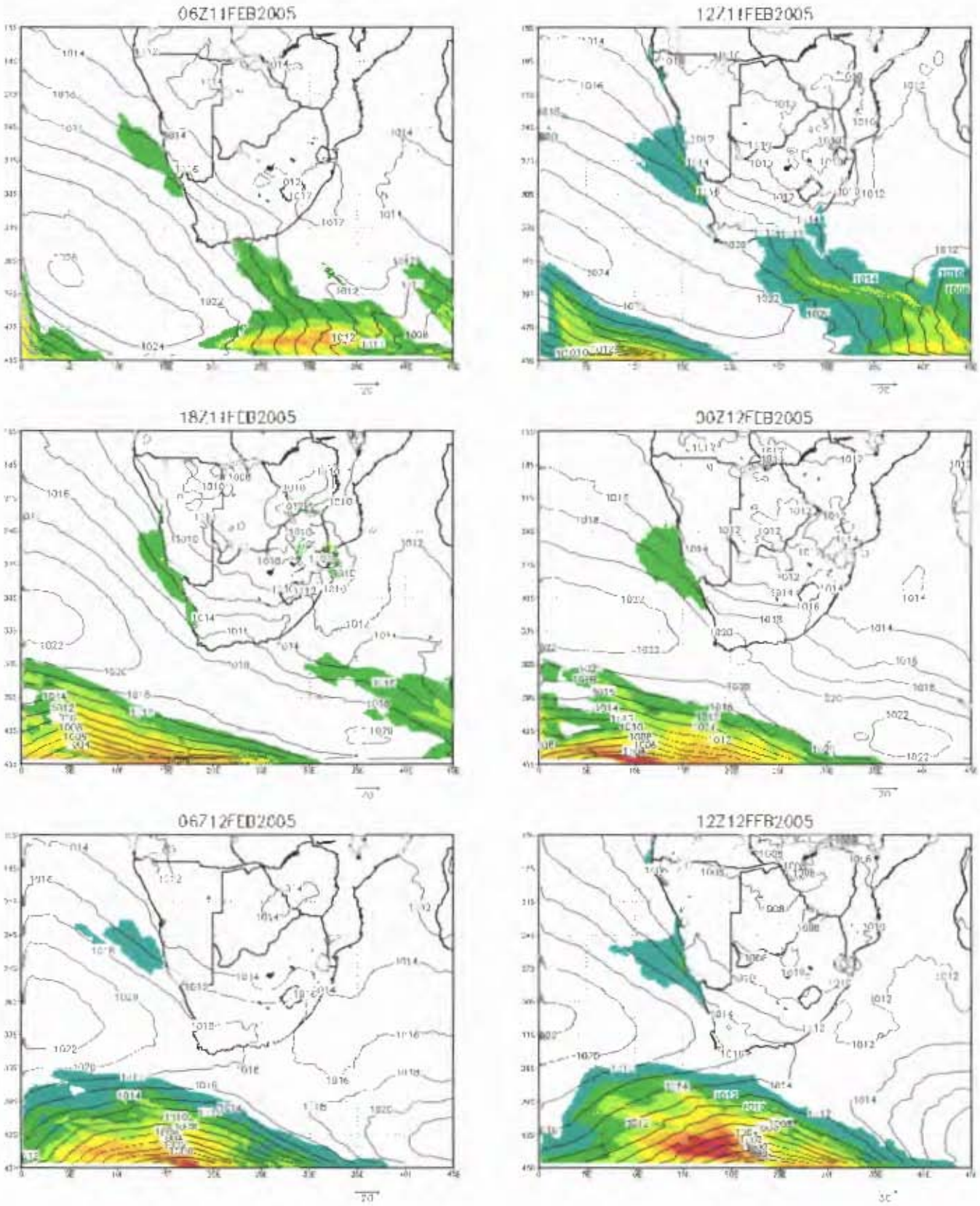

Figure 6.13: Mean sea level pressure (black contours; interval 4 mb) and winds with speeds greater than $10 m.s^{-1}$ at the 0.995 sigma level, derived from the topography sensitivity test. Starting at 06h00 UTC on the 11th and ending at 12h00 UTC 12 February (at 6-hourly intervals).

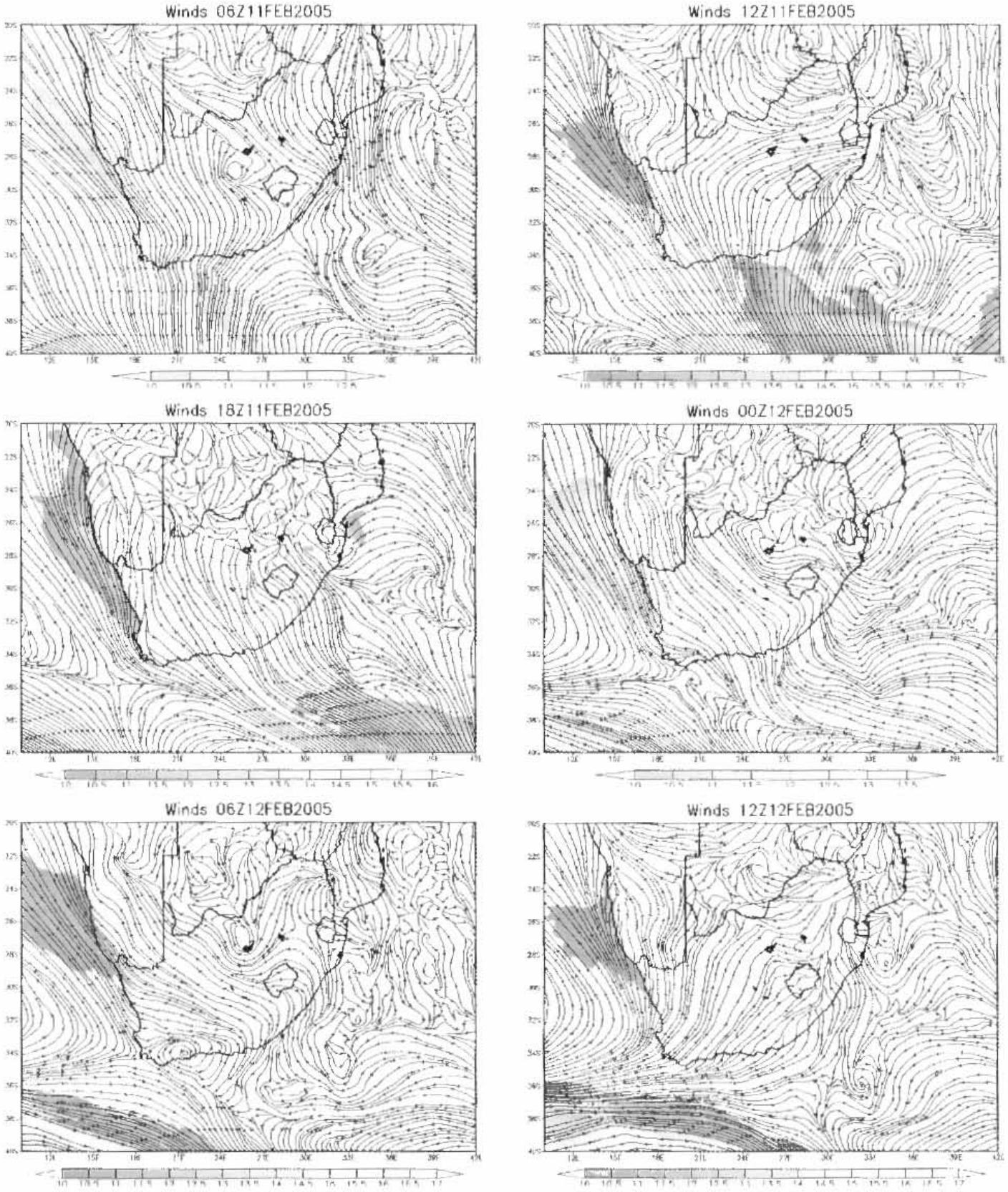

Figure 6.14: Simulated circulation pattern at the 0.995 sigma level and regions where wind speeds greater than 10m.s^{-1} are shaded (interval; 0.5 m.s^{-1}) found in the topography sensitivity test.

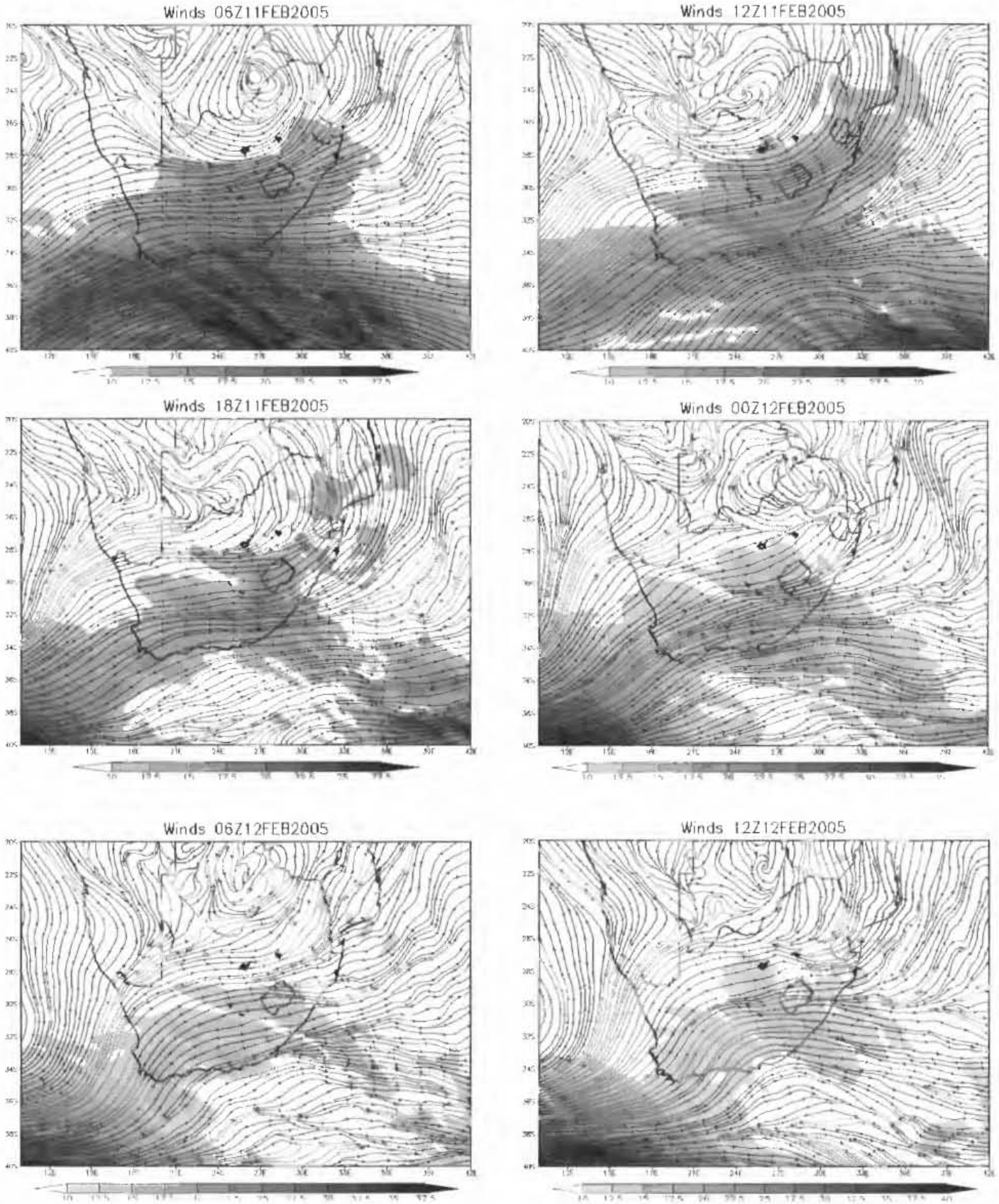

Figure 6.15: Same as figure 6.14, except at the 0.525 sigma level and that the shaded interval is at 2.5 $m.s^{-1}$.

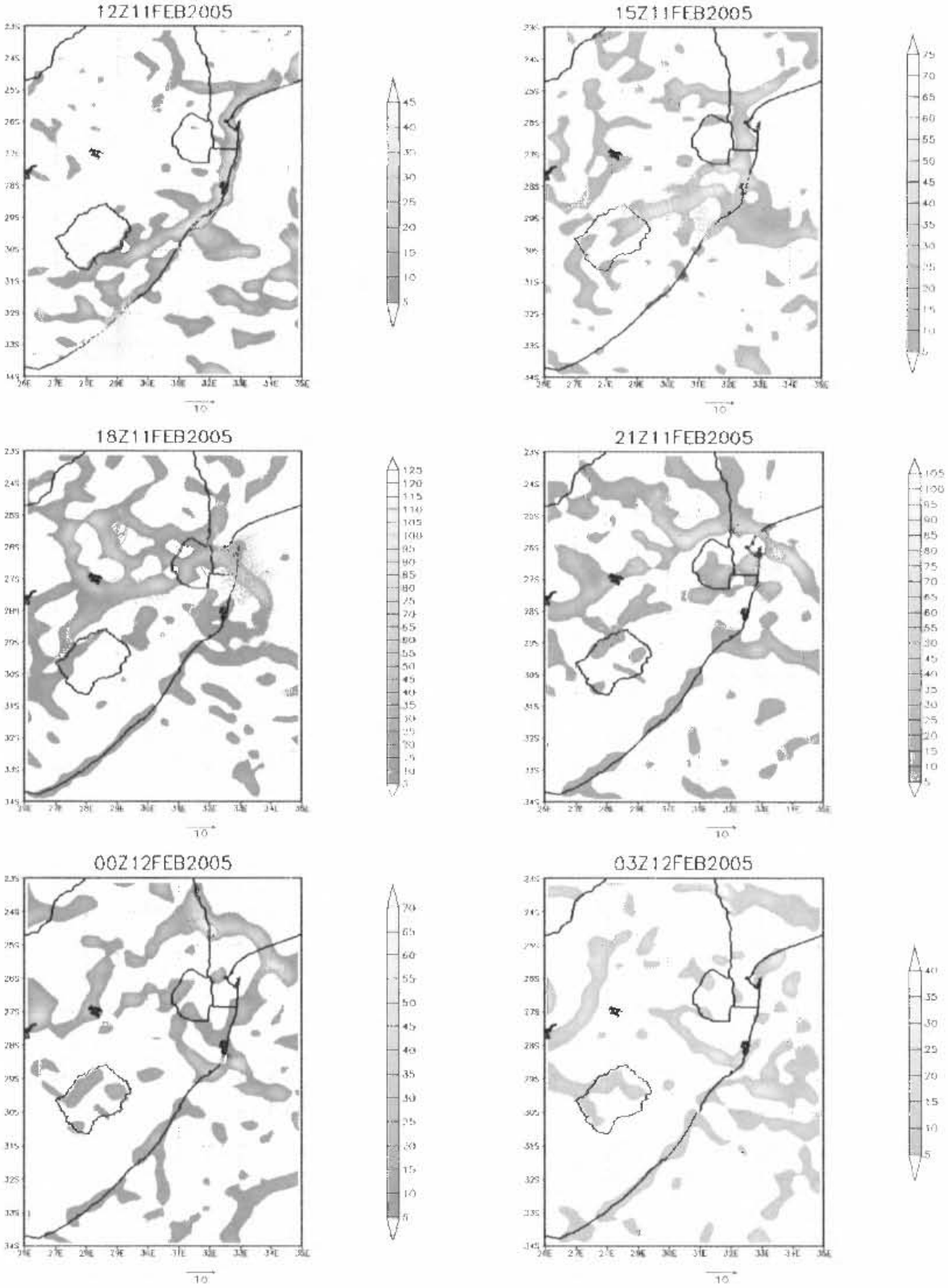

Figure 6.16: Moisture convergence (shaded positive values with interval of 5 $g.kg^{-1}.s^{-1}$) and wind speeds greater than 10 $m.s^{-1}$ at the 0.955 sigma level in the topography test simulation. Starting at 12h00 UTC 11 February through to 03h00 UTC on the 12th, and at 3 hour intervals. Note that divergence has been omitted for clarity.

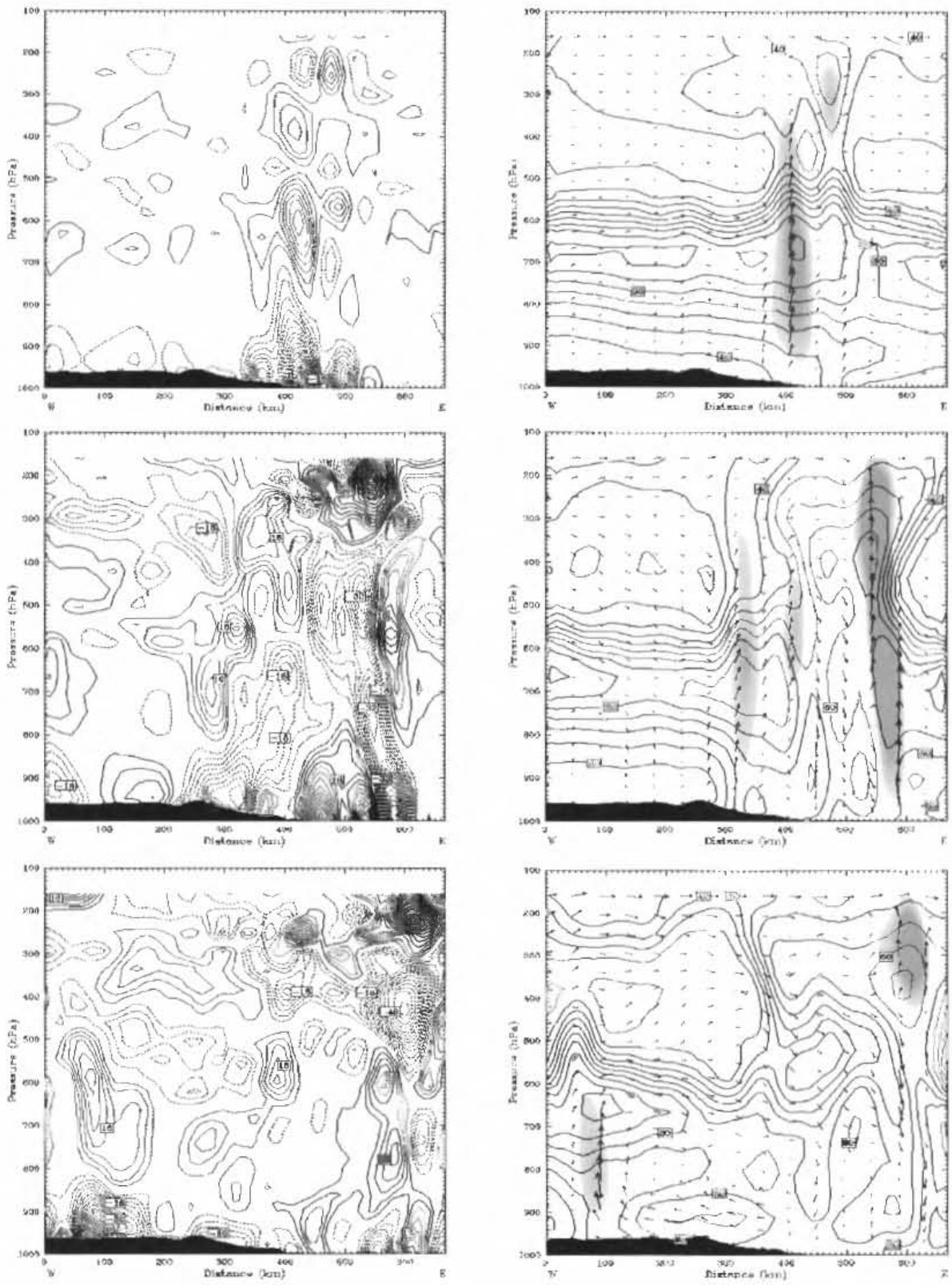

Figure 6.17: Vertical cross-section of divergence (left; interval 4 s^{-1}) and the right figures showing wind vectors, vertical velocity greater than 40 $cm.s^{-1}$ (shaded) and relative humidity (contours with an interval of 10%) along line D-D' found in figure 6.12 Starting at 15h00 UTC on the 11 February (2 hour intervals) and ending at 19h00 UTC. Note that divergence is positive and convergence is negative and dashed.

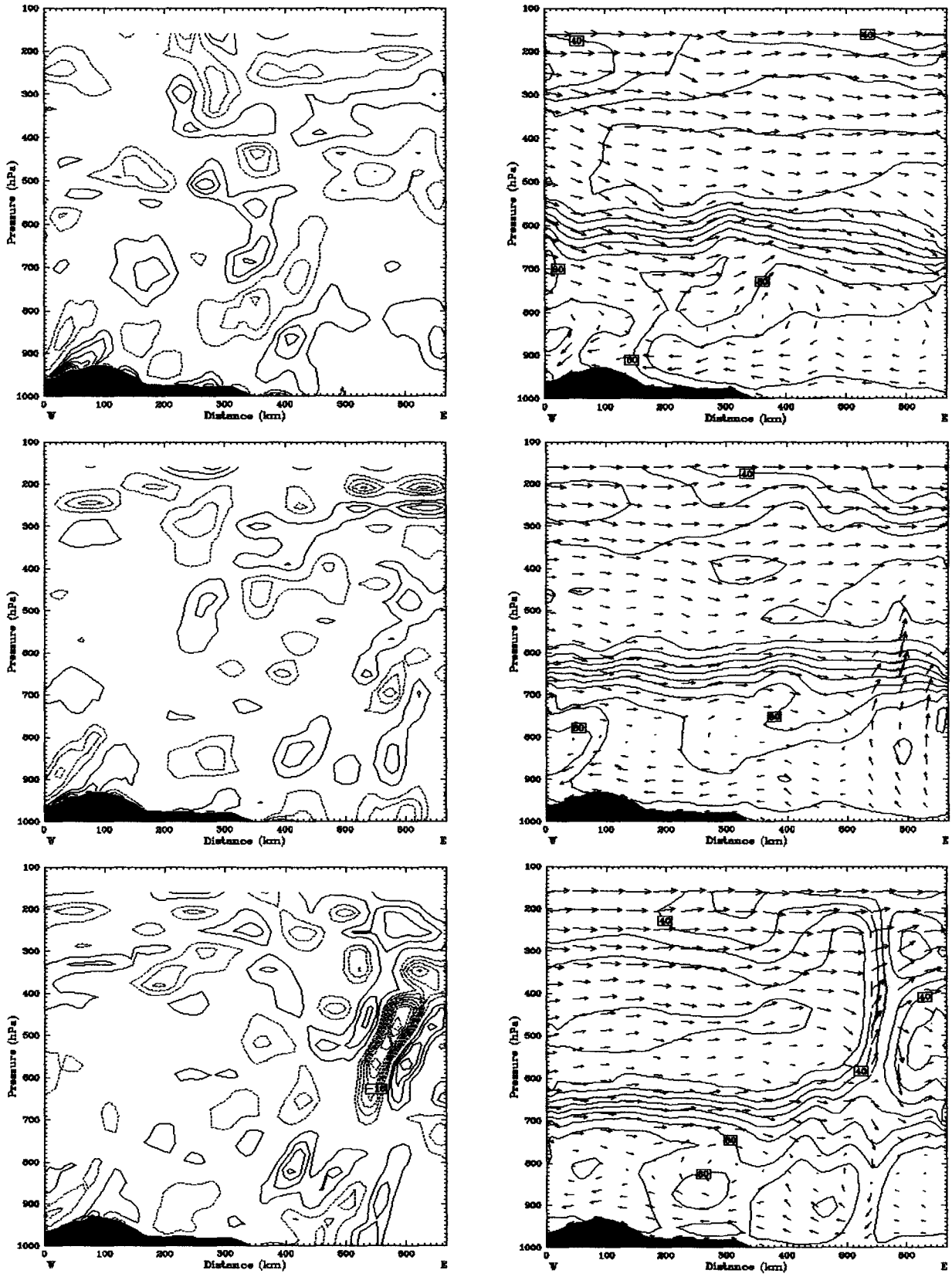

Figure 6.18: Same as figure 6.20, except for along line A-A' in figure 5.9 and starting at 18h00 UTC 11 February (3 hour intervals) and ending at 00h00 UTC. Note that divergence is positive and convergence is negative and dashed.

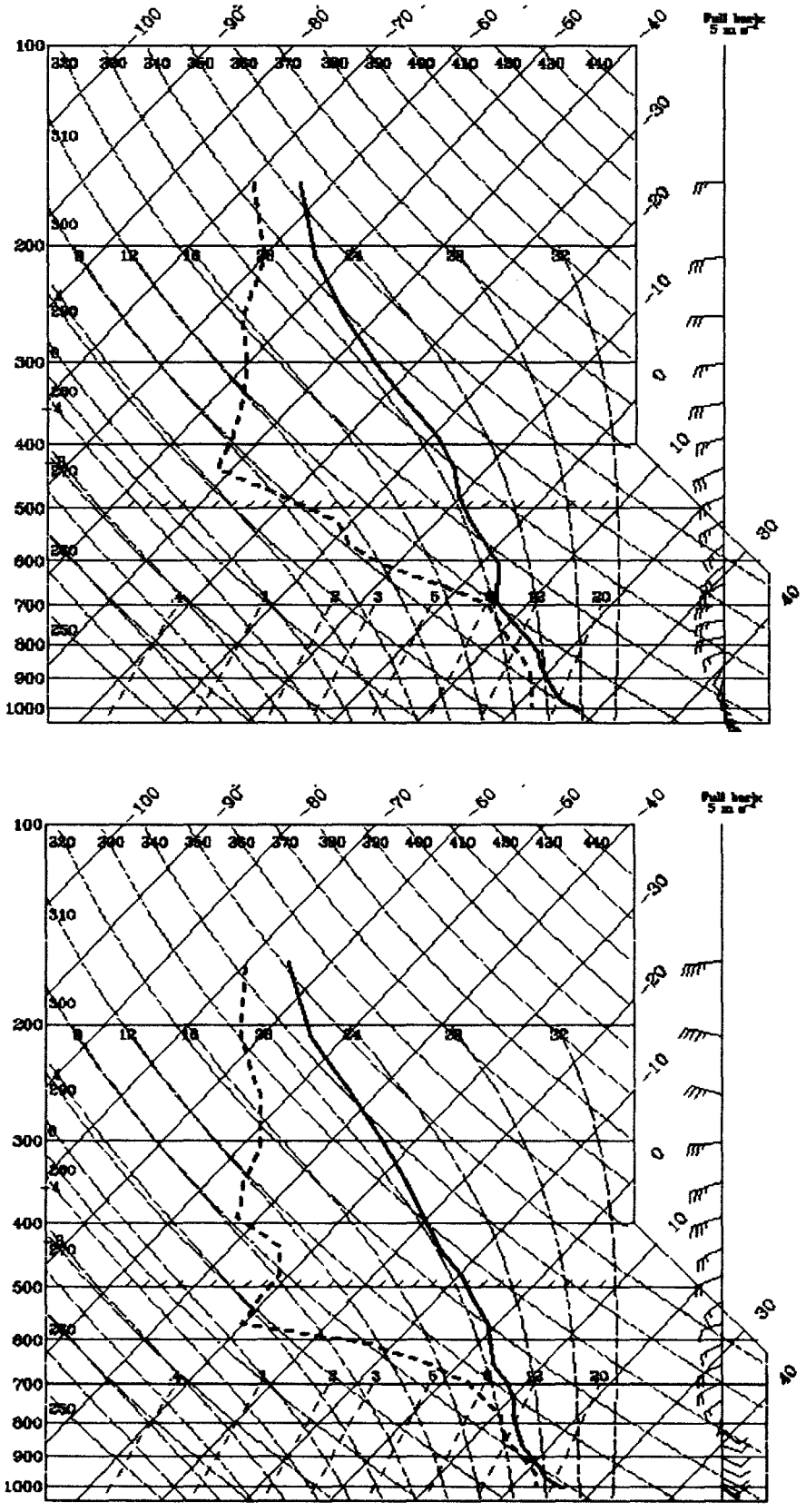

Figure 6.19: Soundings from the topography sensitivity simulation located at 29.97°S; 30.95°E (Location of Durban station) at 12h00 UTC 11 February 2005 (top) and 28.73°S; 32.08°E (Location of Richards Bay station) at 00h00 UTC 12 February 2005 (bottom).

a)

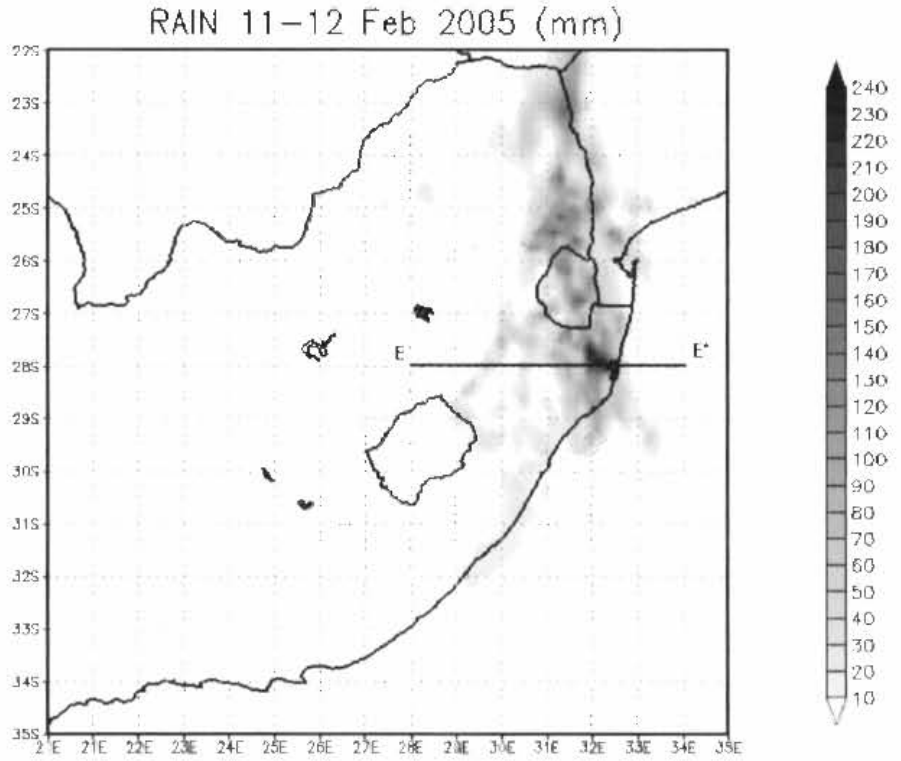

b)

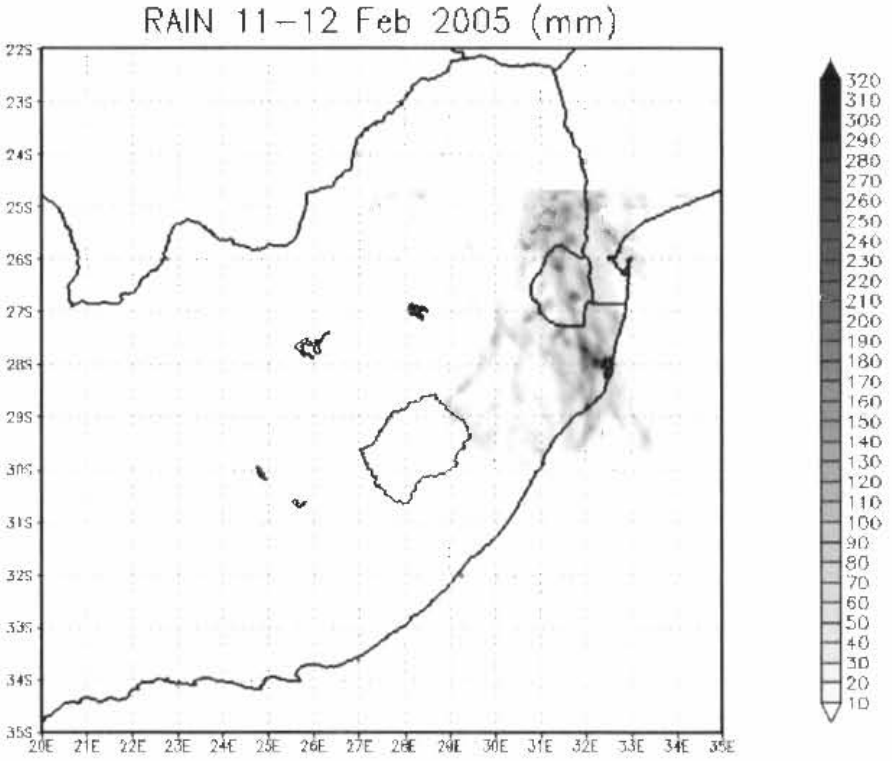

Figure 6.20: Accumulated precipitation for the 11 and 12 February 2005 for a) domain one and b) domain two in the mid-latitude sensitivity test.

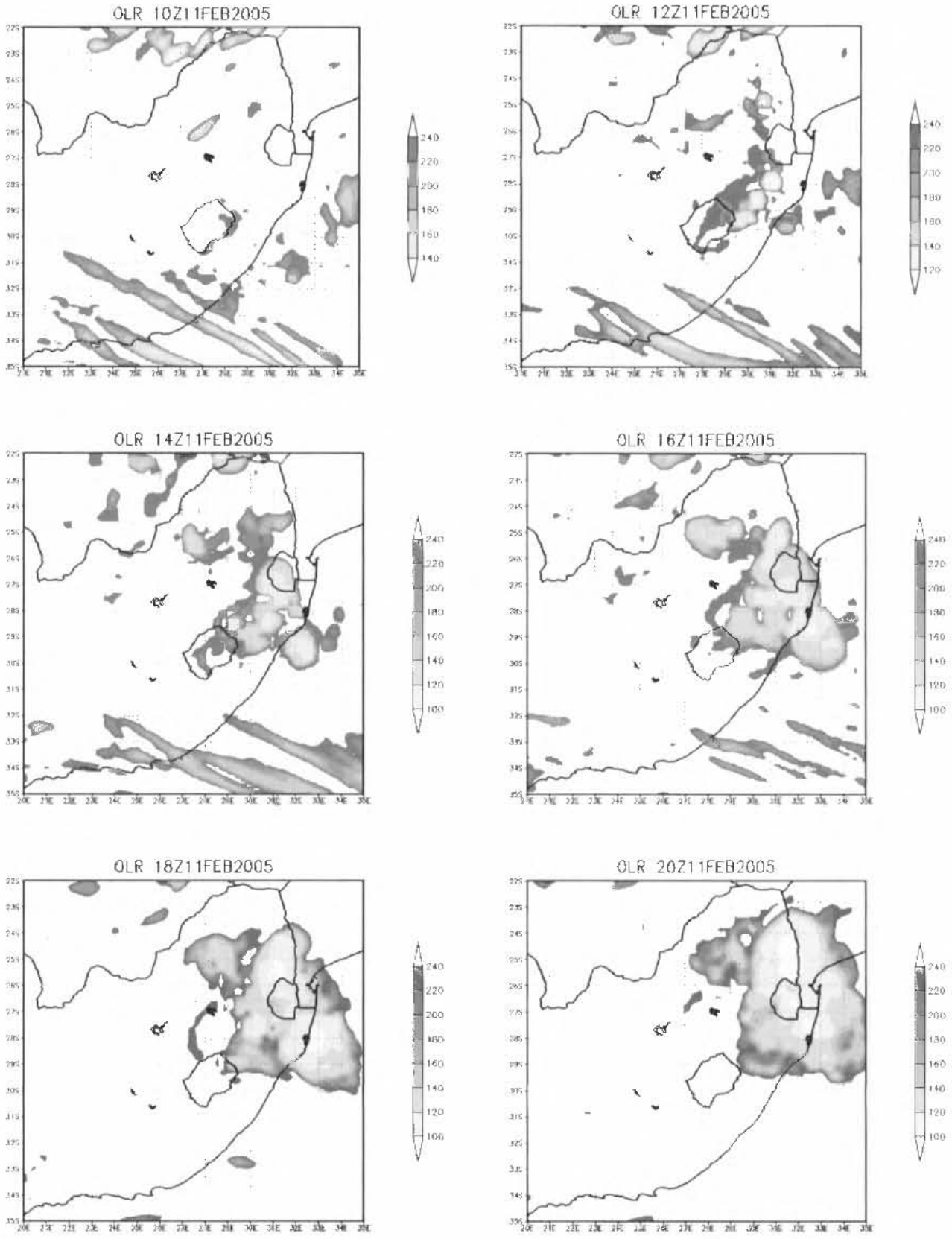

Figure 6.21: Domain one outgoing longwave radiation (interval, 20 w.m^{-2}) derived from the mid-latitude sensitivity simulation. Starting at 10h00 UTC 11 February at 2 hour intervals and ending at 20h00 UTC.

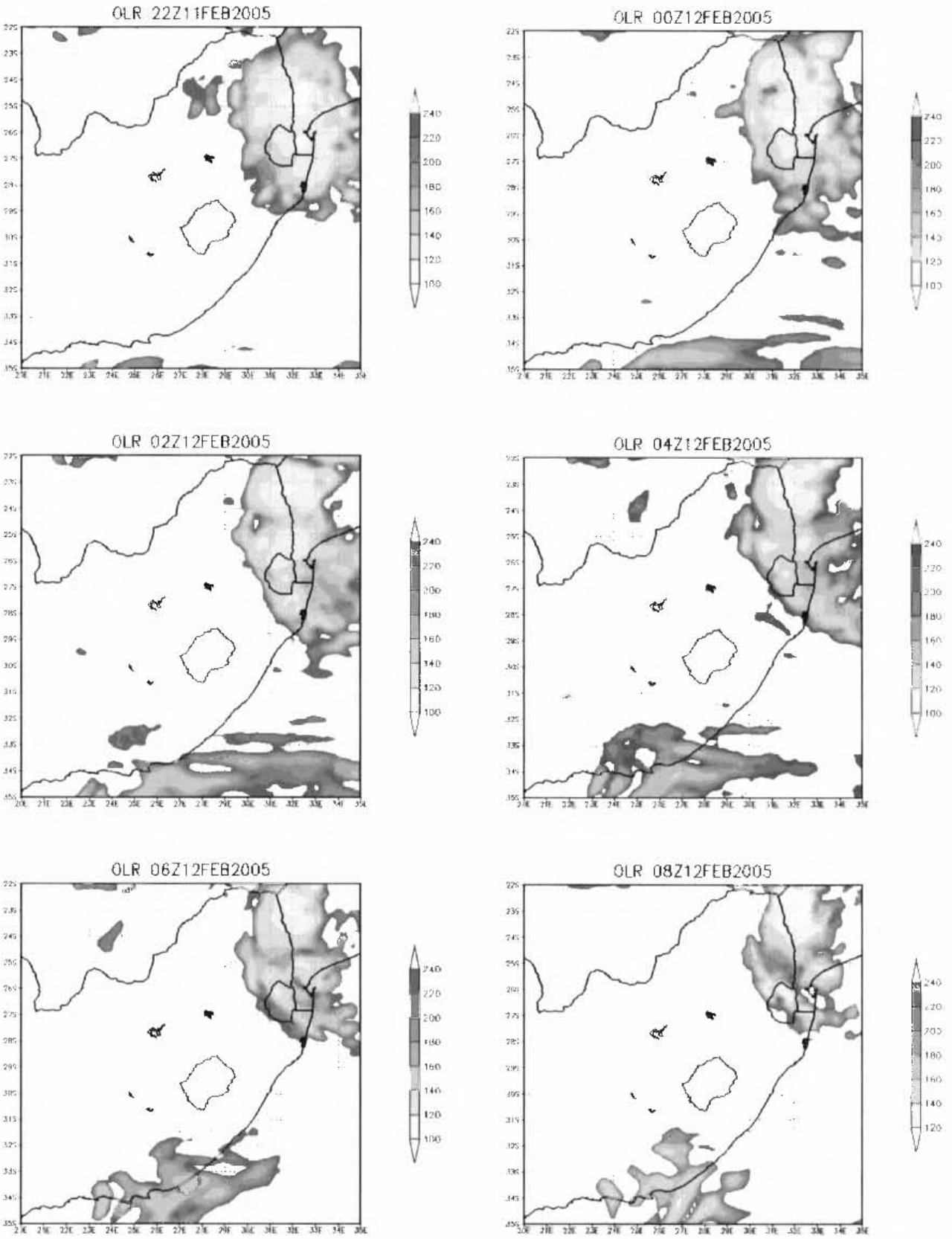

Figure 6.21cont: From 22h00 UTC 11 February at 2 hour intervals and ending at 08h00 UTC on the 12th

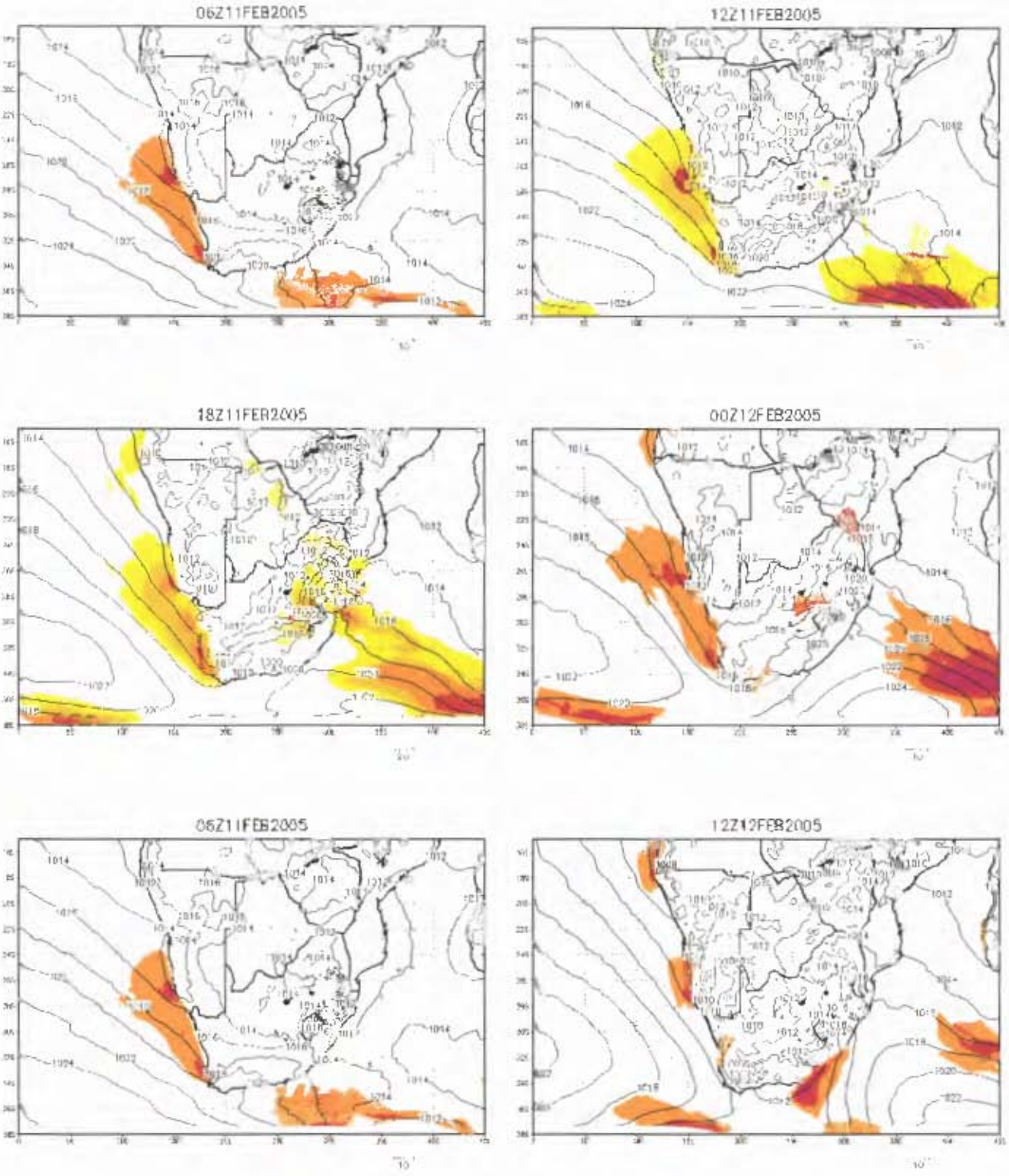

Figure 6.22: Mean sea level pressure (black contours; interval 4 mb) and winds with speeds greater than 10m.s^{-1} at the 0.995 sigma level, derived from the mid-latitude sensitivity test. Starting at 06h00 UTC on the 11th and ending at 12h00 UTC on the 12 February, at 6-hourly intervals.

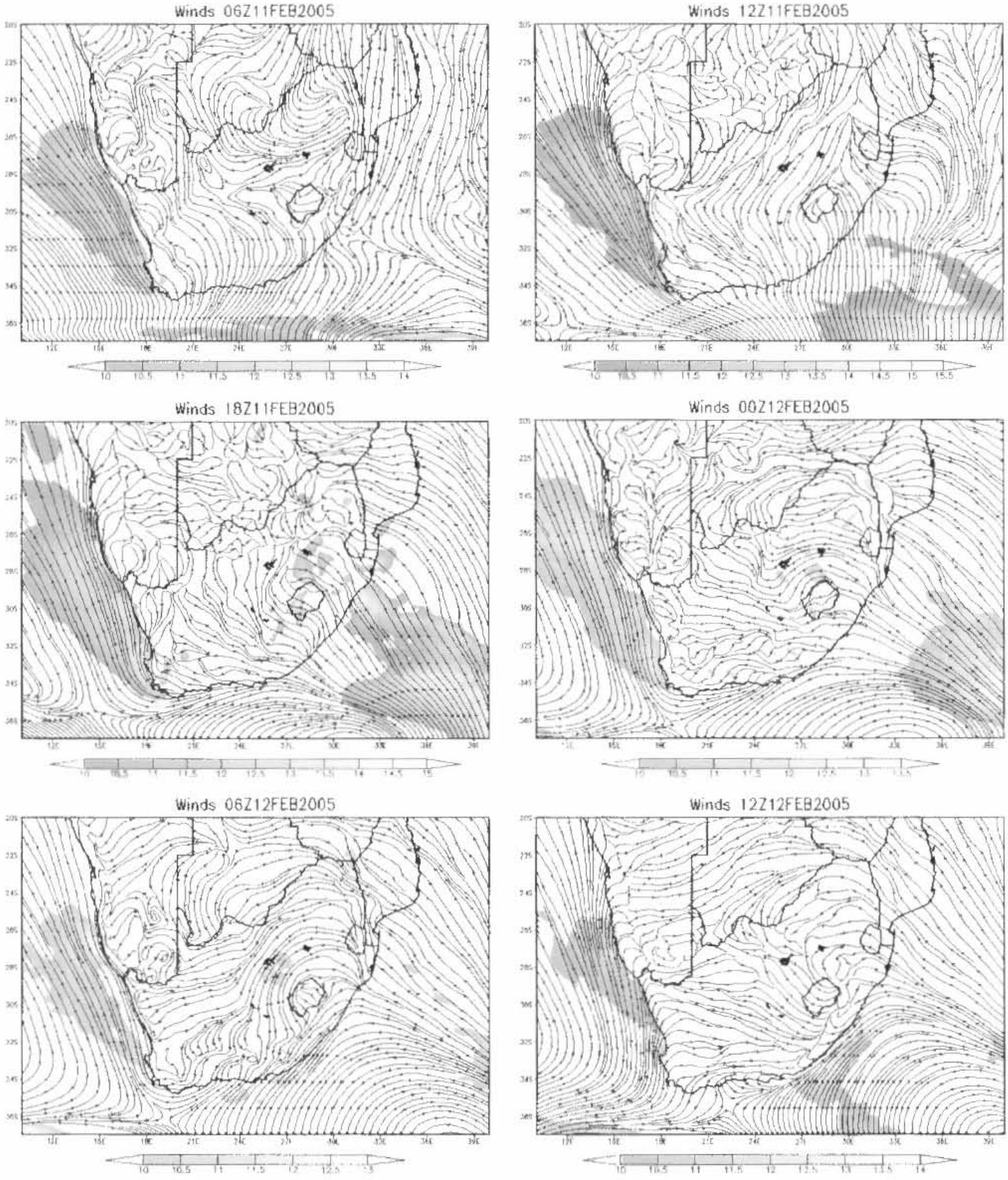

Figure 6.23: Circulation pattern in the mid-latitude sensitivity run at the 0.995 sigma level and regions where wind speeds greater than 10m.s^{-1} are shaded (interval; 0.5 m.s^{-1}).

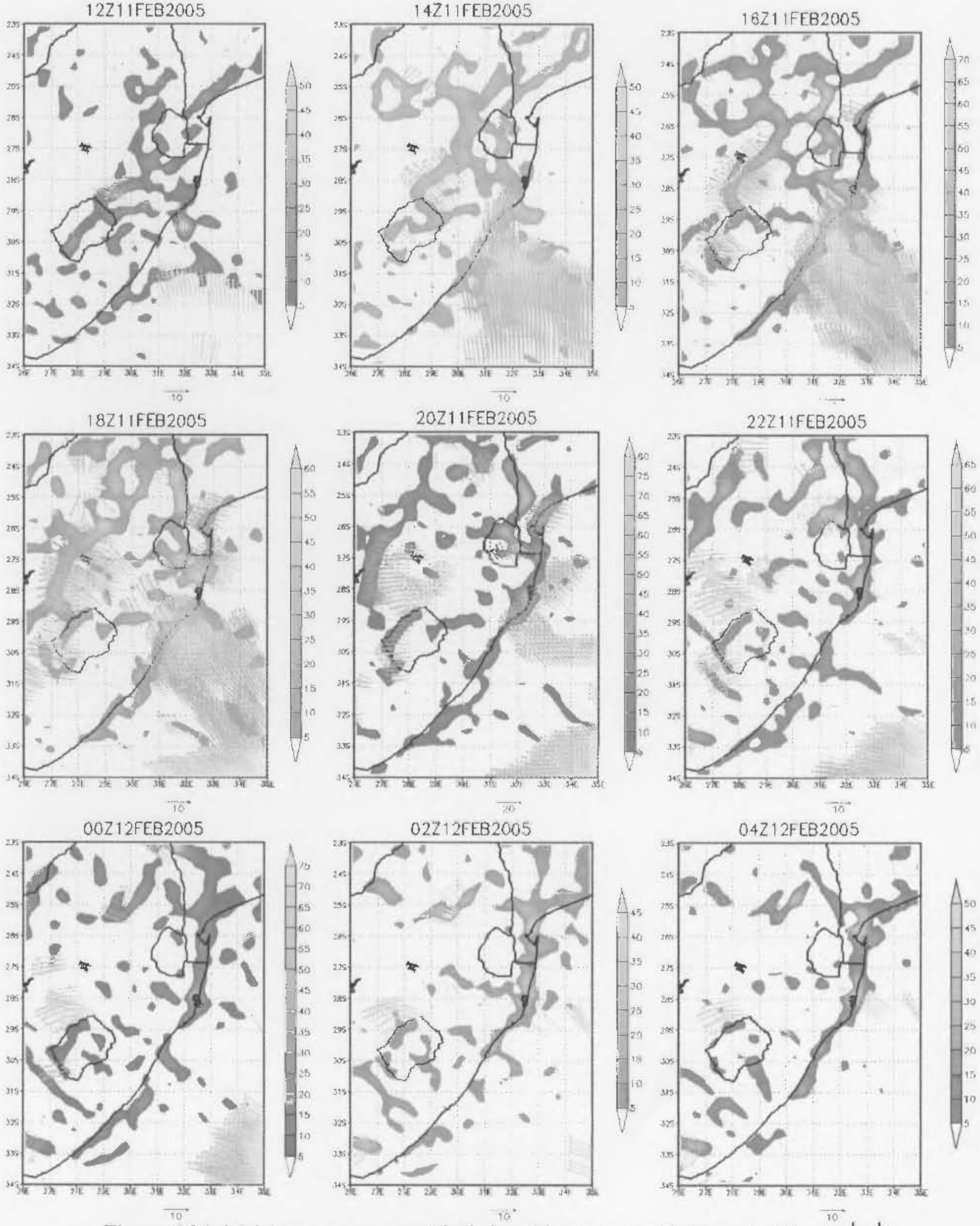

Figure 6.24: Moisture convergence (shaded positive values with interval of 5 $\mathbf{g.kg^{-1}.s^{-1}}$) and wind speeds greater than 10 $m.s^{-1}$ at the 0.955 sigma level from the mid-latitude sensitivity simulation. Starting at 12h00 UTC on the 11th through to 04h00 UTC on the 12th, at 2 hour intervals. Note that divergence has been omitted for clarity.

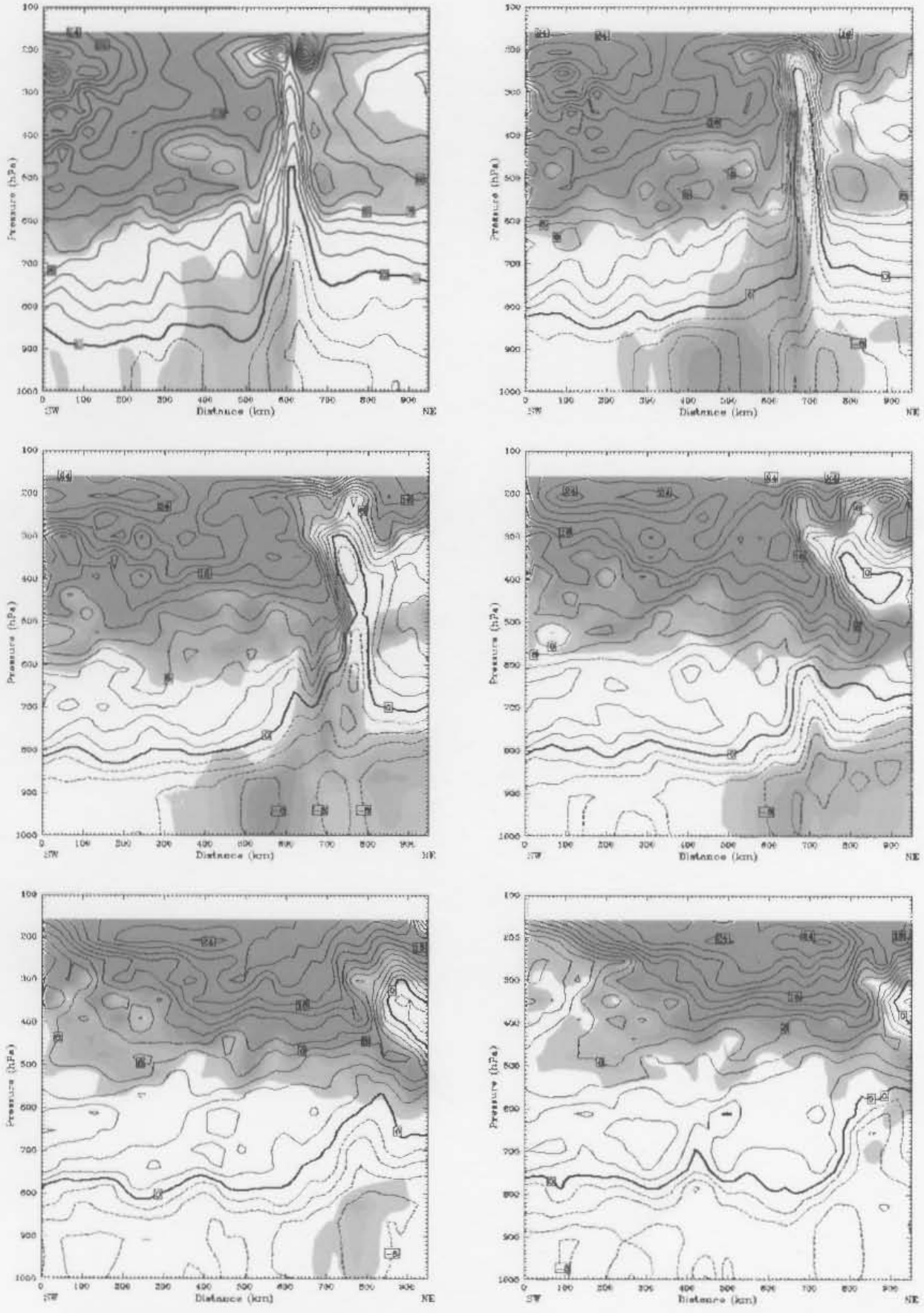

Figure 6.25: Vertical cross-sections of wind speeds starting at 10 $m.s^{-1}$ (shaded; 5 $m.s^{-1}$ interval) and zonal wind speeds (contour; 2 $m.s^{-1}$ interval) along B-B' (see figure 5.9). From left to right, starting at 14h00 UTC (top) and ending at 00h00 UTC (bottom).

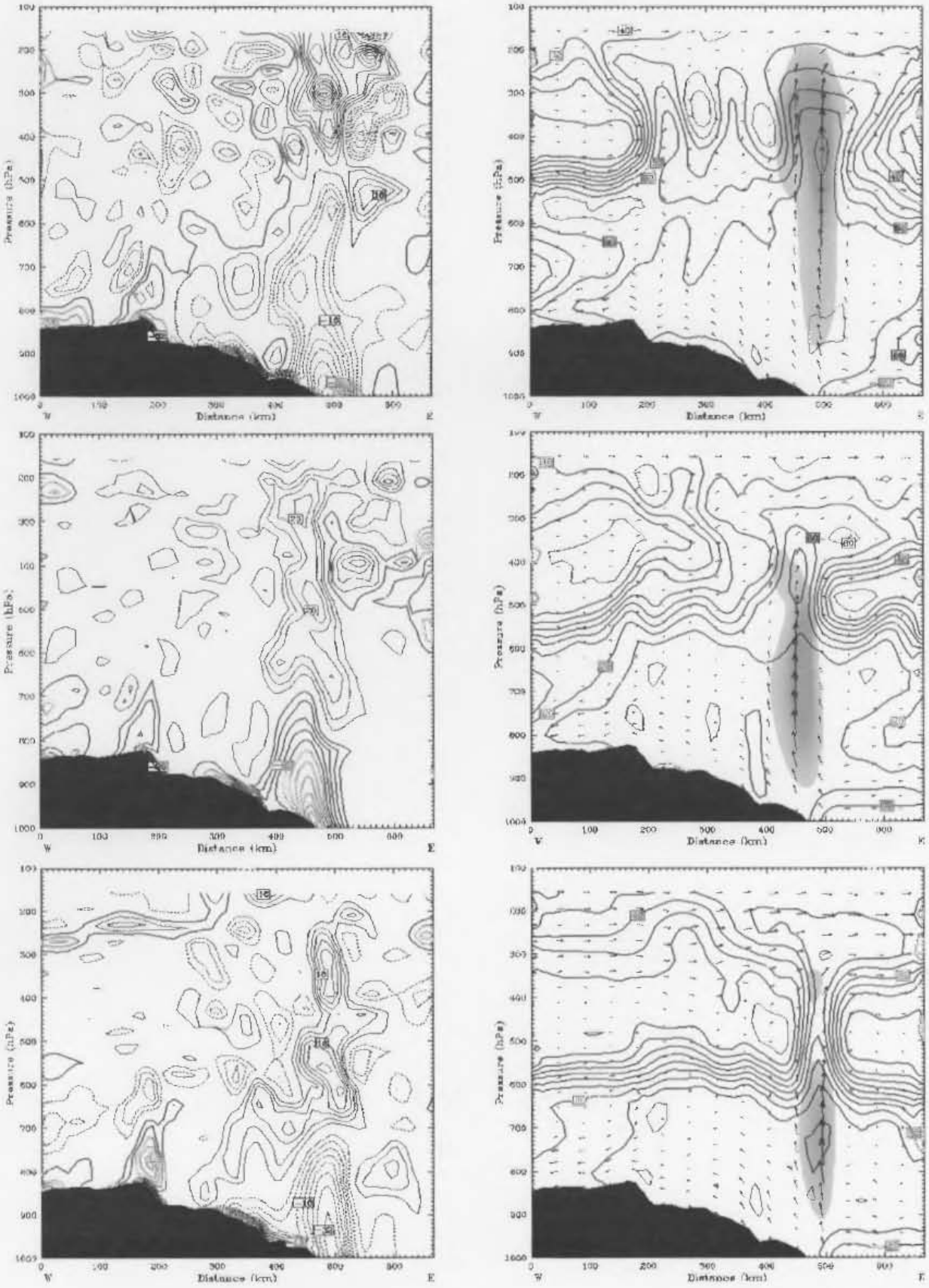

Figure 6.26: Vertical cross-section of divergence (left; interval 4 s^{-1}) and the right figures showing wind vectors, vertical velocity greater than 40 cm.s^{-1} (shaded) and relative humidity (contours with an interval of 10%) along line E-E' found in figure 6.20a. Starting at 17h00 UTC 11 February (4 hour intervals) and ending at 01h00 UTC. Note that Divergence is positive and convergence is negative and dashed.

Chapter 7

Discussion

7.1. General Discussion

South Africa is frequently affected by severe weather events, but the scarcity of observations restricts our understanding of these weather systems. Advancements in technology, particularly in the radar, satellite and computer industry, have resulted in the global research of MCSs being more efficient and accurate. However, the biggest problem is that many areas, especially the poorer nations, do not have sufficient observation technology (especially radar and radiosondes) or equipment to research or monitor these types of convective systems. This is probably one of the main reasons why systems in the United State of America (US) have been documented much better than in other MCS locations. In addition, forecasting MCSs is still a major problem that has to be addressed. From the little research that has been done on Southern African MCSs, it can be seen that these systems are not uncommon to the region and they continuously pose a threat when they occur.

As documented in the literature, a MCS may produce large amounts of precipitation and a host of other severe weather phenomena (see chapter two). Not only do they pose a danger, they are perceived to be an important feature of the South African climate due to the substantial contribution they make to total annual rainfall (Garstang and Tyson, 2000). Thus, a better understanding of their development and evolution is required. In particular, more details about the factors that separate the formation of the different types of convective systems is needed. The understanding of the synoptic and mesoscale conditions that possibly result in the development of these large convective systems remains poor. It should be noted that the synoptic conditions summarised by Maddox et al. (1986) that result in the development of MCCs are those that generally result in the development of convective weather and do not differentiate days when large MCS occur and those that result in the development of scattered thunderstorms. Therefore, further research is required in order to identify features that are important to the development of these systems.

As mentioned previously, most MCSs that have been studied in recent decades have occurred in the Northern Hemisphere, particularly in the US. Comparisons can be made between the systems in the US with those found in South Africa, but this is limited because there are differences in the factors that play a role in the development and location of these systems. For example, the geographic setting of South Africa is different to that of the US. South Africa is a much narrower land mass, is bordered by the surrounding oceans along its western, eastern and southern borders. The South African landmass terminates near 34°S, whereas North America extends into high latitudes. The major moisture source for mesoscale convective systems in the US is the Gulf of Mexico (e.g. Maddox, 1983; Velasco and Fritsch, 1987; Laing and Fritsch, 2000), whereas moisture sources for the South African summer rainfall region include the neighbouring tropical oceans (D'Abreton and Lindesay, 1995; Cook et al. 2004), tropical Africa (D'Abreton and Lindesay, 1993; Cook et al. 2004) and the Agulhas Current region (Jury et al. 1993; Rouault et al. 2002; Singleton and Reason, 2006, 2007). Another key difference is that the US contains large areas of flat plains with significant mountain ranges near each coast, whereas South Africa has much smaller areas of flat terrain. Thus, different features to the U.S. may play a role in the development and life cycle of MCS in South Africa. However, the little research that has been done in South Africa has found that the systems themselves do not differ that much from the global population (e.g. Laing and Fritsch, 1993b, 1997).

In this thesis, a MCS that developed over the eastern parts of South Africa is analyzed. This part of the country has been known to favour the development of these types of convective systems, as documented by Laing and Fritsch (1993b). It should be noted that these authors concentrated on one specific type of MCS, namely, the largest of the convective systems, the mesoscale convective complex (MCC). However, these authors noted two key local features that possibly play a role in MCC development in this region, namely the high-lying topography of the eastern escarpment and the large quantities of moisture available due to the close proximity of the Agulhas Current. A similar trait was identified in this thesis, where it was found that these two features played a key role in the evolution of the MCS. The particular system studied here did not appear to reach MCC status since to it did not contain the correct eccentricity and did not last long enough. Although it just failed to satisfy

these two categories, it did manage to attain the required cloud top temperature and possibly size for MCC status.

In terms of development and evolution, the convective system was triggered over the eastern escarpment as single cells storms in the early afternoon of February 11 2005. The triggering of the event was likely due to a combination of the high-lying topography and strong surface diurnal heating. These single cell storms then merged, forming a large convective system known as a MCS. MRF data suggest that the convective event evolved as result of interaction between an interior trough, a ridging anticyclone located to the south of the country, and a mid-level trough propagating along the southern parts of the country. The timing of the different development stages of the system and the development pattern itself is similar to that identified in similar systems in other regions of the world (Maddox, 1980; Velasco and Fritsch, 1987; Millar and Fritsch, 1991; Laing and Fritsch 1993a; Laing and Fritsch 1997; Anderson and Arritt, 1998). The system then propagated towards the warm waters of the northern Agulhas Current, which is known to be a common propagation pattern of these types of large convective systems in eastern South Africa (e.g. Laing and Fritsch, 1993b). This propagation direction may be due to the combination of the mid-level flow pattern and the inflow of low level high-θ_e air (Corfidi et al. 1996). It was evident that in all the simulations conducted in this thesis, the propagation of the simulated system appeared to be influenced by the prevailing mid-level flow. It was also apparent that most of the moisture used to fuel the system originated from the Agulhas Current region. The Agulhas Current as a moisture source for extreme precipitation events has been identified in numerous cases before (e.g. Rouault et al. 2002; Singleton and Reason, 2006, 2007).

Simulations with a numerical mesoscale model indicated that the heavy precipitation along the coastal regions resulted from a combination of factors. These factors include a convectively unstable atmosphere, which contained a high water content, and a coupled low level convergence and mid-level divergence pattern. The coastal topography may also have provided the initial uplift required for the heavy precipitation. More importantly, the simulations indicated that these favourable patterns for the development of convection persisted for long periods over the coastal regions and resulted in the heavy precipitation. As noted by Doswell et al. (1996),

large local precipitation totals often occur when deep convective cells are organized in such a way that they move repeatedly over a given area.

Ultimately, these synoptic and mesoscale conditions are likely to have favoured the development of an MCS and the heavy precipitation due to them remaining over a specific region and lasting for several hours (Romero et al. 2000). However, there were slight differences identified in the model simulation when compared to the observations. The next section discusses some of the known problems with simulating or forecasting these convective systems and the associated precipitation, which may have influenced the results obtained in this thesis.

7.2. Discussion of Modelling Results

There have been a number of studies dedicated to examining the ability of a mesoscale numerical model to simulate mesoscale convective systems and the associated weather phenomena, and those that have done so have shown some success (e.g. Tucker and Crook, 1998; Romero et al. 1998; Bernardet et al. 2000; Zhang et al. 2003 and many others). However, there is still a lot of room for improvement in simulating these convective systems. MCSs are predominately warm season events, which suggests that numerical models will struggle to accurately simulate these types of systems due to the poor simulation/forecast of convective precipitation (e.g. Kuo et al. 1996; Wang and Seaman, 1997). This problem may be due to deficiencies in the parameterizations (e.g. the convective scheme or the land-surface scheme, etc), which may need to be tailored for local conditions. Currently, there do not appear to be a suite of universal parameterization schemes that produce better results in a range of different environments and situations.

It was found that the precipitation in the control run was over-estimated or under-estimated in certain parts of northeastern KZN but, the spatial distribution was reasonably well produced. However, there also appeared to be some small regions where the model simulated precipitation which did not occur in the observations. It should be noted that even with an increased resolution, there was no difference in the spatial distribution of precipitation, although the intensity changed. The nested domain in the control simulation appeared to have a similar precipitation distribution

when compared to the mother domain, but it had larger errors in the over-estimated precipitation.

Precipitation under- or over-estimation appears to be one of the biggest problems when it comes to accurate simulations of flash flooding associated with mesoscale convective events. As noted by Fritsch et al. (1998), quantitative precipitation forecasting (QPF) skill by the current operational models remains relatively low. Spencer and Stensrud (1998) ran different modelling experiments to find that some sacrifice has to be made in either precipitation totals or areal extent of heavy precipitation. They suggest that it is more useful to under-estimate the total precipitation, but produce a correct distribution of the precipitation than to produce a more accurate total precipitation, but the wrong spatial distribution.

Probably the key for numerical mesoscale models to produce reasonable simulations is that they must accurately predict the development and evolution of convection. Convective processes usually occur on scales smaller than can be resolved by current model resolutions, and hence, have to be parameterized. Zhang and Fritsch (1988a) suggest that two of the most important components in modelling mesoscale events are that of adequate parameterizations of deep convection and the planetary boundary layer (PBL). From the literature it is known that the simulations of convectively generated mesoscale patterns show considerable sensitivity to the formulation of the *trigger function* within a convective (or cumulus) parameterization scheme (CPS; e.g. Kain and Fritsch, 1992 and Stensrud and Fritsch, 1994). The *trigger function* is the complete set of criteria used to determine when and where deep convection occurs in a numerical model (Kain and Fritsch, 1992). Other authors, such as Kuo et al. (1996) and Wang and Seaman (1997), have also identified model sensitivities to differences in the actual construction of the CPS. It should be noted that the problems associated with the construction of CPS is not discussed here due to it being beyond the scope of this thesis. Kuo et al. (1996) also found that the distribution and intensity of precipitation were "extremely sensitive" to the choice of the CPS. As noted by Grell et al. 2000, convective parameterizations are often the source of error in model precipitation.

A large portion of the summer rainfall in South Africa is convective in origin (Tyson and Preston-Whyte, 2000), which means that an effective CPS is required for the model in order to accurately simulate or forecast precipitation patterns. There has been considerable focus on the issue of a reliable or effective CPS (e.g. Kuo et al., 1996; Wang and Seaman, 1997; Kuo et al. 1997; and others), but there does not appear to be a scheme that performs consistently better than others. In this thesis, all simulations used the Grell CPS (Grell et al., 1994) in the mother domain. It has already been established that the CPS used in the simulation will have an influence on the precipitation output. Hence, a CPS that will perform favourably for the selected resolution was used. Based on the literature, it appears that the Grell and Kain-Fritsch schemes (Kain and Fritsch, 1993) are the most appropriate for the resolution chosen for the simulations in this thesis. For example, in a study by Wang and Seaman (1997), where four cumulus schemes were tested at grids of 36 km and 12 km on six heavy precipitation events, results showed that the Kain-Fritsch and Grell schemes did well in predicting total precipitation volume and storm life-cycles, but over-predicted light precipitation. To evaluate the success of the cumulus parameterizations, these authors used as indicators other aspects of precipitation, such as timing, evolution, areal coverage and intensity.

It must be noted that other physical processes that are parameterized will have an influence on convection, which is why sufficient parameterization of these processes is also required. An adequate PBL representation is required because of the large vertical fluxes of heat, moisture and momentum produced by near-surface processes which have a significant effect on the energy supply for PBL-rooted convective storms (Zhang and Fritsch, 1988a). This will apply particularly to the eastern Southern Africa region where the Agulhas current is responsible for large values of heat fluxes off the east coast (Rouault et al. 2003) and is known to have an impact on heavy rainfall events (Rouault et al. 2002; Singleton and Reason 2006, 2007). It was found that when increasing the resolution of the SST in the simulation, a better precipitation spatial distribution was obtained, but the intensity was greatly over-estimated in regions. An improved shape of the model mesoscale system also appeared to be generated when the higher resolution SST data was used, particularly when the system was located over the Agulhas Current.

However, it appears that many of the problems that arise in simulating MCS and the associated precipitation appear to be with the parameterizations used, with the CPS probably being the most troublesome (e.g. Grell et al. 2000). In order to reduce the influence that the convective parameterization scheme has on the model results, high resolution runs, which can explicitly resolve vertical motions causing precipitation, are required (Flory and Gutowski, 2005). Adequate model resolution has been highlighted throughout the literature to be of great importance in simulating MCSs and convection. The need for high model resolution was identified in the early stages of mesoscale modelling development. For example, Zhang et al. (1988) suggested that in order to reproduce a squall line with an explicit (grid-resolved) convective scheme, the grid size may need to be reduced so that individual convective components, such as updrafts and precipitation fallout, can be explicitly resolved. Using the non-hydrostatic version of MM5 to simulate precipitation over the complex terrain of the Alps, Grell et al. (2000) were able to produce more realistic precipitation patterns and increases in precipitation in their higher resolution runs due to a better resolution of the local orographic features. Weisman et al. (1997) found that the accuracy of the representation of mesoscale systems by a numerical model deteriorates significantly at grid resolutions larger than 4km.

From the simulated experiments in this thesis, it was identified that one of the key features of an increased resolution was the over-estimation of precipitation. At a higher resolution (6km compared to 18km), the location of the precipitation did not change drastically, but the intensity of the precipitation did. This difference between the simulated precipitation intensity within the domains could have possibly resulted from more precipitation being explicitly resolved in the nested domain and hence, an increase in precipitation in this particular domain.

However, it is not always the case that a higher resolution simulation will produce a better result compared to a lower resolution simulation. For example, Singleton and Reason (2007) found that MM5 deficiencies in the location of heavy rainfall during cut-off lows were not improved at 3 km resolution compared to the 27 km grid. Flory and Gutowski (2005) also suggest that the benefits derived from high resolution runs may not be worth the computational cost. These authors found that when attempting forecasting summer precipitation in the central US using a lower resolution run (20

km) and a higher resolution run (5 km), the spatial patterns and timings of the precipitation were well reproduced in both runs, but in both cases, the amount of precipitation was overestimated. As discussed by Kuo et al. (1997), model simulations with resolutions between 1-20 km add problems to the CPS due to a portion of the mesoscale convective system being resolved by the model. Mass et al. (2002) studied the effects of horizontal resolution on forecast accuracy and also developed a review on high resolution studies from the past two decades. These authors noted that higher resolution simulations appear more useful for strongly forced convection or convection associated with fronts, drylines or topography.

Bernardet et al. (2000) found that high resolution was needed not only to resolve convection, but that it must also be able to resolve components of the LLJ, such as the jet strength, timing and location. These authors found that changes in the simulated LLJ affected the development of the MCS, resulting in the rapid change in precipitation rate. As discussed in chapter two, a LLJ is usually a prominent feature found in the evolution of MCS. It should be noted that there did not appear to be a LLJ present in the control simulation. However, it was evident that moderate onshore winds still played an important role in providing fuel for the system.

Another important feature in the model setup includes the representation of the physiography (i.e. topography, soil moisture, etc) of the region. Bernardet et al. (2000) analysed four simulations of convective events that took place in the United States to show that the explicit simulation of convection depends on high spatial resolution of physiography. These authors found that their selected convective case studies were initiated by topography, or soil moisture gradients or other mesoscale forcing features. Numerical simulations have previously been used to identify the important role of topography in the initiation and development of MCSs (e.g. Tucker and Crook 1999). Mountains may aid in producing heavy rainfall through orographic uplift of potentially unstable air or they may assist in developing long-lived, stationary low-level convergence zones that provide a source for new convection to develop (Spencer and Stensrud, 1998). It was identified that the local topography appeared to play an important role in the evolution of the convective system presented in this thesis. From the results in the topography sensitivity simulation it indicated that the eastern escarpment in South Africa played an important role in triggering the

convective system as well as influencing the low level circulation patterns. The results also indicated that the coastal topography may have provided additional forcing for the uplift of the moist onshore flow and hence, favoured conditions for heavy precipitation.

However, in the absence of significant terrain features or other noticeable strong large-scale forcing for upward motion, a very accurate representation of the initial conditions is sometimes necessary for the success of numerical simulations. Stensrud and Fritsch (1994) noted that the initiation and evolution of convection is tied to mesoscale features that are not always well observed by the conventional observing network, which makes the structure of the model initial conditions a potentially crucial factor for a successful numerical simulation. These authors obtained a more reasonable representation of events when subjectively altering the mesoscale model's initial conditions by creating artificial stations and soundings. As discussed by Zhang and Fritsch (1986), it appears that the timing, location, and magnitude of mesoscale features within a mesoscale model simulation are subject to large errors when important mesoscale details are missing from the initial conditions imposed on the model. This result highlights the importance of data observing networks that have the ability to observe not only atmospheric conditions on the synoptic scale, but also on the mesoscale.

For this particular case study, it was found that when starting the model run two days prior to the control simulation starting time, a different precipitation pattern was found, with a significant under-estimation of the precipitation along the entire north coast region (not shown). As mentioned previously, the region does not contain any significant topography as found in the interior, so other factors, such as those found in the control simulation, are required for heavy precipitation. As discussed by Xu et al. (2001), highly nonlinear processes are involved in the simulation of an MCS, which increases the likelihood that small errors in the early part of the simulation may accumulate and become amplified as the simulation continues, resulting in large errors at the end. Hence, the longer the spin up time involved in the simulation, the more likely the model will deviate away from the event. Thus, if one has reasonable or accurate initial conditions, it is better to start closer to the event, but at the same time there must be enough time for the model to spin up. As shown in the control run,

starting the simulation at 00h00 UTC 10 February 2005 resulted in a more accurate simulation of the event.

The literature suggests that a possible solution may involve the use of additional data in the initialization of the model to increase the accuracy of the simulation. An example of this is the incorporation of extra sounding data, such as that used by Zhang and Fritsch (1986) that are not typically available from the regular observational network. On the same note, Zheng et al. (1995) found that they could not successfully simulate a flood-producing mesoscale convective system in northwestern Oklahoma with standard observations alone. Thus, if special observations are not obtainable (as in most cases) then other measures have to be taken in order to try and achieve a reasonable simulation of the event. Another method which seems to be used more often in modelling is that of four-dimensional data assimilation (e.g. Yakazami and Orgaz, 2005). Four-dimensional data assimilation (FDDA or 4-DDA) involves processes through which the model is kept in close check with observations. However, for this process to be useful, a reliable and well distributed observation dataset is required, which is problematic for the South African region. It should be remembered that not all regions gather continuous observation coverage due to varying circumstances. Results from the mid-latitude sensitivity simulation highlighted the importance of the Southern Hemisphere mid-latitudes in the simulation of weather systems over South Africa. These results indicated that the large-scale features found in the mid-latitudes need to be well resolved in the models initial and boundary conditions. This is due to these large-scale features having an influence on weather patterns over South Africa. However, the Southern Hemisphere mid-latitudes is a region that cannot provide continuous or well distributed radiosonde or station data due to the lack of land. This region relies on data obtained from other observing systems, such as satellites, which have played a key role in the development of analysis data for the Southern Hemisphere since 1979 (Tennant, 2004).

It should also be noted that there are other factors that play a role in mesoscale modelling. In a modelling case study, Xu et al. (2001) found that in a weakly forced large–scale environment, the successful simulation of an MCS may depend on the size of the time step. These authors found that when time steps in the model set-up

were altered, different results were achieved. They proposed that this sensitivity to the change in time step size may possibly be related to the numerical horizontal diffusivity, which is dependent on the time step. They also noted that the precipitation field was the most sensitive, with both the location and intensity affected.

The setup of a model simulation can be very subjective, so that the simulations could be seen as a trial and error process, used to try and identify the most appropriate configuration. The challenge in modelling mesoscale convective systems is that they occur on a scale of hundreds of kilometres, yet the model resolution must be fine enough to simulate the key formation elements accurately. Also, the different severe weather producing systems all contain different forcings and features that play a role in their evolution, which also differ from case to case. This is why further modelling studies are required to try and identify the best setup for the range of systems. The validation of model simulations is something that also requires further attention, especially in regions that only contain coarse resolution observations. An adequate network of weather stations that continuously record atmospheric conditions is required to validate the model results. These observations could also be included in the initial conditions of the model simulation. In summary, it can be concluded that the key features that require attention when commencing a model simulation include: the horizontal and vertical resolution, the parameterization schemes used, physiography (i.e. topography, soil moisture, etc) and the initial conditions (incl. starting times). Other problematic issues include computational space and time associated with higher resolution model runs.

It is clear that modelling mesoscale convective systems is very complex and that further research is required in order to identify the key factors in the evolution of such systems. It must also be highlighted that most model simulations of convective systems have focused on those outside of the African continent (with the possible exception of the Sahel region), where favourable conditions for the formation of these systems may differ from place to place. Thus, careful attention should be paid to setting up model simulations for the South African region and also direct comparisons of the results with that of the published literature should be viewed with caution. It can be concluded that there is still a great need for further research of such convective systems within the Southern Africa region.

7.3. Future Research

7.3.1. Introduction

The geographical position of South Africa together with sharp regional gradients, topography and sea surface temperatures may help account for the diverse array of weather conditions experienced in the country. Heavy rainfall events along the northern coast of KZN are not uncommon. In the past few decades, this region has been flooded by a range of severe weather producing systems, such as cut-off lows (e.g. November 2000) and tropical cyclones (e.g. Domoina in 1984). It was noted in chapter four that there is a lack of radar coverage in this region, which is something that needs to be addressed. Research such as this thesis should provide motivation for SAWS to install increased radar coverage over the region, because such events will more than likely continue in the future. Possibly one of the most influential features in this region is the close proximity of the Agulhas Current, which has been shown to have a large influence on weather systems developing over South Africa (e.g. Rouault et al. 2002; Singleton and Reason 2006, 2007). Previous research has also highlighted the importance of the eastern escarpment in the development of convective systems in that region, which then propagate towards the coastal regions (e.g. Laing and Fritsch, 1993b), as also occurred in this case study. Thus, a better understanding of regional topography and oceanic features on the development of MCSs and associated heavy rainfall events over the east coast of South Africa is needed.

An important step, once sufficient satellite data are available, is to develop a climatology of mesoscale convective systems within Southern Africa. To the author's knowledge, there does not appear to be any information on how many MCSs occur annually over South Africa. Thus, future studies should determine how frequent these types of systems occur and how much they contribute to the South African summer precipitation. This should be followed with a comprehensive study on the synoptic and local conditions that determine the development and location of the systems. The use of a mesoscale model would allow for the identification of the role that certain local features have on the development on such systems. On the local scale, a greater understanding of what variables differentiate days when large MCS occur and those that result in the development of isolated thunderstorms is also needed. However,

difficulties may arise when trying to develop a classification scheme for detecting days in which MCS may develop. Researching MCSs that developed over the Iberia and Balearic Islands in 2001, García-Herrera et al. (2005) noted that several precursors are essential to guarantee convection, but they do not appear to operate simultaneously when looking at individual events. These authors found that multiple combinations of convective contributors lead to a wide variety of scenarios for MCS genesis, thus making it hard to develop a reliable classification system.

7.3.2. The Role of Satellites

In regions where AWS data collection and radiosonde data are sparse, alternative methods are required. Satellites have played a major role in monitoring weather systems all over the world and collecting atmospheric data, due to these instruments being able to continuously observe large regions. They have been used to identify MCSs as well as their structural properties, location and distribution around the world (e.g. Evans and Shemo, 1996; Hodges and Thorncroft, 1997; Carvalho and Jones, 2001). A key role of satellites was determined early on when their capability for allowing the very-short-range forecasting of such severe weather systems became apparent (e.g. Zipser, 1982).

For this thesis, only data taken from the MSG satellite was utilized. Other instruments that could be used to monitor such events include the precipitation radar and TRMM microwave imager aboard the TRMM satellite (Kummerow et al. 1998). This satellite has previously been used to document a heavy rainfall event in South Africa (Rouault et al. 2002), but for this case study the satellite swath path did not extend over the KZN region during the event.

All channels aboard the MSG satellite are useful for determining different features within the atmosphere, due to the satellite capturing wavelengths ranging from visible wavelengths to infrared wavelengths. In chapter four, the use of individual channels, such as the IR channel, was used in identifying the convective system and the associated cloud top temperatures. These individual channels help in defining an MCS, as well as locating regions where convective precipitation is taking place. Another feature which used is that of false colour composites (also known as RGB

composites). This is due to some channels working better than others in different times of the day.

A typical MCS is usually a nocturnal feature, initiating during the afternoon and continuing to develop through the night. Night time and daytime convection is monitored by using different satellite channels and different Red-Green-Blue (RGB) composites. Certain wavelengths are ineffective at night as a result of there being no sunlight reflected off the cloud tops. Thus, daytime convection may be monitored using the previous mentioned channels, such as the IR and the visible channels, whereas night time convection uses the infrared channels and water vapour channels or a combination of these channels.

Future work on Southern African convective systems could include the use of RGB composites to help identify characteristic features during the development and life cycle of MCSs. These composites may also be used for short range forecasting of heavy precipitation due to this method allowing for the detection of regions of strong convection within the cloud mass. Ultimately, the use of these composites will hopefully broaden our knowledge on detection, monitoring and forecasting such systems.

7.3.3. Mesoscale Modelling

Large increases in computer processing power, the development of sophisticated parameterizations and the availability of global analysis datasets have resulted in mesoscale modelling being widely used over the last few years. This increase in mesoscale modelling has led to more research on mesoscale convective systems with the model able to produce finer details about the structure of these systems and the environment in which they develop. However, there still remains uncertainty in the skill of models to simulate such systems.

Currently, there is still uncertainty on how effective the use of very high resolution simulations are in relation to the high computation costs (e.g. Flory and Gutowski, 2005). This result suggests that possibly more focus should be placed on the development of effective parameterizations. In addition, a better representation of the

models initial and boundary conditions (including the local topography) may be needed. Stensrud and Fritsch (1994) found that if the mesoscale features were not resolved in the initial conditions then the result simulation was somewhat different to the observations. These authors found that the lack of observation data may lead to the poor initialization. Thus, future modelling of South African events should include the use of observational data to try improve initial conditions. However, this is limited to the amount of observational data that is available. In the control simulation and the mid-latitude sensitivity simulation, it was demonstrated that synoptic features in the mid-latitudes played a role in the development of the convective system. Thus, an accurate representation of the mid-latitudes in the re-analysis data is needed since this data is used for the initial and boundary conditions imposed on the model.

Some key questions that need to be addressed in future modelling work include:

1. How to get an accurate forecast without having "special" observations (i.e. best resolution and initial conditions)?
2. What is the ideal resolution when compared to the cost in computational space and time?
3. How does one validate the model results in data sparse regions?
4. How reliable are the NCEP and ECWMF re-analysis data in the mid-latitude Southern Hemisphere, since observations are relatively sparse

The atmospheric community can obtain a lot of information from these types of studies, such as identifying the factors that play a crucial role in the development of MCS. Numerical modelling is a process that can only get stronger as more advanced models become available to the research community or the parameterizations used become more refined. This will hopefully enable forecasters to predict the location and intensity of these types of systems in South Africa, which may benefit local communities and reduce loss of life and damage to infrastructure. Disaster management groups would also be able to properly prepare and mitigate the damage that these systems may produce. It will also be able to benefit the agricultural sector, because these systems are known to produce a large fraction of the summer rainfall.

Chapter 8

Conclusions

In this thesis, a mesoscale convective system that resulted in a copious amount of precipitation along the northeast coast of South Africa was investigated. From SAWS rainfall data, it was evident that this single event had a large impact on the February 2005 rainfall over northern KZN. Thus, the main emphasis for this thesis was on the identification of the processes that resulted in the development of the system as well as the associated heavy precipitation. This was possible with the use of the MM5 mesoscale model, which allows for the detection of features at a higher temporal and spatial resolution when compared to analysis or re-analysis datasets, such as MRF model output or NCEP re-analysis data. Various sensitivity tests, using the MM5 model, were also conducted in order to identify the role certain local features played in the development of the particular convective event. An attempt was also made to highlight the use of satellite and radar technologies to detect and monitor such storms in South Africa. Due to the coarse resolution of the South African observation and upper-air sounding network, only satellite and radar images were used to verify the development and propagation of the system. These technologies used to monitor storm development are very useful, but there are still shortcomings that need to be addressed. One such shortcoming is the lack of radar data over the north coast of KwaZulu-Natal.

From satellite images, it was evident that during the early afternoon of 11 February 2005, single cell convective systems initiated over the topography of the eastern escarpment of South Africa. These individual systems then merged and developed into a mesoscale convective system during the late afternoon and strengthened during the night, resulting in the heavy precipitation found along parts of KZN. A similar propagation pattern as identified in MCCs over South Africa by Laing and Fritsch (1993b) was found in this case study. After initiating over the eastern escarpment, the system began to propagate to the east/northeast, towards the northern Agulhas Current region. The results have shown that conditions on the synoptic scale and mesoscale

were favourable for the development of an MCS and the associated heavy precipitation found along the eastern region of South Africa.

The analysis of the MRF model data reveals that the convective event resulted from an interaction of a ridging anticyclone, a surface trough in the interior and a weak westerly wave in the mid-levels. It developed in an atmosphere that was favourable for the development of convection and was likely to have been triggered by high diurnal surface heating as well as the high-lying topography of the eastern escarpment. Moisture transports, which were derived from NCEP reanalysis data, suggested that moisture from the Agulhas Current then fed and strengthened the system during the late afternoon and night. Changes in the synoptic conditions during the morning of the 12th resulted in the system decaying. These changes included the propagation of the ridging anticyclone out into the Southwest Indian Ocean, which resulted in the core of the strong onshore, moisture advecting winds weakening and moving further offshore.

It was found that the development of the MCS was successfully simulated in the control run at a resolution of 18 km and a nested grid of 6 km. This was assessed by the presence of key development features of the system, as well as by the timing of the different stages through its evolution. It is encouraging to find that the MM5 model appeared to be capable of simulating such a convective system over the eastern parts of South Africa. However, there were some differences found between the control simulation and the observations. These differences include the shape of the simulated system and the excess precipitation produced in some regions. These differences could possibly be explained by the low resolution MRF data used in the initial and boundary conditions or issues related to the parameterization of convection and cloud microphysics.

Through the use of the numerical model it was established that the heavy precipitation along the north coast was due to sustained periods of favourable conditions for deep convection. This result was identified through variables such as convective instability, low level moisture content and strong vertical motions. The simulation results suggest that the pattern of low level convergence and upper level divergence along the coastal regions aided in intensifying the system during the night. Results from the simulation

also suggested the presence of strong onshore winds in the lower levels during the evolution of the convective system. This wind pattern likely played a key role in supplying moisture into the region during the late afternoon and night, which was then forced to ascend due to the coastal topography. Backward trajectories supported the findings in the NCEP and MRF data, since it was also apparent that moisture used to fuel the system was transported into the region after travelling above the Agulhas Current. However, one noticeable absent feature during the event was that of a strong LLJ, which is usually documented in these types of convective events.

Various sensitivity simulations were preformed in order to identify the role certain features, namely the surrounding SST, the local topography and the large-scale mid-latitudes circulation, played in the development of the convective system. The results from these simulations highlighted the importance of accurately resolving these three features in the initial and boundary conditions since different properties in the MCS evolution and the associated heavy nocturnal precipitation were identified in each simulation. It is suggested that the differences found in the sensitivity simulations were related to different circulation patterns in the low- to mid-levels, which played a significant role in advecting moisture into the region and determining the propagation path of the system. A key feature identified in all but one of these simulations was that the heavy nocturnal precipitation was linked to sustained conditions favouring the development of convection along the coastal regions, as identified in the control simulation. In the topography sensitivity simulation, these conditions only occurred for a short while and hence, a much reduced precipitation pattern occurred.

Some key points emerged from the numerical modelling, with the most obvious being the complexity of modelling convective systems. This complexity points to the need for further model simulations using different initial conditions, starting times, parameterizations, and resolutions to test for the optimum setup of the MM5 model since the experience from this event does not necessarily mean that similar results will be achieved for other South African events. The major challenge in modelling these systems is that they occur on a scale of hundreds of kilometres, yet the model resolution must be fine enough to accurately represent the small scale features. Hence, the representation of sub-grid scale atmospheric processes needs to be improved. However, the results do suggest the potential for forecasting such mesoscale systems

24 hours in advance at the selected resolution. Although, it must again be recognized that this thesis is based on a single case study and further tests are required in order to determine the ability to model other cases.

The mechanisms that result in the development of these types of storms are not completely understood, yet these systems play a large role in the weather and rainfall patterns in parts of Southern Africa. More research is required on these large convective systems, to enable the identification of regional conditions and synoptic pre-cursors that may lead to such events in South Africa. The sensitivity tests suggest that more attention needs to be paid to the representation of the local topography and SSTs of the surrounding oceans in the initial conditions applied to the model. These tests also highlighted the importance of accurately representing the mid-latitudes in numerical simulations of weather events in South Africa. However, further investigation is required to see if other types of extreme precipitating events are influenced by these features. Other variables that should be investigated further include the effects of local land usage and soil moisture content. A future challenge with numerical mesoscale models also includes improving quantitative precipitation forecasting since these systems may be associated with heavy precipitation. Thus, careful attention should be paid to the development of the convective parameterization schemes, as well as the incorporation of extra observational data into the initial conditions to obtain a more accurate representation of the state of the atmosphere in simulations.

Future research should include the development of a climatology of these convective systems found in South Africa, as well as obtaining a better understanding of the synoptic and mesoscale environment in which they develop. The need for better forecasting of such events will continue to grow, which is why a greater understanding of these systems is required. With increases in satellite and radar technology, better monitoring and detection of the systems should occur, which should lead to a better understanding. These convective systems are known to produce an array of severe weather phenomenon, including large quantities of precipitation, which at times can be vital for this semi-arid country. An accurate assessment of the contribution of these systems to the summer precipitation of eastern South Africa

remains unknown, which further motivates for more research into these large, powerful convective systems.

References

Anderson, C.J. and R.W. Arritt, 1998: Mesoscale Convective Complexes and Persistent Elongated Convective Systems over the United States during 1992 and 1993. *Monthly Weather Review*. Vol. 126 (3), 578–599.

Anderson, C.J. and R.W. Arritt, 2001: Mesoscale convective systems over the United States during the 1997-98 El Niño. *Monthly Weather Review*: Vol. 129 (9), 2443-2457.

Ashley, W. S., T.L. Mote, P Grady Dixon, S. L. Trotter, E. J. Powell, J. D. Durkee, and A. J. Grundstein. 2003: Distribution of Mesoscale Convective Complex Rainfall in the United States. *Monthly Weather Review*: Vol. 131, (12), 3003–3017.

Bartels D.L. and R.A. Maddox, 1991: Midlevel Cyclonic Vortices Generated by Mesoscale Convective Systems. *Monthly Weather Review*. Vol. 119, 104-118.

Bartels, D.L., J.M. Skradski and R.D. Menard, 1984: Mesoscale convective systems: A satellite-data-based climatology. NOAA Tech. Memo. ERL ESG 8, Dept. of Commerce, Boulder, CO, 63 pp. [NTIS PB-85-187904]

Bartels, D.L, J. M. Brown, and E. I. Tollerud, 1997: Structure of a midtropospheric vortex induced by a mesoscale convective system. *Monthly Weather Review*. Vol. 125 (2), 193–211.

Bernardet, L. R., L. D. Grasso, J. E. Nachamkin, C. A. Finley and W. R Cotton, 2000: Simulating convective events using a high-resolution mesoscale model. *Journal of Geophysical Research*. Vol. 105 (D11). 14, 963-14,982.

Bluestein, H.B. and M.H. Jain, 1985: Formation of Mesoscale lines of precipitation: Severe Squall Lines in Oklahoma during the spring. *Journal of the Atmospheric Sciences*. Vol. 42 (16), 1711-1732.

Buzzi, A. and L. Foschini, 2000: Mesoscale meteorological features associated with heavy precipitation in the southern Alpine region. *Meteorology and Atmospheric Physics*. Vol. 72 (2-4). 131-146.

Carvalho, L.M.V. and C. Jones, 2001: A Satellite Method to Identify Structural Properties of Mesoscale Convective Systems Based on the Maximum Spatial Correlation Tracking Technique (MASCOTTE). *Journal of Applied Meteorology*: Vol. 40 (10), 1683–1701.

Chen, C., W.-K Tao, P.-L. Lin, G. S. Lai., S.-F. Tseng and T.-C. C. Wang. 1998: The Intensification of the Low-Level Jet during the Development of Mesoscale Convective Systems on a Mei-Yu Front. *Monthly Weather Review*. Vol. 126 (2), 349-371.

Chen. S.-J., W. Wang, K.-H. Lau, Q.-H. Zhang and Y.-S. Chung. 2000: Mesoscale convective systems along the Meiyu front in a numerical model. *Meteorology and Atmospheric Physics*. Vol. 75, 149-160.

Chen. C, W. Chen, Y.L, Chen, P. Lin and H. Lai, 2005: Investigation of orographic effects on two heavy rainfall events over southwestern Taiwan during mei-yu season. *Atmospheric Research*. Vol. 73; 101-130.

Cook, K.H. 2000: The South Indian Convergence Zone and Interannual Rainfall Variability over Southern Africa. *Journal of Climate*. Vol. 13 (21), 3789-3804.

Cook, C., C.J.C. Reason and B.C. Hewitson, 2004: Wet and dry spells within particularly wet and dry summers in the South African summer rainfall region. *Climate Research*. Vol. 26 (1), 17-31

Corfidi, S.F., 2003: Cold Pools and MCS Propagation: Forecasting the Motion of Downwind-Developing MCSs. *Weather and Forecasting*. Vol.18, 997-1017

Corfidi, S.F., J.H. Meritt, and J.M. Fritsch, 1996: Predicting the Movement of Mesoscale Convective Complexes. *Weather and Forecasting*. Vol. 11 (1), 41–46.

Cosjin, C. and Tyson, P.D., 1996: Stable discontinuities in the atmosphere over South Africa. *South African Journal of Science*. Vol. 92 (8), 381-386.

Cotton, W.R., 2000: An overview of mesoscale convective systems. Chapter 31 in *Storms vol. II.* [Pielke Jr., RA and RA Pielke Sr. (eds.)]. Routledge, London, pp. 3–25.

Cotton, W. R., M.-S. Lin, R.L. McAnelly, and C.J. Tremback, 1989: A composite model of mesoscale convective complexes. *Monthly Weather Review*. Vol. 117 (4), 765–783.

Crimp S.J. and S.J. Masson, 1999: The extreme precipitation event of 11-16 February 1996 over South Africa. *Meteorology and Atmospheric Physics*. Vol 70 (1-2). 29-42.

D'Abreton, P.C and J.A. Lindesay. 1993: Water vapour transport over Southern Africa during wet and dry early and later summer months. *International Journal of Climatology*. Vol. 13, 151-170.

D'Abreton, P.C and J.A. Lindesay. 1995: Divergent and non-divergent water vapour transport over southern Africa during wet and dry conditions. *Meteorology and Atmospheric Physics*. Vol. 55, 297-306.

D'Abreton P.C. and P.D. Tyson, 1996: Three-dimensional kinematic trajectory modelling of water vapour transport over southern Africa. *Water SA*. Vol. 22, 297-306.

Davis, C.A., and M.L. Weisman (1994), Balanced dynamics of mesoscale vortices produced in simulated convective systems., *Journal of the Atmospheric Sciences*. Vol. 51, 2005–2030.

Dixion, M., 2005: TITAN users guide: Overview. NCAR, Boulder, Colorado. Pp.1-4

Doswell, C.A. III, 1987: The distinction between large scale and mesoscale contribution to severe convection: A case study example. *Weather and Forecasting.* Vol. 2, 3-16.

Doswell, C. A., III, H. E. Brooks, and R. A. Maddox, 1996: Flash flood forecasting: An ingredients-based methodology. *Weather and Forecasting.* Vol. 11, 560–581.

Draxler R.R., and A. D. Taylor, 1982: Horizontal dispersion parameters for long-range transport modelling. *Journal of Applied Meteorology.* Vol. 21, 367-372.

Draxler, R.R., and G.D. Hess, 1997: Description of the Hysplit_4 modeling system, NOAA Technical Memorandum ERL ARL-224, December, 24p.

Dudhia, J., 1993: A non-hydrostatic version of the Penn State-NCAR Mesoscale Model: Validation tests and simulation of an Atlantic cyclone and cold front. *Monthly Weather Review.,* Vol. 121, 1493–1513.

Dudhia, J., 1996: A multi-layer soil temperature model For MM5. *Preprints, 6th Annual MM5 Users Workshop*, Boulder, CO.

Dyson, L.L. and J. van Heerden, 2001: The heavy rainfall and floods over the northeastern interior of South Africa during February 2000. *South African Journal of Science.* Vol. 97, 80-86.

Evans, J.L. and R.E. Shemo, 1996: A Procedure for Automated Satellite-Based Identification and Climatology Development of Various Classes of Organized Convection. *Journal of Applied Meteorology*: Vol. 35, (5), 638–652.

Federal Meteorological Handbook, 2005: Doppler Radar Meteorological Observations. Part B: Doppler Radar theory and meteorology. Federal Meteorological Handbook number 11. Washington, DC. Pp 1-219

Flory. D.M, and W.J. Gutowski Jr. 2005. Summer Precipitation Dynamics in High Resolution Climate Simulations. Submitted to *Journal of Climate.*

Fowler, G. 2006: MSG Level 1.5 Image Data Format Description. V4, EUM/MSG/ICD/105, 1-125

Fritsch, J.M., R.J. Kane, and C.R. Chelius, 1986: The contribution of mesoscale convective weather systems to the warm season precipitation in the United States. *Journal of Climate and Applied Meteorology.* Vol. 25, 1333 – 1345.

Fritsch, J., Houze, R. J., Adler, R., Bluestein, H., Bosart, L., Brown, J., Carr, F., Davis, C., Johnson, R., Junker, N., Kuo, Y., Rutledge, S., Smith, J., Toth, Z.,Wilson, J., Zipser, E., and Zrnic, D. 1998: Quantitative precipitation forecasting: report of the 8th prospectus development team, US Weather Research Program, *Bulletin of the American Meteorology Society.* Vol. 79, 285-299.

García-Herrera, R., D. Barriopedro, E. Hernández, D. Paredes, K.F. Correoso and L. Prieto, 2005: The 2001 Mesoscale Convective Systems over Iberia and the Balearic Islands. *Meteorology and Atmospheric Physics*. Vol. 90, 225-243.

Garstang, M. and P. Tyson, 2000: Mesoscale convective systems over South Africa. Chapter 38 in *Storms vol. II.* [Pielke Jr., RA and RA Pielke Sr. (eds.)]. Routledge, London, pp. 146–162.

Garstang, M., B.E. Kelbe, G.D. Emmit, and W.B. London, 1987: Generation of convective storms over the escarpment of NE South Africa. *Monthly Weather Review*. Vol. 115 (2), 429-443.

Geerts, B., 1998: Mesoscale convective systems in the southeast United States during 1994–95: A survey. *Weather and Forecasting*. Vol. 13, 860– 869.

Grell, G. 1993: Prognostic evaluation of assumptions by cumulus parameterizations. *Monthly Weather Review*. Vol. 121 (3), 764-787.

Grell, G.A., J. Dudhia and D. R. Stauffer, 1994: A description of the fifth generation Penn State/NCAR Mesoscale Model Version 5 (MM5). NCAR Tech. Note NCAR/TN-398, 138 pp.

Grell, G., L. Schade, R. Knoche, A. Pfeiffer, and J. Egger, 2000: Non-hydrostatic climate simulations of precipitation over complex terrain. *Journal of Geophysical Research*, Volume 105, (D24), 29595-29608.

Hilgendorf, E.R and R.H. Johnson, 1998: A study of the evolution of Mesoscale Convective Systems using WSR-88D data. *Weather and Forecasting*. Vol. 13, 437-452.

Hodges, K.I., and C.D. Thorncroft, 1997: Distribution and Statistics of African Mesoscale Convective Weather Systems Based on the ISCCP Meteosat Imagery. *Monthly Weather Review*. Vol. 125, (11), 2821–2837.

Holland, G.J. and L.M. Leslie, 1986: Ducted coastal ridging over southeast Australia. *Quarterly Journal of the Royal Meteorology Society*. Vol. 112 (473), 731-748.

Hong, S.-Y., and H.-L. Pan, 1996: Nonlocal boundary layer vertical diffusion in a medium-range forecast model. *Monthly Weather Review*. Vol. 124, 2322–2339.

Houze, R.A. Jr. 1997: Stratiform precipitation in regions of convection: A meteorological paradox. *Bulletin of the American Meteorology Society*. Vol. 78, 2179–2196

Houze, R.A. Jr. 2004: Mesoscale Convective Systems. *Reviews of Geophysics*, 42. 10.1029/2004RG000150, 1-43

Houze, R. A., S. A. Rutledge, M. I. Biggerstaff, and B. F. Smull, 1989: Interpretation of Doppler weather radar displays of midlatitude mesoscale convective systems. *Bulletin of the American Meteorology Society*. Vol. 70 (6), 608–619.

Houze, R.A., Jr., B.F. Smull, and P. Dodge, 1990: Mesoscale organization of springtime rainstorms in Oklahoma. *Monthly Weather Review.* Vol. 118 (3), 613–654

Huffman, G.J., R.F. Adler, M. Morrissey, D.T. Bolvin, S. Curtis, R. Joyce, B McGavock, J. Susskind, 2001: Global Precipitation at One-Degree Daily Resolution from Multi-Satellite Observations. *Journal of Hydrometeorology.* Vol. 2, 36-50.

Jirak, I.L., W.R. Cotton, and R.L. McAnelly, 2003: Satellite and Radar Survey of Mesoscale Convective System Development. *Monthly Weather Review*: Vol. 131 (10), 2428–2449.

Johnson, R.H. and P.J. Hamilton, 1988: The relationship of surface pressure features to the precipitation and air floe structure of an intense midlatitude squall line. *Monthly Weather Review.* Vol. 116. 1444-1472.

Juneng, L., F.T. Tangang and C.J.C. Reason, 2006: Numerical Case Study of an Extreme Rainfall Event during 9-11 December 2004 over the East Coast Peninsular Maylaysia. Submitted to *Meteorology and Applied Physics.*

Jury, M.R., H.R. Valentine and J.R.E. Lutjeharms. 1993: Influence of the Agulhas Current on summer rainfall on the southeast coast of South Africa. *Journal of Applied Meteorology.* Vol. 32, 1282-1287.

Kain, J. S. and J.M. Fritsch, 1992: The role of the convective "trigger function" in numerical forecasts of mesoscale convective systems. *Journal of Meteorology and Applied Physics.* Vol. 49, 93-106.

Kain, J.S. and J.M. Fritsch, 1993: Convective parameterization for mesoscale models: The Kain-Fritsch scheme. *In The Representation of Cumulus Convection in Numerical Models, Meteorological Monograph.* K.A. Emanuel and D. J. Raymond, Eds. No. 46, American Meteorology Society, 165-170.

Kalnay, E., M. Kanamitsu and W.E. Baker, 1990: Global Numerical Weather Prediction at the National Meteorological Center. *Bulletin of the American Meteorology Society.* Vol. 71, 1410-1428.

Kalnay, E., Kanamitsu, M., Kistler, R., Collins, W., Deaven, D., Gandin, L., Iredell, M., Saha, S., White, G., Woollen, J., Zhu, Y., Chelliah, M., Ebisuzaki, W., Higgins, W., Janowiak, J., Mo, K. C., Ropelewski, C., Wang, J., Leetmaa, A., Reynolds, R., Jenne, R. and Joseph, D. 1996: The NCEP/NCAR 40-year reanalysis project. *Bulletin of the American Meteorology Society.* Vol. 77(3): 437-471.

Kanamitsu, M., 1989: Description of the NMC global data assimilation and forecast system. *Weather and Forecasting.* Vol. 4, 334-342.

Kanamitsu, M., J.C. Alpert., K.A. Campana., P.M. Caplan., D.G. Deavan., M. Iredell., B. Katz., H.-L. Pan., J. Sela and G.H. White, 1991: Recent changes implemented into the global forecast system at NMC. *Weather and Forecasting.* Vol. 6, 425-435.

Kane, R.J., C.R. Chelius, and J.M. Fritsch, 1987: Precipitation characteristics of mesoscale convective weather systems. *Journal of Climate and Applied Meteorology.* Vol. 26, 1345-1357.

Katzfey, J. J., 1995: Simulation of extreme New Zealand precipitation events. Part I: Sensitivity to orography and resolution. *Monthly Weather Review*. Vol. 123, 737–754.

Kingsmill, D.E., and R.A. Houze Jr. 1999: Kinematic characteristics of air flowing into and out of precipitating convection over the west Pacific warm pool: An airborne Doppler radar survey. *Quarterly Journal of the Royal Meteorology Society.*, Vol. 125, 1165–1207.

Kummerow, C., W. Barnes, T. Kozu, J. Shiue and J. Simpson, 1998: The Tropical Rainfall Measuring Mission (TRMM) sensor package. *Journal of atmospheric and oceanic technology.* Vol. 15, 808-816.

Kuo Y.-H., R.J. Reed, and Y.-B. Liu, 1996: The ERICA IOP 5 storm. Part III: Mesoscale cyclogenesis and precipitation parameterization. *Monthly Weather Review.* 124 (7), 1409-1434.

Kuo Y.-H., J. F. Bresch., M. –D. Cheng., J. Kain., D. B. Parsons, W. –K. Tao and D. –L. Zhang, 1997: Summary of a mini workshop on cumulus parameterization for mesoscale models. *Bulletin of the American Meteorology Society*. Vol. 78 (3), 475-491.

Lafore, J.-P. and M.W. Moncrieff, 1989: A numerical investigation of the organisation and interaction of the convective and stratiform regions of tropical squall lines. *Journal of Atmospheric Science*. Vol. 46, 521-544

Laing, A.G. and J.M. Fritsch, 1993a: Mesoscale convective complexes over the Indian Monsoon region. *Journal of Climate.* Vol. 6, 911-919.

Laing, A.G. and J.M. Fritsch, 1993b: Mesoscale convective complexes in Africa. *Monthly Weather Review*. Vol.121, 2254-2263.

Laing, A.G. and J.M. Fritsch, 1997: The global population of mesoscale convective complexes. *Quarterly Journal of the Royal Meteorology Society*. Vol. 123, 389-405.

Laing, A.G. and J.M. Fritsch, 2000: The Large-Scale Environments of the Global Populations of Mesoscale Convective Complexes. *Monthly Weather Review*: Vol. 128, (8), 2756–2776.

Laing, A.G., J.M. Fritsch, and A.J. Negri, 1999: Contribution of Mesoscale Convective Complexes to Rainfall in Sahelian Africa: Estimates from Geostationary Infrared and Passive Microwave Data. *Journal of Applied Meteorology*: Vol. 38 (7), 957–964.

Laurent, H., N. D'Amato, and T. Lebel, 1998: How important is the contribution of mesoscale convective complexes to the Sahelian rainfall. *Physics, Chemistry and Earth Sciences*. Vol. 23 (5-6), 629-633.

Leary, C.A. and E.N. Rapport, 1987: The life cycle and internal structure of a Mesoscale convective complex. *Monthly Weather Review*. Vol. 115 (8), 1503-1527.

Loehrer, S.M. and R.J. Johnson, 1995: Surface pressure and precipitation life cycle characteristics of PRE-STORM mesoscale convective systems. *Monthly Weather Review*. Vol. 123, 600-621.

Machado, L.A.T., W. B. Rossow, R. L. Guedes, and A. W. Walker, 1998: Life Cycle Variations of Mesoscale Convective Systems over the Americas. *Monthly Weather Review*: Vol. 126, (6), 1630–1654.

Maddox, R.A. 1980: Mesoscale convective complexes. *Bulletin of the American Meteorology Society*. Vol. 61, 1374-1387.

Maddox, R.A. 1983: Large-scale meteorological conditions associated with mid-latitude, mesoscale convective complexes. *Monthly Weather Review*: Vol. 111 (7), 1475-1493.

Maddox, R.A. and C.A. Doswell, III, 1982: An examination of jet stream configurations, 500 mb vorticity and low-level thermal advection patterns during extended periods of intense convection. *Monthly Weather Review.*, 110, 184-197.

Maddox, R.A, C.F. Chappell, and L. R. Hoxit, 1979: Synoptic and meso-α-scale aspects of flash flood events. *Bulletin of the American Meteorology Society*. Vol. 60 (2), 115 – 123.

Maddox, R.A, K.W. Howard, D.L. Bartels, and D.M. Rogers, 1986: Mesoscale convective complexes in the middle latitudes. Mesoscale Meteorology and Forecasting. P.S. Ray, Ed., American Meteorology Society, 390-413.

Mapes, B.E. 1993: Gregarious tropical convection. *Journal of the Atmospheric Sciences*. Vol. 50, 2026-2037.

Mapes, B.E., T.T. Warner, and M. Xu. 2003: Diurnal patterns of rainfall in northwestern South America, Part III: Diurnal gravity waves and nocturnal convection offshore. *Monthly Weather Review*. Vol. 131 (5), 830 – 844.

Mass, C.D., Ovens, K. Westrick, and B. Colle, 2002: Does increasing horizontal resolution produce more skillful forecasts? *Bulletin of the American Meteorology Society*. Vol. 83 (3), 407–430.

Mathon, V., H. Laurent and T. Lebel. 2002: Mesoscale Convective System Rainfall in the Sahel. *Journal of Applied Meteorology*. Vol. 41, 1081-1092.

McAnelly, R.L. and W. R. Cotton, 1986: Meso-β-scale aspects of an episode of meso-α-scale convective complexes. *Monthly Weather Review*. Vol. 114 (9), 1740 – 1770.

McAnelly, R.L. and W. R. Cotton, 1989: The precipitation life cycle of mesoscale convective complexes over the central united states. *Monthly Weather Review*. Vol. 117 (4), 784-808.

Menard, R.D., and J.M. Fritsch, 1989: A mesoscale convective complex-generated inertially stable warm core vortex. *Monthly Weather Review*. Vol. 117, 1237–1261.

Miller, D. and J.M. Fritsch, 1991: Mesoscale convective complexes in the western Pacific region. *Monthly Weather Review*. Vol. 119, 2978-2992.

Mounier, F., G.N. kiladis and S. Janicot, 2005: The West African Monsoon Dynamics. Part III: Evidence of Convectively Coupled Kelvin waves. Submitted to *The Journal of Climate*.

Orlanski, I. 1975: A rational subdivision of scales for atmospheric processes. *Bulletin of the American Meteorology Society*. Vol. 56, 527-530.

Pan, Z., M. Segal. and R.W. Arritt, 2004: The role of topography in forcing Low-level Jets in the Central United States during the 1993 Flood-Altered Terrain Simulations. *Monthly Weather Review*. Vol. 32 (1), 396-403.

Parker, M.D. and R.H. Johnson, 2000: Organizational Modes of Midlatitude Mesoscale Convective Systems. *Monthly Weather Review*: Vol. 128, (10), 3413–3436.

Parker, M.D., and R.H. Johnson, 2004a: Structures and dynamics of quasi-2D mesoscale convective systems. *Journal of the Atmospheric Sciences*. Vol. 61 (5), 545-567.

Parker, M.D., and R.H. Johnson, 2004b: Simulated convective lines with leading precipitation. Part I: Governing dynamics. *Journal of the Atmospheric Sciences.* Vol. 61 (14), 1637-1655.

Parker, M.D., and R.H. Johnson, 2004c: Simulated convective lines with leading precipitation. Part II: Evolution and maintenance. *Journal of the Atmospheric Science.* Vol. 61 (14), 1656-1673.

Perrin, G.M. and C.J.C. Reason, 2000: Monsoonal influences on a mesoscale convective system over midlatitude South Australia. *Meteorology and Atmospheric Physics*. Vol. 74, 63-82.

Pettit, and R.H. Johnson, 2003: Airflow and precipitation structure of two leading stratiform mesoscale convective systems determined from operational datasets. *Weather and Forecasting.* Vol, 18, 685–699.

Pielke, R.A. 2002: Mesoscale Meteorological Modeling. San Diego: Academic Press. 1-676.

Preston-Whyte, R.A. 1970: Land Breezes and rainfall over the Natal coast. *South African Geographical Journal*. Vol. 52, 38-43.

Preston-Whyte, R.A., R.D. Diab and R. Washington, 1991: Diurnal variation of rainfall events by synoptic type in Natal. *South African Geographical Journal.* Vol. 73, 22-28.

Reason, C.J.C., 2001: Evidence for the influence of the Agulhas Current on regional atmospheric circulation patterns. *Journal of Climate.* Vol. 14, 2769–2778.

Reason C.J.C. 2006: A review of interannual climate variability over Southern Africa and its relationship with surface gradient forcing. South African Society Atmospheric Sciences (SASAS) Conference, Bloemfontein, South Africa.

Reason, C.J.C. and A. Keibel. 2004: Tropical Cyclone Eline and Its Unusual Penetration and Impacts over the Southern African Mainland. Weather and Forecasting. Vol.19 (5), 789-805.

Reisner J., R. M. Rasmussen, and R. T. Bruintjes, 1998: Explicit forecasting of supercooled liquid water in winter storms using the MM5 mesoscale model. *Quarterly Journal of the Royal Meteorological Society.* Vol. 124, 1071–1107.

Reynolds, R.W. and Smith, T.M. 1994: Improved global sea surface temperature analyses using optimum interpolation. *The Journal of Climate.* Vol. 7, 929-948

Reynolds, R.W., Rayner, N.A., Smith, T.M., Stokes, D.C. and Wang, W. 2002: An Improved In Situ and Satellite SST Analysis for Climate, *The Journal of Climate.* Vol. 15 (13), 1609 – 1625.

Romero, R., C. Ramis and S. Alonso, 1998: Mesoscale model simulations of three heavy precipitation events in the western Mediterranean region. *Monthly Weather Review.* Vol. 126 (7), 1859-1881.

Romero, R., C.A. Doswell III and C. Ramis, 2000: Mesoscale numerical study of two cases of long-lived quasi-stationary convective systems over eastern Spain. *Monthly Weather Review.* Vol. 128 (11), 3731-3751

Rotunno, R., J.B. Klemp, and M.L. Weisman, 1988: A theory for strong, long-lived squall lines. *Journal of the Atmospheric Sciences.* Vol. 45, 463–485.

Rouault, M., A.M. Lee-Thorp and J.R.E. Lutjeharms, 2000: The atmospheric boundary layer above the Agulhas Current during along current winds. *Journal of Physical Oceanography.* Vol. 30, 40-50

Rouault, M., S.A. White., C.J.C. Resaon., J.R.E. Lutjeharms and I. Jobard. 2002: Ocean-Atmosphere interaction in the Agulhas Current region and a South African extreme weather event. *Weather and Forecasting.* Vol. 17, 655-669.

Rouault, M., C.J.C. Reason, J.R.E. Lutjeharms and A.C.M. Beljaars, 2003: Underestimation of latent and sensible heat fluxes above the Agulhas Current in NCEP and ECMWF analyses. *Journal of Climate.* Vol. 16, 776-782.

Smith, J. A., M. L. Baeck, Y. Zhang and C. A. Doswell III, 2001: Extreme Rainfall and Flooding from Supercell Thunderstorms. *Journal of Hydrometeorology.* Vol. 2, 469-489.

Schmetz J., P. Pili, S. Tjemkes, D. Just, J. Kerkman, S. Rota and A. Ratier, 2002: An introduction to Meteosat Second Generation (MSG). *Bulletin of the American Meteorological Society*. Vol. 83, 977-992

Schmidt J.M. and W.R. Cotton, 1990: Interactions between upper and lower troposheric gravity waves on squall line structure and maintenance. *Journal of the Atmospheric Sciences*. Vol. 47. pp 1205-1222.

Schumacher, R.S. and R.H. Johnson, 2005: Organization and Environmental Properties of Extreme-Rain-Producing Mesoscale Convective Systems. Monthly Weather Review. Vol. 133 (4), 961-976

Singleton, A.T. and C.J.C. Reason, 2006: Numerical Simulations of a Severe Rainfall event over the Eastern Cape coast of South Africa: Sensitivity to sea surface temperature and topography. *Tellus A*, Vol. 58 (3), 355-367.

Singleton, A.T. and C.J.C. Reason, 2007: A numerical model study of an intense cut-off low pressure system over South Africa. *Monthly Weather Review*. Vol. 135 (3), 1128-1150.

Skamarock,W.C., M.L.Weisman, and J.B. Klemp 1994: Three-dimensional evolution of simulated long-lived squall lines, *Journal of the Atmospheric Sciences*., Vol. 51, 2563–2584.

Smull, B.F., and R.A. Houze Jr., 1987: Rear inflow in squall lines with trailing-stratiform precipitation. *Monthly Weather Review*. Vol. 115, 2869–2889.

Smull, B.F., and J.A. Augustine, 1993: Multi-scale analysis of a mature mesoscale convective complex. *Monthly Weather Review*. Vol. 121, 103–132.

Spencer P.L. and D.J. Stensrud, 1998: Simulating Flash Flood Events: Importance of the Subgrid Representation of Convection. *Monthly Weather Review*. Vol. 126, 2884-2912.

Stein, U., and P. Alpert, 1993: Factor separation in numerical simulation. *Journal of the Atmospheric Sciences*. Vol. 50, 2107-2115.

Stensrud, D.J. and J.M. Fritsch, 1993: Mesoscale convective systems in weakly forced large-scale environments. Part I: Observations. *Monthly Weather Review*. Vol. 121 (12), 3326-3344.

Stensrud, D.J. and J.M. Fritsch, 1994: Mesoscale convective systems in weakly forced large-scale environments. Part II: Generation of a Mesoscale Initial Condition. *Monthly Weather Review*. Vol 121 (9), 2068-2083.

Stowe, L. L., E. P. McClain, R. Carey, P. Pellegrino, G. G. Gutman, P. Davis, C. Long, and S. Hart, 1991. Global distribution of cloud cover derived from NOAA/AVHRR operational satellite data, *Advances in Space Research*, Vol. 11 (3), 51-54.

Tennant, W. 2004: Considerations when using pre-1979 NCEP/NCAR reanalyses in the southern hemisphere, *Geophysical Research Letters*. Vol. 31 (11), L11112, doi:10.1029/2004GL019751.

Trier, S.B. and D.B. Parsons, 1993: Evolution of environmental conditions preceding the development of a nocturnal mesoscale convective complex. *Monthly Weather Review*. Vol. 121, 1078-1098.

Trier, S.B., C.A. Davis, and J.D. Tuttle, 2000a: Long-Lived Mesoconvective Vortices and Their Environment. Part I: Observations from the Central United States during the 1998 Warm Season. *Monthly Weather Review*. Vol. 128 (10), 3376-3395.

Trier, S.B., C.A. Davis, and W.C. Skamarock. 2000b: Long-Lived Mesoconvective Vortices and Their Environment. Part II: Induced Thermodynamic Destabilization in Idealized Simulations. *Monthly Weather Review*. Vol. 128 (10), 3396-3411.

Tucker, D.F. and N.A. Crook, 1999: The generation of mesoscale convective systems from mountain convection. *Monthly Weather Review*. Vol. 127 (6), 1259 – 1273.

Tucker, D.F. and K.S. Zentmire, 1999: On the Forecasting of Orogenic Mesoscale Convective Complexes. *Weather and Forecasting*: Vol. 14 (6), 1017–1022.

Tyson, P.D. and R.A. Preston-Whyte, 2000: *The atmosphere and weather of southern Africa*. Oxford University press. Cape Town. 396pp.

Velasco, I. and J.M. Fritsch, 1987: Mesoscale convective complexes in the Americas. *Journal of Geophysical Research*, Vol. 92, 9591-9613.

Vera, C., J. Baez, M. Douglas, C. B. Emmanuel, J. Marengo, J. Meitin, M. Nicolini, J. Nogues-Paegle, J. Paegle, O. Penalba, P. Salio, C. Saulo, M. A. Silva Dias, P. Silva Dias, and E. Zipser, 2005: The South American low-level jet experiment (SALLJEX). *Bulletin of the American Meteorology Society*. Vol. 89 (1), 63-77.

Wang, W. and N. Seaman, 1997: A comparison of convective parameterization schemes in a mesoscale model. *Monthly Weather Review*. Vol. 125 (2), 252-278.

Weisman, M.L. 1992: The role of convectively generated rear-inflow jets in the evolution of long-lived mesoscale convective systems. *Journal of the Atmospheric Sciences*. Vol. 49, 1826 – 1847.

Weisman. M.L., 1993: The genesis of severe, long-lived bow-echoes. *Journal of the Atmospheric Sciences*. Vol. 50, 645–670

Weisman. M.L., and J.B. Klemp., 1982: The Dependence of Numerically Simulated Convective Storms on Vertical Wind Shear and Buoyancy. *Monthly Weather Review*: Vol. 110 (6), 504–520.

Weisman. M.L., and J.B. Klemp., 1986: Characteristics of Convective Storms. Mesoscale Meteorology and Forecasting. P.S. Ray, Ed., American Meteorology Society, 331-358.

Weisman, M.L. and C. A. Davis, 1998: Mechanisms for the generation of mesoscale vortices within quasi-linear convective systems. *Journal of the Atmospheric Sciences*. Vol. 55, 2603–2622.

Weisman, M.L., W.C. Skamarock, and J.B. Klemp, 1997: The resolution dependence of explicitly modelled convective systems. *Monthly Weather Review*. Vol.125 (4), 527 – 548.

Xu M., J-W. Bao, T.T. Warner and D. J. Stensrud, 2001: Effect of time size in MM5 simulations of a mesoscale convective complex. *Monthly Weather Review*. Vol. 129 (3), 502-516.

Yamazaki, Y. and M.D.M. Orgaz. 2005: Forecasting mesoscale precipitation using the MM5 model with the four-dimensional data assimilation (FDDA) technique. *Global NEST Journal*. Vol. 7 (3), 258-263.

Zhang, D.-L and J.M. Fritsch 1986: A case study of the sensitivity of numerical simulation of mesoscale systems to varying conditions. *Monthly Weather Review*. Vol. 114 (12), 2418-2431.

Zhang, D.-L. and J.M. Fritsch, 1988a: Numerical sensitivity experiments of varying model physics on the structure, evolution and dynamics of two mesoscale systems. *Journal of the Atmospheric Sciences*. Vol. 45 (2), 261 – 293.

Zhang, D.-L. and J.M. Fritsch, 1988b: A numerical simulation of a convectively generated inertially stable, warm core extratropical mesovortex over land. *Monthly Weather Review*. Vol. 116, 2660-2687.

Zhang, D.-L., E. –E. Hsie, and M.W. Moncrieff, 1988: A comparison of explicit and implicit predictions of convective and stratiform precipitating weather systems with a meso-beta-scale numerical model. *Quarterly Journal of the Royal Meteorology Society*. Vol. 114, 31-60.

Zhang, Q-H.; K-H, Lau; Y-H, Kuo and S-J. Chen, 2003: A Numerical Study of a Mesoscale Convective System over the Taiwan Strait. *Monthly Weather Review*. Vol. 131. 1150-1170

Zheng, Y., Q. Xu and D.J. Strensrud, 1995: A numerical simulation of the 7 May 1985 mesoscale convective system. *Monthly Weather Review*. Vol.123, 1781-1799

Zipser, E.J. 1982: Use of a conceptual model of the life-cycle of mesoscale convective systems to improve very-short-range forecasts. *Nowcasting*. K.A. Browning (Ed.), Academic Press, London, 191-204.

Appendix A:

Additional Figures

a)

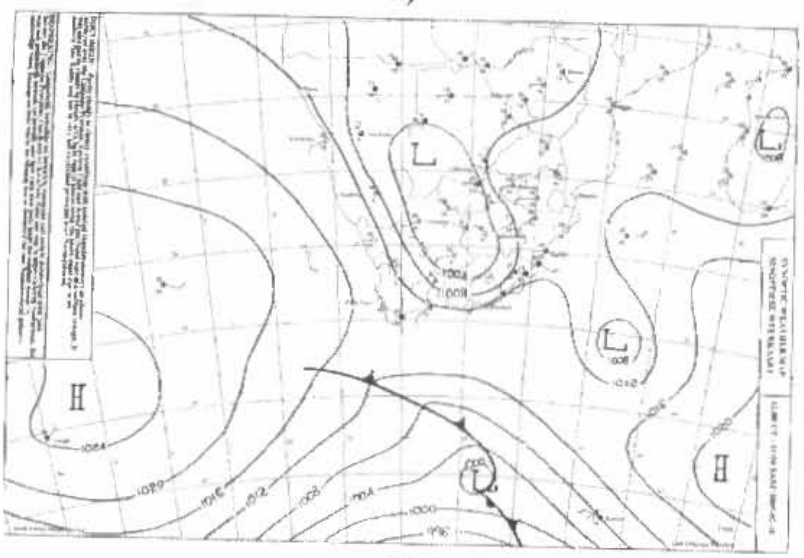

b)

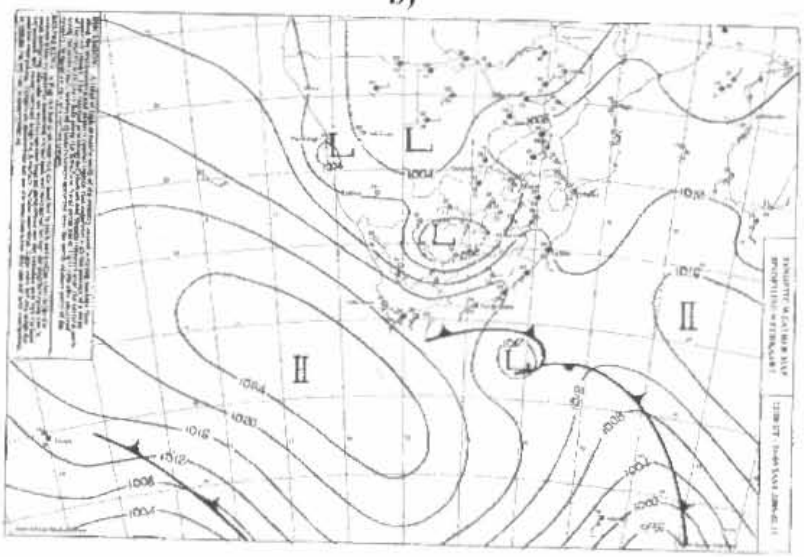

c)

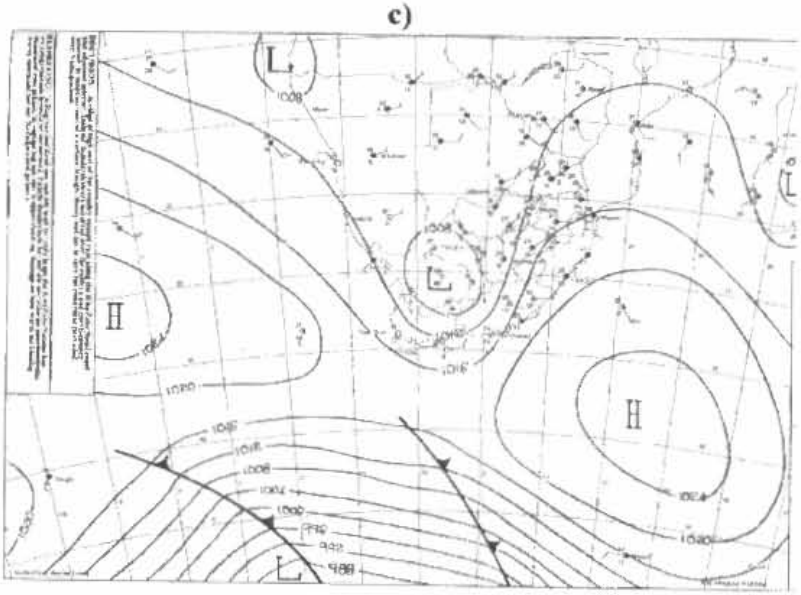

Figure A4.1: SAWS synoptic charts for the a) 10th, b) 11th and c) 12th February 2006

a) 12h00 UTC 11 February 2005

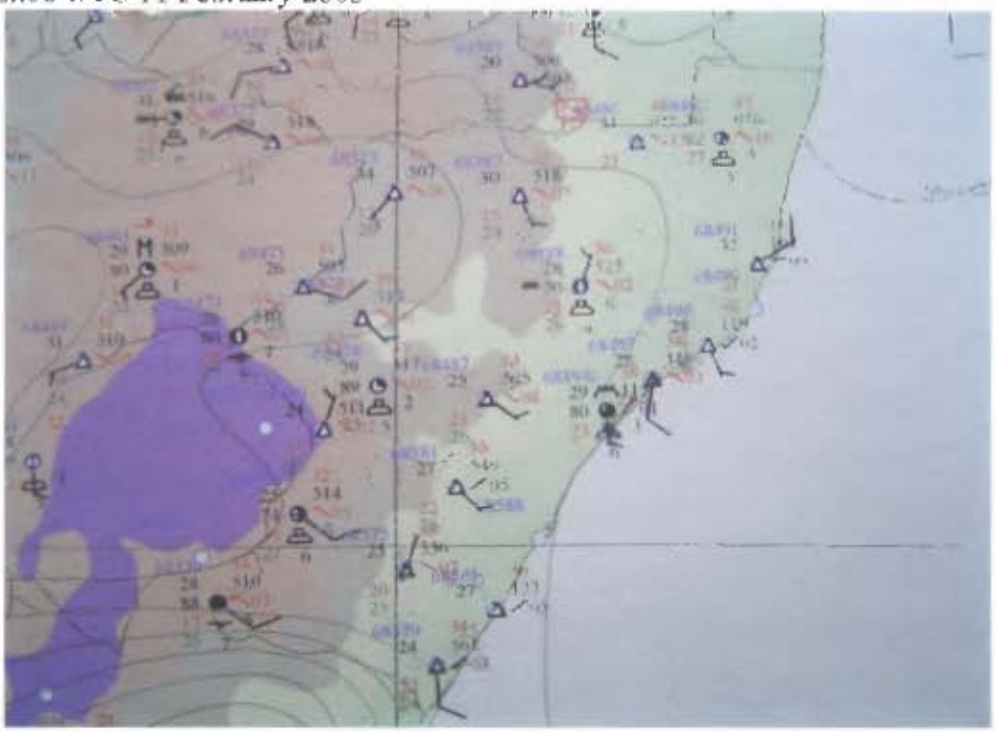

b) 00h00 UTC 12 February 2005

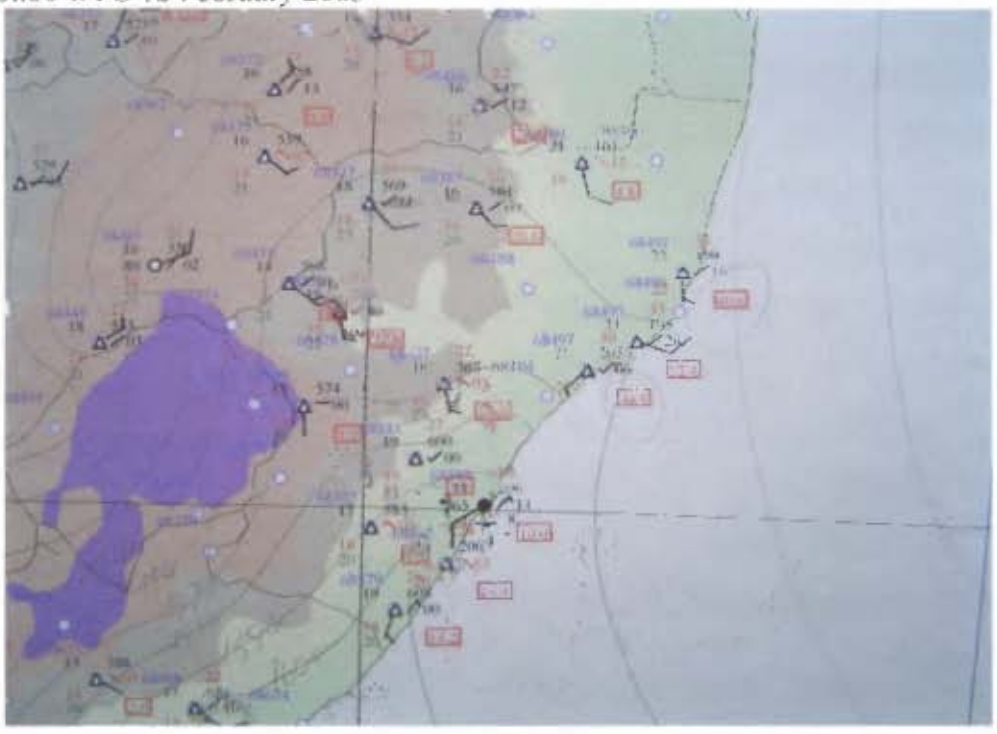

Figure A4.2: Mesoscale charts showing surface conditions (derived from SAWS weather stations) over eastern South Africa at a) 12h00 UTC and b) 00h00 UTC on the 11 and 12 February 2005, respectively.

a) 12h00

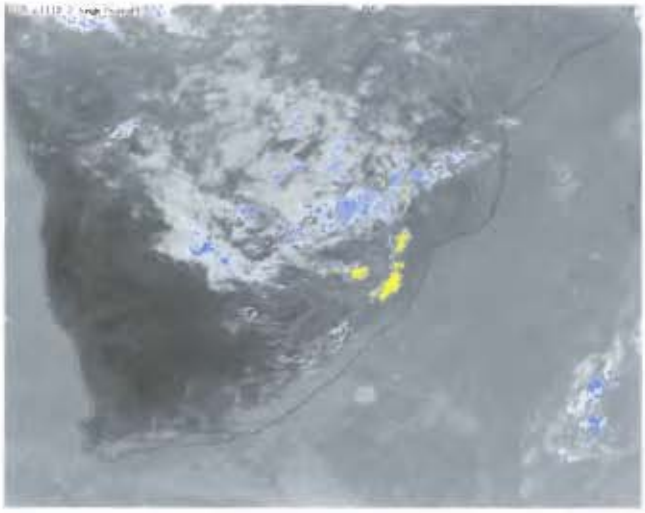

b) 14h00

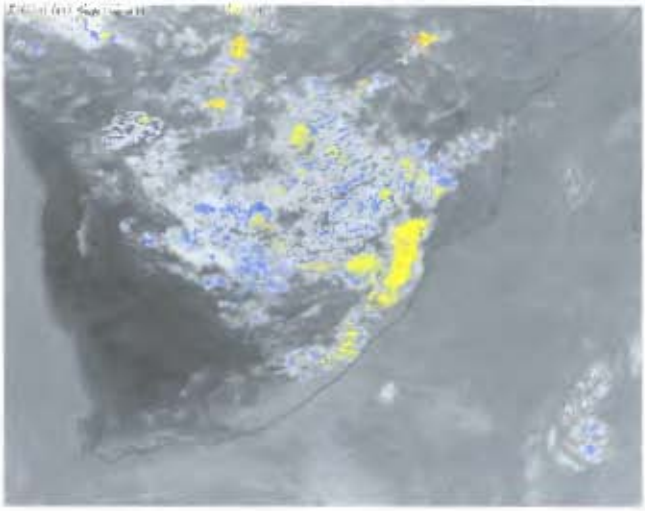

c) 16h00

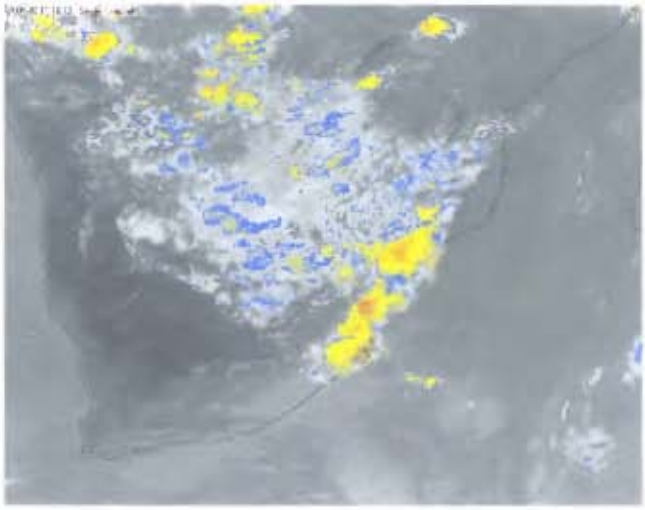

d) 18h00

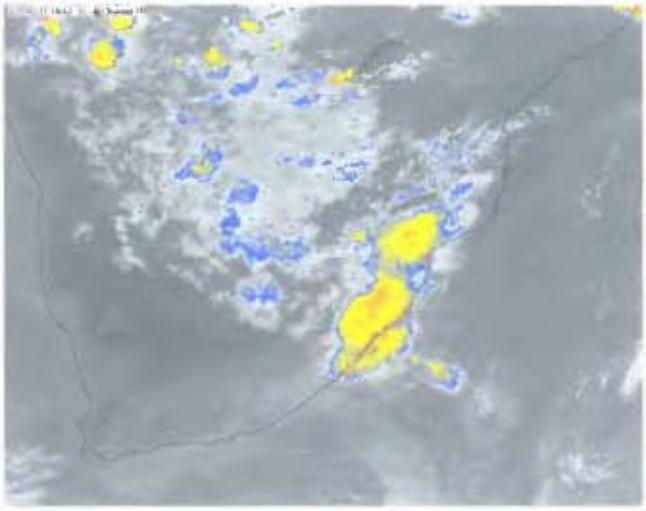

e) 20h00

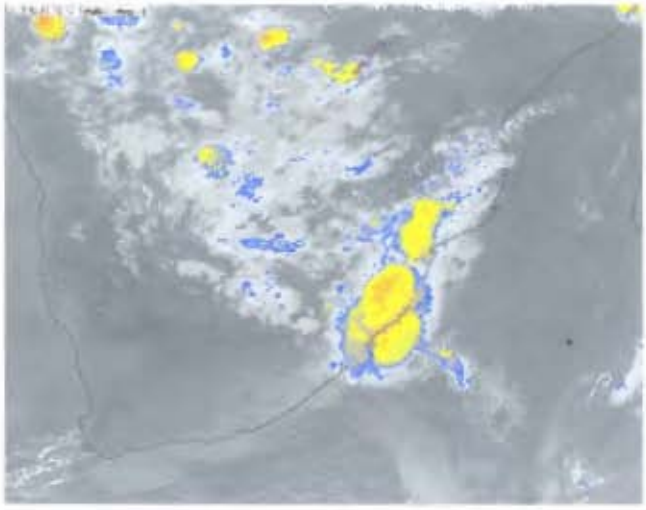

f) 22h00

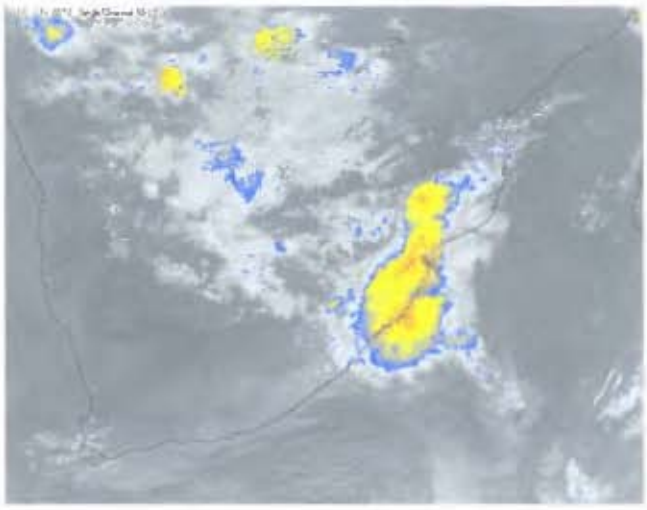

Figure A4.3: MSG infrared satellite images, with colour mapping applied to cloud top temperatures. Starting at top left (a) at 12h00 UTC and at 2 hour intervals, to j) at 06h00 UTC. Where: Blue = -32.4°C, Yellow = -52.5°C and Red = -72.0°C.

g) 00h00

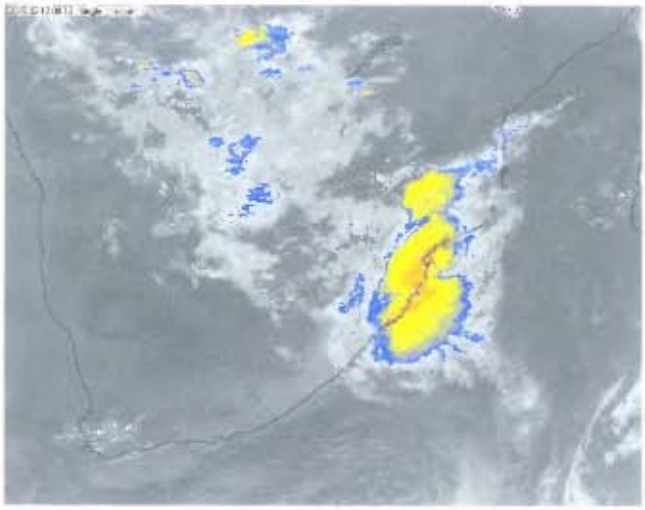

h) 02h00

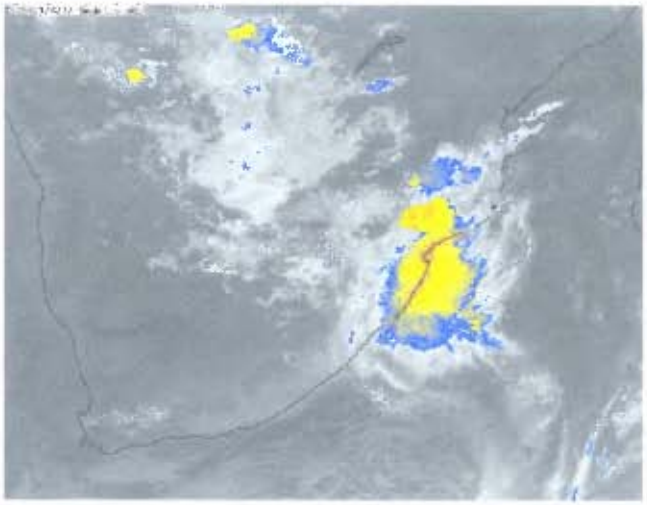

i) 04h00

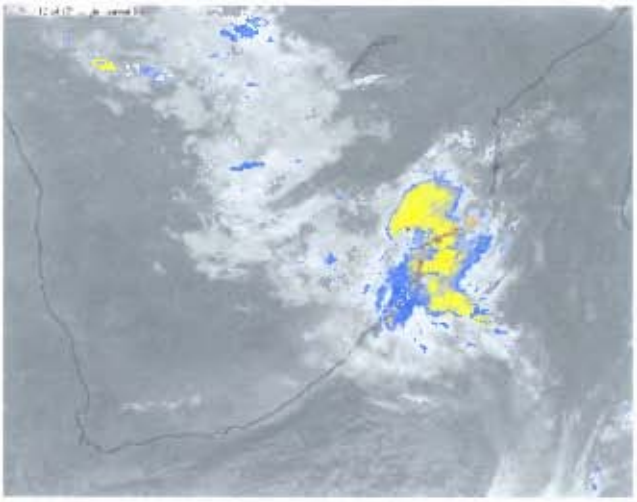

j) 06h00

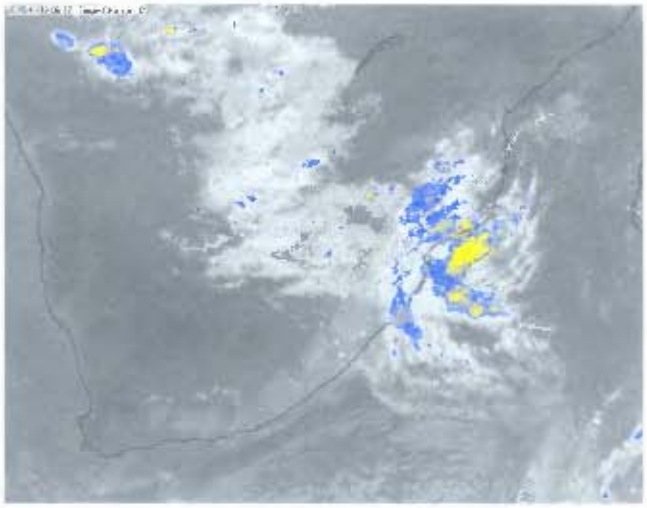

Figure A4.3 cont: MSG infrared satellite images, with colour mapping applied to cloud top temperatures from g) 00h00 UTC through to j) 06h00 UTC.

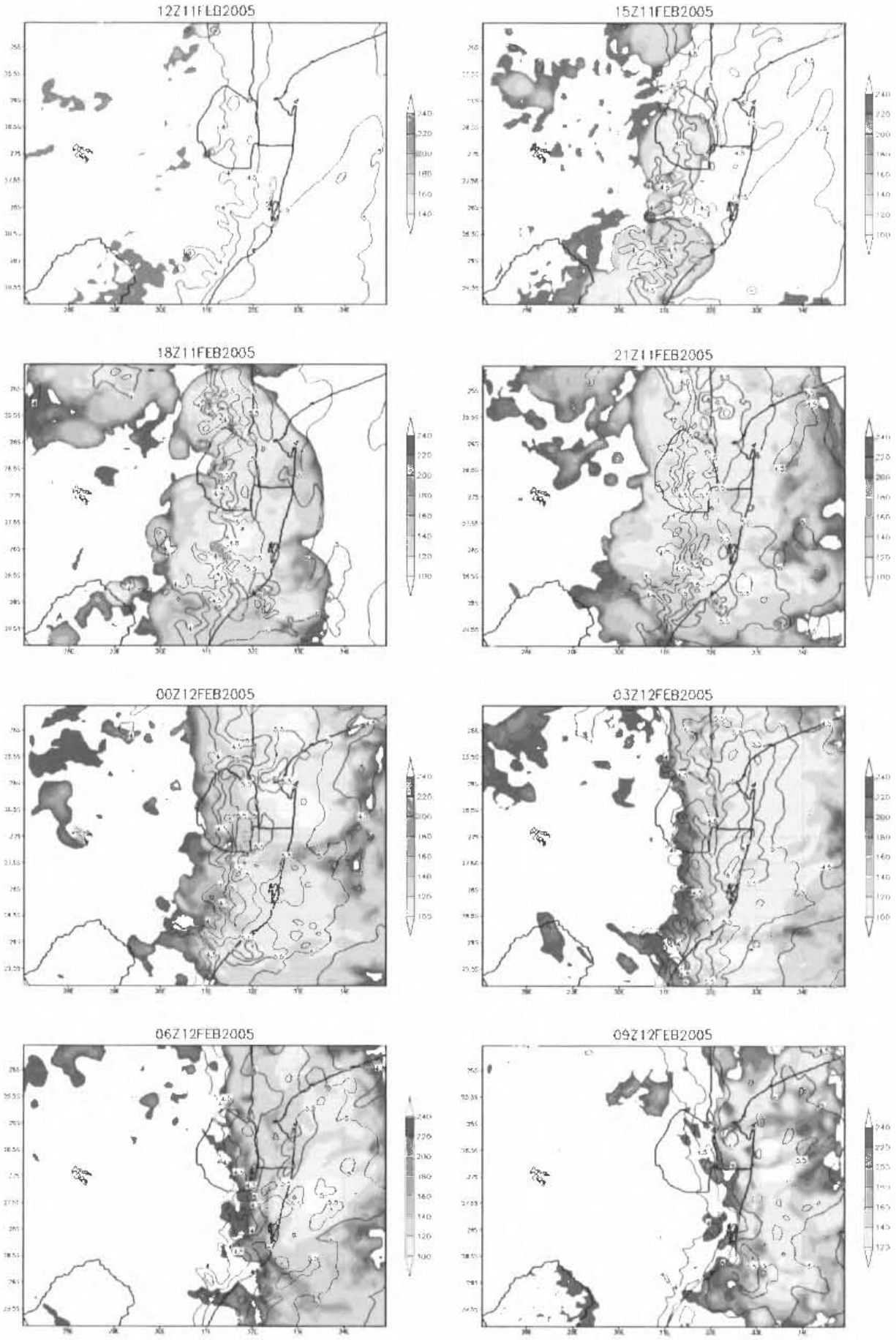

Figure A5.1: Simulated domain two outgoing longwave radiation (shaded with interval of 20 W.m^{-2}) and precipitable water (contour starting at 4 cm with interval of 0.5 cm) at 3 hour intervals starting at 12h00 UTC on the 11 February 2005.

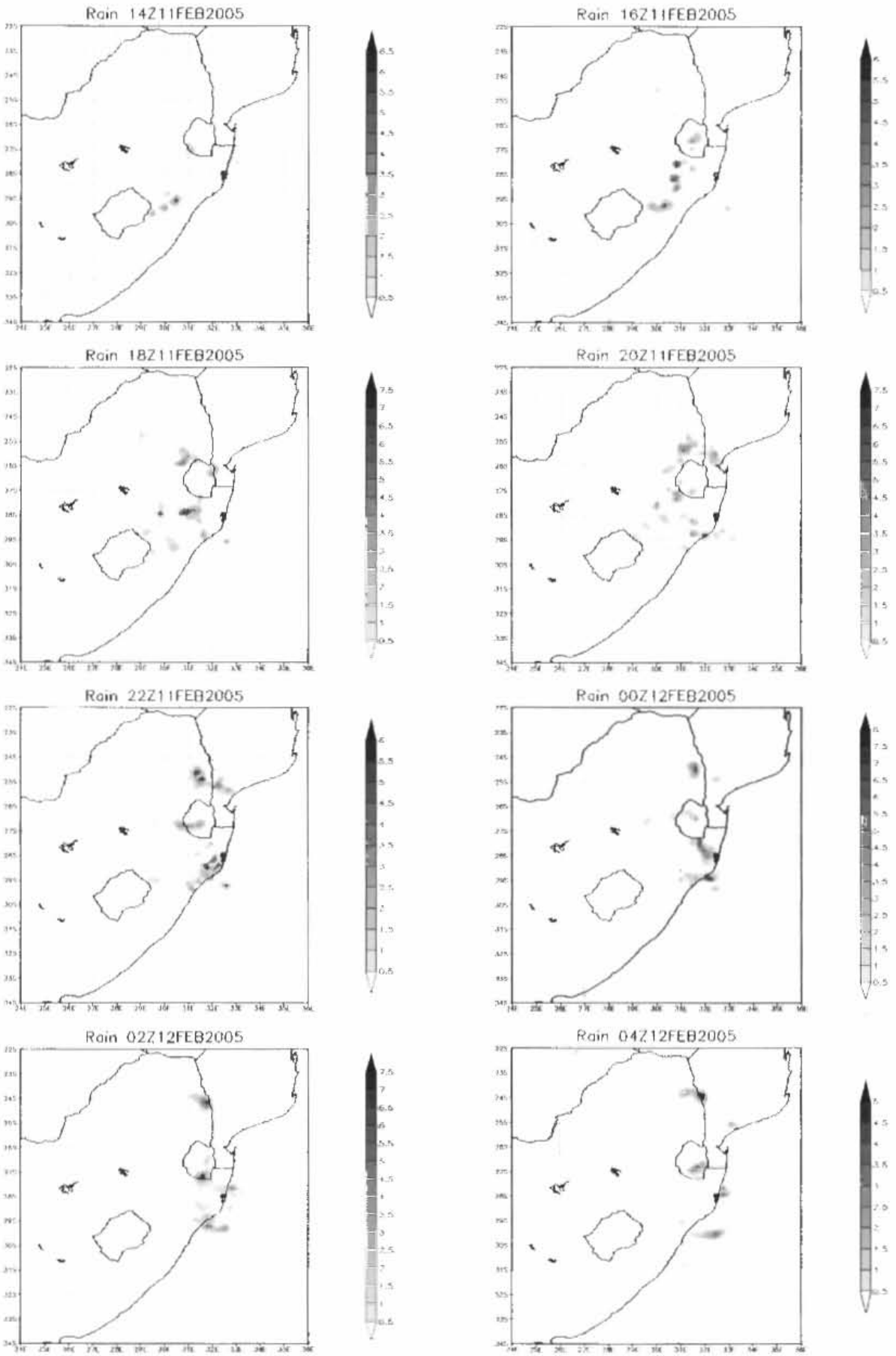

Figure A 6.1: Hourly simulated precipitation (interval at 0.5 cm) from the SST sensitivity run. Displayed every two hours, starting at 14h00 UTC 11 February to 04h00 UTC on the 12th.

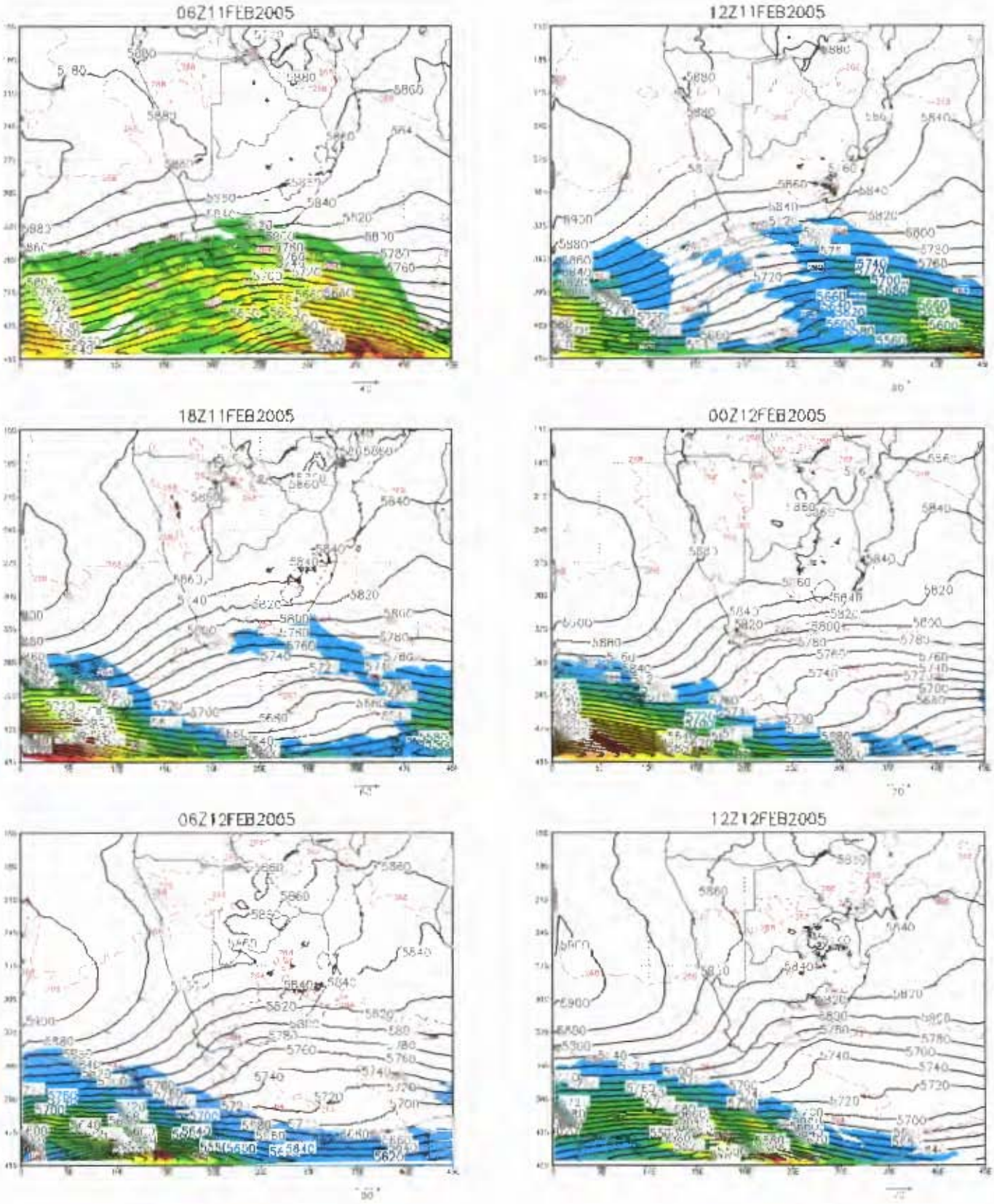

Figure A6.2: Temperature (dashed contours; interval 4 degrees k), geopotential height (thick contours; interval 20m) and winds with speeds greater than 20m.s^{-1} at the 500 hPa level, derived from the SST sensitivity simulation. Starting at 06h00 UTC on the 11th and ending at 12h00 UTC 12 February, at 6-hourly intervals.

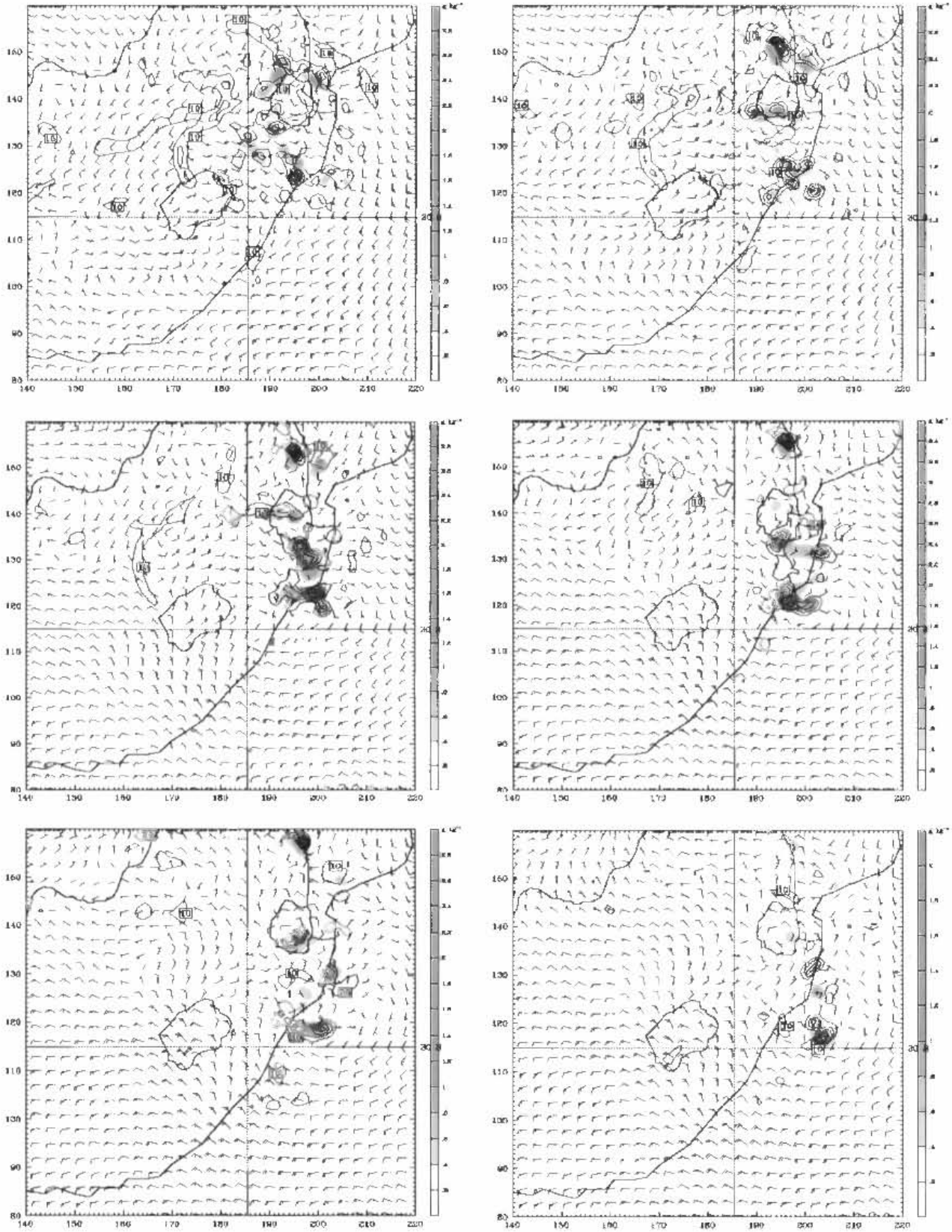

Figure A6.3: Simulated winds, vertical velocity (contour; interval 25 cm.s^{-1}) and rain water mixing ratio (shaded; starting at 0.4 g kg^{-1}) at the 750 hPa level in the SST sensitivity simulation. Starting at 19h00 UTC on the 11th and ending at 05h00 UTC on the 12th, at 2 hour intervals (left to right). Only areas with upward motion (greater than 10 cm s^{-1}) are shown for clarity.

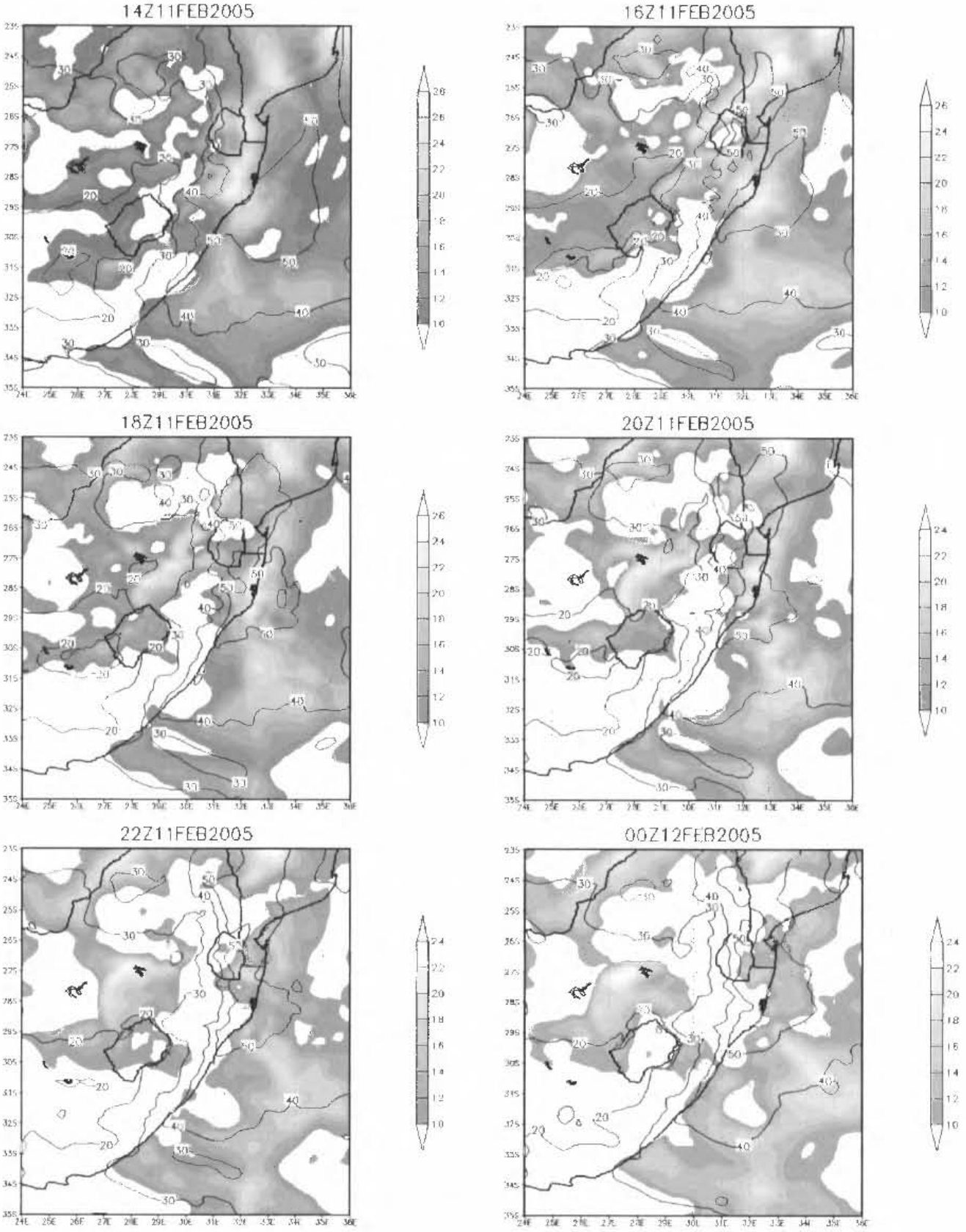

Figure A6.4: Convective instability (shaded; 2 °C interval starting at 10 °C) and precipitable water (contour, 10 mm interval) over the eastern parts of South Africa in the SST sensitivity run. Starting at 14h00 UTC and ending at 00h00 UTC, at 2 hour intervals.

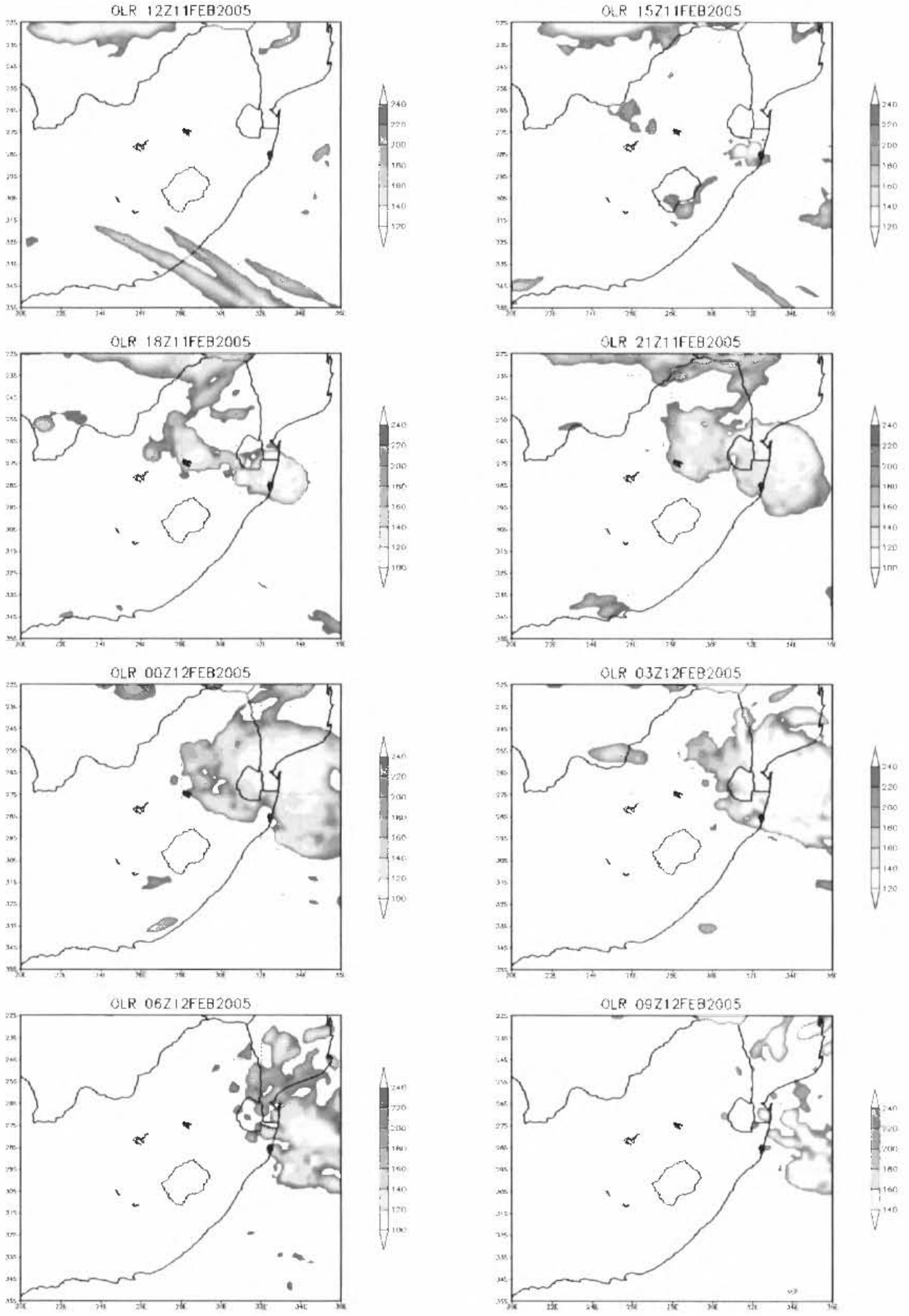

Figure A6.5: Domain one OLR (interval, 20 w.m^{-2}) derived from the SST test simulation starting at 12h00 UTC 11 February at 3 hour intervals (from left to right) and ending at 09h00 UTC.

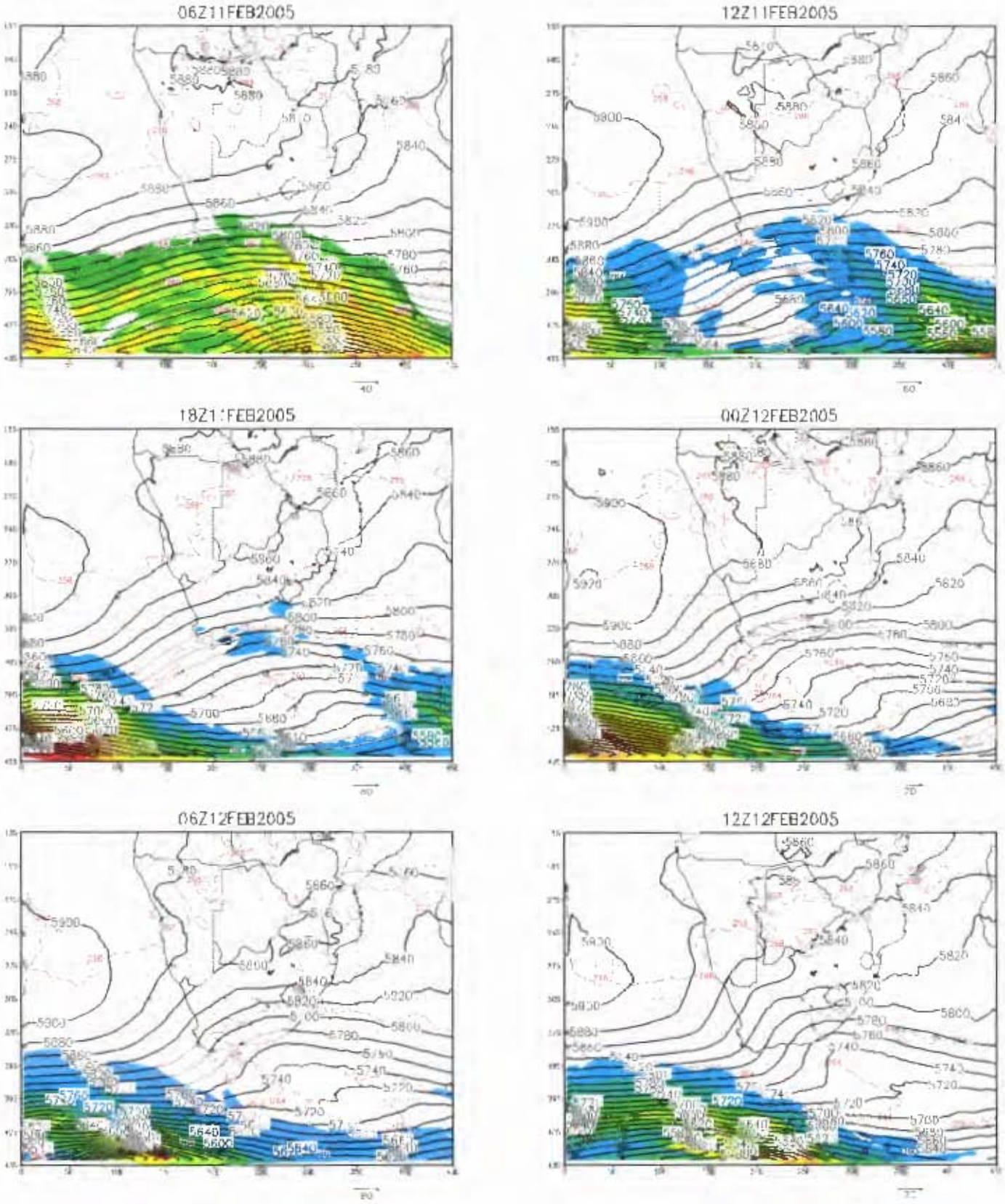

Figure A6.6: Temperature (dashed contours; interval 4 degrees k), geopotential height (thick contours; interval 20m) and winds with speeds greater than 20m.s^{-1} at the 500 hPa level, derived from the topography test simulation. Starting at 06h00 UTC on the 11th and ending at 12h00 UTC 12 February, at 6-hourly intervals.

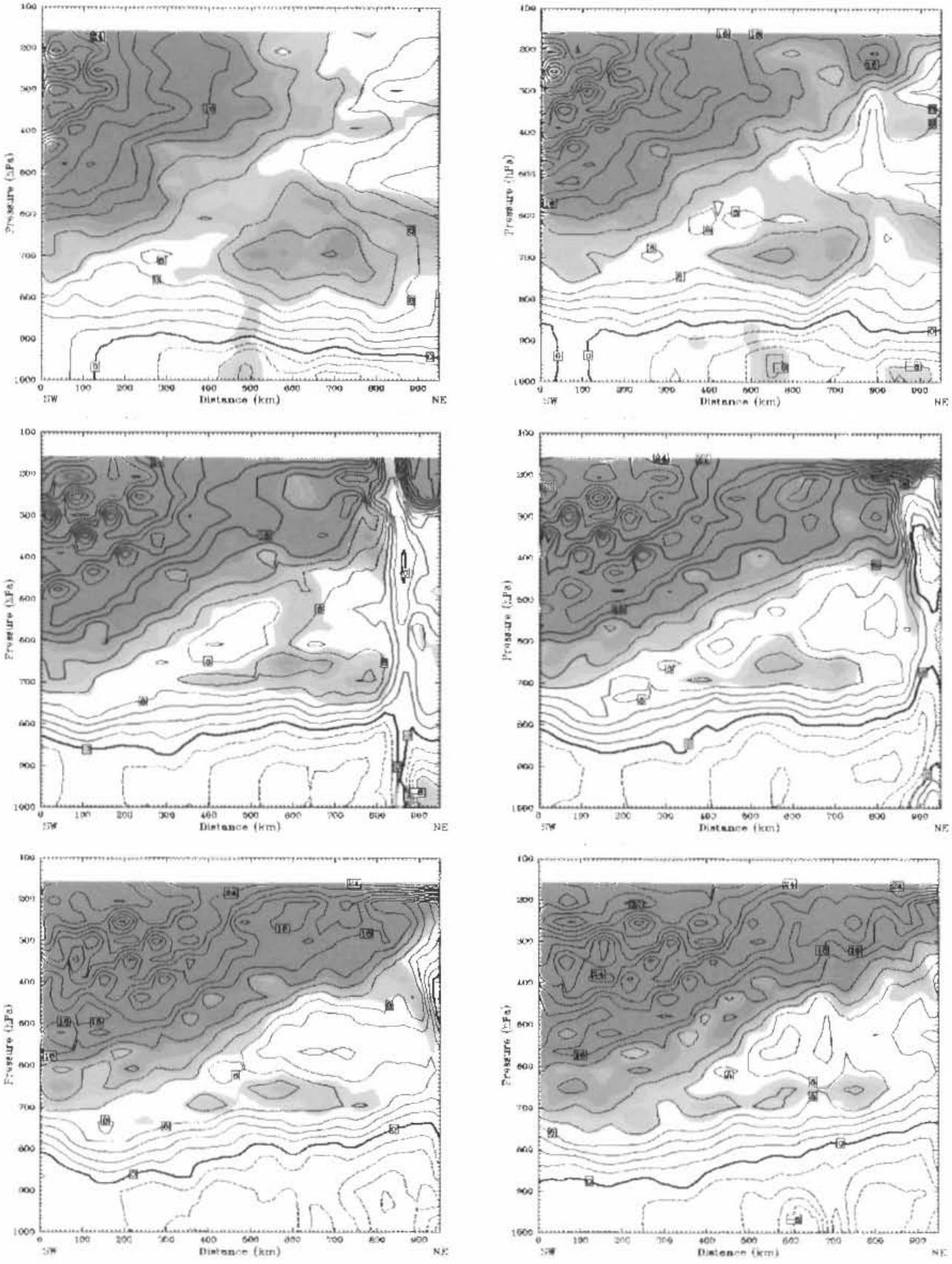

Figure A6.7: Vertical cross-sections of wind speeds starting at 10 $m.s^{-1}$ (shaded; 5 $m.s^{-1}$ interval) and zonal wind speeds (contour; 2 $m.s^{-1}$ interval) from the topography sensitivity simulation along B-B' in figure 5.9. From left to right starting at 14h00 UTC (top) and ending at 00h00 UTC (bottom).

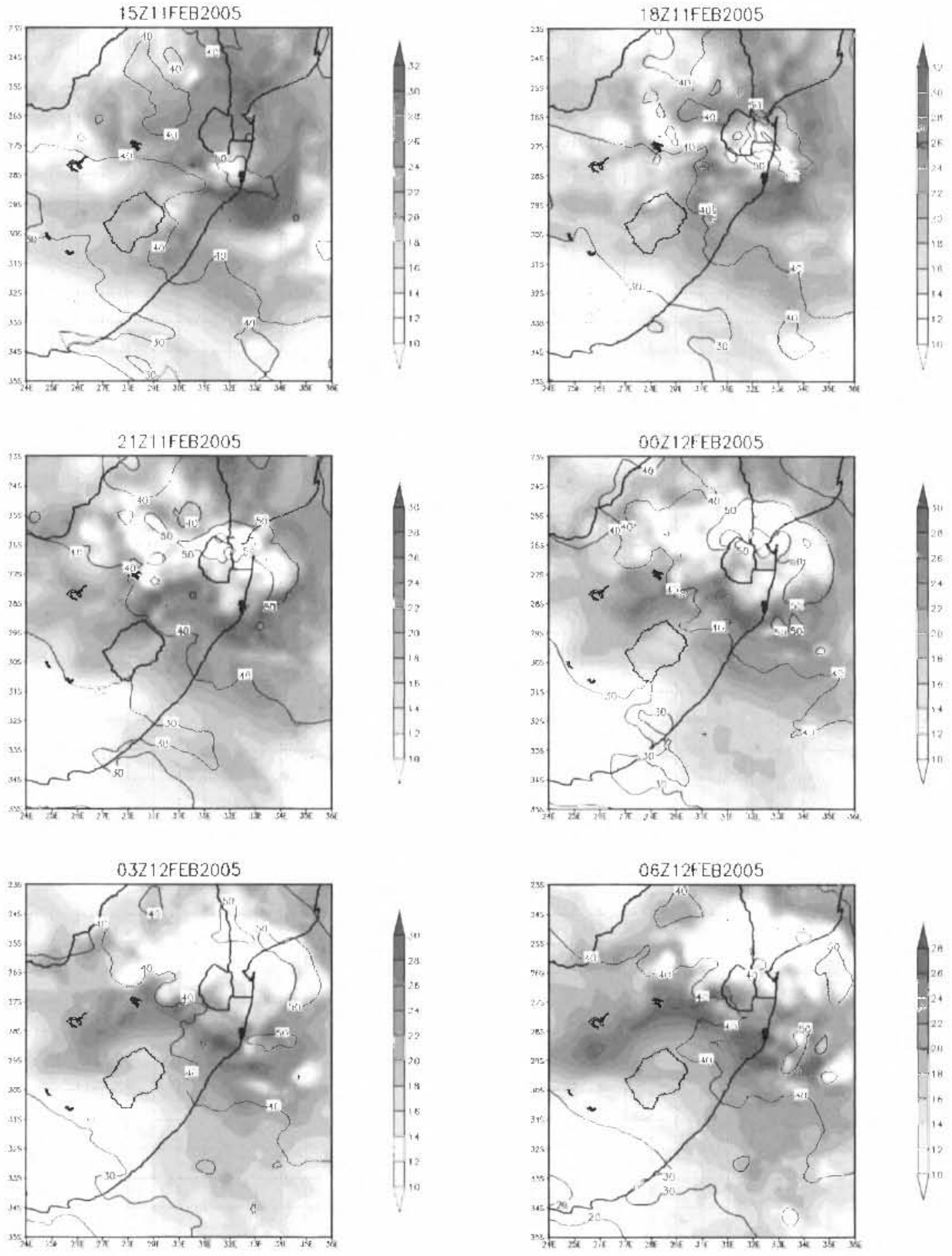

Figure A6.8: Convective instability (shaded; 2 °C interval starting at 10 °C) and precipitable water (contour, 10 mm interval) over the eastern parts of South Africa in the topography sensitivity simulation. The convective instability is calculated by the difference between equivalent potential temperature at the 0.955 – 0.525 sigma levels. Starting at 15h00 UTC and ending at 06h00 UTC, at 3 hour intervals.

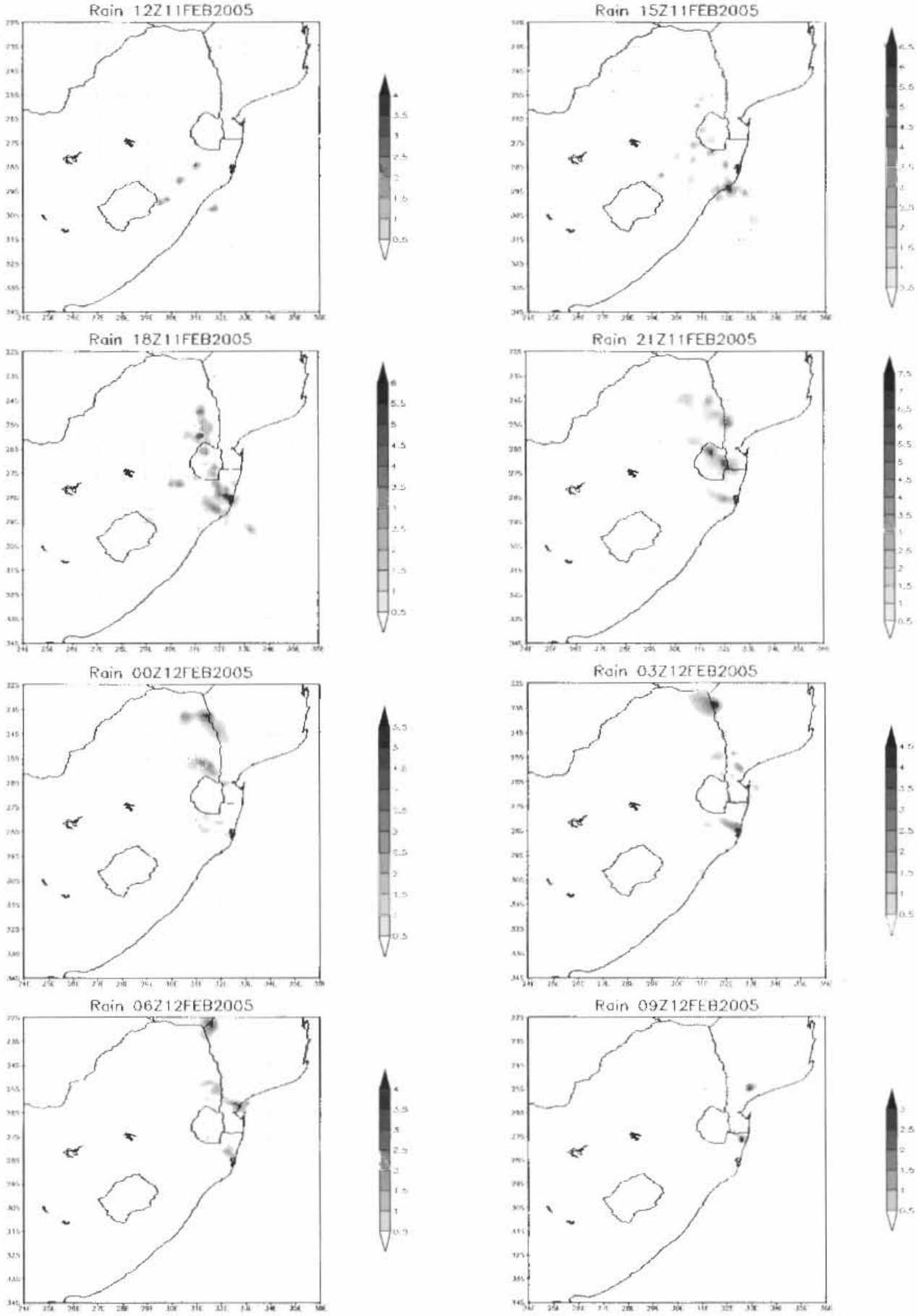

Figure A6.9: Hourly simulated precipitation (interval at 0.5 cm) from the mid-latitude sensitivity run, which is displayed every three hours starting at 12h00 UTC 11 February to 09h00 UTC on the 12th.

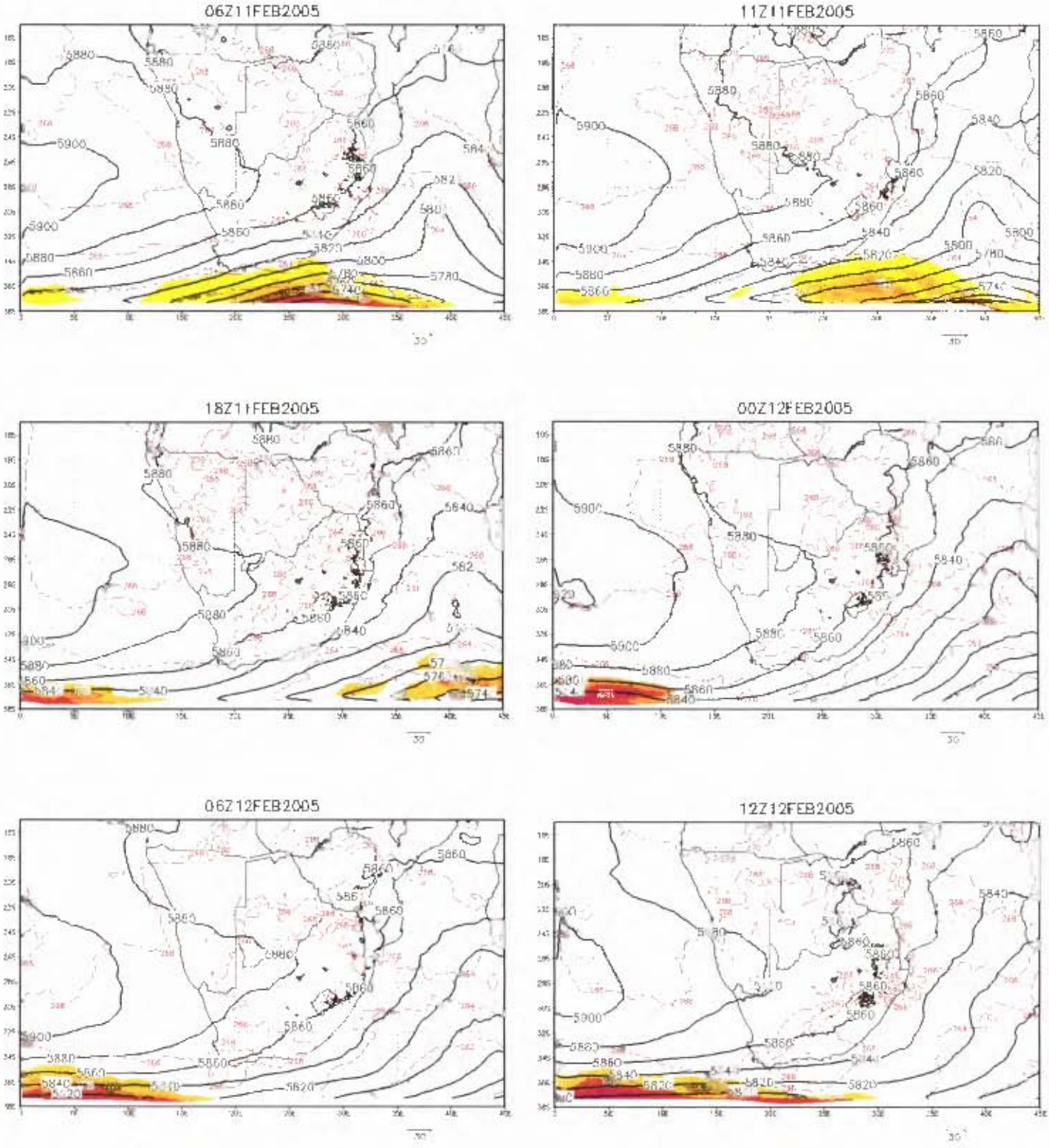

Figure A6.10: Temperature (dashed contours; interval 2 degrees k), geopotential height (thick contours; interval 20m) and winds with speeds greater than 20 $m.s^{-1}$ at the 500 hPa level, derived from the mid-latitude sensitivity test. Starting at 06h00 UTC on the 11th and ending at 12h00 UTC 12 February, at 6-hourly intervals.

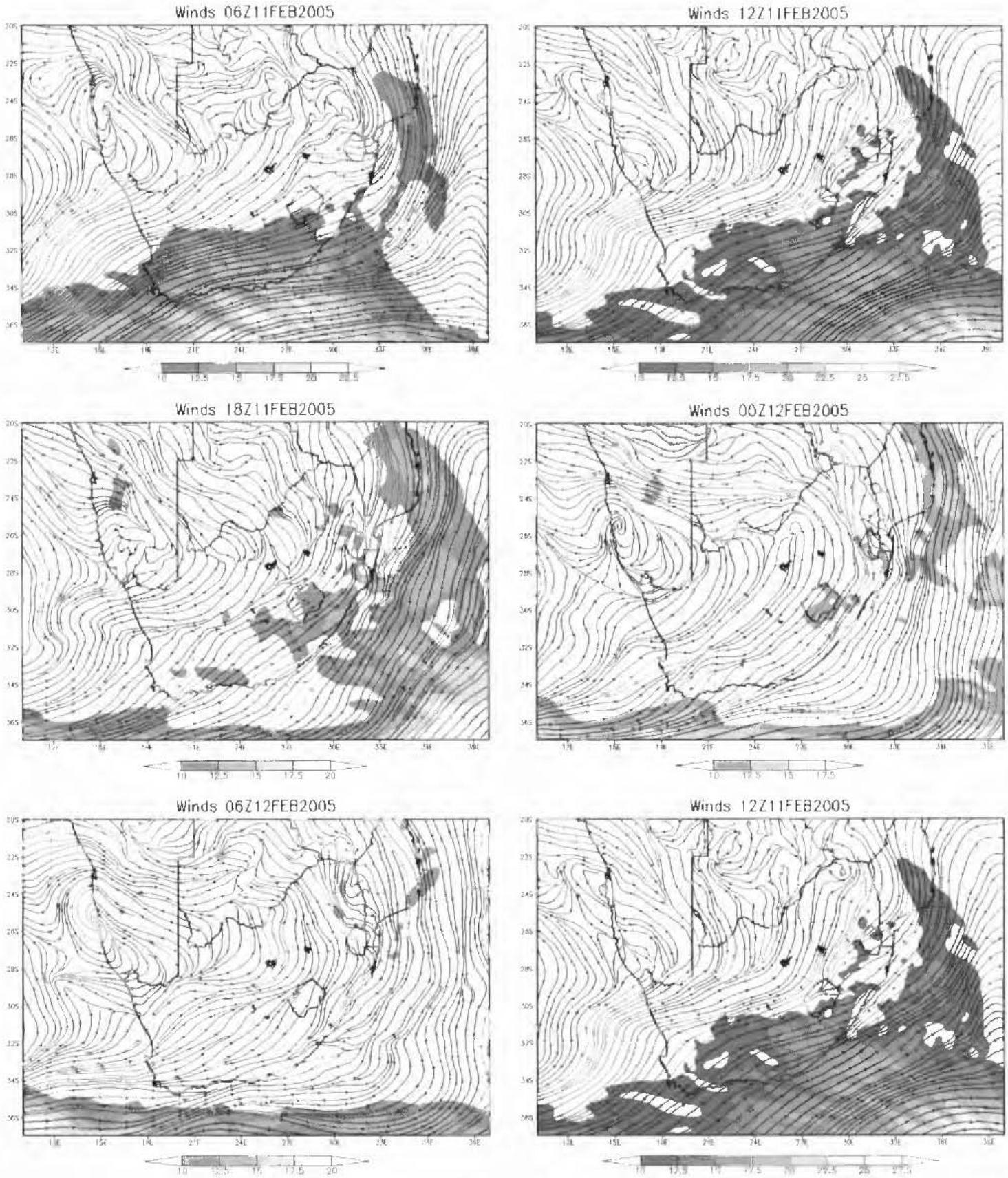

Figure A6.11: Same as figure 6.23, except at the 0.525 sigma level and regions where wind speeds greater than 10m.s^{-1} are shaded (interval; 2.5 m.s^{-1}).

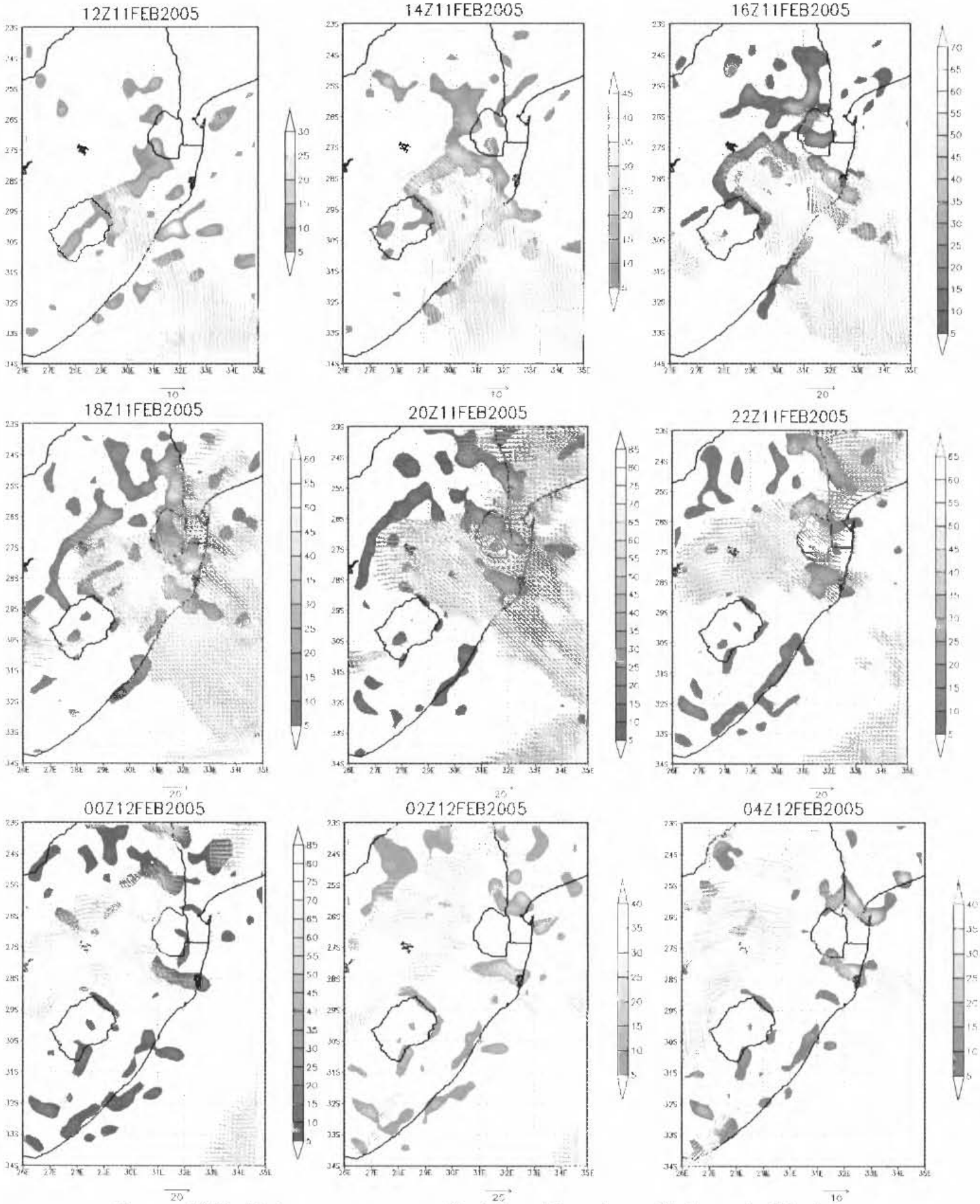

Figure A6.12: Moisture convergence (shaded positive values with interval of 5 $g.kg^{-1}.s^{-1}$) and wind speeds greater than 10 $m.s^{-1}$ at the 0.870 sigma level from the mid-latitude sensitivity simulation. Starting at 12h00-04h00 UTC 11/12 February, at 2 hour intervals. Note that divergence has been omitted for clarity.

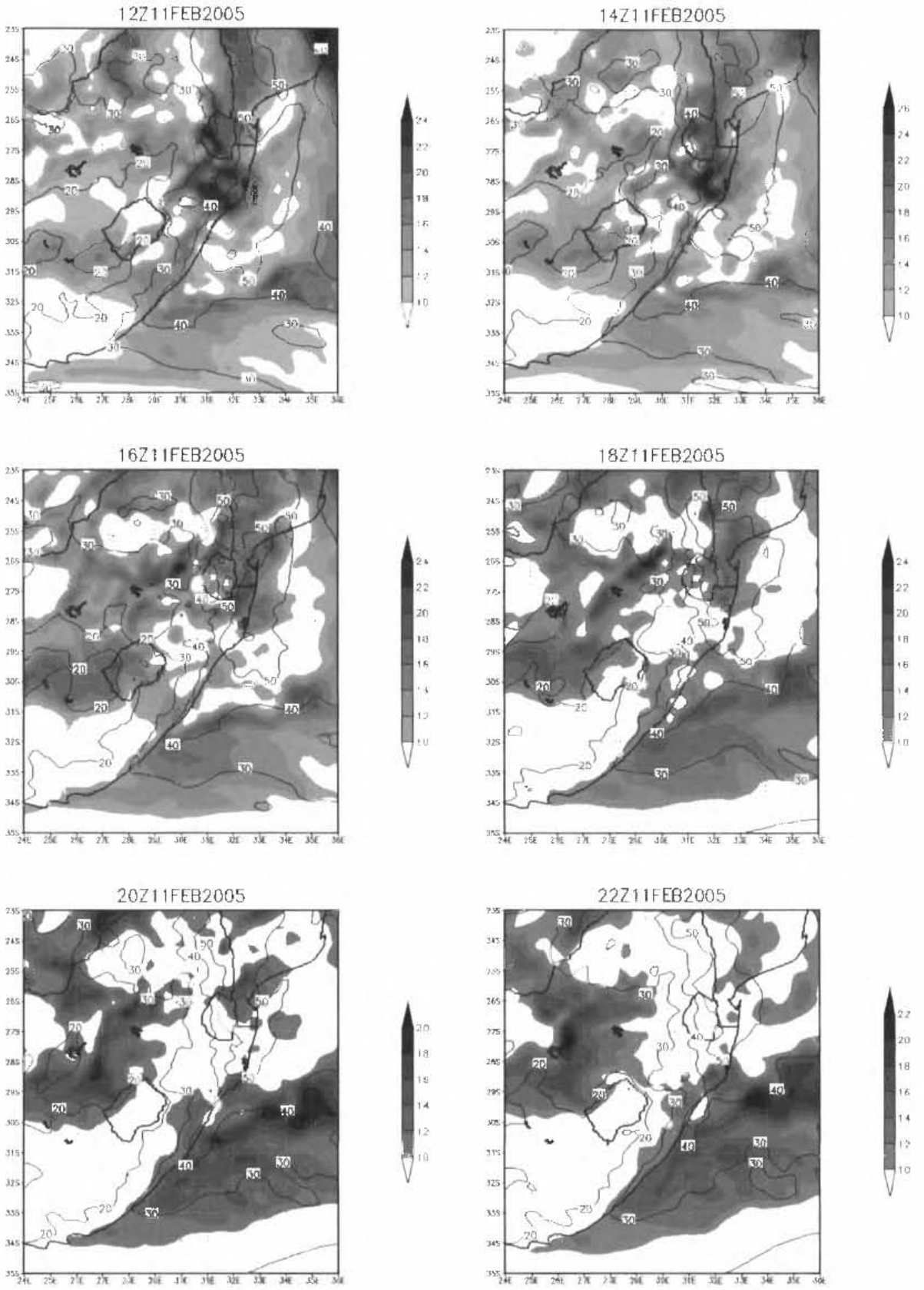

Figure A6.13: Convective instability (shaded; 2°C interval starting at 10 °C) and precipitable water (contour, 10 mm interval) over the eastern parts of South Africa in the mid-latitude sensitivity simulation. Starting at 12h00 UTC and ending at 06h00 UTC, at 2 hour intervals.

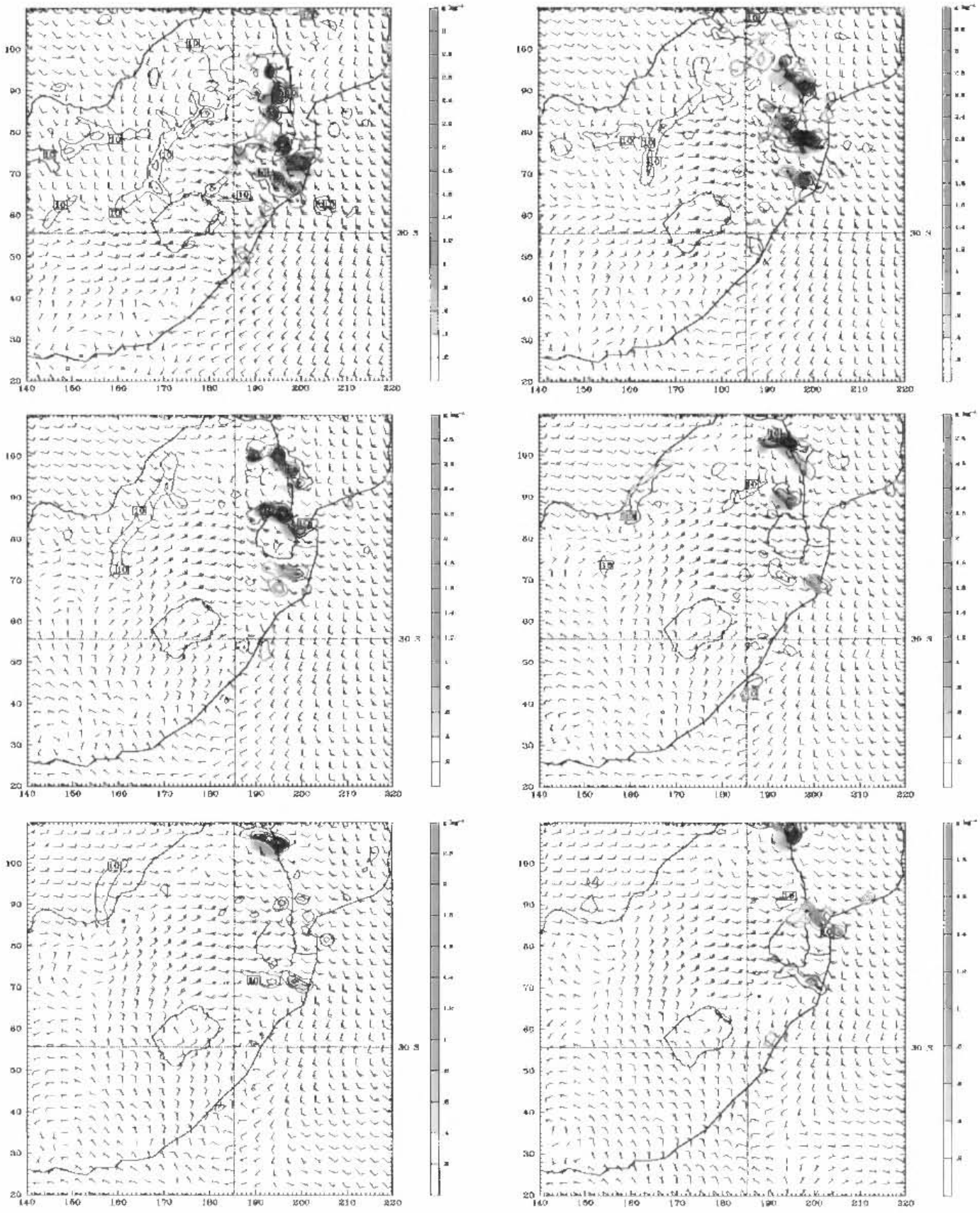

Figure A6.14: Winds, vertical velocity (contour; interval 25 cm.s^{-1}) and rain water mixing ratio (shaded; starting at 0.4 g kg^{-1}) at the 750 hPa level in the mid-latitude sensitivity run. Starting at 18h00 UTC on the 11th and ending at 04h00 UTC on the 12th, at 2 hour intervals (left to right). Only areas with upward motion (greater than 10 cm s^{-1}) are shown for clarity.

Appendix B:

Basic Severe Weather Parameters:

- As used by the NOAA National Weather Service (www.crh.noaa.gov/)

B.1. Convective Available Potential Energy – CAPE

CAPE represents the amount of buoyant energy created in the process whereby a parcel of air passes its level of free convection and continues to rise due to it becoming warmer than its environment. This energy is then available to accelerate the parcel of air upwards. This parameter is determined from the positive area on a sounding between the parcel's ascent along a moist adiabat and the environmental temperature curve from the level of free convection (LFC) to the equilibrium level (EL).

$$\mathbf{CAPE} = g \int_{LFC}^{EL} \left\{ \left[(T_{parcel} - T_{envir}) / T_{envir} \right] dz \right.$$

Where:
g = gravity
EL = equilibrium level
LFC = level of free convection
"{" = vertical integration between the LFC and the EL
dz = incremental depth
Tparcel = temperature of a parcel from the lowest 500 m of the atmosphere, raised dry adiabatically to the LCL and moist adiabatically thereafter
Tenvir = temperature of the environment

B.2. Lifted Index – LI

This parameter (in degrees Celsius) is a measure of stability which measures the difference between a lifted parcel's temperature at 500 mb and the environmental temperature at 500 mb.

$$\mathbf{LI} = T(500\text{ mb envi}) - T(500\text{ mb parcel})$$

Where:

T (500 mb envi) = 500 mb environmental temperature
T (500 mb parcel) = rising air parcel's 500 mb temperature.

B.3. Precipitable Water – PW

Precipitable water, which is measured in mm, is the amount of precipitable water for the entire sounding (i.e. through the entire atmosphere column).

B.4. Severe Weather Threat Index - SWEAT:

The SWEAT Index evaluates the potential for severe weather by combining several parameters into one index. These parameters include:

- Temperature in Celsius at 850 mb - (T850mb)
- Total Totals Index – (TT)
- 850 and 500mb wind speeds (f8 and f5) and direction (S)

These parameters are then incorporated into one equation:

$$\mathbf{SWEAT = 12\ [Td850\ mb] + 20\ (TT - 49) + 2\ (S8K) + S5K + 125\ (S + 0.2)}$$

Where:
S8K and S5K = 850 mb and 500 mb wind speed in knots, respectively,
S = sin (500 mb minus 850 mb wind direction)

B.5. Total Totals Index - TT:

This method uses the combination of two other parameters, which are Vertical Totals (VT) and the Cross Totals (CT). These two parameters utilize three values at two different levels, which are:

- Temperature in Celsius at 850 mb - (T850mb)
- Dewpoint in Celsius at 850 mb – (Td850 mb)
- Temperature in Celsius at 500 mb – (T500mb)

This then results in the TT being calculated as:

$$\mathbf{TT = VT + CT}$$
$$\mathbf{VT = T850mb - T500\ mb}$$
$$\mathbf{CT = Td850mb - T500\ mb}$$

B.6. Bulk Richardson number – BRN:

This relationship between the buoyancy and wind shear is represented in the form of the bulk Richardson number (BRN), R, a non-dimensional convective parameter defined as:

$$\mathbf{R = B / (1/2\ U^2)}$$

Where B is the buoyant energy (or CAPE) in the storms environment and U is a measure of the vertical wind shear. The vertical wind shear is calculated by taking the difference in the mean wind over the lowest 6 km.

Appendix C:

List of Acronyms

AMSR-E – Advanced Microwave Scanning Radiometer for EOS

ARL - Atmosphere Resources Laboratory

AWS – Automatic Weather Station

BRN – Bulk Richardson's Number

CAPE – Convective Available Potential Energy

CDC – Climate Diagnostic Center

CISK – Conditional Instability of the Second Kind

CPS – Convective Parameterization Scheme

DJF – December, January and February

ECMWF – European Centre for Medium-range Weather Forecasting

FDDA – Four-Dimensional Data Assimilation

GCM – Global Circulation Model

GMT – Greenwich Mean Time

GPCP – Global Precipitation Climatology Project

HRV – High Resolution Visible

HYSPLIT – Hybrid Single Particle Lagrangian Integrated Trajectory

IR – Infrared

ITCZ – Intertropical Convergence Zone

KZN – KwaZulu-Natal

LI – Lifted Index

LLJ – Low Level Jet

LST – Local Standard Time (UTC + 2)

MBE – Meso-beta Scale Convective Elements

MCS – Mesoscale convective system

MCC – Mesoscale Convective Complex

MCV – Mesoscale Convective Vortex

MCWS – Mesoscale Convection Weather Systems

MM5 – Mesoscale Model 5th Generation

MRF – Medium Range Forecast

MSG – Meteosat Second Generation

MW - Microwave

NASA – National Aeronautics and Space Administration

NCAR – National Center for Atmospheric Research

NCEP – National Center for Environmental Prediction

NOAA – National Oceanic and Atmospheric Administration

OI – Optimally Interpolated

OISST – Optimum Interpolation Sea Surface Temperatures

OLR – Outgoing Longwave Radiation

PBL – Planetary Boundary Layer

PECS – Persistent Elongated Convective Systems

PSU – Pennsylvania State University

PW – Precipitable Water

QPF – Quantitative Precipitation Forecasting

RGB – Red, Blue and Green

RIJ – Rear Inflow Jet

SAWS – South African Weather Service

SICZ – South Indian Convergence Zone

SST – Sea Surface Temperature

SWEAT – Severe Weather Threat Index

TMI - TRMM Microwave Imager

TRMM – Tropical Rainfall Measuring Mission

TT – Total Totals Index

ULJ – Upper Level Jet

US – United States of America

USGS – United States Geological Survey

UTC – Coordinated Universal Time

WPR – Western Pacific Region
